Department of Astronautics, Electrical and Energetics Engineering

Ph.D. Program: Sciences and Technologies for Complex Systems

Curriculum: Electrical Engineering
ING-IND/33–ELECTRICAL POWER SYSTEMS

Final Dissertation

Power system planning methods and experiences in the energy transition framework

---

by
Michela Migliori

Supervisors:

Prof. Stefano Lauria

Ing. Enrico Maria Carlini

Coordinator of Ph.D Program:
Prof. Luigi Martrano

Course n°33, 2017-2020

Index

Introduction

In recent years, the unbundling of the electricity market together with the profound "energy landscape" transformation have made the transmission network development planning a very complex multi-objective problem. The climate and energy objectives defined at the European level aim for a deepening integration of the European power markets and the electricity sector is recognized as one of the main contributors to the energy transition from a thermal-based power system to a renewable-based one.

In the deregulated framework, network planners have to satisfy multiple different objectives, including: facilitating competition between market participants, providing non-discriminatory access to all generation resources for all customers, including green resources, mitigating transmission congestions, efficiently allocating the network development actions, minimizing risks associated with investments, enhancing power system security and reliability and minimizing the transmission infrastructure environmental impact. Further complexities are related to the significant uncertainty about future energy scenarios and policy rules. In particular, the increasing distributed renewable energy source integration dictated by the European energy targets, raises several issues in terms of future power flow patterns, power system flexibility and inertia requirements, and cost-effective development strategies identification.

The thesis aims to investigate various aspects concerning the transmission network planning, with particular reference to the Italian power system and the experience gained working in the "Grid Planning and Interconnections Department" of Terna, the Italian Transmission System Operator.

One of the main topics of this work is the use of the series compensation to exploit operating limits of underused portions of the HV – EHV transmission network in parallel to critically loaded ones, in order to control and provide alternative paths for power flows. The purpose is to extend the allowable transmission capacity across internal market sections. To this aim, a specific application of series compensation (together with reconductoring) to exploit the transfer capacity of a 250 km long, 230 kV-50 Hz transmission backbone spanning the critical section Centre South – Centre North is illustrated in **Chapter 1**. The results are validated by means of static assessment and similar applications could be hypothesized for grid portions in the South of Italy where the primary network is mainly unloaded whereas the sub-transmission network reaches high levels of loading because of the huge renewable generation capacity situated there.

A further characteristic of modern power systems is the need to integrate high levels of renewable energies while fulfilling reliability and security requirements. In **Chapter 2**, the offshore wind farms perspectives in the Italian transmission system are evaluated, considering policies, environmental and technical aspects. Furthermore, the adoption of the HVDC technology in parallel to the AC traditional system topic is addressed: planning static and dynamic studies involving a real HVDC Italian project are proposed. In particular, the impact of the planned HVDC link on the loadability and the dynamic performance of the system is investigated in medium and in long-term future planning scenarios.

The evaluation of the thermal performance of a specific grid portion in the South of Italy affected by significant increase of power generation by variable energy sources is proposed both in the current situation and in the future scenarios in order to highlight the benefits related to the presence of the planned network reinforcements. Finally, some issues of the prospective reduced inertia systems are illustrated and a possible methodology to evaluate the economic impact of inertia constraints in long-term market studies is proposed.

In the light of the emerging concept of power system flexibility, traditional planning evolved to assess the ability of the system to employ its resources when dealing with the changes in load demand and variable generation. Flexibility analyses of the Italian power system, carried out in terms of some market studies-based metrics and grid infrastructure-based indexes, are provided in **Chapter 3**. The flexibility requirements assessment in planning scenarios are of interest to evaluate the impact of network development actions and have been included in the yearly National Development Plan.

The last research topic involves the cost-effective target capacity assessment methodology developed by Terna in compliance with the Regulator directives and presented in **Chapter 4**, together with the results yielded by its application to each significant market section of the Italian power system. The methodology has been positively evaluated from academic independent expert reviewers, and its outputs are relevant for the policy makers, regulatory authority and market participant to assess and co-design the energy transition plan of a future European interconnected power system.

1. Series compensation

Reactive compensation methods have been devised with the aim of realize voltage control and increase power transfer capability, especially when generators are located far from the load areas. The effectiveness of these methods is proved by the common practice in the power industry, due to the active power flows sensitivity to reactive power changes. Furthermore, the reactive power propriety to be generated at any location without external energy sources makes the reactive compensation relatively inexpensive [1].

Series capacitors allow to control the longitudinal impedance of the network, while also providing reactive power. By reducing the total reactance of the transmission line, the series compensation improves power system stability and helps to control the voltage drop along the line. Since the series capacitors are passive elements in the system, they perform these functions function without external controls or operator action.

The main application of series capacitors is nowadays represented by the compensation of long EHV transmission lines connecting power plants to distant consumption areas, with the aim of increasing the power transfer under angle stability constraints. This occurs mainly in countries characterized by an important geographic extension: in ENTSO-E space, the use of series compensation is basically limited to center-north Sweden [2] and Turkey.

In comparatively smaller countries, such as Italy, the meshed electrical grids and the shorter transmission lines make angle stability less constraining for power system operation. However, an interesting application of series compensation in a densely meshed system is represented by their use to regulate active power flows, in order to allow the loading of underused grid portion in parallel with critically loaded ones, expecially in case of contingencies. In fact, power system reliability is a primary concern for power system engineers both in planning and operation phases, to meet security and adequacy standards. Moreover, the most straightforward solution to extend the operational limits of strategic transmission paths (additional transmission lines building) is hardly practicable nowadays due to the increasing public opposition.

All these aspects have led to the investigation of the possible application of the series compensation to exploit the capability of selected backbones which span critical sections of the Italian power system. Series compensation has been employed in transmission systems worldwide since the 1950s. It represents an effective means of improving steady state voltage regulation since series capacitors are inherently self-regulating [3], raising the voltage collapse limit, increasing power transfer capability of transmission lines by raising the transient stability margin, improving the reactive power balance. It could also be used for active load sharing

between adjacent transmission corridors by changing impedances and damping of system oscillations, by resorting to Thyristor Controlled Series Capacitors (TCSC), [4 – 6].

In planning studies, series capacitors represent a less capital intensive solution (which also requires minimal permitting and siting requirements) to increase the capacity of existing transmission lines, allowing the optimization of the overall asset utilization, as well as the minimization of risk through the preservation of right of ways and corridors for future needs.

In the following, a real case study is presented showing different scenarios involving the present configuration (with and without series compensation included) and the re-equipment of the backbone under study (with and without series compensation included).

1.1 Introduction

The idea of using the series compensation to exploit the operating limits of underused grid portions and providing alternative paths for large active power transfers, expecially during important contingencies affecting the EHV transmission network, can be attractive if series capacitors are located within the TSO's sub-stations as this solutions is less capital intensive than mid-line compensation and has minimal permitting and siting requirements.

Starting from the analysis of the critical sections of the Italian power system, a specific application of series compensation (in conjunction with reconductoring with modern high-temperature conductors) has been studied for a 250 km long, 230 kV-50 Hz transmission backbone spanning the critical section Centre South – Centre North. The latter has been considered a strategic one as it could allow significant power transfers in the South to North direction, as confirmed by the planned development "Removal of 230 kV Centre South – Centre North restrictions" (included in the National Development Plan since year 2014).

Actually the 250 km long, 230 kV-50 Hz transmission backbone under study is subject to severe thermal rating limitations since it is equipped with old conductors. Besides the limited thermal rating, the high longitudinal impedance of a long line equipped with single conductors compounds the difficulty of loading a 230 kV with several important 400 kV transmission paths in parallel.

The uprating studies carried out for the 230 kV backbone are presented in sub-section 1.2. Firstly, the operating envelopes of the line under study have been evaluated in the "as is" and "after reconductoring" configurations, without series compensation.

Series compensation requirements are then assessed and the capability of both the present line and the reconductored in the presence of series compensation have been obtained.

Extensive steady-state load-flow calculations have been performed both for the isolated backbone and considering its effective loading within the meshed grid, in order to verify the usefulness of the proposed approach.

Finally, sub-section 1.3 reports the results yielded by a parametric analysis of the impact of series compensation on fault quantities in the Italian 230 kV – 50 Hz backbone under consideration. The main results of the short circuit parametric analysis in terms of fault levels (short-circuit currents, earth fault factor, voltage shift between neutral and ground, ratio between the single-line-to ground fault current and the three-phase fault current and impedances ratios) are illustrated both in the reconductored scenario without series capacitors and in the reconductored and series compensated ones.

1.2 Uprating studies for a 230 kV – 50 Hz backbone in central Italy

One possible avenue of intervention on active power flows is represented by the structural grid modification, by varying the longitudinal reactance of some network branches through the series insertion of reactive components characterized by a fixed impedance.

This section deals with a possible application of the series compensation, presenting a case study with series compensation used to increase power transfer in an underused grid.

The Italian power system zonal market configuration of the year 2018 [7] included six different market zones (Fig. 1.1): North, Centre North, Centre South, South, Sardinia and Sicily. Moreover, there is one "virtual zone" in the south of nation around the Rossano power plant, where production is limited due to network constraints.

This structure naturally lends itself to the individuation of "critical sections", which are more likely to undergo grid congestions in some operational conditions. Once the proper zones of the grid are identified, the maximum admissible transfer capacity between them must be assessed by considering the grid topology, the power flows distribution in most probable operational conditions, the thermal ratings of the lines and the associated security criteria [8].

The adoption of a zonal market provides several benefits such as the compatibility between the power transfers between nodes and the grid constraints, as well as the definition of price signals encouraging the Transmission System Operator to locate network developments in an efficient way. It ultimately provides an assessment of the economic value of transfer capacity between zones.

This study assesses the feasibility of upgrading a 230 kV transmission line (Fig 1.1) capability to increase the power transfer capacity between Centre North and Centre South market zones, especially in case of severe contingencies affecting the Tyrrhenian EHV backbone.

Straightforward technical solutions (from the use of bundled phase conductors to a full reconstruction of the line at 400 kV) are not viable, due to increasing authorization difficulties and public opposition to new infrastructures. Therefore, the only practical approach is to retain the present single-conductor 230 kV line structure, replacing the old Aluminum steel-reinforced (ACSR) conductors with modern high-temperature ones; however in order to actually extend the operational limits of the 230 kV transmission line, the use of series compensation is also necessary.

The assessment of power transfer capability of the line under study is carried out before and reconductoring. Then, the compensation requirements are evaluated both for the present

configuration and for the reconductored one, as well as the assessment of new power transfer capacities. Finally, load-flow calculations verify the feasibility of results previously obtained.

Fig. 1.1. Market zones of the Italian power system (year 2018) with the f 230 kV transmission line under study.

1.2.1 Methodology and case study

The maximum transfer capacity of the line under study was analysed in two different scenarios: the present scenario named “as is” and the “after reconductoring” scenario, with a greatly enhanced thermal rating of conductors; in both cases, the line is analysed as an isolated system with the reference single-line diagram shown in Fig 1.2. To obtain the operating envelopes, thermal (i.e. maximum current) and voltage constraints are enforced at each node in turn.

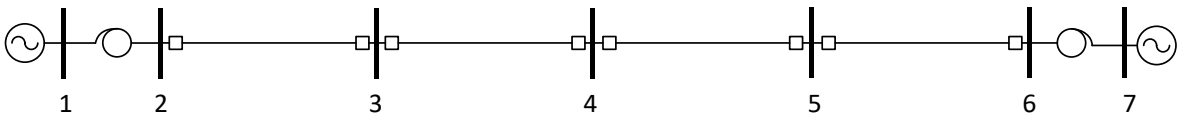

Fig. 1.2. Single-line diagram of the existing line under study, in the present uncompensated configuration.

1.2.1.1 Present Line – Operating Envelopes

The line is composed by four stretches, all realized in single circuit with one conductor per phase, with a total length of 250 km. Its main characteristics are listed in Table 1.1.

Table 1.1. Specifications and parameters of the 230 kV existing line under study.

Stretch	Length (km)	S (mm^2)	Thermal rating (A)	r_l (Ω/km)	x_l (Ω/km)	c_l (nF/km)
2 – 3	49.7	509	618	0.069	0.40	9.01
3 – 4	69.1	509	618	0.069	0.40	9.01
4 – 5	67.5	509	618	0.069	0.40	9.01
5 – 6	65.5	428	559	0.082	0.40	9.01

The remarkable overall length and the use of a single conductor per phase (with a relatively small cross-section) limit the maximum power transfer. Due to the presence of important 400 kV lines running in parallel along the Tyrrhenian backbone, the 230 kV line under study is largely unloaded in normal operational conditions.

Considering a grid configuration with no intermediate loads, the 230 kV backbone under study is equivalent to a single 252 km long non-homogeneous line whose maximum power transfer can be determined by enforcing thermal and maximum/minimum voltage constraints at each node in turn.

An example of the procedure used to obtain the operating envelopes is shown below in a (P,Q) plane referred to receiving end of the line, namely those dictated by the maximum current at node 2; similar developments dictated by voltage constraints are omitted because not significant.

Starting from the two-port equations [9 – 11], the sending node (1, or "S") and the receiving node (7 or "R") phase voltages can be expressed as:

$$\bar{E}_S = \bar{A}_{12} \cdot \bar{E}_2 + \bar{B}_{12} \cdot \bar{I}_2 \tag{1.1}$$

$$\bar{E}_R = \bar{D}_{27} \cdot \bar{E}_2 - \bar{B}_{27} \cdot \bar{I}_2 \tag{1.2}$$

The receiving end current is given by:

$$\bar{I}_R = -\bar{C}_{27} \cdot \bar{E}_2 + \bar{A}_{27} \cdot \bar{I}_2 \tag{1.3}$$

Simple manipulations yield the desired expressions of receiving-end voltage and current as a function of current at node 2:

$$\bar{E}_{R\_\bar{I}_2\, max} = \frac{\bar{D}_{27} \cdot \bar{E}_S - \bar{B}_{tot} \cdot \bar{I}_2}{\bar{A}_{12}} \tag{1.4}$$

$$\bar{I}_{R\_\bar{I}_2\, max} = \frac{-\bar{C}_{27} \cdot \bar{E}_S + \bar{A}_{tot} \cdot \bar{I}_2}{\bar{A}_{12}} \tag{1.5}$$

Lastly, the complex power at receiving end is now obtained:

$$\bar{N}_{R\_\bar{I}_2\,max} = 3 \cdot \bar{E}_{R\_\bar{I}_2\,max} \cdot \bar{I}_{R\_\bar{I}_2\,max} \tag{1.6}$$

By taking the magnitude of $\bar{I}_2$ equal to the thermal rating (618 A) of the conductor of the line first stretch (bottleneck) and varying the phase angle of $\bar{I}_2$ between 0° and 360°, a (P,Q) "capability" curve is obtained.

A similar operation is carried out to impose the maximum and the minimum admissible voltages at each node, yielding two different voltage-limited capability curves (max/ min voltage respectively). The resulting curves are, generally, ellipses in the complex plane (P_R, Q_R), as shown in Fig. 1.3.

The combination of voltage and current constraints shows that operation is limited by maximum current at line terminals and minimum bus voltage at node 7 resulting in a 206 MW maximum active power at the receiving end, i.e. node 7. The attendant steady-state bus voltages and line currents are summarized in Table 1.2. Note that both the voltage drop (ΔU=7.5 %) and the phase shift (Δϑ=32.1°) are quite large compared to values normally found at HV levels.

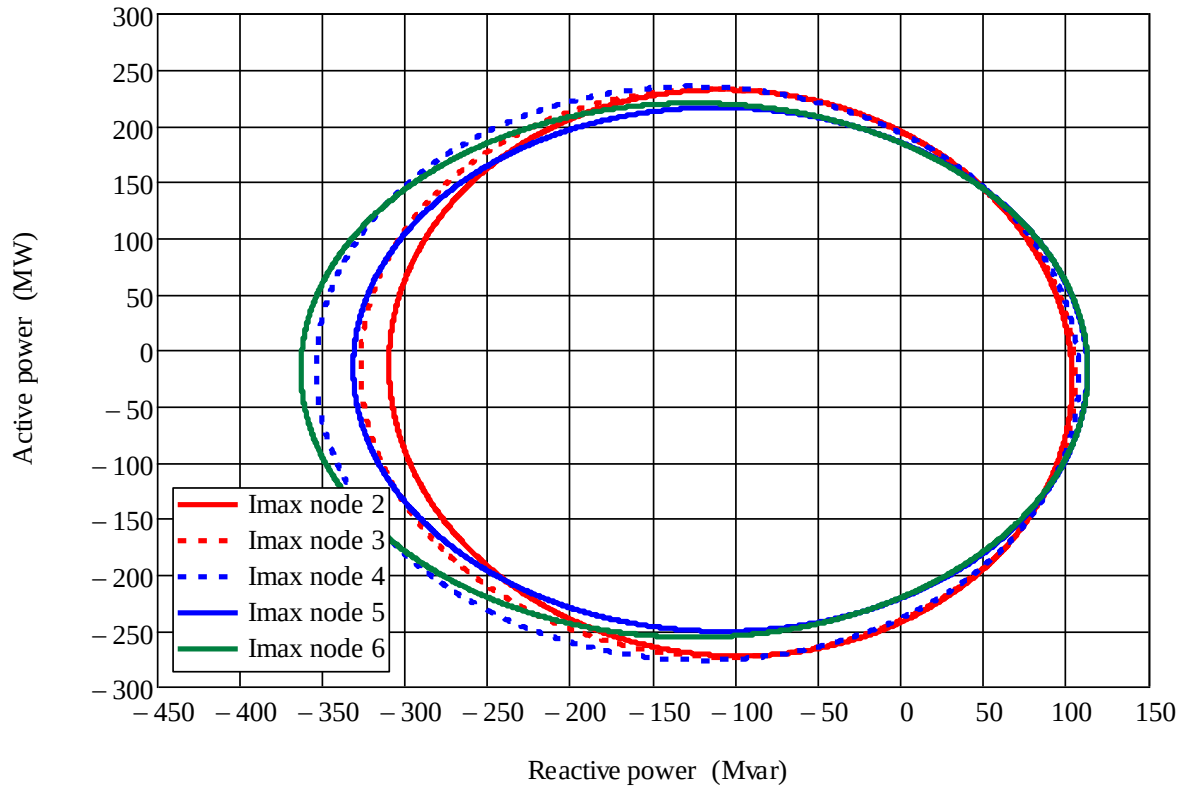

Fig. 1.3. Receiving-end (P,Q) capability curves of the existing, non-compensated line as dictated by maximum current in each segment.

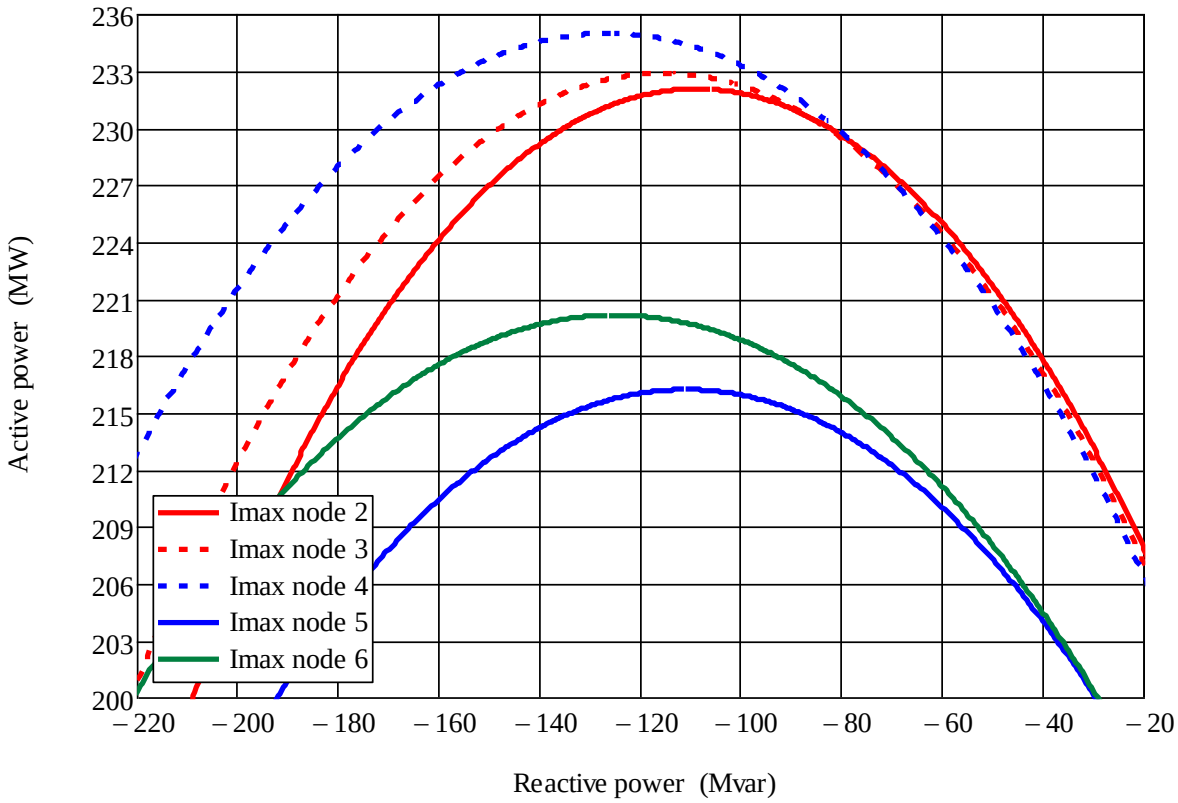

Fig. 1.4. Detail of the current-limited capability curves in Fig. 1.4.

Table 1.2. Voltage (amplitude and phase) and current values along the present line, at maximum power (P_R =205.5 MW).

Node	Current (A)	Voltage (kV)	$\Delta\vartheta_{1n}$ (n=1,…,7)
1	318.5	410	0°
2	554	233.5	-3.5°
3	555.8	228.3	-8.2°
4	556.8	222.7	-14.9°
5	556	219.1	-21.6°
6	553.5	216.6	-28.4°
7	318.2	381.3	-32.1°

1.2.1.2 Reconductoring

In order to accommodate much higher currents, the existing ACSR phase conductors could be replaced by "high temperature" ones such as the 27.5 mm Aluminium Conductor Steel Supported (ACSS).

The conductor cross-section is shown in Fig. 1.5 while conductor data are reported in Table 1.3.

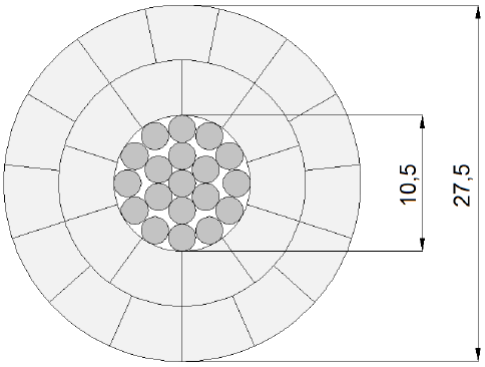

Fig. 1.5. Cross-section of the new 27.5 mm ACSS conductor.

Table 1.3. ACSS conductor technical specifications.

High Temperature ACSS Conductor			
Formation		AL0	20 (10+15) conci
		MUHST	19 x 2.10
Theoretical sections	(mm^2)	AL0	466.79
		MUHST	65.81
		Total	535.60
Theoretical mass	(kg/m)	AL0	1.291
		MUHST	0.516
		Total	1.807
Electrical resistance at 20 °C	(Ω/km)		0.06116
Internal breaking load of whole conductor	(daN)		15620
Breaking load of nucleus	(daN)		12931
Final elastic module under knee point	(daN/mm^2)	Whole conductor	7050
Final elastic module over knee point	(daN/mm^2)		18000
Coeff. of thermal expansion under knee point	(K^{-1})	Whole conductor	19.4×10^{-6}
Coeff. of thermal expansion over knee point	(K^{-1})		11.5×10^{-6}

The 20 °C resistance per unit of length of the ACSS conductor is r_{20}=0.06 Ω/km: assuming a 1300 A maximum operating current the operating temperature given by the thermal equilibrium equation is T_c=122 °C and the attendant resistance value is r_l=0.089 Ω/km.

After the change of conductors, all the line stretches have the same electrical constants and thermal rating: the parameters after reconductoring are listed in Table 1.4.

Table 1.4. Specifications and parameters of the 230 kV existing line under study after reconductoring.

Stretch	**Length (km)**	**Sez. (mm2)**	**Thermal rating (A)**	r_l **(Ω/km)**	x_l **(Ω/km)**	c_l **(nF/km)**
2 – 3	49.7	532.6	1300	0.089	0.41	8.76
3 – 4	69.1	532.6	1300	0.089	0.41	8.76
4 – 5	67.5	532.6	1300	0.089	0.41	8.76
5 – 6	65.5	532.6	1300	0.089	0.41	8.76

Receiving-end capability curves in the (P,Q) plane for the line after reconductoring are shown in Fig 1.6.

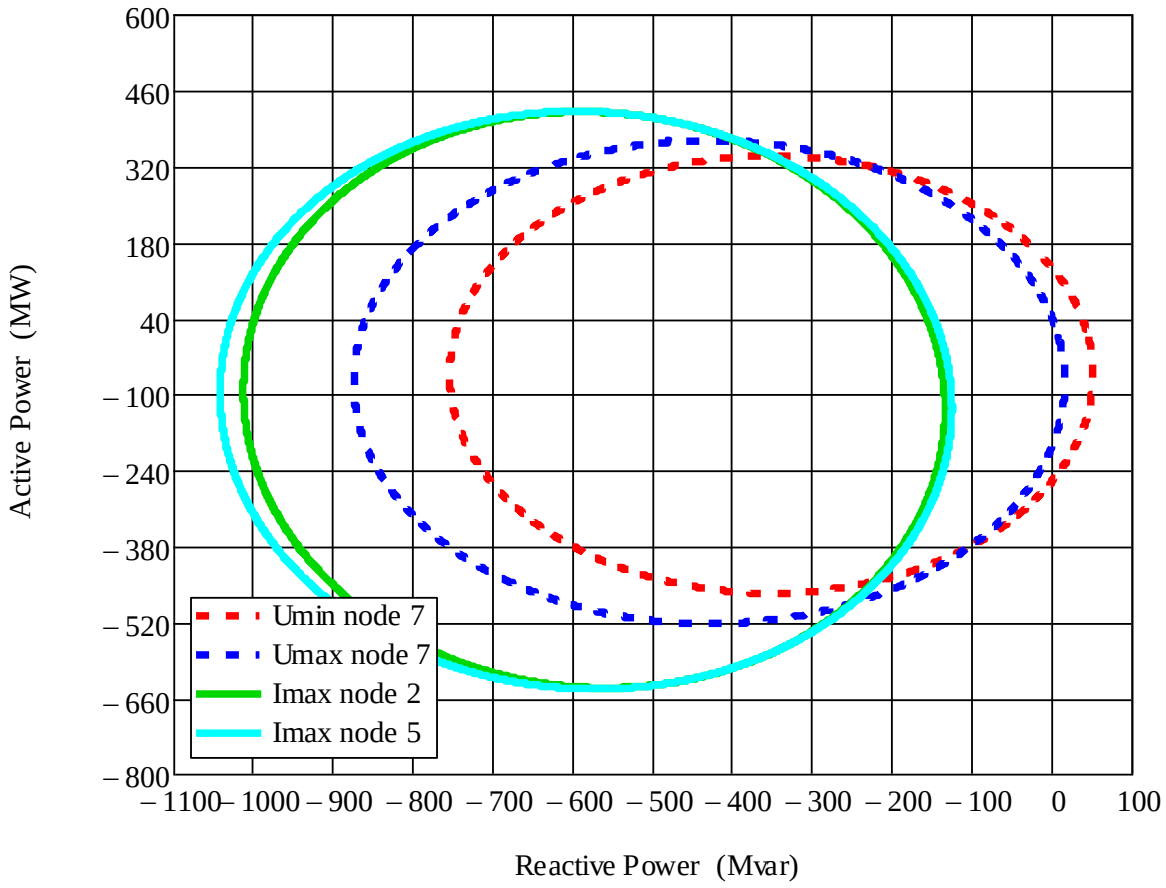

Fig. 1.6. Receiving-end (P,Q) capability curves of the uncompensated, reconductored line as dictated by maximum current in each segment.

In this case, only part of the area enclosed by voltage-limited and current-limited capability curves in the (P,Q) plane is viable: notably, “maximum current” operating points entail unacceptably large values for both the phase shift between terminal voltages, and the reactive power drawn by the line.

By adding a further constraint on angular separation, i.e. a (-45°÷+45°) limit, the actual operating area shown in Fig. 1.7 is obtained. The resulting maximum allowed active power transfer is 263.7 MW (+57.7 MW).

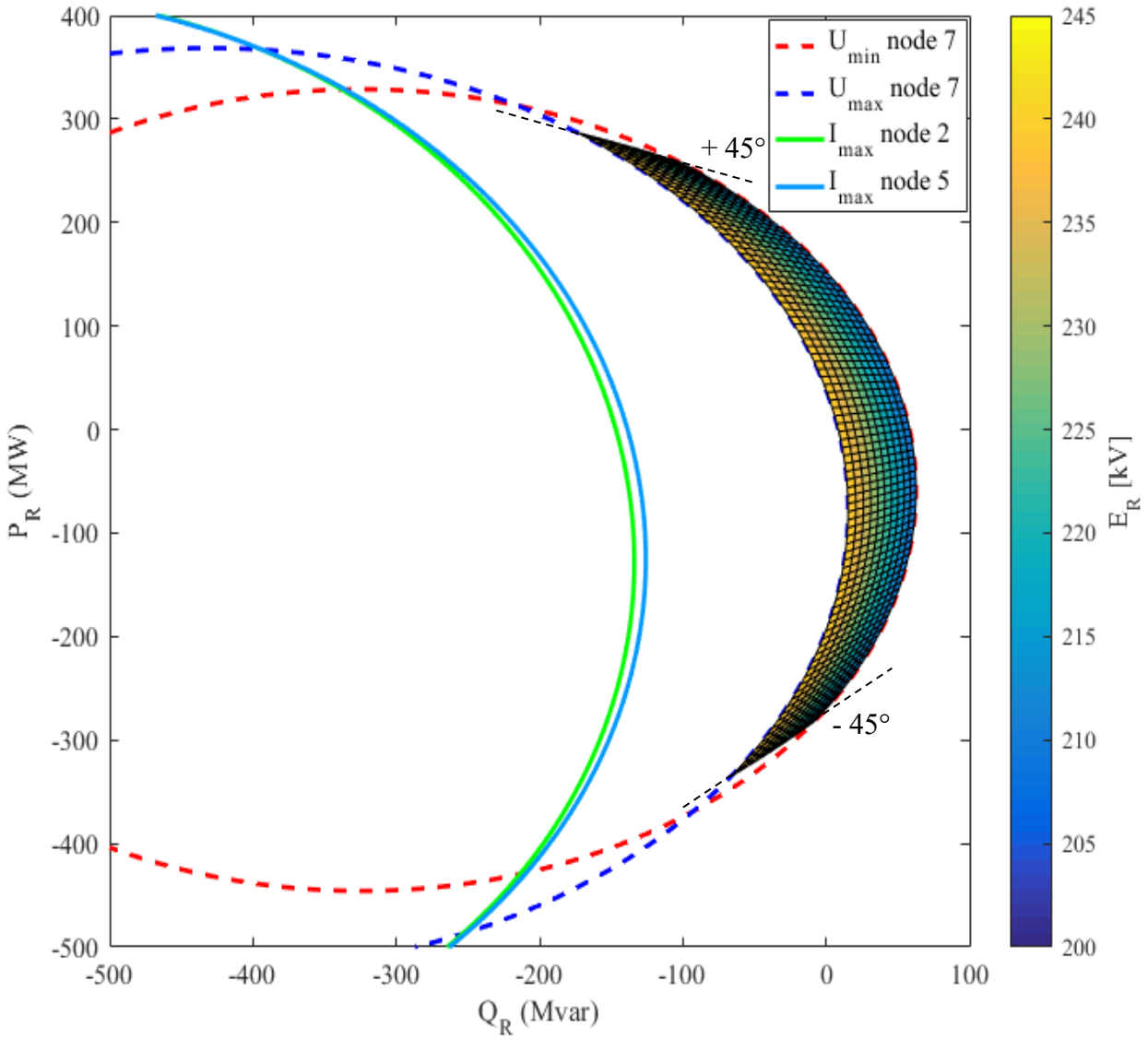

Fig. 1.7. Detail of voltage- and current-limited capabilities for uncompensated, reconductored line (see Fig. 1.6) with voltage magnitude color map and phase angle limits added.

Current and voltage (magnitude and phase) values in each node of the system for the maximum power transfer regime are summarized in Table 1.5: it should be pointed out that the line currents do not even attain the 60% of the 1300 A thermal rating. Despite the large phase shift,

the increase in power transfer is just 50 MW over the base case because is not possible to load the line after reconductoring at thermal limit while keeping terminal voltages within acceptable magnitude and phase limits.

Table 1.5. Voltage (amplitude and phase) and current values along the reconductored, uncompensated line, at maximum power (P_R =263.7 MW).

Node	Current (A)	Voltage (kV)	$\Delta\vartheta_{1n}$ (n=1,…,7)
1	441	410	0°
2	767	232.2	-3.9°
3	770	222.6	-10.5°
4	770	213.7	-20.4°
5	767.2	210.2	-30.6°
6	761.3	212.4	-40.5°
7	437.7	380	-44.5°

In order to overcome the severe constraint on line loading imposed by phase angle separation, line compensation by means of series capacitors is the most straightforward solution.

1.2.2 Series compensation

A preliminary evaluation of the series compensation requirements could be obtained by considering the ideal distributed compensation of a lossless line [12]. If a distributed capacitive reactance x_c is added to the inductive per unit length line reactance x, the p.u.l. reactance of the series compensated line becomes:

$$x_{se} = x - x_c = (1 - k_{se}) \tag{1.7}$$

The attendant series compensation degree is defined as:

$$k_{se} = \frac{x_c}{x} \tag{1.8}$$

The propagation constant and the characteristic impedance of the compensated line are:

$$K''_{se} = \sqrt{\omega \cdot c \cdot x_{se}} = \sqrt{\omega \cdot c \cdot (1 - k_{se})} = K'' \cdot (1 - k_{se}) \tag{1.9}$$

$$Z_{cse} = \sqrt{\frac{x_{se}}{\omega \cdot c}} = \sqrt{\frac{x}{\omega \cdot c} \cdot (1 - k_{se})} = Z_c \cdot \sqrt{(1 - k_{se})} \tag{1.10}$$

With the equal terminal voltages, the resulting expression for the active power flow is:

$$P_{se} = \frac{U^2 \cdot \sin\vartheta}{Z_c \cdot \sqrt{(1 - k_{se})} \cdot \sin\left(K'' \cdot \sqrt{(1 - k_{se})}\right) \cdot L} \tag{1.11}$$

By setting P=420 MW, U=230 kV, ϑ=20°, the value is k_{se}=0.58. This preliminary estimation is based on a very conservative 20° value for the phase angle separation between the terminal voltages of the 230 kV line. However, for stability purposes the overall phase angle separation

at 400 kV level, i.e. transformers included, is of interest, which requires a significant margin towards the 30° – 35° target value.

1.2.2.1 Compensation requirements assessment

Uniformly distributed compensation is not feasible in practice, and compensation is concentrated, either along the line at some convenient location or at the ends.

Three different locations are usually envisaged for the series capacitors banks:

- at mid-line [13], [14];
- at 1/3 and 2/3 of the length;
- at the line ends [15].

The last location is probably the most convenient and common and the two banks are usually identical. This solution was also adopted in the present study. With capacitors banks installed, the system shown in Fig. 1.2 becomes that in Fig. 1.8, with 15 nodes.

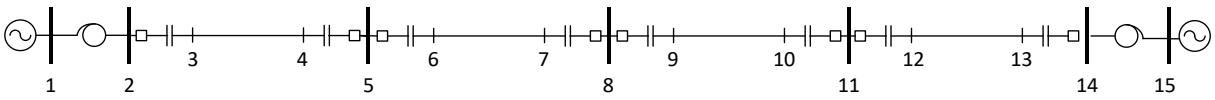

Fig. 1.8. Single line diagram of line under study with series compensation included.

The compensation requirements for the real line could be assessed analytically, with some small algebraic complication due to the number of banks involved and the different length of individual line stretches. A very good estimate, however, can be obtained by following simplified approach [1], [5], which takes line resistance into account while neglecting shunt capacitances. This yields the following expression of the optimal series compensation reactance:

$$X_{eq,opt} = R \cdot \sqrt{4 \cdot \left(\frac{U_R}{U_S}\right)^2 - 1} \tag{1.12}$$

where U_S and U_R are respectively the sending-end and receiving-end voltages.

Assuming as a further approximation U_S=U_R, (12) becomes:

$$X_{eq,opt} = \sqrt{3} \cdot R \tag{1.13}$$

This yields the "optimal" series compensation degree:

$$k_{se,opt} = 1 - \frac{X_{eq,opt}}{X_L} \tag{1.14}$$

Based on the R and X_L values for the present and the reconductored, still uncompensated line, the above approach yields the series compensation degrees are summarized in Table 1.6.

Table 1.6. Optimal series compensation degree for the present and the reconductored line.

Scenario	$k_{se,opt}$
Present configuration	0.67
Reconductored configuration	0.62

In the following, a slightly lower compensation degree of 60% was assumed for each of the 4 line stretches with two equal line-end series capacitors banks whose ohmic impedances are summarized in Table 1.7.

Table 1.7. Ohmic impedances of series capacitor banks located along the line in the present (Scenario A) and the reconductored (Scenario B) configuration.

Series Capacitor Banks	Scenario A Ohmic Reactances [Ω]	Scenario B Ohmic Reactances [Ω]
$Z_{sc\,1}$, $Z_{sc\,2}$	6.0 Ω	6.1 Ω
$Z_{sc\,3}$, $Z_{sc\,4}$	8.3 Ω	8.5 Ω
$Z_{sc\,5}$, $Z_{sc\,6}$	8.1 Ω	8.3 Ω
$Z_{sc\,7}$, $Z_{sc\,8}$	7.9 Ω	8.1 Ω

1.2.2.2 Operating envelopes

The evaluation of the operating envelope of the present line with compensation added is carried out assuming a 410 kV voltage at the sending end (node 1 in Fig 1.2). Only the current-limited capability curves are reported since voltage profiles at high line loading are not critical in this case given the series capacitors effect. As shown by current-limited curves in Fig 1.9, the limiting factor is current intensity at node 4, i.e. at the sending-end of the 230 kV line (see also the detail in Fig 1.10): the attendant maximum value of receiving-end active power is P_{RMAX}=213.6 MW, only +3.6% compared with the uncompensated line (+8 MW).

The installation of series capacitors provides a negligible power transfer capacity increase for the present line, since it does not affect the thermal limits. The benefits provided in terms of voltage drop mitigation and phase shifting between terminal nodes are however evident, as shown in Table 1.8. The voltage drop along the line decreases to the 1.9%, while the phase shift between terminal nodes is reduced to 17.4°.

Fig 1.11 and Fig 1.12 respectively show the voltage and reactive power profiles along the line, highlighting the discontinuities due to the presence of capacitor banks along the line. The voltage “jumps” across individual capacitor do not raise concerns.

Table 1.8. Voltage (amplitude and phase) and current values along the existing compensated line, at maximum power (P_R =213.6 MW).

Node	Current (A)	Voltage (kV)	$\Delta\vartheta_{1n}$ (n=1,…,15)
1	327.4	410	0°
2	569.4	238.1	-3.59°
3	569.4	237.0	-2.19°
4	565.8	237.3	-6.98°
5	565.8	236.2	-5.60°
6	565.8	234.8	-3.65°
7	560.9	235.3	-10.32°
8	560.9	233.6	-8.39°
9	560.9	232.3	-6.49°
10	556	232.8	-13.02°
11	556	231.2	-11.13°
12	556	229.9	-9.28°
13	551.3	230.0	-15.69°
14	551.3	228.1	-13.84°
15	316.9	402.4	-17.37°

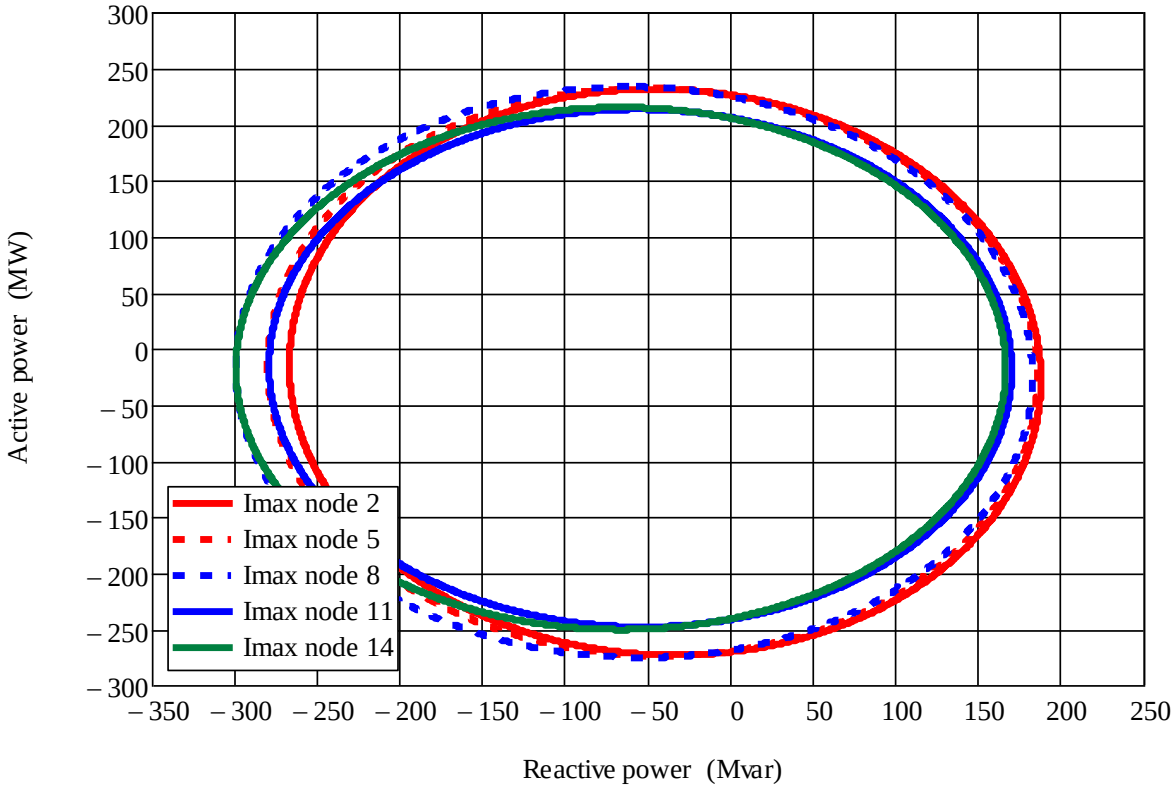

Fig 1.9. Receiving-end (P,Q) capability curves of the existing, compensated line as dictated by maximum current in each segment.

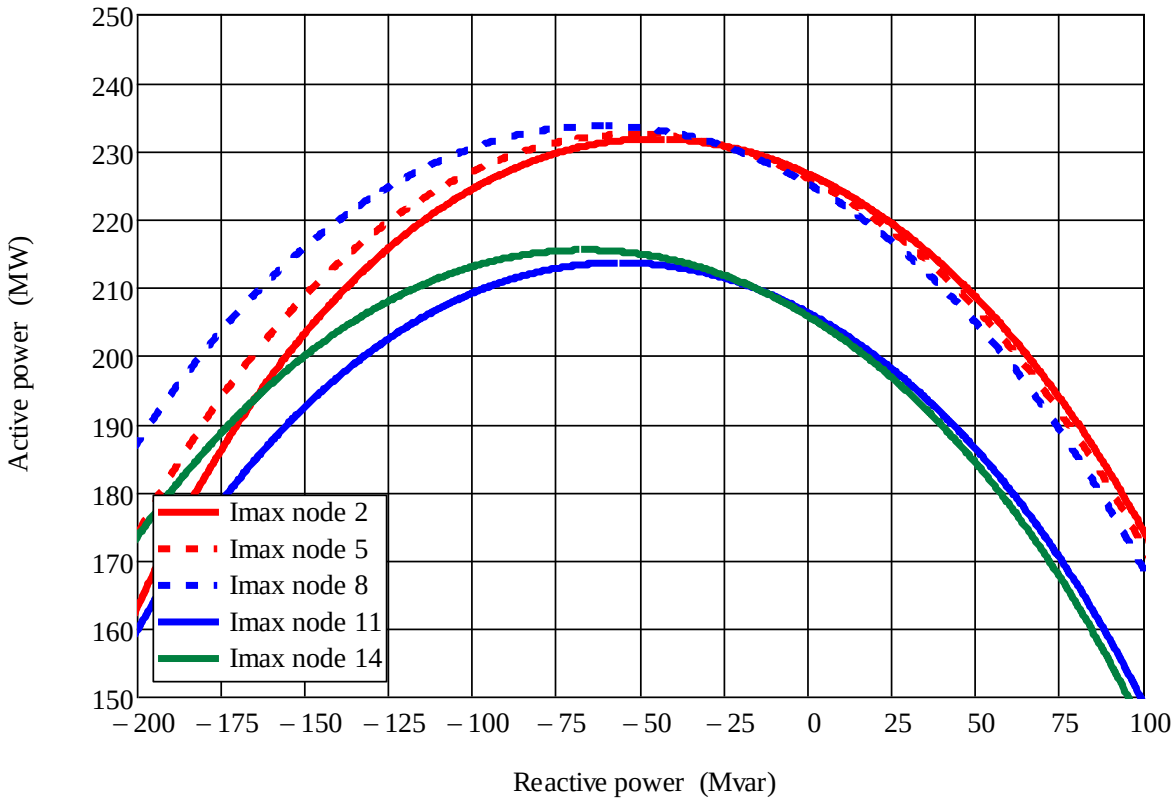

Fig 1.10. Detail of the current-limited capability curves Fig. 1.9.

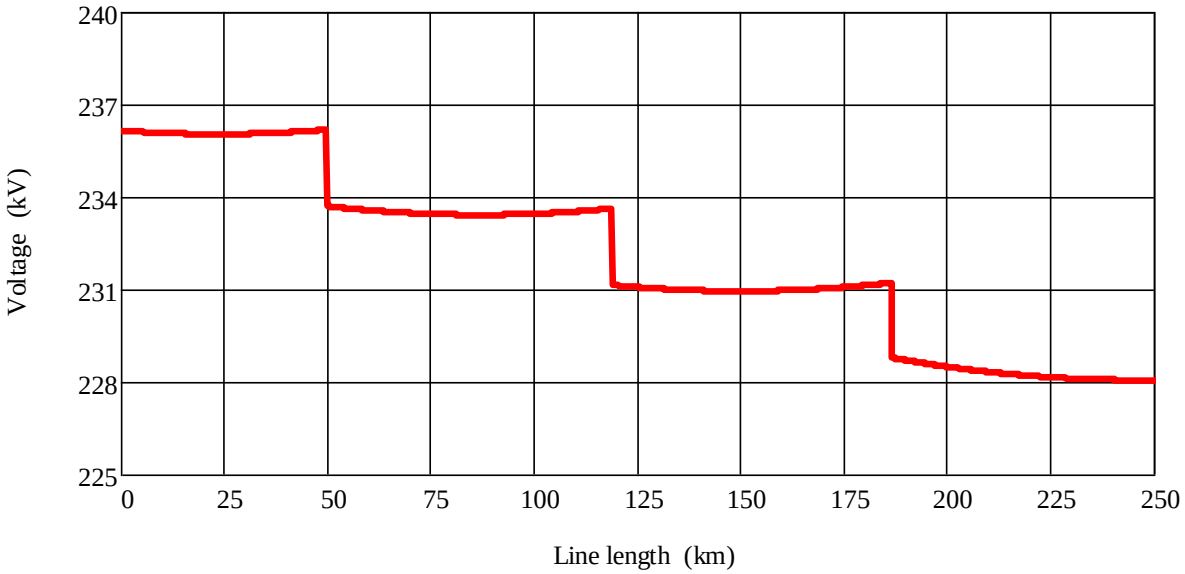

Fig 1.11. Maximum power (P_R=213.6 MW) operation of existing the line (with 60% series compensation): voltage magnitude profile along the 230 kV line.

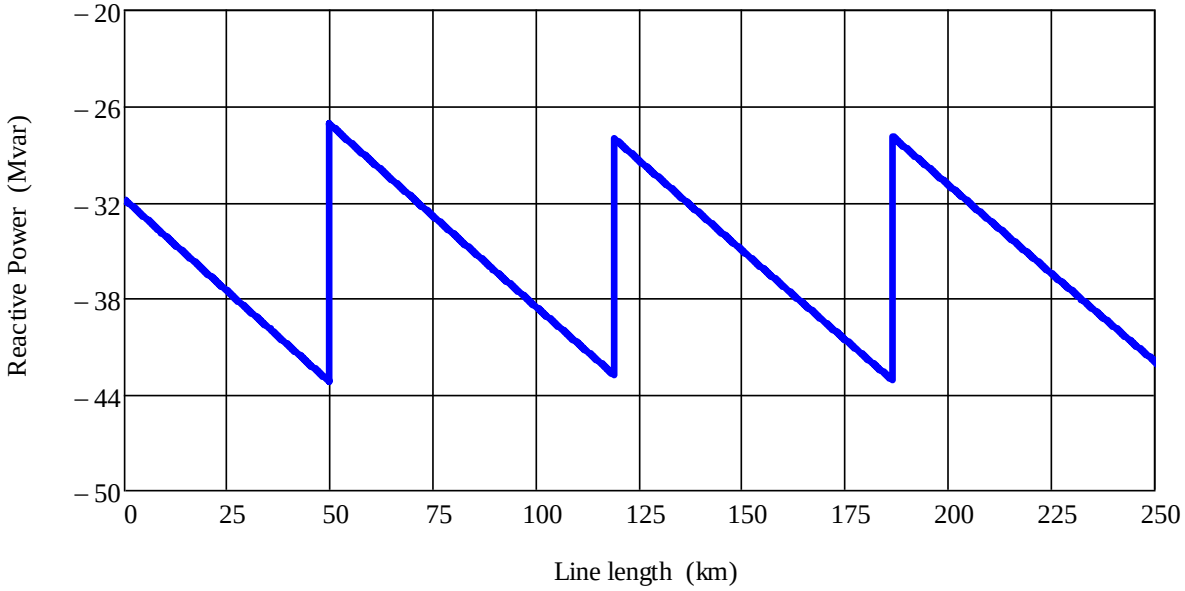

Fig 1.12. Maximum power (P_R=213.6 MW) operation of the line (with 60% series compensation): reactive power profile along the 230 kV line.

The evaluation of the operating envelope of the reconductored, compensated line is carried out assuming a 410 kV voltage at the sending end (node 1 in Fig 1.8). Only the current-limited capability curves are reported since voltage profiles at high line loading are not critical given the effect of series capacitors. As shown by current-limited curves in Fig. 1.13, the limiting factor is current intensity at node 2, i.e. at the sending-end of the 230 kV line (see also the detail in Fig. 1.14): the attendant maximum value of receiving-end active power is P_{RMAX}=419.1 MW. To allow this power transfer, a large amount of reactive power must be provided at the receiving-end, despite the series capacitors, (-302.3 Mvar), while the phase shift between terminal nodes is $\Delta\vartheta_{SR}$=38.8°. The increase of power transfer capacity of the reconductored line under study is substantial when series compensation is added (compare P_{RMAX}=419 MW with the previously achieved 263 MW, i.e. +59%; the increase over the base case is indeed more than 100%). Table 1.9 summarizes the "maximum power" operating point, reporting the current and voltage (amplitude and phase) values in each node of the system. As shown in Table 1.9, the overall voltage drop along the line is significantly reduced in comparison to the uncompensated case [16], since at receiving end the voltage amplitude is 407.9 kV (it was just 380 kV without series compensation). All line current magnitudes are very close to the 1300 A thermal rating of the ACSS conductor; this means that it is possible to take advantage of new conductors' performance only in presence of series compensation whereas in the in previous scenario (line after reconductoring in absence of series capacitors), line current could only reach 770 A.

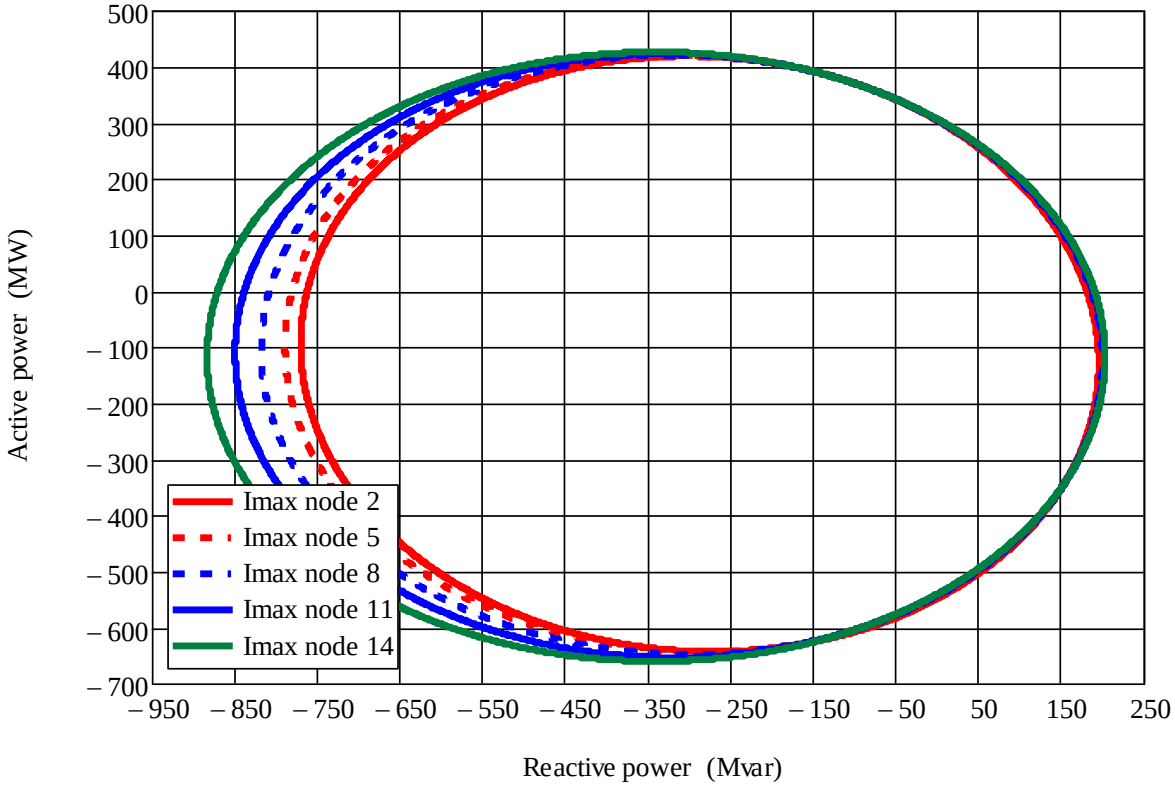

Fig 1.13. Receiving-end (P,Q) capability curves of the existing, compensated, reconductored line as dictated by maximum current in each segment.

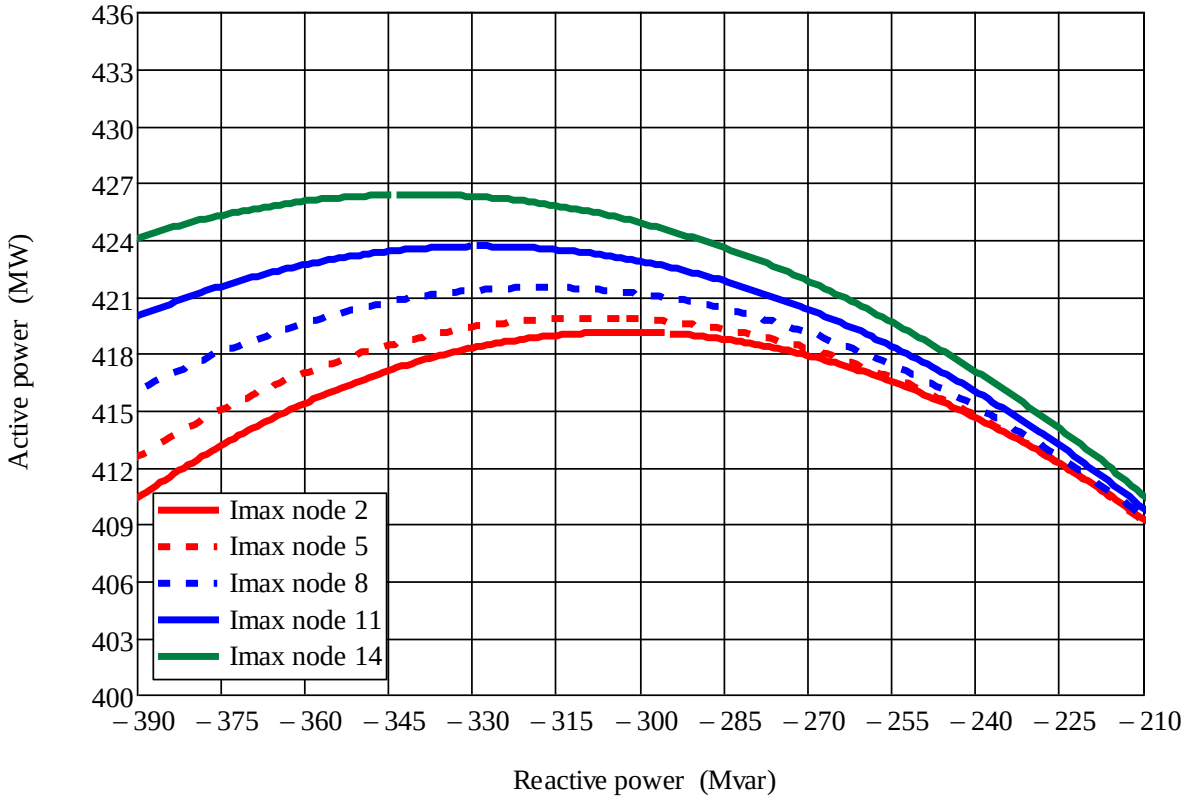

Fig 1.14. Detail of the current-limited capability curves in Fig 1.13.

Fig. 1.15 and Fig. 1.16 respectively show the voltage and reactive power profiles along the line, highlighting the discontinuities across the capacitor banks along the line.

Table 1.9. Voltage (amplitude and phase) and current values along the reconductored-compensated line, at maximum power (P_R =419.1 MW).

Node	Current (A)	Voltage (kV)	$\Delta\vartheta_{1n}$ (n=1,…,15)
1	747.5	410	0°
2	1300	237.8	-6.8°
3	1300	236.4	-3.5°
4	1297	234.2	-14.9°
5	1297	231.1	-11.6°
6	1297	228	-6.9°
7	1291	230.6	-23.2°
8	1291	224.1	-18.7°
9	1291	219.2	-14.1°
10	1282.2	228.4	-30.1°
11	1282.2	220.3	-25.9°
12	1282.2	213.7	-21.5°
13	1272	229.5	-36.8°
14	1272	219.6	-33.0°
15	731.3	407.9	-38.8°

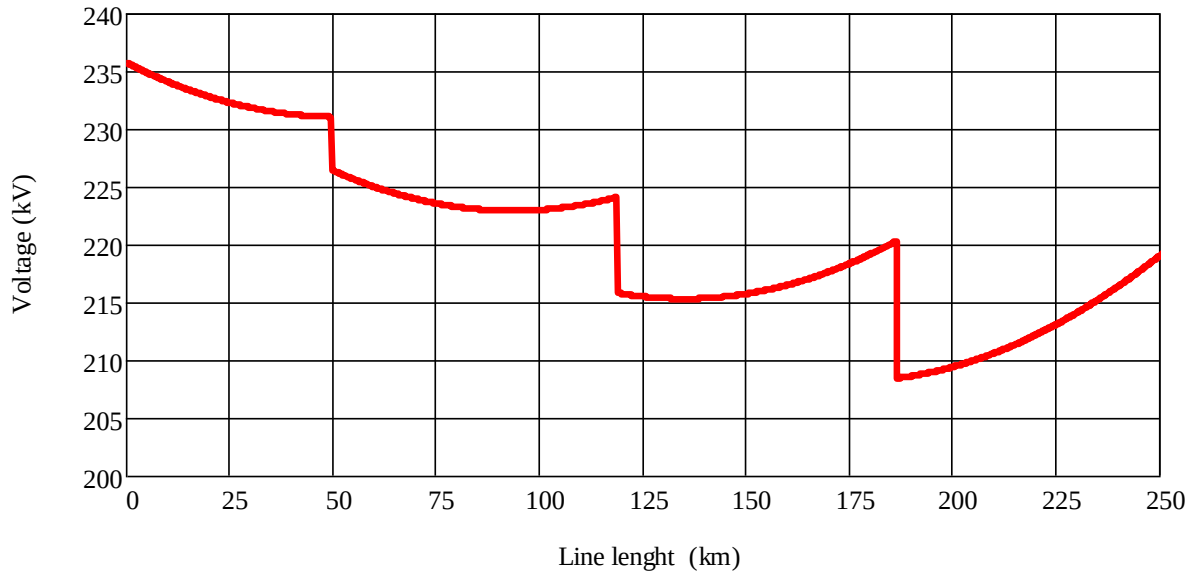

Fig 1.15. Maximum power (P_R=419.1 MW) operation of the line (with ACSS conductors and 60% series compensation): voltage magnitude profile along the 230 kV line.

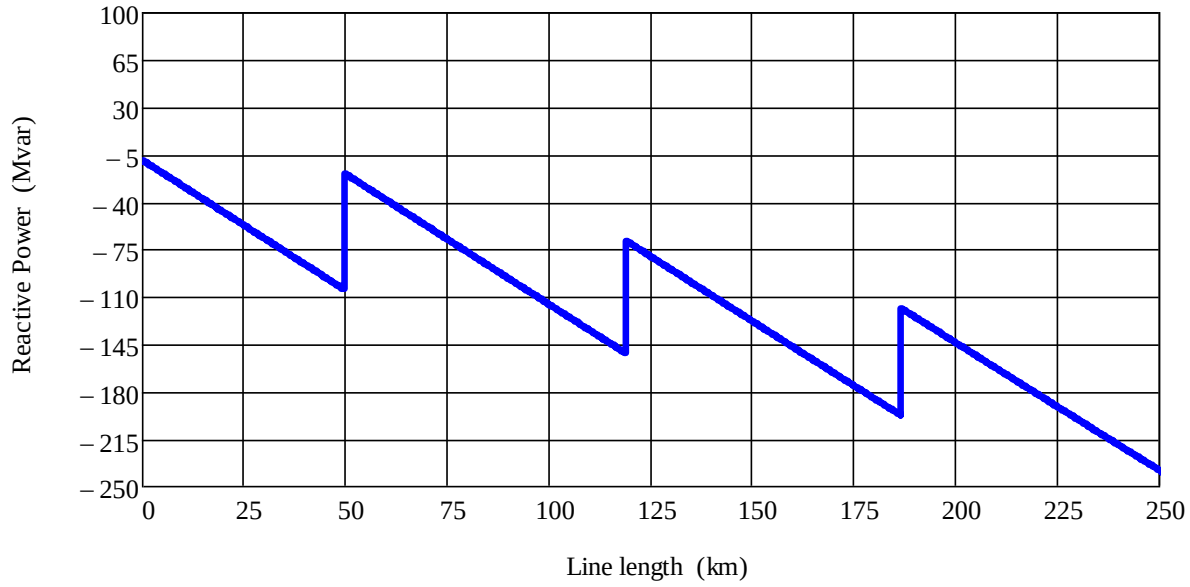

Fig 1.16. Maximum power (P_R=419.1 MW) operation of the line (with ACSS conductors and 60% series compensation): reactive power profile along the 230 kV line.

1.2.3 Load – flow results

In order to show the effectiveness of the proposed approach, many steady-state operating points of line under study at different stages of the development have been simulated by means of a commercial power flow simulation program. Results for the following cases are summarized below:

1. Current-limited operating condition of the existing line without series compensation (410 kV sending-end voltage, 205.5 MW receiving-end active power);
2. Current-limited operating condition of the existing line with series compensation included (410 kV sending-end voltage, 213.6 MW receiving-end active power)
3. Voltage-limited operating point of the line after reconductoring, without series compensation (410 kV sending-end voltage, 263.7 MW receiving-end active power);
4. Current-limited operating point of the line after reconductoring with 60% series compensation (410 kV sending-end voltage, 419.1 MW receiving-end power).

Load flow results for the above described cases are summarized in Fig. 1.17.

Results are very satisfactory, with all line currents and node voltages (amplitude and phase) very close to those obtained by the application of two-port circuit equations in previous paragraphs.

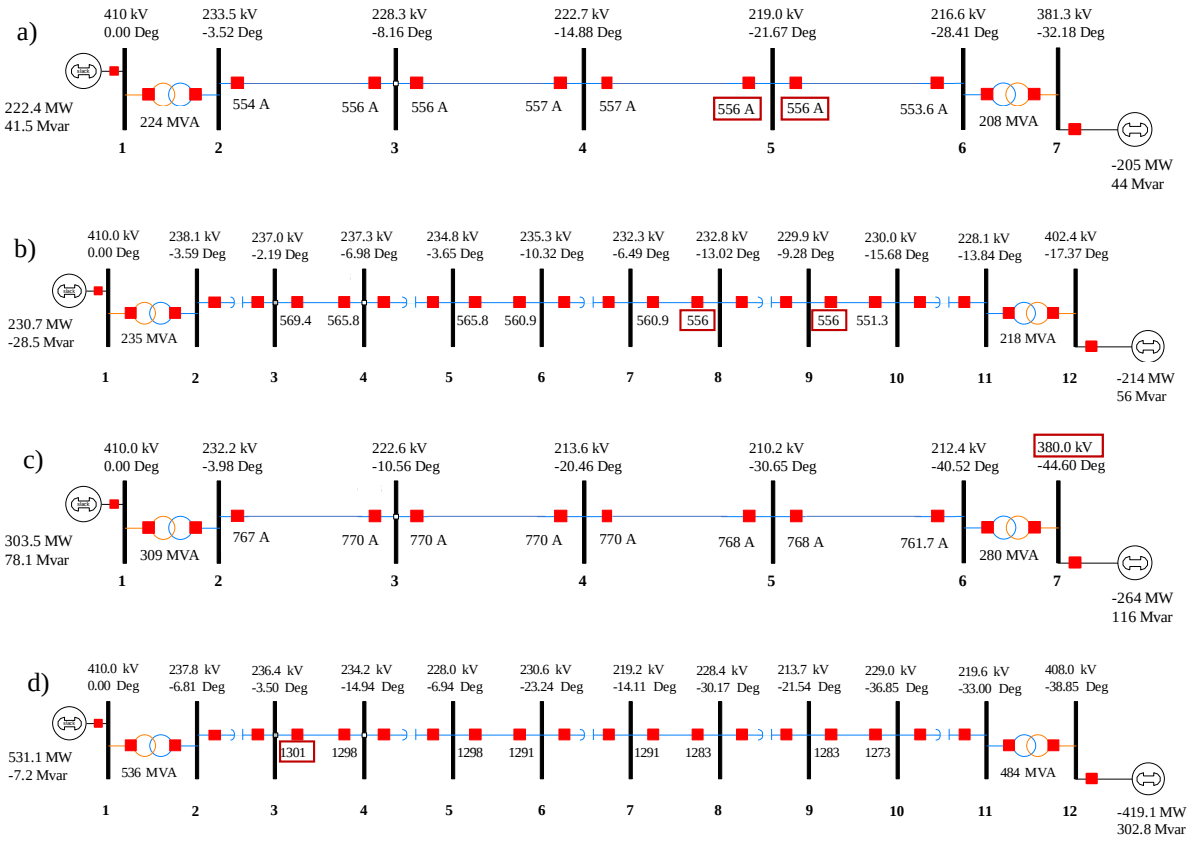

Fig 1.17. Load flow results for: (a) the present line (old conductors, no compensation) at maximum power P_R=205 MW, operation limited by maximum current (556 A) at the 230 kV line stretches bordering node 5; (b) the present line with series compensation included at maximum power P_R=213.6 MW, operation limited by maximum current (556 A) at the 230 kV line stretches bordering nodes 8 and 9; (c) the reconductored line (ACSS conductors, no compensation) at maximum power P_R=263.7 MW, operation limited by minimum voltage (380 kV) at node 7 (receiving-end); (d) the reconductored line with 60 % series compensation at maximum power P_R=419.1 MW, operation limited by maximum current (1300 A) at the line stretch bordering node 3.

1.2.4 Test within the meshed grid

This Section provides the results in terms of power flows obtained by the load-flow simulations performed by the means of PSS-E tool considering the whole meshed transmission network during the normal operation and in case of an important contingency along the 400 kV Tyrrhenian backbone in order to verify the effectiveness of the considered solutions to increase the power transfer across the critical section Centre South – Centre North. The simulations have been carried out in all four analysed scenarios, both in the normal operational conditions and when the critical contingency (outage of a 400 kV double circuit) occurs. The results are shown in Table 1.10: the 230 kV backbone under study active power transfer "P_{LOAD}" is compared in each analysed scenario with the maximum allowable capability "P_{MAX}" defined in the previous sections in order to state the feasibility or not.

Table 1.10. Results obtained from the load-flow tests within the meshed transmission network.

Scenario	P_{MAX} **[MW]**	P_{LOAD} **[MW]**	**Feasibility**
Existing line in normal operational conditions	205.5	127.8	yes
Existing line during the critical contigency		211	no
Existing compensated line in normal operational conditions	213.6	245.7	no
Existing compensated line during the critical contigency		388	no
Reconductored line in normal operational conditions	263.7	124.1	yes
Reconductored line during the critical contigency		205.2	yes
Reconductored-compensated line in normal operational conditions	419.1	230.9	yes
Reconductored-compensated during the critical contigency		381.1	yes

The results show how the reconductored-compensated line can ensure higher levels of security and reliability.

1.3 Impact on fault quantities

A specific application of series compensation together with reconductoring has been presented in the previous sub-section: the power transfer capacity of an Italian 250 km long, 230 kV-50 Hz transmission line spanning the Centre North – Centre South section presently restricted by its low thermal rating, was increased by re-equipping the line with high-temperature Aluminium Conductor Steel-supported (ACSS) conductors with a much higher thermal rating than the old Aluminium Steel-Reinforced (ACSR) ones; the simultaneous installation of fixed 60% series compensation is also foreseen. This solution allows to fully exploit the capability of the new conductors, resulting in a 104% increase of power transfer capacity over the original configuration.

The addition of series compensation to a transmission line presents complexities with regards to the behavior during transmission line faults and to the relay protection of the line itself, and in many cases the relay protection of adjacent and parallel lines. Said complexities will obviously depend on the system configuration, degree of series compensation, series capacitor protection and control schemes.

In the system under study, the capacitors are supposed located at the line terminals, with the advantages of use of available space within the substations, and much easier access to the equipment for maintenance and operations. Possible disadvantages of this solution are increased requirements on line protection (possible voltage and current inversion phenomena) and a less favorable voltage profile in comparison with the location of series compensation at mid-point of the line.

1.3.1 Parametric analysis

For the purposes of this study, neither loads nor connections to the rest of the system are taken into account at intermediate locations along the line, as the backbone is supposed to operate exclusively in support of the 400 kV system, as illustrated in Fig. 1.18.

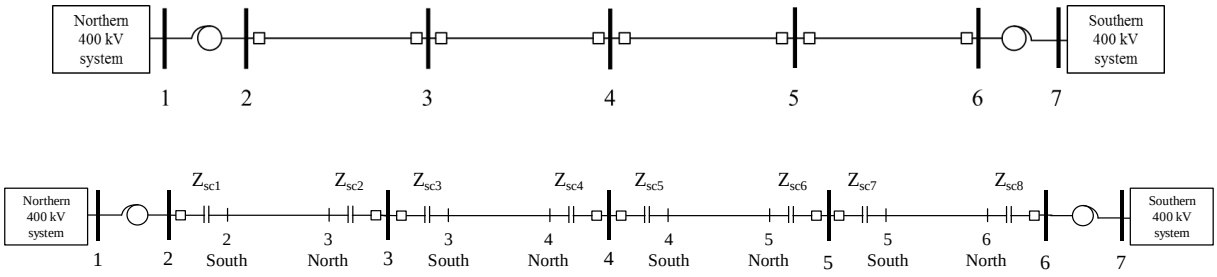

Fig. 1.18. Single line diagram of line under study: uncompensated configuration (top) and with series compensation included (bottom).

The uprated series-compensated line should be connected to the 400 kV system via a dedicated 600 MVA, 400/230 kV autotransformer at each end. Such autotransformers are of course instrumental in dictating short-circuit levels at the 230 kV supply busbars; the foreseen three-limb core construction also has a strong influence on the zero-sequence impedance at said busbar.

This substantial recourse to capacitive series compensation is obviously bound to change the line behavior during fault, namely a marked increase of fault currents is expected for all types of faults and at all locations along the line compared to the corresponding quantities calculated for the original line configuration. In case of single-phase-to-ground faults a limited but noticeable increase of the earth faults factor, i.e. of the healthy phase voltages to ground is also in order, due to the lower equivalent series compensation degree of the line's zero-sequence reactance.

Increased fault currents are obviously relevant to the line circuit breakers installed along the line which moreover have to cope with a substantial rise of transient recovery voltages. The increase of zero-sequence currents, albeit less marked, might be significant for the older substations grounding systems, as well as for the single shield wire of the line.

In order to evaluate the short circuit levels increase related to the presence of the series capacitors, a parametric analysis of fault currents is carried out in two different scenarios, i.e. considering the reconductored line without and with series compensation. The existing line in the present configuration is not studied since its re-equipment with high temperature conductors

is already planned in the National Network Development Plan and is an prerequisite in order to extend the operational limits in a significative manner.

The symmetrical components analysis is an effective way to evaluate unbalanced faults in a power system by using positive, negative, and zero sequence impedances (Z_1, Z_2 and Z_0 respectively) seen from the fault point. As the system is supposed to be symmetrical and balanced before the fault occurs, sequence impedances are not coupled; in the subtransient time interval the positive and the negative sequence impedances match [17].

For each scenario, the four different fault types are considered:

- Symmetrical three-phase fault without ground (3L);
- Single-line to ground fault (SLG);
- Line to line fault without ground (LL);
- Line-to-line to ground fault (LLG).

After reconductoring the whole backbone with the new ACSS line stretches have the same electrical constants: the positive and zero-sequence parameters of the 230 kV line under study are listed in Table 1.11.

Table 1.11. Positive and zero sequence parameters of the 230 kV existing line under study after reconductoring.

Positive-sequence			**Zero-sequence**		
r_l **(Ω/km)**	x_l **(Ω/km)**	c_l **(nF/km)**	r_{l0} **(Ω/km)**	x_{l0} **(Ω/km)**	c_{l0} **(nF/km)**
0.06	0.41	8.76	0.23	1.1	5.4

The three-phase networks at the terminals of the system under study are supposed to have a short circuit power of 15000 MVA with $X_0 = X_1$ the magnitude of the voltage source is set at $c \cdot U_n/\sqrt{3}$ where U_n is the nominal system phase-to-phase voltage (400 kV), and c is the voltage factor, intended to give a worst-case condition for fault current intensity and assumed equal to 1.05 [18].

In order to assess the fault currents magnitudes profiles along the line, the equivalent line impedance is firstly expressed as a function of the line length both for the positive and for the zero sequences:

$$Z_{l_n} = (r_l + i \cdot x_l) \cdot d_{l_n} \tag{1.15}$$

where d_{l_n} is the variable length of the line:

$$d_{l_n} = d_{min} + n \cdot \Delta L \tag{1.16}$$

$$n \, \epsilon \, (0, \dots, L) \tag{1.17}$$

$$L = \frac{d_{lmax} - d_{lmin}}{\Delta L} \tag{1.18}$$

and ΔL is the length discretization step.

An example of procedure used to obtain the short circuit currents expressions is shown below for the line stretch 2 – 5 in the series compensated configuration of Fig. 1.18; similar developments can be replicated for the remaining stretches.

Starting from the uncoupled sequence networks (Fig. 1.19) the Thévenin impedance Z_{eq,l_n} seen at fault location for a fault along the stretch 2 – 5 of the 230 kV – 50 Hz backbone under study in the scenario B (see Fig. 1.18) is defined as:

$$Z_{eq,l_n} = \left(\frac{Z_{a,l_n} \cdot Z_{b,l_n}}{Z_{a,l_n} + Z_{b,l_n}} \right) \tag{1.19}$$

Where:

$$Z_{a,l_n} = Z_{1-2} + Z_{sc1} + Z_{L_f} \tag{1.20}$$

And:

$$Z_{b,l_n} = \left(Z_L - Z_{L_f} \right) + Z_{sc2} + Z_{5-15} \tag{1.21}$$

Therefore, once the equivalent impedances are defined for the positive and the zero sequences, the short circuit currents for the different considered fault types can be calculated.

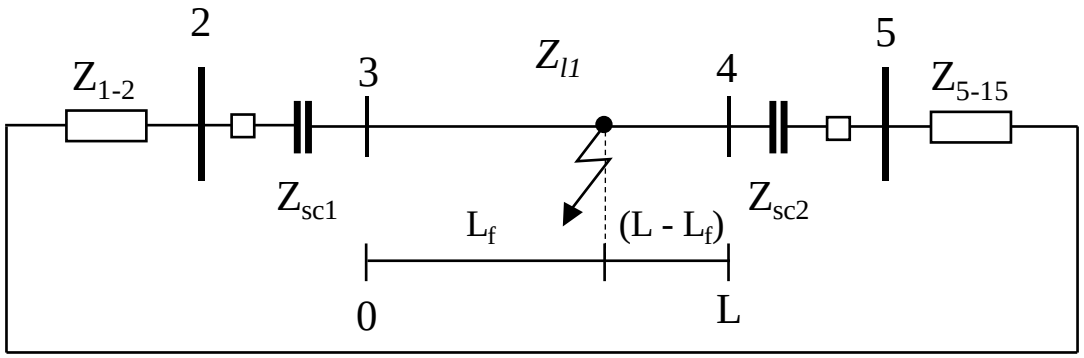

Fig. 1.19. Uncoupled sequence networks for a generic portion of the system in Fig. 1.18.

For the sake of clarity, the expressions of short-circuit currents are recalled below. The arc resistance and the fault impedance in general are neglected in order to obtain the maximum possible fault levels.

1. Three-phase symmetrical fault: both the negative and the zero sequence networks are omitted due to the balanced three-phase fault assumption. The three-phase short circuit $\bar{I}_{3L}$ is given by:

$$\bar{I}_{3L} = \frac{\frac{c \cdot U_n}{\sqrt{3}}}{\bar{Z}_{eq\ 1,l_n}} \tag{1.22}$$

2. The single line to ground short circuit current $\bar{I}_{SLG_n}$ is given by:

$$\bar{I}_{SLG_n} = \frac{3 \cdot \frac{c \cdot U_n}{\sqrt{3}}}{\bar{Z}_{eq\ 0,l_n} + 2 \cdot \bar{Z}_{eq\ 1,l_n}} \tag{1.23}$$

3. The line-to-line fault current $\bar{I}_{LL_n}$ without earth is given by:

$$\bar{I}_{LL_n} = \frac{-i \cdot c \cdot U_n}{2 \cdot \bar{Z}_{eq\ 1,l_n}} \tag{1.24}$$

4. The line-to-line to ground fault current $\bar{I}_{LLG_n}$ is given by:

$$\bar{I}_{LLG_n} = -i \cdot cU_n \cdot \frac{(\bar{Z}_{eq\ 0,l_n} - \alpha \cdot \bar{Z}_{eq\ 1,l_n})}{2 \cdot \bar{Z}_{eq\ 1,l_n} \cdot \bar{Z}_{eq\ 0,l_n} + (\bar{Z}_{eq\ 1,l_n})^2} \tag{1.25}$$

Furthermore, the Earth Fault Factor (EFF) in case of line-to-ground faults is calculated at each node of the system in order to verify the neutral grounding status of the backbone. By definition, in an effectively grounded system the voltage to ground of the healthy phases during a line-to-ground fault does not exceed 80% of the line-to-line voltage and consequently the EFF does not exceed $0.8 \cdot \sqrt{3}$, i.e 1.4 p.u.. Therefore, the system can be considered as effectively grounded if [19]:

- the ratio of zero-sequence reactance to positive-sequence reactance $a = X_0/X_1$ is positive and not greater than 3;
- the ratio of zero-sequence resistance to positive-sequence reactance R_0/X_1 is positive and smaller than 1.

By neglecting the resistive parameters, the EFF assumes the simplified expression:

$$EFF = \frac{\sqrt{3 \cdot (1 + a + a^2)}}{|2 + a|} \tag{1.26}$$

Another significant parameter for the circuit-breakers stresses is the ratio between the single-line-to ground fault current and the three-phase fault current. With the same assumptions adopted for the EFF, the i_m parameter can be expressed as:

$$i_m = \frac{I_{SLG}}{I_{3L}} = \frac{3}{|2 + a|} \tag{1.27}$$

When the ratio a is positive and smaller than 1, the single-line-to-ground fault current overcomes the three-phase fault current and becomes instrumental in selecting the rated breaking current of the circuit breakers along the line.

Finally, the voltage shift between neutral and ground e_0, i.e. the zero-sequence voltage E_0 in p.u. of the pre-fault voltage equal to the nominal voltage E_n, neglecting the resistances is given by [20]:

$$e_0 = \frac{E_0}{E_n} = \left|\frac{X_0}{X_1 + X_2 + X_0}\right| = \left|\frac{X_0}{2X_1 + X_0}\right| = \left|\frac{a}{2 + a}\right| \tag{1.28}$$

1.3.2 Results and discussion

The Table 1.12 summarizes the fault quantities assessed for the system after reconductoring, without series compensation (Fig. 1.18 top). It can be observed that the 3L fault currents are larger than the single line to ground ones in all locations along the line. The higher fault levels occur at the line terminals, being around 10 kA at 230 kV voltage level. Conditions for an effectively grounded neutral, i.e. $a \leq 3$ and $R_0/X_1 \leq 1$, are fulfilled in all nodes.

Table 1.12. Fault-quantities in the Scenario A (after reconductoring, no series compensation).

Fault Location	I_{3L} **(kA)**	**Single line to ground fault**			I_{LL} **(kA)**	I_{LLG} **(kA)**	**Impedance ratio**		**EFF**
		I_{SLG} **(kA)**	i_m	e_0 **(p.u.)**			R_0/X_1	X_0/X_1	
Node 2	**9.862**	9.833	0.997	0.335	8.541	9.832	0.009	1.009	1.002
Node 3	**5.227**	3.880	0.742	0.503	4.527	4.872	0.347	2.024	1.149
Node 4	**4.116**	2.878	0.699	0.531	3.564	3.797	0.428	2.268	1.177
Node 5	**4.748**	3.433	0.723	0.516	4.112	4.404	0.382	2.129	1.161
Node 6	**9.862**	9.833	0.997	0.335	8.541	9.832	0.009	1.009	1.002

Table 1.13 summarizes the fault quantities assessed for the system after reconductoring and the installation of series capacitors (Fig. 1.18 bottom). A remarkable increase in terms of short circuit levels can be observed: the most relevant fault levels occur at 6-North (Fig. 1.18 top) where I_{SLG} approaches 20 kA. Moreover, it can be seen that the single-line-to-ground fault current I_{SLG} is greater than the symmetrical three-phase fault current at nodes 2 South and 6 North where the ratio a is smaller than one. On the other hand, with series capacitors installed the X_0/X_1 ratio is greater than 3 between nodes 3-South and 5-North (the R_0/X_1 ratio stays below 1). EFF values along the line increase in comparison with the scenario A, up to 1.3;

however, the limit EFF≤1.4 is still complied with, due to the effect of non-negligible positive-sequence impedance of the line.

Finally, Fig. 1.20, Fig. 1.21, Fig. 1.22, Fig. 1.23 show the faults currents profiles along the reconductored, compensated line (as the case more interesting in this context) separately representing for the four line stretches for the sake of the clarity.

Table 1.13. Fault-quantities in the Scenario B (after reconductoring and series capacitors installed).

Fault Location	I_{3L} **(kA)**	**Single line to ground fault**			I_{LL} **(kA)**	I_{LLG} **(kA)**	**Impedance ratio**		**EFF**
		I_{SLG} **(kA)**	i_m	e_0 **(p.u.)**			R_0/X_1	X_0/X_1	
Node 2	**11.003**	10.605	0.963	0.358	9.528	10.690	0.016	1.115	1.019
Node 2 South	16.161	16.202	1.002	0.332	13.996	**16.285**	0.008	0.993	0.999
Node 3 North	**7.681**	4.965	0.648	0.568	6.652	6.940	0.524	2.629	1.215
Node 3	**8.475**	5.380	0.638	0.575	7.340	7.673	0.569	2.704	1.222
Node 3 South	**11.110**	6.411	0.580	0.613	9.621	9.954	0.743	3.174	1.264
Node 4 North	**7.716**	4.227	0.549	0.634	6.682	6.826	0.821	3.468	1.286
Node 4	**7.468**	4.414	0.562	0.625	6.467	6.665	0.787	3.334	1.279
Node 4 South	**7.941**	4.307	0.543	0.638	6.877	7.048	0.844	3.522	1.290
Node 5 North	**9.887**	5.502	0.559	0.628	8.563	8.817	0.806	3.371	1.279
Node 5	**8.070**	4.860	0.605	0.597	6.989	7.260	0.657	2.958	1.245
Node 5 South	**7.440**	4.541	0.612	0.592	6.444	6.671	0.616	2.906	1.241
Node 6 North	19.516	**19.885**	1.019	0.321	16.901	19.806	0.006	0.945	0.991
Node 6	**11.003**	10.605	0.963	0.358	9.528	10.939	0.016	1.115	1.019

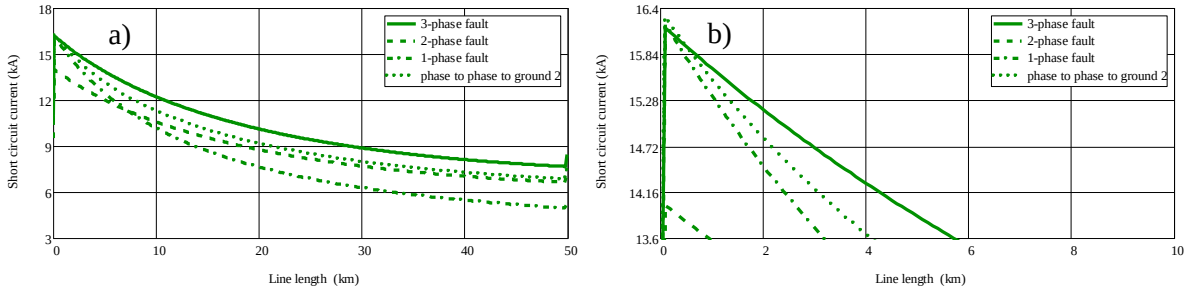

Fig. 1.20. Fault current profiles for the reconductored, series compensated line: (a) along the first line stretch; (b) detail of maximum fault level reached at "Node 2-South" in the phase-to-phase to ground short-circuit.

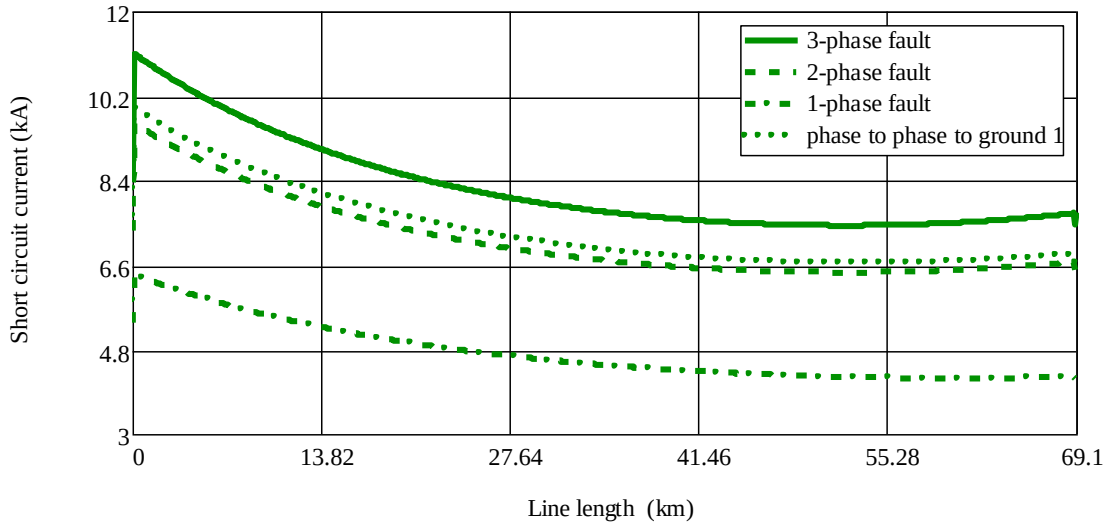

Fig. 1.21. Fault current profiles for the reconductored, series compensated line along the second line stretch: the three-phase short circuit current is always major than the others and the maximum fault level is reached at “Node 3-South”.

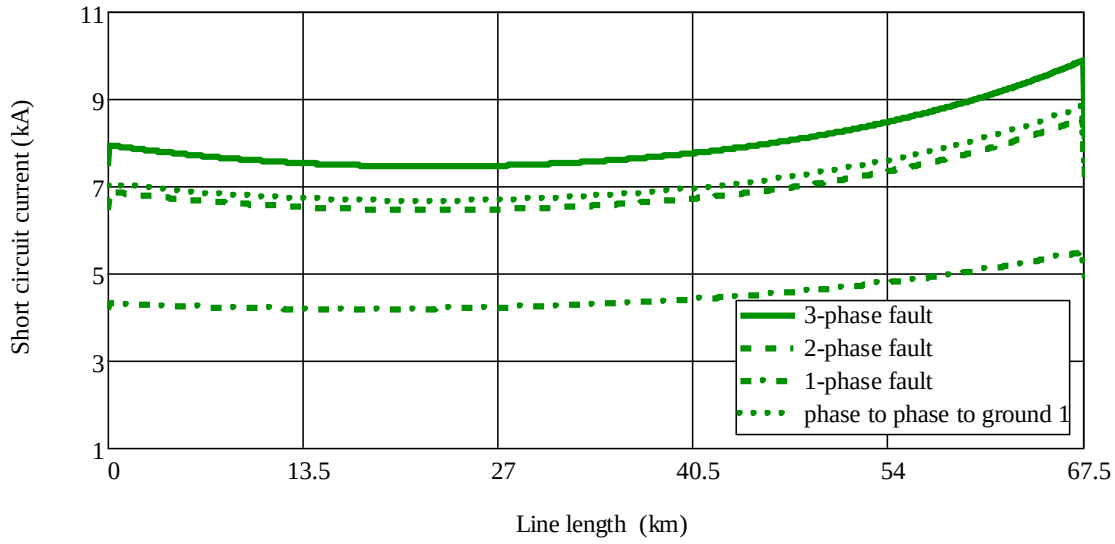

Fig. 1.22. Fault current profiles for the reconductored, series compensated line along the third line stretch: the three-phase short circuit current is always major than the others and the maximum fault level is reached at “Node 5-North”.

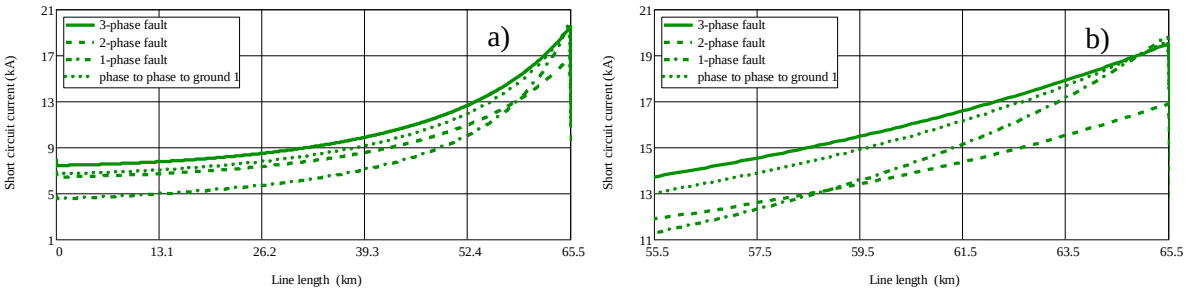

Fig. 1.23. Fault current profiles for the reconductored, series compensated line: (a) along the fourth line stretch; (b) detail of maximum fault level reached at “Node 6-North” in the single-to-phase to ground short-circuit.

1.4 Conclusions

The operating envelopes of an existing 250 km long, 230 kV-50 Hz line spanning Centre South – Centre North market zones of the Italian power system was evaluated by directly enforcing the relevant voltage- and current-based constraints.

As the resulting 205 MW limit was not satisfactory, in order to enhance the power transmission capacity, design improvements such as re-equipping the line with high-temperature conductors and use of series capacitors were evaluated via the same approach.

Main results can be summarized as follows:

1. Despite a 133% increase in maximum current at thermal limit (from a 556 A to 1300 A), replacing existing conductors with ACSS high-temperature ones does not allow a significant power transfer increase because minimum voltage constraints limit the capability to 263 MW, i.e. only 28% more than the present value;
2. The installation of 60 % series capacitive compensation located at the ends of each stretch of the line allows to fully take advantage of the new ACSS conductor, leading to a significant capability increase: a 419 MW maximum power can be achieved (i.e. +104% over the existing line).

In order to investigate the feasibility of the proposed series compensation solution, an assessment of short circuit quantities has been performed by the means of symmetrical components method.

The fault quantities have been evaluated in each node of the system under study, comparing their values before and after the installation of series compensation. This predictably leads to a remarkable increase of short circuit levels in comparison with the uncompensated configuration, up to 20 kA (i.e. +102 %) at the line-side terminals of the southernmost series capacitor bank. Despite X_0/X_1 ratios greater than 3 along the central stretches of the compensated line, the EFF does not exceeds 1.3 anywhere, confirming the viability of the solution.

2. New approaches in power system planning to evaluate system performance and enable high levels of renewables

In 2014 the European countries agreed on the renewable energy target of supplying at least 27% of their final energy consumption from renewable energy sources (RES) by 2030, as dictated by the European Union's energy and climate objectives for 2030. In 2016 the European Commission proposed a revised Renewable Energy directive [21] and, in 2018 a renewable energy target of 32% for European Union by 2030 has been set [22].

In this context, the whole interconnected European network is involved in the energy transition towards power systems based on renewable generation, mostly interfaced to the system through power electronic converters. Moreover, all relevant planning future energy scenarios, defined at European and National level, confirm an increasing trend of renewable capacity installed and progressive decommissioning of thermal power plants in the medium/long term horizon.

In this context, the major concerns for both network planning and operation are:

- the network reinforcements planning with the aim of ensuring a growing share of variable RES integration into the system;
- the static and dynamic stability evaluation of the future power systems during critical contingencies;
- the "loadability" assessment of backbones spanning critical sections of the transmission system potentially overloaded in presence of important power transfers;
- the thermal performances of power system portions expected to collect significant amounts of RES generation (in order to identify overstressed paths and plan additional countermeasures);
- the inertia reduction and the frequency control due to the progressive decommissioning of thermal units, partially counteracted by the installation of synchronous generators.

In this Section, a comprehensive transmission planning assessment including these topics is provided considering different real case studies related to the Italian power system.

Sub-section 2.1 reports offshore wind perspectives considering policies and scenarios drivers. The impact of the planned HVDC "Adriatic Link", considered in both the alternative Voltage Source Converter (VSC) and Line Commutated Converter (LCC) implementations, is analysed in both static and dynamic conditions (in the presence of faults) in sub-section 2.2, together with the Centre North – Centre South critical section loadability increase afforded by the new HVDC connection. Sub-section 2.3 focuses on the thermal performance of a selected set of overhead lines spanning the Centre South – South critical section both in the current and in the

future energy scenario at 2040 year horizon in presence and in absence of planned network reinforcements. Finally, a brief dissertation on the reduced inertia power system topic and possible countermeasures in planning studies is illustrated in the sub-section 2.4

2.1 Transmission system and offshore wind farms: challenges and chances

Offshore wind energy is gaining significant ground in electric transmission systems, due to the large size of installations, higher and relatively stable energy yields, and to policy objectives. The diffusion of offshore wind farms, in view of the increasing renewable share, poses specific issues for their proper integration in the electric network, accounting for a wide range of technical and economic aspects. The aim of this section is to provide a broad perspective of transmission system operator on the influence of offshore wind farms, along with current situation and prospects in the Italian framework.

2.1.1 Introduction

The development of offshore wind energy is growing all over the world, due to the increasing interest in reducing the environmental footprint of power generation by exploiting renewables as well as in ensuring the exploitation of local energy sources, limiting the dependency on external suppliers. At the end of 2017, the total offshore wind installed capacity worldwide amounted to 18.8 GW in 17 countries, as detailed in Fig. 2.1 [23]: a remarkable growth is observed in the three leading countries.

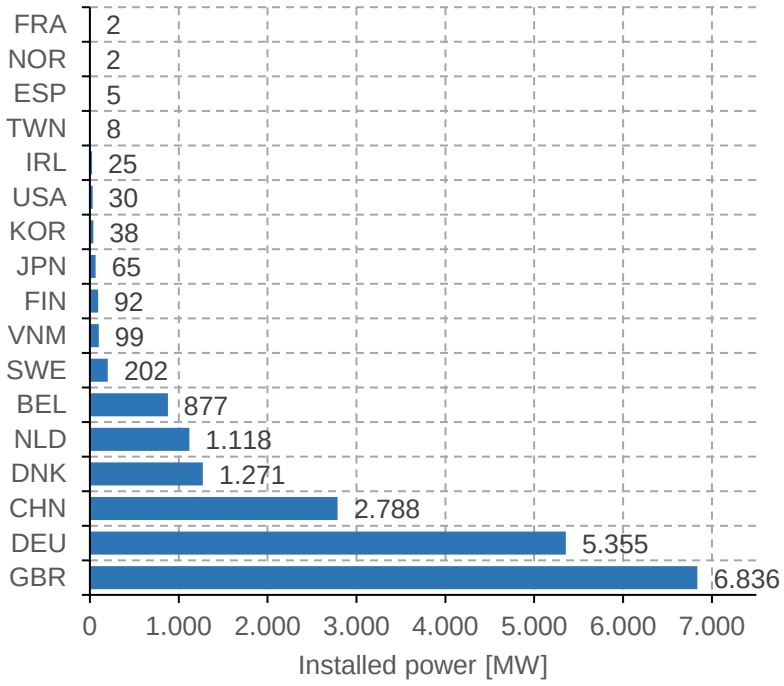

Fig. 2.1. Offshore wind installed power by country at the end of 2017.

Moreover, higher and more uniform wind speeds are generally observed offshore compared to onshore, and the availability of space allows more regular building schemes, leading to higher

energy yields. In offshore wind farms, wind turbines can have larger diameters and rated power, resulting in turn in a better exploitation of strong wind conditions as well as less short-term speed variations. Furthermore, the capacity of new offshore wind farms is usually in the range of hundreds of MW i.e. it is appropriate for direct connection to EHV transmission systems. In order to draw the optimal level of wind energy and to make it available to the transmission system, particular care is paid to the exploitation of specific technologies [24], related to:

- wind turbines, usually with greater dimensions and adapted for marine environment;
- substructure and foundation, where currently monopile solutions are most employed in shallow waters;
- internal wind farm network, including the connections between turbines, the transformer substation and increasingly advanced control systems;
- power transmission to shore, usually realized at EHV level, where the discussion for AC or DC solutions is still open.

All these topics involve remarkable technological challenges, from design to operation and maintenance. The aim of this section is to provide a broad view of the transmission system operator perspective on the influence of offshore wind farms. For this reason, different aspects concerning the integration of offshore wind energy in electric transmission systems are evaluated, involving policy, market and technical impacts. Eventually, the current situation and a possible scenario for the development of offshore wind in the framework of Italian transmission network are also presented.

2.1.2 Policies, scenarios and planning

Several scenarios are evaluated for the diffusion of offshore wind. In particular, [25] individuates for 2022 an amount of 2.9 GW of offshore wind farm projects under construction and awaiting grid connection across Europe, as well as 13.2 GW of projects approved with a final decision, as reported in Fig. 2.2, and the 2030 diffusion scenarios (low, central and high) between 50 GW and 100 GW (roughly) are expected, as illustrated in Table 2.1.

As regards network development plans ENTSO-E [26] develops the “best evolution” scenario at 2025, individuating roughly 45 GW, as well as different evolutionary scenarios at 2030, namely Sustainable Transition (ST), EUCO and Distributed Generation (DG), ranging between 41 and 66 GW; data are summarized in Table 2.2.

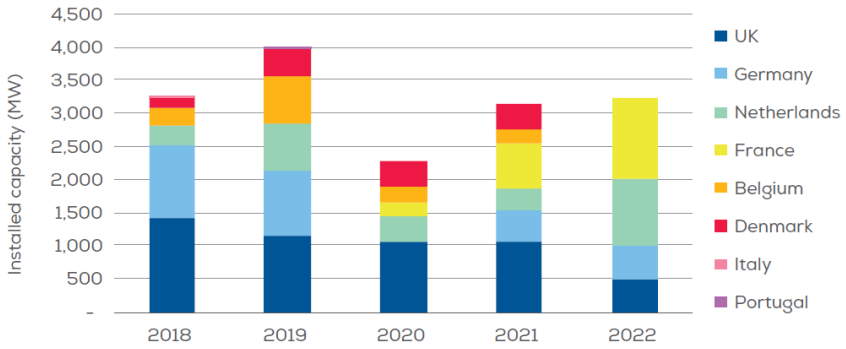

Fig. 2.2. Expected new offshore wind capacity in Europe.

Table 2.1. Wind offshore scenarios at 2030.

Country	LOW	CENTRAL	HIGH
GBR	18.000	22.500	30.000
DEU	14.000	15.000	20.000
NLD	4.500	11.500	18.500
FRA	4.300	7.000	11.100
DNK	3.400	4.300	6.130
BEL	1.600	4.000	4.000
POL	2.200	3.200	6.000
IRL	1.200	1.800	2.000
EST	-	600	1.200
SWE	300	300	800
POR	-	150	175
ITA	-	-	650
Total	**49.500**	**70.350**	**100.555**

Table 2.2. Wind offshore scenarios by ENTSO-E.

Country	**2025 BEST**	**2030 DG**	**2030 EUCO**	**2030 ST**
GBR	17.130	22.182	13.326	22.182
DEU	11.300	14.964	9.883	15.000
NLD	6.500	11.500	2.561	11.500
FRA	3.500	7.000	6.035	7.000
DNK	2.717	2.905	2.833	2.905
BEL	2.310	2.310	3.240	2.310
POL	600	2.250	777	2.250
FIN	500	700	119	700
ITA	447	655	3	655
SWE	190	190	227	190
POR	60	60	27	60
LAT	56	150	49	150
IRL	0	700	131	700
GRE	0	150	0	300
NOR	0	0	1.840	0
ESP	0	0	63	0
Total	**45.310**	**65.716**	**41.116**	**65.902**

The diffusion of offshore wind farms, both at the present stage of technological development and in a subsequent timeframe associated to the exploitation of more challenging sites (e.g. greater water depths) is influenced by policy decisions. In this framework, [27] compares policy and laws adopted in UK with the first steps moved by U.S.A. and India to deal with offshore wind, and [28] analyses incentives and barriers for massive wind power integration, including offshore, in Denmark. Whereas [29] describes the current status in Spain pointing out the consenting procedure for individuating candidate areas and selecting the initiatives, and [30] illustrates policies in China, exploiting SWOT analysis to delineate possible evolutions.

Apart from technical issues related to grid integration, two main aspects are worth of attention for a sound planning of the diffusion of offshore wind farms: market integration and siting assessment.

2.1.2.1 Market integration

A first aspect to be inspected is related to the capacity of current market schemes to cope with increasing shares of offshore wind. In [31], increasing levels of penetration of offshore wind are evaluated in the framework of PJM market, involving day-ahead, intermediate and real-time stages in different seasons and wind production levels, pointing out to an increase of possible shortfalls along with a reduction of network average prices and of emissions. The additional value of advanced wind turbines, exploiting higher towers and bigger rotors as in offshore wind farms, can involve smoother generation profiles, as discussed in [32], in terms of wholesale market, balancing costs, and grid investments.

Energy storage devices, even in hybrid configuration, can be adopted to improve the performance of wind energy in market environment, in order to make proper offers to increase benefits and to manage prediction uncertainties [33]. In particular, [34] presents an analysis of the long-term cost impact of a compressed-air storage on an offshore wind farm.

Finally, the development cost of offshore wind farms has a key role in their diffusion, as analysed in [35], where levelized cost of energy (named “LCoE”) evaluations for different wind farms operating in Europe shows almost constant trend, even with the exploitation of farther sea zones, thanks to learning processes. Differences between countries and the need of reducing the realization time are remarked, however.

2.1.2.2 Siting assessment

In order to obtain suitable positions of offshore wind farms, yielding maximum possible effect while minimizing the negative impacts on the system, several studies have been carried out in

literature. For instance, in [36] a database individuating sites for wind installations in the U.S.A. is introduced, involving a 2 km x 2 km mesh extended onshore and offshore, where unfeasible locations are excluded, and providing simulated forecasted datasets based on weather conditions. Moreover, in [37] a GIS-based tool is presented for the evaluation of offshore wind installation areas in the UK, drawing considerations about the LCoE value according to shore distance, sea depth and wind speed. Analogously, a GIS based approach is described in [38] for the selection of candidate offshore areas, involving the determination of wake effect and the comparison of wind offshore potential to the energy production and demand framework, presenting a case study based on the Canary Islands. In [39], the determination of maximum allowable capacity of offshore wind farms in specific regions of Taiwan is carried out for each node of the transmission network, by means of N and N-1 contingency analysis in peak and off-peak conditions. Finally, in [40], a multi-criteria assessment method for offshore wind sites is introduced, based on Analytic Hierarchy Process ("AHP"), involving network operation security indexes, investment cost, operation cost and capacity performance analysis. The method is applied to the case study of the Baltic States in 2020 horizon.

In addition, several other studies focus on a single offshore wind farm, inspecting connection topologies and related aspects of losses and reliability in [41], whereas in [42] the selection of components for electricity transmission to shore is assessed, taking into account stochastic processes and risk analysis as well.

2.1.3 Grid integration issues

2.1.3.1 Forecasts and curtailment

The correct exploitation of offshore wind energy resources should take particular care of the electricity network connection. At a first stage, it can be inferred that steady-state operation conditions can be affected by wind power diffusion, particularly due to the difficulty of predictions. In [43], deterministic and probabilistic load flow methods in the presence of offshore wind farms are compared.

Suitable wind forecast models should therefore be exploited in order to properly assess the expected production levels. In [44], a method for evaluating day-ahead and intermediate-term wind power forecast error for offshore wind farms is reported, exploiting a numerical weather prediction model and a stochastic model based on historical wind levels, and applied to the PJM system. In [45] the analysis of historical time series for the determination of UK wind capacity factor is carried out, obtaining lower variations for offshore installations, and studying the influence of persistent low or high wind generation periods and of ramping events. Moreover

in [46] it is shown that, in order to respect renewable diffusion targets in Germany, a remarkable share of offshore wind, although involving slightly higher generation costs, yields lower costs for flexibility thanks to more affordable forecasts.

The envisaged increased penetration of wind farms, as in general of non-synchronous generation, can lead to wind power curtailment [47]. In [48], a deep analysis of wind power curtailment events in Spain over four years of operation is illustrated, highlighting possible correlation of curtailment severity with generation levels, load demand, seasonality. In [49], the analysis of the future Irish power system is carried out in order to determine the amount of wind curtailment according to different scenarios, finding that offshore wind can help in the reduction of wind curtailment, thanks to the wider spatial spread of offshore wind turbines and their higher overall capacity factors.

2.1.3.2 Small signal and dynamic stability

In addition to the well-known power balance problems, electric networks can suffer from stability issues due to the increasing amount of wind generation. In [47] a distinction is made among transient stability, as the ability to withstand a fault, and small signal stability, related to normal operating variations. These two analyses involve the definition of suitable dynamic models for power system components, and in particular for wind farms. Both small signal and transient stability are evaluated in [50] in a simplified Taiwan power system and in [51] on future European power system under different scenarios, with particular attention to frequency stability. In this field, a thorough review of grid code requirements for wind farm participation in frequency control and of relevant methods involving deloading techniques and synthetic inertia, is reported in [52], and a synthetic representation is depicted in Fig. 2.3 [53].

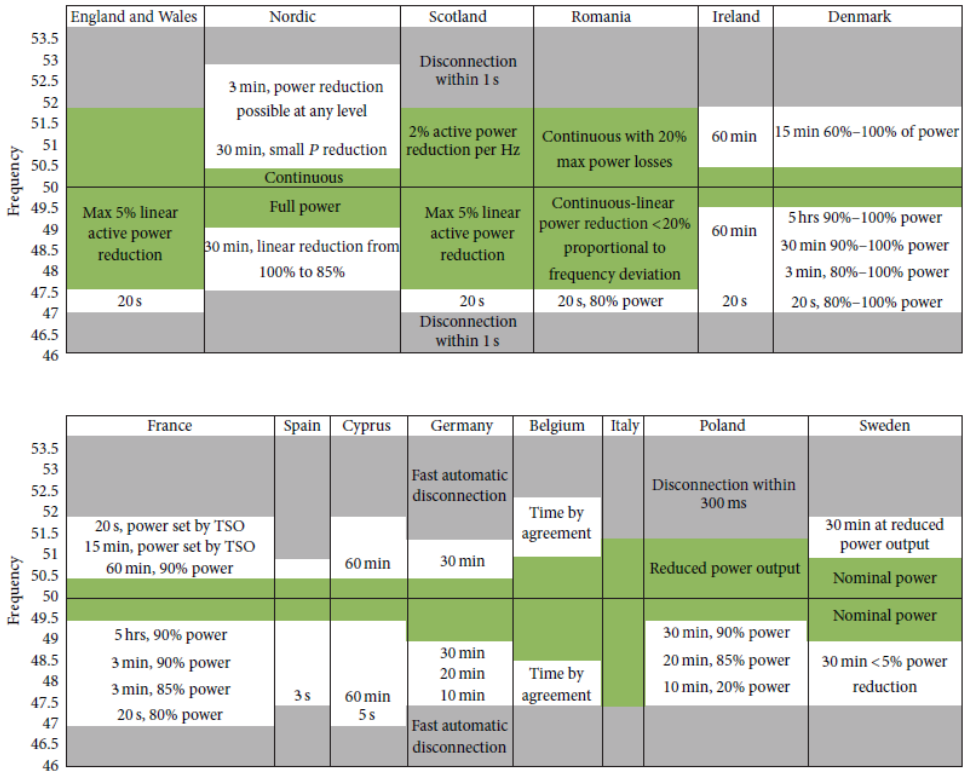

Fig. 2.3. Frequency regulation fields in different countries.

2.1.3.3 Voltage stability and reactive power regulation

Another aspect is related to voltage variations induced by wind farms. As reported in [47], wind turbines are nowadays required not to hinder power system restoration after a fault, by ensuring with low-voltage ride through conditions during transients, as exemplified in Fig. 2.4.

However, in the presence of a wind farm made by many turbines, some further actions could be required. In order to provide fault ride through ability for an offshore wind farm, in [54] a coordinated control scheme is proposed, based on the computation of instability proximity index, either exploiting communicated measures or by an estimator.

The main way to provide voltage support is the reactive power control of wind farm. For this aim, different implementations are thoroughly analysed in [55]. In particular, in [56] the enhancements to a wind power plant voltage stability by means of a STATCOM are investigated, whereas the influence of SVC installation in combination with wind farms on power system stability and on reactive power response is investigated in [57], [58]. In [59], the optimization of reactive power exploitation is carried out, taking into account steady state and dynamic constraints and fault ride through requirements, as well as the possibility of exploiting reactive production from wind farms and ad-hoc compensators. The methodology is applied to a model of the Danish power system, with a remarkable degree of wind power penetration. Moreover, the analysis of the impact of offshore wind farm on voltage profiles and stability curves is inspected in [60].

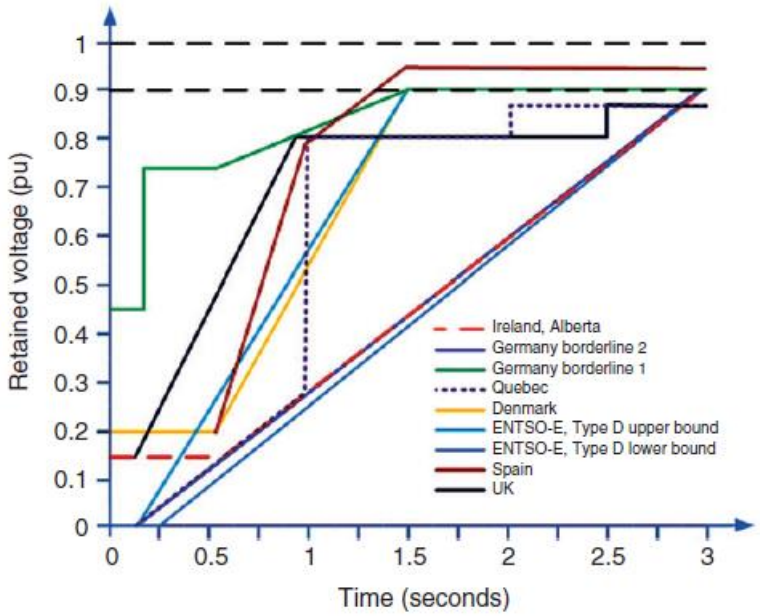

Fig. 2.4. Low voltage ride through conditions of wind turbines as specified by different transmission system operators.

2.1.3.4 The horizon of direct current connections

The exploitation of high voltage direct current (HVDC) systems for the connection of offshore wind farms is increasing due to the higher installed power and larger distance to shore, ensuring lower installation costs for the direct current option; several realizations are presently in commercial operation. In [61], a review of HVDC components for offshore wind farm connection to the mainland power system is carried out, along with suitable control rules. In this field, specific network code requirements for HVDC are envisaged in [62]. In particular, Voltage Source Converter (VSC) technology can be able to ensure several regulation abilities, from active/reactive power control to dynamic performance improvements. Analyses of all the integration challenges and chances in the presence of VSC-HVDC are of great interest indeed. A specific VSC-HVDC control scheme for the provision of ancillary services from offshore wind farms is proposed in [63]. In [64], a proper model of the VSC-HVDC is illustrated, and the analysis of the influence on their implementation of AC network short-circuit ratio and impedance angle is carried out. The integration of VSC-HVDC-interfaced offshore wind farms in the security-constrained day-ahead scheduling of the power system is dealt with in [65] by exploiting coupling models. A dynamic control of VSC-HVDC during faults in order to comply with fault ride through requirements is assessed in [66], where multi-terminal DC networks are introduced. Finally, the impact of VSC on small-signal and transient stability of an AC system is analysed in [67] and stability assessment of multi-terminal VSC-based DC network is developed in [68].

2.1.4 Situation and perspective in Italian transmission system

Although more than 9 GW of onshore wind power plants are currently connected to the Italian transmission network, there are no offshore installations. However, the procedure for technical authorization and for consenting of different entities involved (also considering the influence of state propriety over seas) has been defined. So far, only one offshore wind farm in southern Italy is authorized for construction in the next years.

Note that 83% of Italian onshore wind farms are installed in the south of the Country as shown in Fig. 2.5. However, the Italian TSO has also received requests for offshore farms to be connected to the system, amounting to approximately 2 GW: these are in the process of being authorized. These plants are localized in the areas with high penetration of onshore wind farms due to the favourable weather conditions prevailing in these sites.

As regards technical requests for the authorization, specific prescriptions for wind farms concerning over- and low-voltage ride through, reactive power control and frequency response

features have been recently revised in the Italian network code [59], imposing more challenging target, as illustrated in the following Fig. 2.6, Fig. 2.7 and Fig. 2.8 respectively.

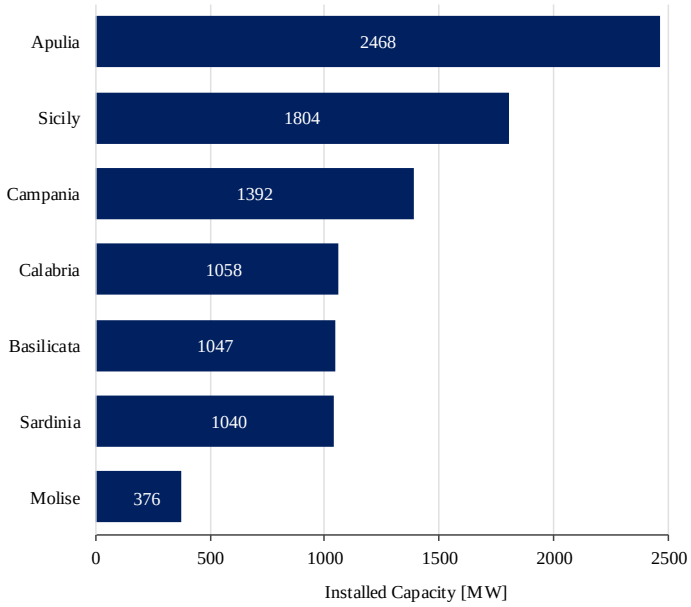

Fig. 2.5. Current installed capacity of onshore wind farms in south of Italy and islands, divided by region.

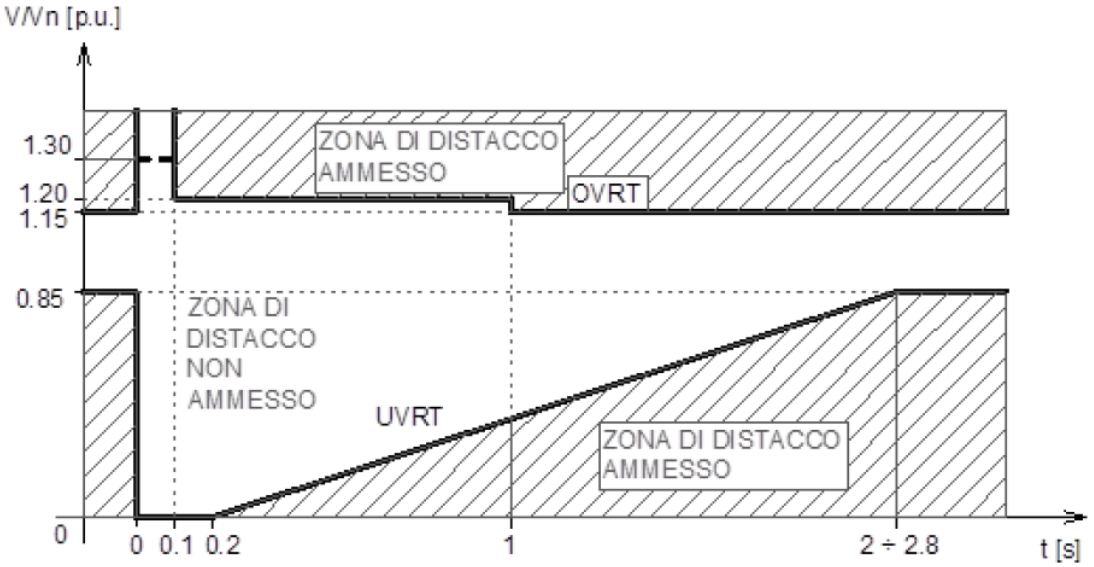

Fig. 2.6. Over- and low-voltage ride through requirements for wind farms in Italy.

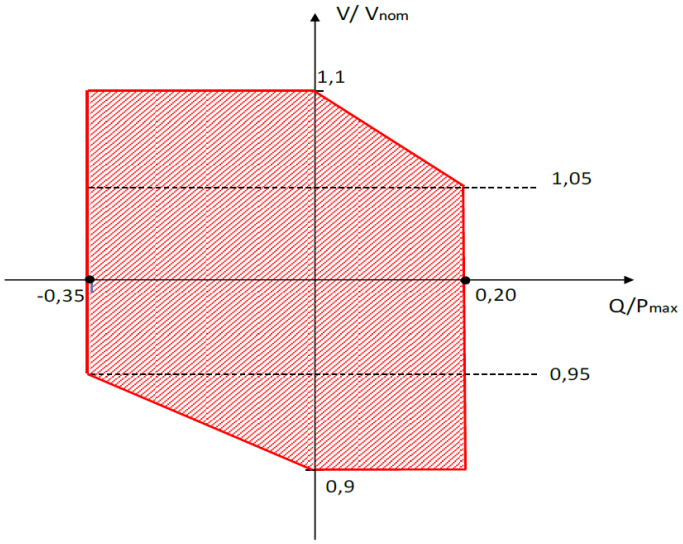

Fig. 2.7. Voltage-reactive power regulation chart for wind farms in Italy.

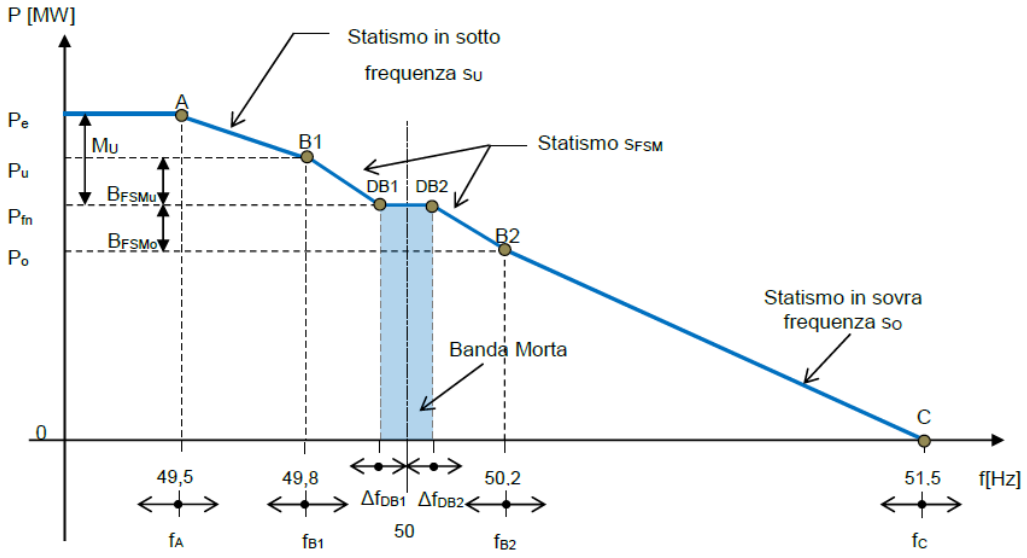

Fig. 2.8. Frequency-active power regulation characteristic for wind farms in Italy.

One additional aspect of interest for the TSO in offshore wind farms is their connection scheme to the National Transmission System. In particular, due to higher amount of installed power in a site, the wind farm should be connected to the EHV system (400 kV preferably). Even if a single radial connection has a gross capacity of 1.500-2.000 MW, the connection scheme has to be studied in a context of system security and maximum loss of active power. In fact, the connection of any power generation initiative, although improving the power provision security, shall be configured in such a way that, in the case of a loss of its active power injection, the impact on the synchronous area shall be limited to a specified value, according to considerations on steady-state conditions and dynamic evolution. Therefore, as the installed power increases, a meshed connection to the system (e.g. in-and-out) is requested.

Fig. 2.9 shows the secondary and tertiary reserve demand of in a low consumption day in the current situation of the Italian Transmission System (no offshore wind farms installed till now).

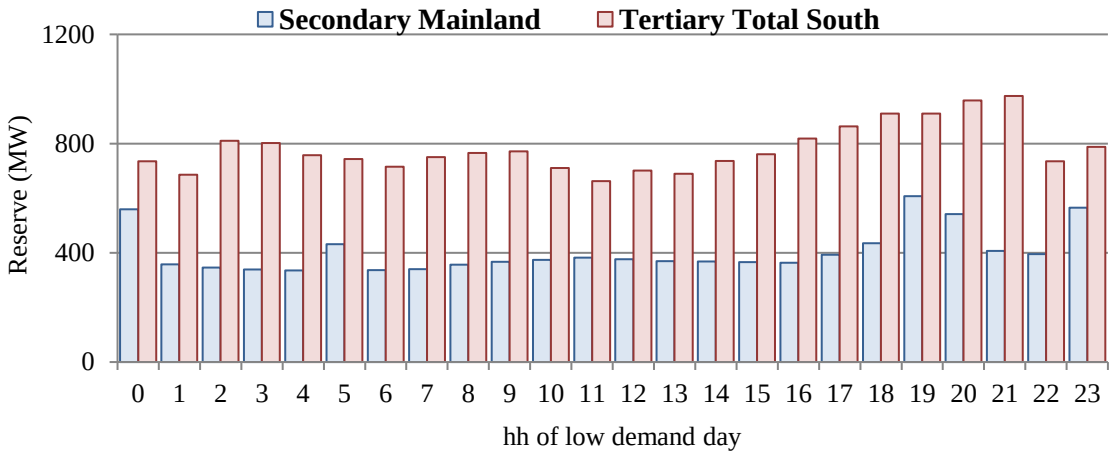

Fig. 2.9. Current Secondary and Tertiary reserve in a low consumption day.

The figure suggests that in a 0-400 MW capacity range, a radial connection of the offshore wind farms to the system day could have no impact on the reserve demand even in a low demand, while in the 400-800 MW range an in-and-out connection would be strongly recommended in order to significantly reduce the reserve request. Over 800 MW of installed offshore wind farms a fully meshed connection seems to be necessary.

2.1.5 Conclusions

In this section, perspectives for the integration of offshore wind farms in power transmission systems have been reviewed and classified, focusing on scenario targets and innovative market regulation for the diffusion of this technology and pointing out several technical aspects to be investigated to improve the effectiveness of offshore wind power production. In particular, the Italian system situation has been analysed, highlighting the increasing interest in offshore wind farms, and the emerging technical challenges for their connection to the transmission network. This study can pose the basis for future considerations as the offshore wind penetration is expected to increase in the Italian system.

2.2 Renewable sources integration using HVDC in parallel to AC traditional system: the Adriatic project

The use of High-Voltage Direct Current (HVDC) transmission in modern power systems is mainly driven by the need to increase the power transfer over long distances in a cost-efficient and controllable way. HVDC controls can ensure fast and accurate power flow control, improving the whole system performance as well as increasing flexibility in the management of flows from remote renewable generation and towards load centers, especially in a zonal market configuration. However, in the network planning phase the implications of a new HVDC connection, on both the steady-state and dynamic operation of a power system, must be carefully evaluated with particular reference to possible outage events, with a view to the operating conditions and to the control schemes. In this study, a real HVDC project within the Italian transmission network is considered, looking at both the Voltage Source Converter and Line Commutated Converter technological options. The study implies a methodology to analyse the impact on steady-state and dynamic performances in the presence of faults, with a focus on grid security and on market efficiency. The behavior of the interconnected Italian power system is simulated from a development planning viewpoint by means of the relevant software tools used by the system operator.

Furthermore, the capability assessment of the critical section Centre South – Centre North affected by the planned HVDC project is provided both in the present and in the future conditions.

2.2.1 Introduction

Modern interconnected power systems are designed to operate efficiently in order to supply load consumption areas with high levels of reliability [70]. In the energy transition context, transmission interconnections in meshed electrical networks guarantee adequate reliability with minimum cost of supply [71] and provide significant benefits in terms of load diversity, availability of sources and flexibility in operation.

In fact, a reliable and flexible transmission grid allows to face new demand typologies and dynamics, and to realize a major integration of renewable generation while keeping system stability [72]. Currently, an effective transmission infrastructure should ensure that cheap renewable energy is unconstrained by transmission capacity and that active power flows can be rapidly directed from the surplus generation areas to the deficit ones, in order to maintain the power system frequency (as the main balancing quality indicator) close to its nominal value [73].

Power systems performances can be improved by the presence of HVDC links, which are characterized by inherent advantages related to fast and accurate controllability, enabling the Transmission System Operator (TSO) to directly control the energy flows [74]. The combined HVDC – AC system also has enhanced capabilities in terms of dynamic performances [75], thanks to the HVDC control scheme not being affected by frequency deviations [76]. In order to realize an efficient and stable operation and to maximize power control flexibility, a hierarchical framework can be implemented for both normal and critical conditions, as illustrated in [77].

In order to take advantage from HVDC diffusion, the attention of researchers and planning engineers is devoted to modeling and control in different time frames [78]. In particular, the classical LCC systems are characterized by usually larger sizes are quite well known, however their impact on power and voltage control should be carefully evaluated by means of performance indexes for stability interactions, as proposed in [79], [80]. In the presence of grid faults, LCC-HVDC can suffer from commutation failures, due to the lack of inherent AC voltage regulation ability [81]. Therefore, the use of reactive power control at both ends, either by means of synchronous compensators or with power electronic-based solutions such as FACTS, can be very useful [82], [83].

However, the VSC is more and more investigated due to its potential for improved dynamic performances. Different schemes have been proposed in order to achieve proper control of both active power and voltage [84], [85], and to obtain frequency response patterns [86], [87] enhancing the inertial behaviour of the power system in the energy transition, which involves more and more renewable-based systems, equipped with power electronic interface. The HVDC integration can remarkably affect power system dynamic stability behaviour. In particular, the analysis of Critical Clearing Time (CCT) is carried out on different controllers in [88], on frequency control in [89] and according to distance and power transfer level in [90]. It can be argued that the influence of different HVDC dynamic control schemes is usually assessed on test networks or simplified real cases.

The control system notwithstanding, the presence of HVDC in actual market framework should be carefully accounted, as proposed by [91], [92]. In this framework, different methods for defining power allocation to HVDC embedded in AC transmission systems have been proposed in [93] – [95]: in [96], HVDC placement in market framework using flow-based indexes and N-1 analysis is described. Whereas, the influence of HVDC in flow-based market coupling has been considered in [97] on a continent-size network and in [98] for the determination of zonal exchange levels comparing net transfer capacity and critical contingencies. In addition, the

potential of reducing unscheduled and loop flows in a meshed zonal market framework is depicted in [71], [99], and the ability of HVDC technologies to provide ancillary services is studied in [100]. It stems from this brief review that the implications of new HVDC link on market framework are often examined in steady-state conditions.

The aim of the present study is to evaluate from a TSO development planning viewpoint the contribution of a new HVDC link located in the mainland of the Italian transmission network. System stability is analysed both under static and dynamic conditions, determining the influence of different HVDC architectures and controls on zonal exchange limits and on CCT. The analysis is carried out on specific operating conditions considering the possible critical event that can lead to maximum loading limit and to system dynamic instability. Network development plan is therefore implemented with different cases by further addition of combinations of synchronous compensators and HVDC, either in the VSC and LCC configuration. The concept is developed and applied in the framework of Italian transmission system.

The main contributions of this study can be individuated in:

- Set-up of a method to evaluate the influence on static and dynamic performances of a network development, in a zonal market framework;
- Individuation of real critical operation scenarios according to N-1 dynamics;
- Analysis of different HVDC architectures and controls for the development of a real transmission system;
- Assessment of the maximum power transfer capacity of the 400 kV Adriatic backbone at year 2030 horizon, without and with the planned Adriatic HVDC project.

2.2.2 Static and dynamic evaluation of different architectures for the HVDC project

2.2.2.1 Italian power system features

The Italian transmission system, managed by Terna as TSO, consists of 11,079 km of 400 kV lines, 11,082 km of 230 kV lines, 47,324 km of 150-132 kV lines, and accounts for several AC interconnections with other countries (France, Switzerland, Austria, Slovenia, Malta), as well as for two HVDC connections with Sardinia and other HVDC links with Greece, Montenegro, and one under construction with France.

The transmission network is densely meshed in the North, where main load areas are located and several connections with European network are present, whereas in the South and in the

islands the high renewable installed capacity, which requires power routing towards North, has to rely on a weakly meshed grid. In particular, along the Adriatic coast, where the load is comparatively low, a single 400 kV North-South corridor is present, and the secure power transfer capacity can result severely constrained as a result.

In fact, due to the physical configuration of the Country (long and narrow with mountain chains), the Italian power system is dealt with by considering six different market zones (Fig. 2.10), among which transport limitations are posed for sake of secure operation: North, Centre-North, Centre-South, South, Sardinia and Sicily. This structure naturally lends itself to the individuation of "critical sections", which are subjected to grid congestions in some operational conditions [101].

The adoption of a zonal market provides several benefits in terms of power transfers compatibility between nodes and grid constraints compliance, as well as the definition of price signals encouraging the TSO to efficiently locate network developments and to provide an economic assessment of the transfer capacity between zones.

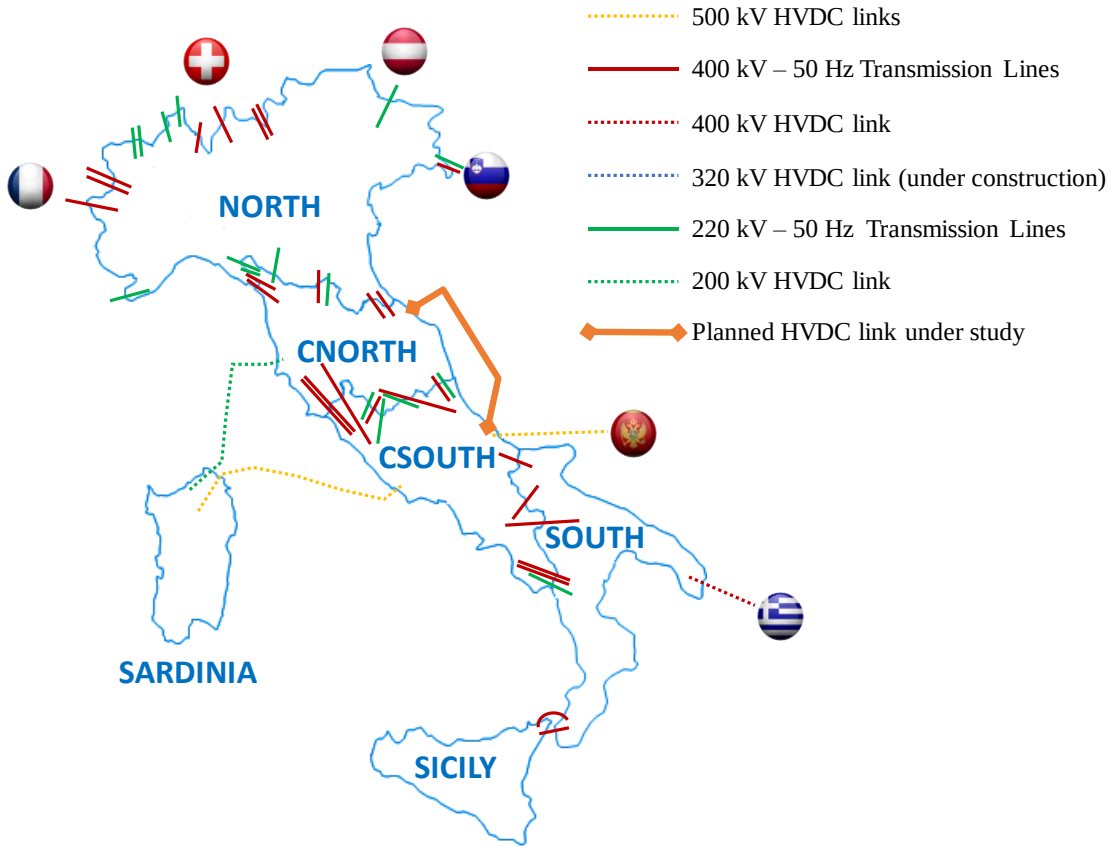

Fig. 2.10. Italian market zone division and interzonal connections.

The zonal representation of the high voltage National Transmission Grid describes the transmission constraints by the means of a set of topological and electrical parameters [102]:

- C_{ij}, defined as the element of connection matrix between zones *i* and *j* (1 if connected, 0 otherwise);
- S_{ij}^{k}, defined as the contribution of zone *k* to the energy exchange F_{ij} between zones *i* and *j*, defined according to electrical characteristics of network branches and to zone connection matrix.

Moreover, $EN_k$is defined as the energy balance of the zone *k*, as the difference of total sales of power production PP_g and total purchases of power demand PD_l within that zone:

$$EN_k = \sum_{g \in k} PP_g - \sum_{l \in k} PD_l \tag{2.1}$$

Therefore, the energy exchange F_{ij} between zones *i* and j can be determined as follows:

$$F_{ij} = \sum_{k=1}^{N} S_{ij}^{k} \cdot EN_k \tag{2.2}$$

The market solution procedure maximizes the social welfare considering technical limits for production/demand levels, with relevant bids b_g and b_l, and imposing boundaries for zonal energy exchange F_{ij} in both directions:

$$\max_{PP,PD} \left[\sum_{g} b_g(PP_g) - \sum_{l} b_l(PD_l) \right] \quad s.t. \begin{cases} \sum_{g} PP_g - \sum_{l} PD_l = 0 \\ PP_g^{min} \le PP_g \le PP_g^{max} \\ F_{ji}^{max} \le F_{ij} \le F_{ij}^{max} \end{cases} \tag{2.3}$$

In fact, a market zone can be defined as a grid portion characterized by physical limits to power exchanges with neighbouring zones dictated by system security reasons. The identification of these limits is based on the following criteria:

- the power transfer capacity between bordering zones must result limited in most common operational conditions, in accordance to security criteria;
- power injections and withdrawals programs shall not cause significant congestions to varying injections and withdrawals within each geographical zone;
- the dislocation of power injections and withdrawals within each zone shall not have remarkable influence on power transfer capacity between zones.

The maximum admissible transfer capacity between zones must be assessed according to the grid topology, the power flows distribution, the thermal rating of individual lines and the associated security criteria. In the steady-state analysis, this requires the solution of multiple

AC power flow problems, accounting for different possible contingencies in several operating conditions. For each condition, the vector of net nodal injections of active power $\boldsymbol{P}$ is defined as the difference of PP_g and PD_l, and by defining the vector of reactive power injection $\boldsymbol{Q}$ in the same way, the power flow problem can be posed in the following standard form:

$$\boldsymbol{P} - \boldsymbol{P}(\boldsymbol{\vartheta}, \boldsymbol{V}) = \boldsymbol{0} \tag{2.4}$$

$$\boldsymbol{Q} - \boldsymbol{Q}(\boldsymbol{\vartheta}, \boldsymbol{V}) = \boldsymbol{0} \tag{2.5}$$

where the vectors $\boldsymbol{P}(\boldsymbol{\vartheta}, \boldsymbol{V})$ and $\boldsymbol{Q}(\boldsymbol{\vartheta}, \boldsymbol{V})$ derive from nodal admittance matrix, and the vectors of nodal voltage amplitude $\boldsymbol{V}$ and phase $\boldsymbol{\vartheta}$ are obtained, along with branch flows.

The security criteria in load flow analysis are represented by maximum power flow limits on branches, estimated at 120% of rating, or by maximum/minimum voltage ranges at nodes, fixed at ±10% of nominal voltage [10], [103].

Even under acceptable steady-state conditions, the lack of a strong redundancy can expose the system to the risk of instability. This can occur in the case of severe contingencies and in the presence of limited inertia on the network, e.g. in low load conditions or in the presence of massive renewable production, even if more stringent requirements for voltage and frequency regulators are currently being adopted [104]. Therefore, time-domain simulations for transient stability analysis have to be carried out, with the aim of solving a system of non-linear differential-algebraic equations:

$$\begin{cases} \dot{\boldsymbol{x}} = \boldsymbol{f}(\boldsymbol{x}, \boldsymbol{v}, \boldsymbol{r}) \\ \boldsymbol{I}(\boldsymbol{x}, \boldsymbol{v}) - \boldsymbol{Y} \cdot \boldsymbol{v} = \boldsymbol{0} \end{cases} \tag{2.6}$$

where $\boldsymbol{x}$ is the vector of state variables for devices with dynamic behavior (e.g. generator rotor angle, electromotive force components), $\boldsymbol{v}$ is the vector of nodal voltage components, $\boldsymbol{r}$ is the vector of control inputs, $\boldsymbol{Y}$ is the nodal admittance matrix and $\boldsymbol{I}$ is the vector of nodal current injections.

In order to manage the evolution of generation/demand and the overall energy transition, several grid reinforcement projects are studied by Terna in the National Development Plan (NDP). In this context, development actions are evaluated according to a cost-benefit analysis method involving the economic evaluation of the impact of their implementation on electricity market and on steady-state operation, whereas the dynamic impacts are considered as additional effects [105].

The aim of this study is to estimate the effect of a capital-intensive initiative as a new HVDC link on static and dynamic technical aspects in the zonal market framework, to add evaluation elements in cost-benefit analysis. In particular, as envisaged in the NDP, an HVDC link is to

be placed between Centre-South and Centre-North market zones, with the aim of increasing power transfer capacity and enhancing voltage and frequency stability in the whole national power system [106], [107]. The location of the planned HVDC is shown in Fig. 2.10, between VLL node (Centre-South) and FNO node (Centre-North). The HVDC is supposed to be built in a bipolar configuration with a total size of 1000 MW, in order to have a higher power rating for the chosen 400 kV DC voltage level, and in order to increase the reliability of the connection, able to carry half of rated power acting as a monopolar HVDC in the case of single pole failure or maintenance [108]. However, the exploitation of either consolidated LCC technology (in use on connections with Sardinia, Greece and Montenegro) or VSC technology (to be installed on Italy-France border) should be analysed.

2.2.2.2 Methodology

The study is intended to start from situations detected in the Italian power system via field measurements, fully feasible from the steady-state analysis viewpoint, but potentially revealing possible stability issues in case of severe grid faults, e.g. due to the reduced levels of inertia. These potentially critical situations, named scenarios, are analysed in different cases considering a set of network development solutions, involving the planned HVDC link as well. For each scenario under different network development cases, an early transient stability analysis in N-1 condition is considered, by assuming as critical contingency a three-phase fault in the middle point of a double-circuit 400 kV transmission line on the Tyrrhenian coast spanning across the investigated Centre-North – Centre-South market section "border" (Fig. 2.11). This line is chosen due to its usual high flows with respect to other single-circuit lines of the section. The system stability behaviour is assessed by evaluating the CCT of line fault as transient stability index and by testing performances as fault duration increases.

The second part of the analysis involves the determination of steady-state power exchange limit across the investigated section. For this aim, the power generation levels of active generators placed in the adjacent zones and boundaries, are modified according to development scenarios given by national policies [109], [110], until maximum reliable power production is attained. The load of the same zones and the export/import levels with other Countries are modified accordingly, by exploiting power injection shifting in compliance with network sensitivities [97]. Under these assumptions, different N-1 AC load flow analyses are carried out by eliminating the grid elements across the investigated section one at a time, shown in Fig. 2.11, for a total of 9 events (one double-circuit 400 kV line, four 400 kV single-circuit lines, four 230 kV lines). The loading condition is increased until line rating or nodal voltage limits described

in Section 2.2.2.1 are reached on network elements of the zones in any of the analysed N-1 events. From this analysis, the critical N-1 event is pointed out, and the power flowing on branches across the market zone border in that event is assumed as the steady-state contingency-based maximum zonal exchange.

Finally, a transient stability analysis is carried out, under the steady-state limit loading condition obtained in the previous stage, and considering – for the reasons explained before – that the critical N-1 dynamic event is the opening of the same line indicated in Fig. 2.11 due to a mid-length three-phase line fault with a fixed 100-ms duration, corresponding to maximum tripping time of line protective relays. If the dynamic stability of the steady-state limit loading condition is not satisfactory, the loading is decreased according to the rules described in the previous stage, until the considered fault does not imply network instability. In this way, the dynamic contingency-based maximum zonal exchange is determined.

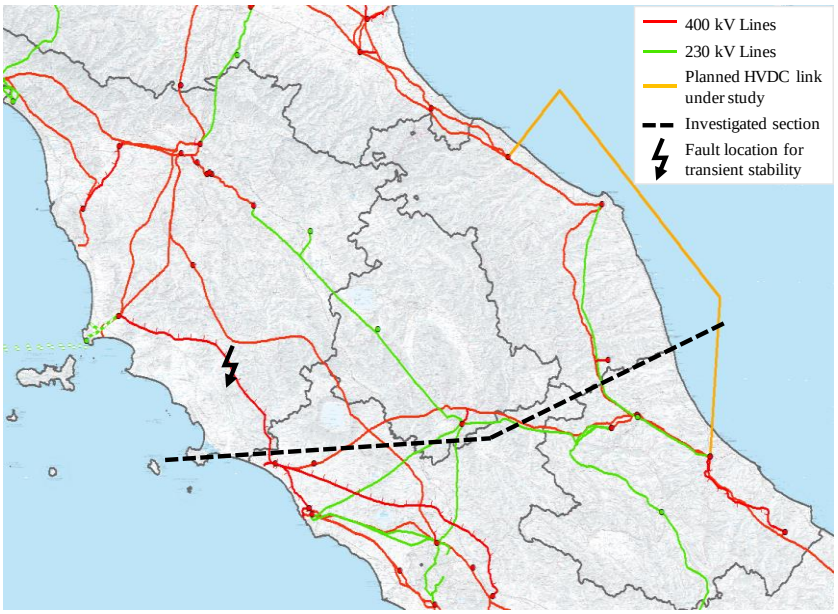

Fig. 2.11. Identification of Investigated Section and fault location (HVDC line path is merely indicative).

2.2.2.3 Tools

Simulations are performed using SPIRA and SICRE/CRESO tools [111], which define the Terna software environment for the secure and economic operation planning of the Italian transmission grid for both static and dynamic studies. In particular, static and dynamic modeling of HVDC in these tools, based on benchmark models, has been described and discussed, with comparison to other commercial software tools and literature-based models, in [112], [113].

Power flow analyses are carried out by exploiting a Newton-Raphson solution method, with power mismatch thresholds set at 0.1 MW and 0.1 MVAr as convergence criteria. For dynamic

stability analysis, aimed at system-level electromechanical transients rather than device-level electromagnetic phenomena, the employed integration method is Runge-Kutta2, with a timestep of 0.005 s in order to catch possible spikes in grid-side quantities due to switching of power electronic interfaces.

Dynamic models of generators and of SCs involve a 4th order model of the electric machine, including angle, rotating speed and electromotive force components in the d-q frame, and an AVR-4 model for voltage regulation, involving further 5 state variables. Whereas, the mechanical part of either thermoelectric or hydroelectric plants is tailored according to manufacturer data, involving valving systems to control mechanical power. Moreover, the system is equipped with power system stabilizer of type PSS IEEE1, with 5 state variables. Loads are described through static exponential models, function of voltage and frequency, in order to account for specific features and limit the stiffness of response. In order to evaluate the CCT, protective relays at the faulted line terminals are blocked, whereas, all other devices involved in network defence plan (e.g. frequency relays) are considered active with intervention characteristics according to Italian Network code [114].

The LCC-HVDC model involves:

- Algebraic equations for converter power at each terminal, voltage/current references, and DC lines;
- Ramping limits on references and dynamic evolutions;
- Firing angle and DC current control at rectifier side, extinction angle and DC voltage control at inverter side;
- Additional inverter firing angle advance to reduce commutation failure;
- Primary Frequency Regulation (PFR) with synthetic droop and PSS effect on the inverter side.

In addition, VSC-HVDC control has the following features:

- A control linking active power to converter voltage phase, and reactive power to voltage magnitude;
- Additional firing angle is absent;
- Droop-based PFR on both converters;
- Voltage/reactive power PI regulators on both converters, working independently

2.2.2.4 Tests

The proposed procedure has been tested on a model of the Italian transmission system, involving a full representation of the 400 kV and 230 kV network, and of directly connected generation plants, and considering a reconstruction of power injections at high-voltage nodes and a proper equivalent model of EHV network of external Countries. The model includes roughly 2200 nodes and 3300 branches (lines and transformers). In this framework, two different scenarios are investigated, representing actual network operating conditions of the Italian transmission network registered during winter season.

The main data of Scenario A and Scenario B are reported in Fig. 2.12 and Fig. 2.13, respectively. It can be observed that both scenarios are characterized by a power exchange close to the 3300 MW maximum limit on the Centre South – Centre North boundary, with the lines on the Tyrrhenian side loaded close to maximum rating. The identification of critical scenarios is performed according to offline transient stability studies on the actual network operation conditions, revealing possible stability issues in case of a line fault.

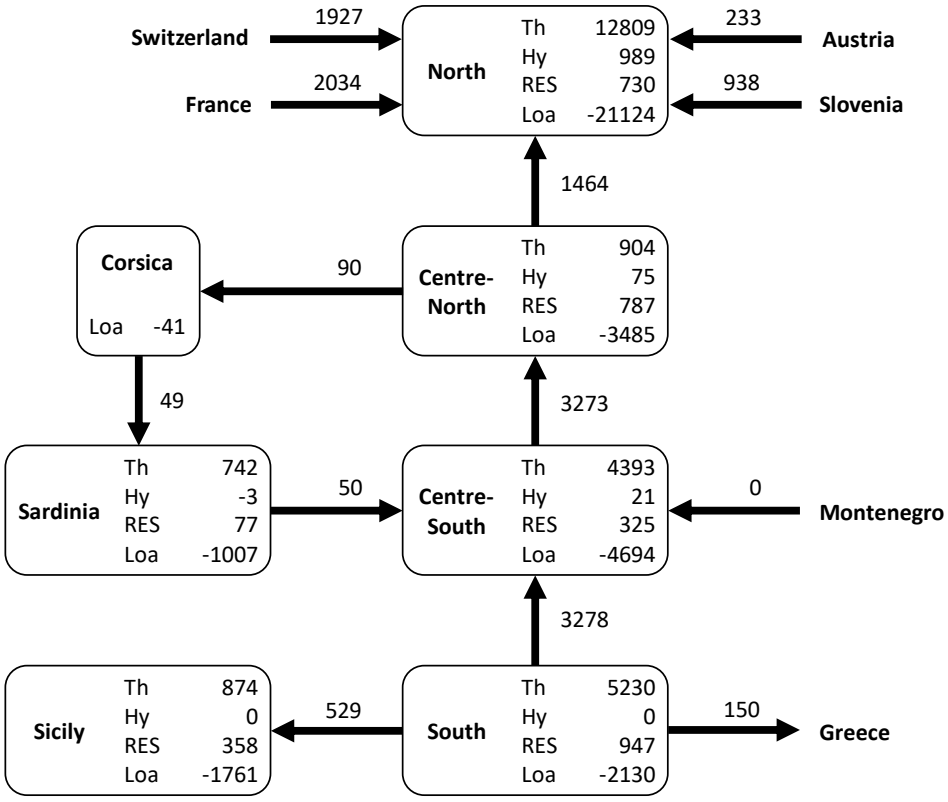

Fig. 2.12. Input data of Scenario A: zonal balances and exchanges [MW].

In Scenario A, total load (Loa) amounts to 34.2 GW, representing an average situation, and it is covered by 72.8% by thermal generators (Th), 3.2% by hydroelectric plants (Hy), 9.4% by

renewables (RES), and 14.4% by imports. The South zone exports due to excess low-cost generation. Along the peninsular network, all the exchanges are directed towards the North zone. A total of 140 thermoelectric units and 42 hydroelectric units are active, most of them are placed in the North zone, with a limited amount of pumped hydro in Sardinia.

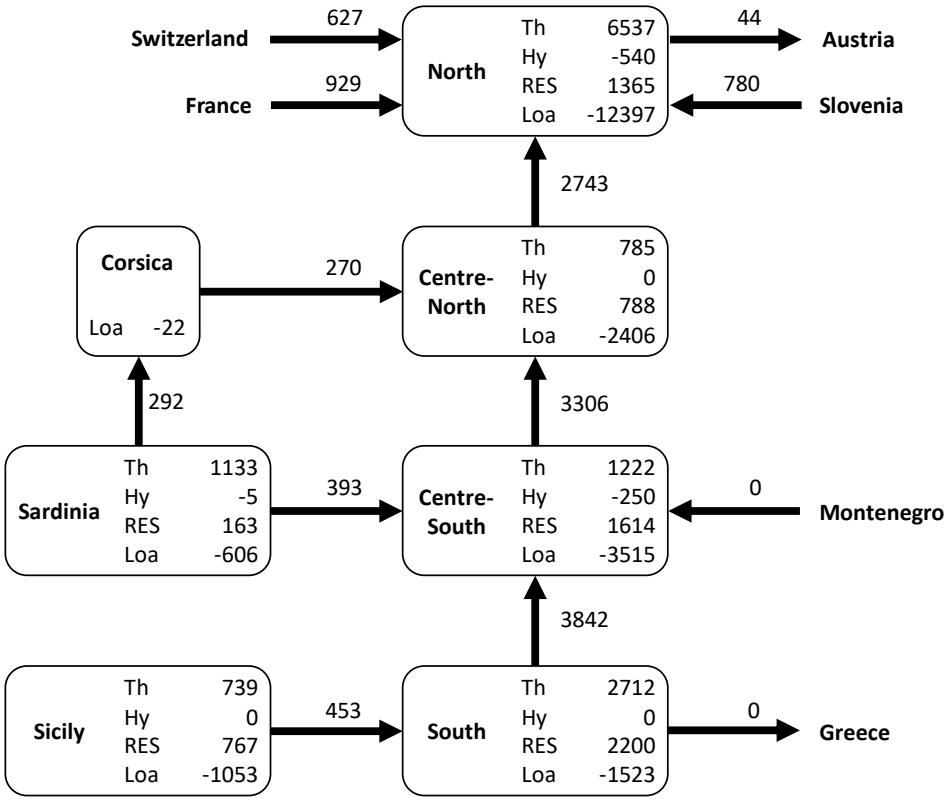

Fig. 2.13. Input data of Scenario B: zonal balances and exchanges [MW].

In Scenario B a low demand condition is considered, where the load is equal to 21.5 GW, close to minimum registered values, and the renewables and distributed generation supply 32% of load, with a remarkable increase in Centre-South, South and Sicily with respect to Scenario A. Thermoelectric plants cover 60.9% of the load, and 10 pumping hydro units are exploited to support the demand. The flows on the peninsular network towards North are larger. Power production is provided by 104 thermoelectric units, (of which only a small part is located in zones with high RES contribution), and 13 hydroelectric plants. This configuration can imply more challenging conditions on dynamic behavior due to lower levels of inertia.

For each Scenario, six cases are considered, in order to inspect the effects of different decisions about network developments, as summarized in Table 2.3. With current network configuration as a reference, the NDP provisions at year 2025 (new lines and regulating transformers, new outline of the Adriatic backbone) are considered to enhance RES integration. In addition,

voltage control devices are included: although the use of SVCs and STATCOMs for several applications is currently being investigated [58], in this study the presence of synchronous compensators (SCs) at key transmission nodes is accounted, since they have a limited footprint, improve inertial response and short circuit levels, do not raise particular issues in modeling and control integration [115], [116]. Finally, the presence of the planned HVDC link also taken into account, considering either LCC control, or LCC control with SC for voltage regulation, or VSC control (VSC-HVDC together with SC would provide concurrent regulation and it is not analysed).

As regards operation strategy, the target of SCs is to keep voltage values within the allowable range 0.95-1.05 p.u., whereas the HVDC connection is supposed to carry its rated capacity (i.e. 1000 MW) from Centre-South to Centre-North to reduce the stress on the AC network elements.

Table 2.3. Explanation of investigated cases of network development.

Case	Current network	NDP@2025 network	SCs	LCC	VSC
Case 1	X				
Case 2		X			
Case 3		X	X		
Case 4		X		X	
Case 5		X	X	X	
Case 6		X			X

2.2.2.5 Results and discussion

The transient stability assessment of Scenario A leads to the results reported in Table 2.4. It can be noted that the CCT is close to protection system intervention time in the Case 1, thus denoting the impending stability issue. The network developments of Case 2 allow a slight increase of the CCT, whereas the presence of SC in Case 3, ensuring prompt voltage support, results in a remarkable time margin increase. The presence of LCC-HVDC in Case 4 does not imply a significant advantage with respect to Case 3, but the combination of SC and LCC in Case 5 makes the CCT much longer. Finally, Case 6 shows the highest value of CCT, proving VSC-HVDC effectiveness.

As an example, in Fig. 2.14 and Fig. 2.15 trends of voltage and frequency values the planned HVDC link terminals are shown for Cases 1, 3, 4 and 6 (Cases 2 and Case 3 are very similar, and the same is observed between Case 5 and Case 6, therefore they are not shown for the sake of readability). It can be noted that fault recovery in Case 1 is slow, with the first voltage oscillation below 0.8 at FNO node and below 0.7 at VLL node. In fact, the southern part of the system is characterized by a lower inertia and comparatively looser voltage control; plots show

that at t=20 s oscillations are less damped than in the northern part. The presence of SCs in Case 3 allows reduced oscillations, and the presence of HVDC further contributes to a better recovery.

Table 2.4. Scenario A: CCT determination.

Case	CCT [ms]
Case 1	100
Case 2	115
Case 3	200
Case 4	205
Case 5	290
Case 6	310

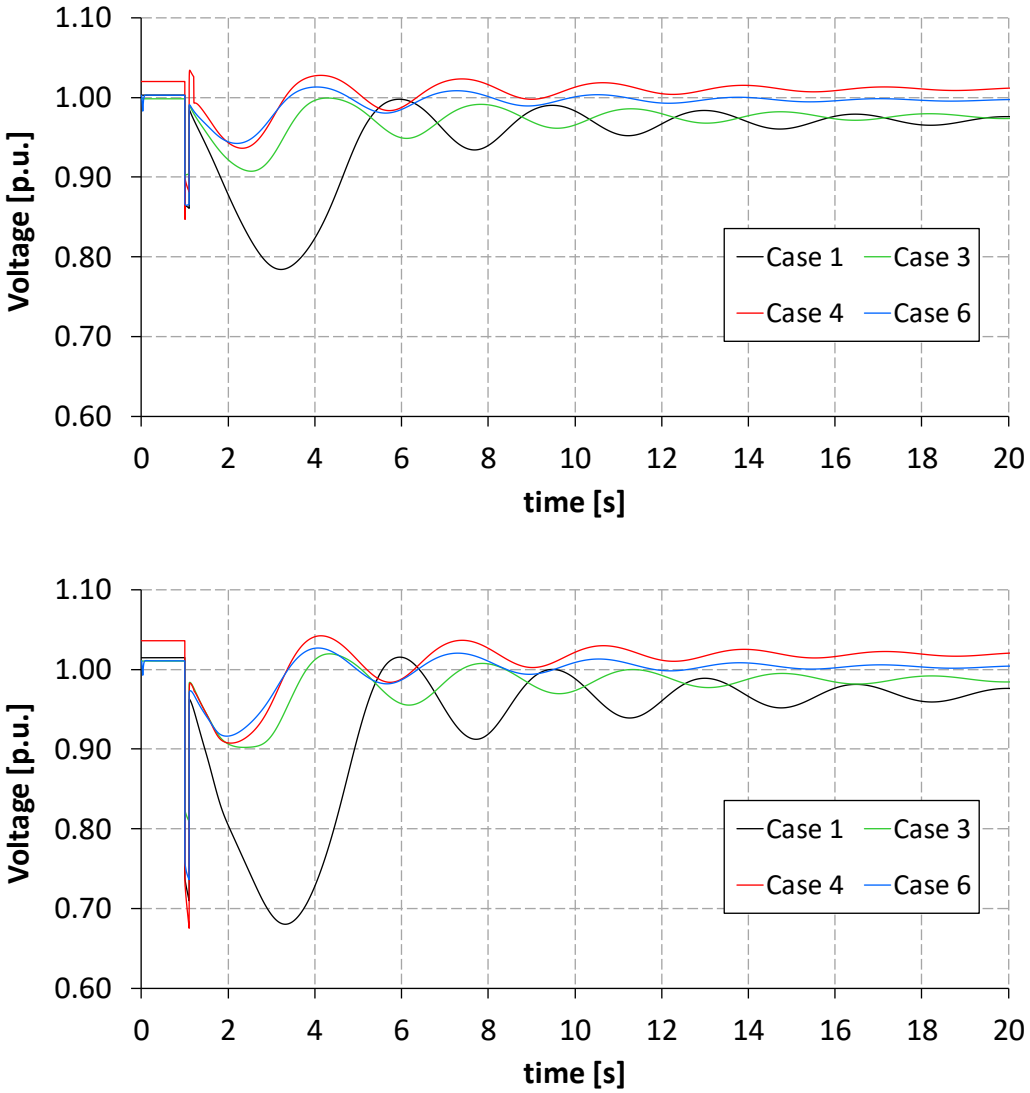

Fig. 2.14. Scenario A. Nodal voltage at FNO node (top) and VLL node (bottom) in different cases.

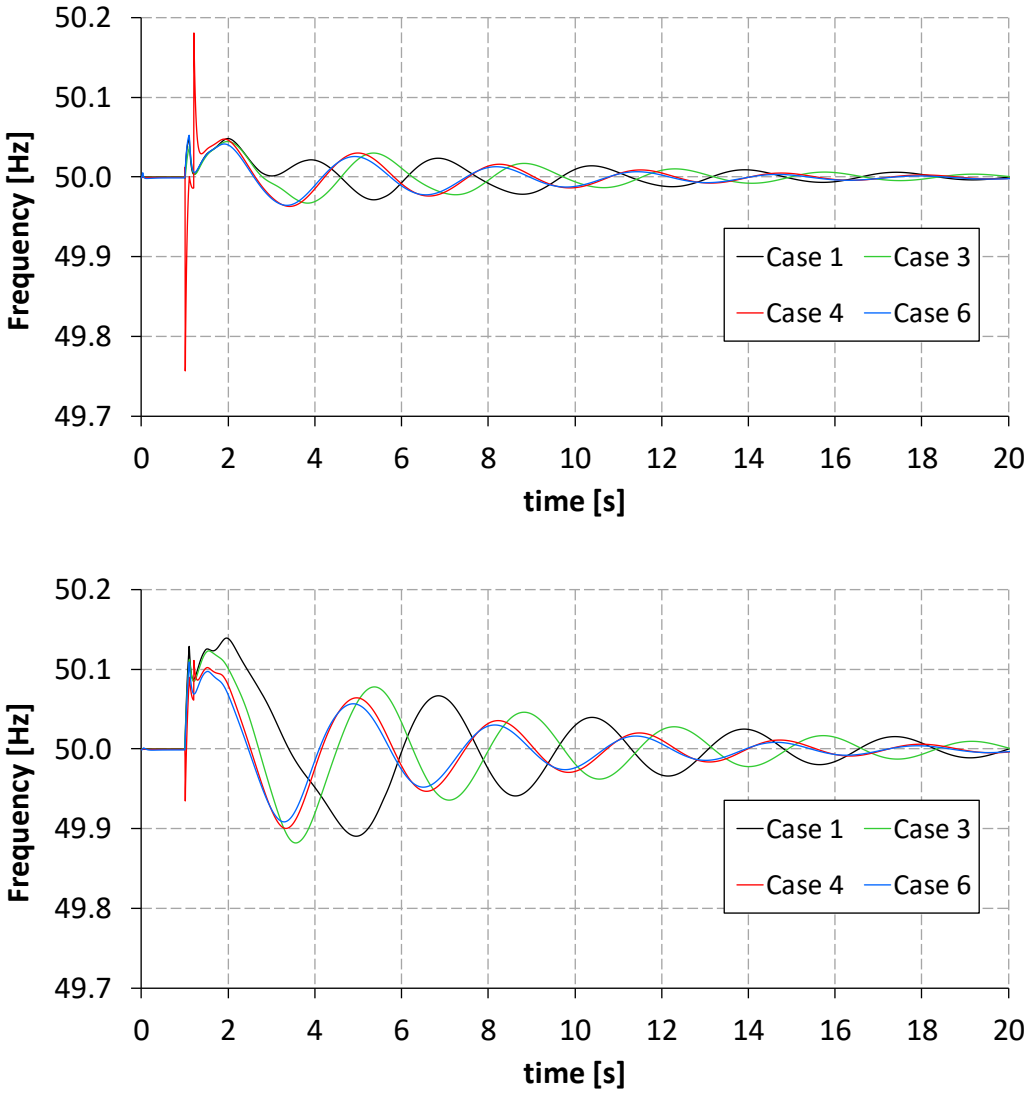

Fig. 2.15. Scenario A. Values of frequency at FNO node (top) and VLL node (bottom) in different cases.

However, in Case 4, significant frequency spikes are apparently observed at FNO node during and after the fault. This is ascribable to the commutation failure affecting the converter station of the HVDC link acting as inverter as shown in Fig. 2.16 [117], [118]. Commutation failure is avoided in Case 5 thanks to SCs, whereas VSC in Case 6 is not affected.

Reactive power injections at terminal buses in Cases 3 and 6 are reported in Fig. 2.17.

For the sake of comparison, the reactive power output of a SC placed in South region in Cases 3, 4 and 6 is reported in bottom part of Fig. 2.17, showing that the presence of HVDC implies smaller oscillations and a new steady-state regime value closer to initial one.

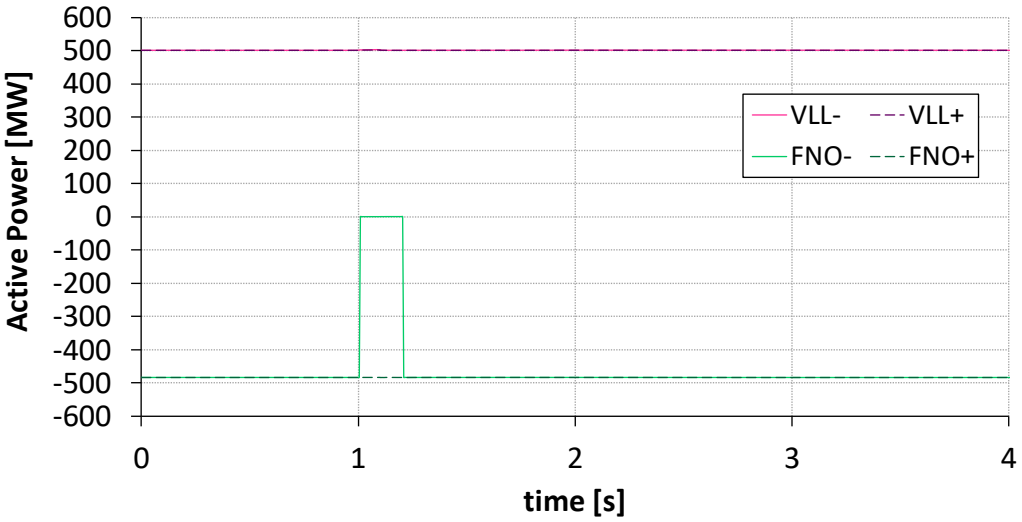

Fig. 2.16. Scenario A. Active power trends at HVDC terminals in Case 4.

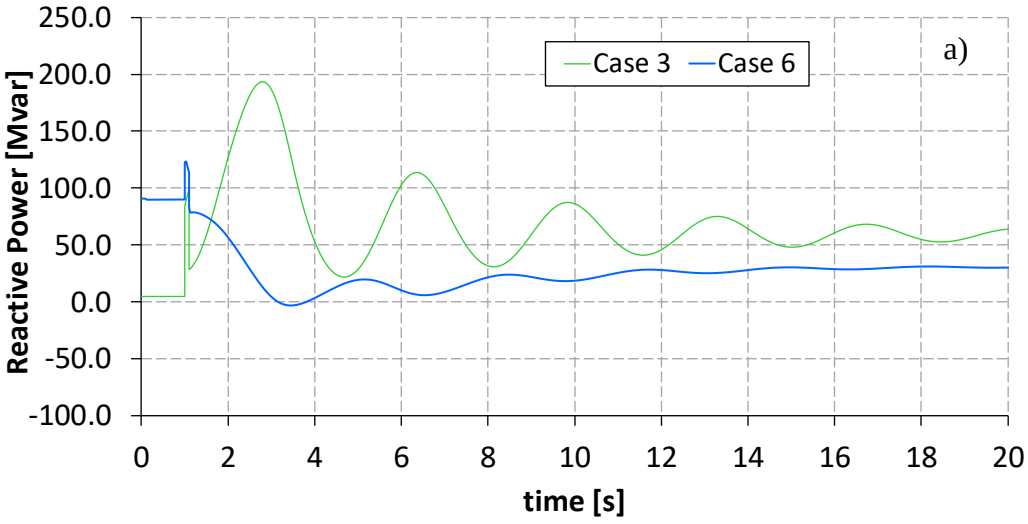

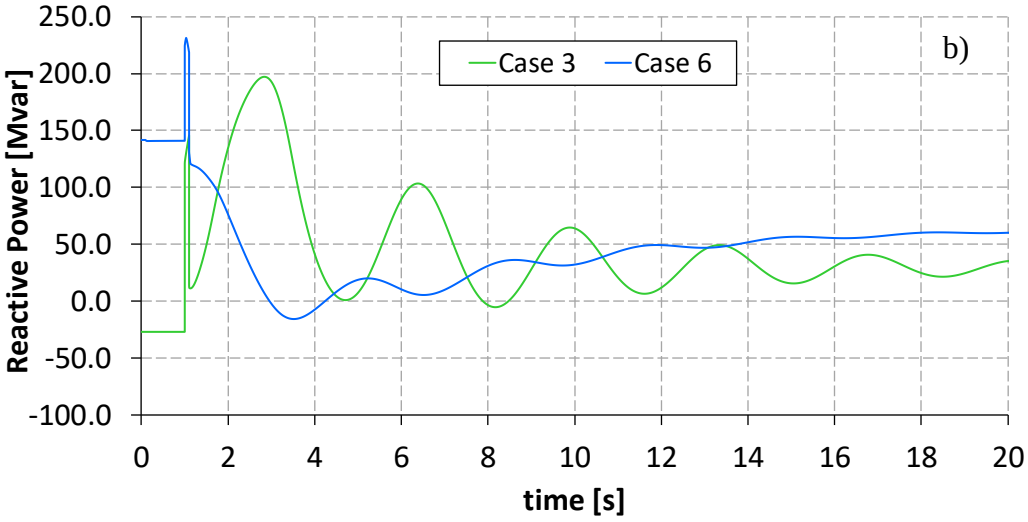

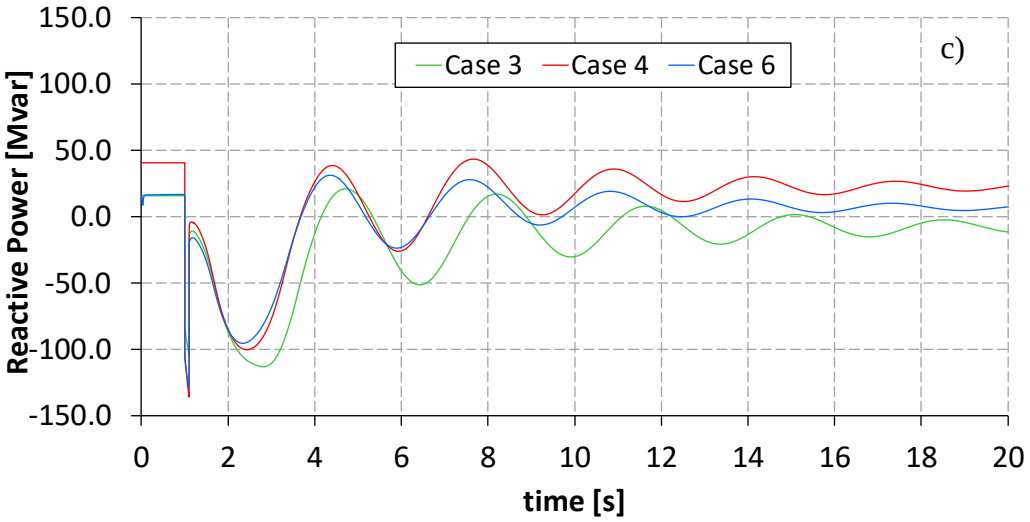

Fig. 2.17. Scenario A. Reactive power injections at FNO nodes (a), VLL node (b) and at an SC in South zone (c) in different cases.

As regards steady-state and dynamic contingency-based maximum zonal exchanges, a synthetic overview is provided in Table 2.5. A slight advantage in steady-state is obtained in Case 2, whereas no remarkable improvement in transient is registered. In these two cases, the limiting N-1 condition is observed for low-voltage bounds (Vmin in Table 2.5) on the Adriatic corridor. Case 3 shows the first increase of margin in dynamic analysis, and the presence of SCs implies the alleviation of voltage problems, in fact the limiting N-1 condition is detected for line rating (Imax) of a 220-kV line. Cases 4, 5 and 6 involve a remarkable steady-state increase, but the presence of LCC without SC in Case 4 does not give remarkable dynamic advantages with respect to Case 3. Cases 5 and 6 show close performances in both steady-state and dynamic tests. In any case, the critical N-1 event corresponds to the double-circuit line outage analysed in the CCT study. Moreover, it can be seen that the presence of the 1000-MW HVDC link implies an increase of static margin close than its nominal power, whereas dynamic margin is always well below this value.

Table 2.5. Scenario A: Contingency-based maximum zonal exchange on Centre-North – Centre-South border.

Case	Zonal exchange [MW]	Static max [MW]	Static margin [MW]	Static limiting N-1 condition	Dynamic max [MW]	Dynamic margin [MW]
Case 1	3273	3318	45	Vmin	3273	0
Case 2	3291	3516	225	Vmin	3291	0
Case 3	3293	3608	315	Imax	3516	223
Case 4	3304	4348	1044	Vmin	3666	362
Case 5	3304	4432	1128	Imax	4031	727
Case 6	3304	4432	1128	Imax	4126	822

The results of CCT determination in Scenario B are illustrated in Table 2.6. It can be noted that, in the presence of low loading conditions and high contributions from renewable and distributed generators, the involvement of a lower number of conventional plants can jeopardize system stability, with CCT slightly lower than 100 ms. Planned development projects in Case 2 already imply a remarkable improvement of dynamic features, due to higher meshing and to the inertial contribution of SCs, but without dynamic reactive support the LCC architecture for the new HVDC link in Case 4 could even downgrade system performances, i.e. a lower CCT. On the other hand, SCs in Case 3 result in strong enhancement of dynamic performances, and the presence of HVDC with voltage regulation ability (LCC+SC in Case 5 and VSC in Case 6) do not imply remarkable advantages under this regard.

Table 2.6. Scenario B: CCT determination.

Case	CCT [ms]
Case 1	95
Case 2	230
Case 3	350
Case 4	210
Case 5	340
Case 6	360

The determination of contingency-based maximum zonal exchange is summarized in Table 2.7. It can be seen that the maximum base exchange level increase is found in Case 2; however, no remarkable advantage is yielded by the presence of grid developments nor by additional SCs in Case 3, both in steady-state and dynamic conditions. In all these cases, the critical N-1 event is detected on the Adriatic corridor, and the binding condition is represented by a line rating on the same side. This issue is overcome by the installation of HVDC, in fact for Cases 4, 5 and 6 the critical N-1 event corresponds to the double-circuit line outage analysed in CCT study, and the binding condition is minimum voltage. A remarkable increase of maximum power exchange is therefore observed, even higher than in Scenario 1 for static analysis. Whereas, the dynamic margin in Case 6 is lower than in Case 5; this can be ascribable to the initial criticality registered for the Adriatic side, requiring a further level of control that SCs can provide. This shows that the dynamic margin depends on the effect of the adopted control scheme on the different operating conditions, and it is always lower than HVDC power rating.

In Fig. 2.18 and Fig. 2.19, trends of voltage and frequency values at HVDC link extreme nodes are shown for Cases 4, 5 and 6, respectively (Case 1 is unstable therefore it is not plotted). It can be seen that in this Scenario, with a different starting point and lower inertia, the oscillations

are more severe and higher spikes are present, though staying below intervention threshold of protection system.

Table 2.7. Scenario B: Contingency-based maximum zonal exchange on Centre-North – Centre-South border.

Case	Zonal exchange [MW]	Static max [MW]	Static margin [MW]	Static limiting N-1 condition	Dynamic max [MW]	Dynamic margin [MW]
Case 1	3306	3306	0	Imax	3210	-96
Case 2	3529	3529	0	Imax	3529	0
Case 3	3537	3537	0	Imax	3537	0
Case 4	3328	4188	860	Vmin	3706	378
Case 5	3343	4533	1190	Vmin	4246	903
Case 6	3349	4533	1184	Vmin	4070	721

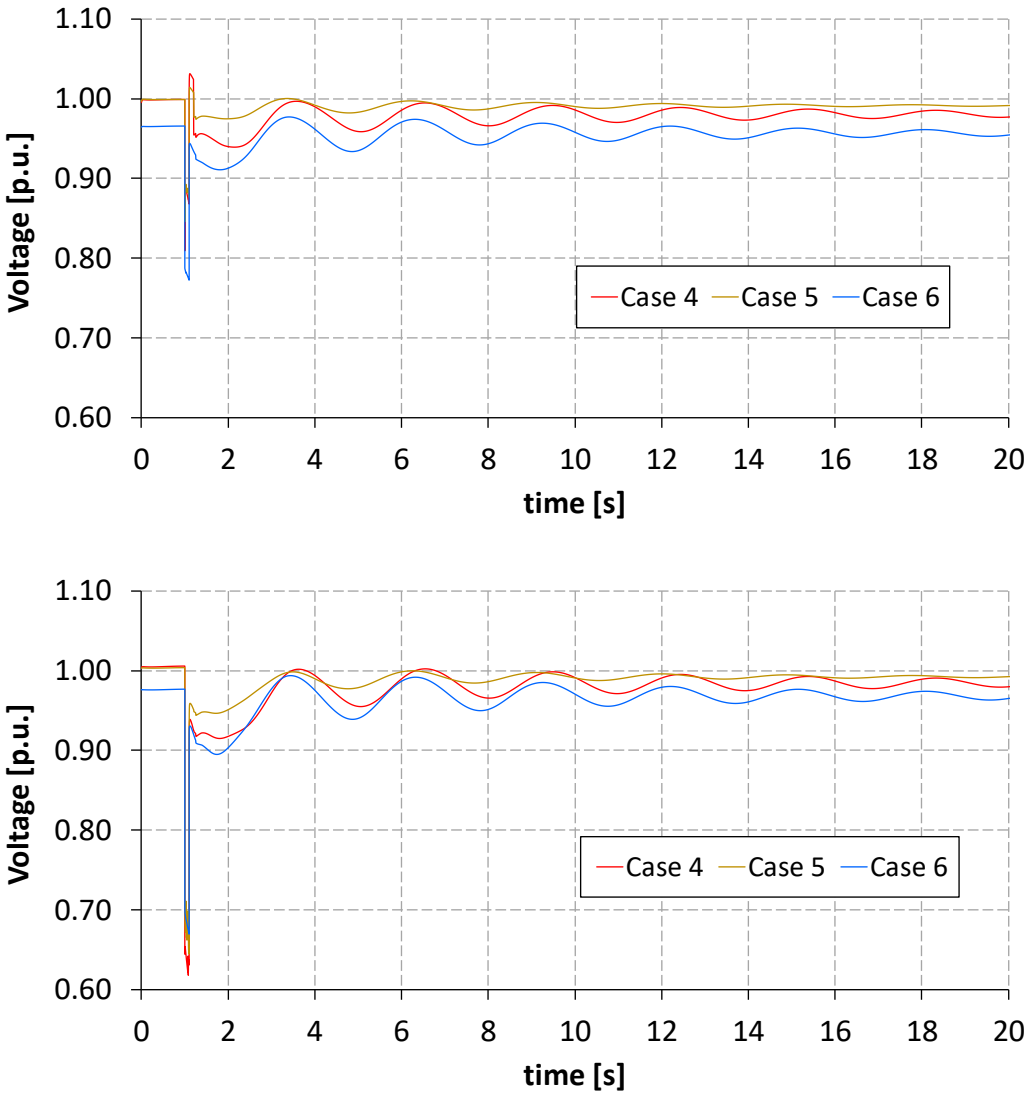

Fig. 2.18. Scenario B. Nodal voltage at FNO node (top) and VLL node (bottom) in different cases.

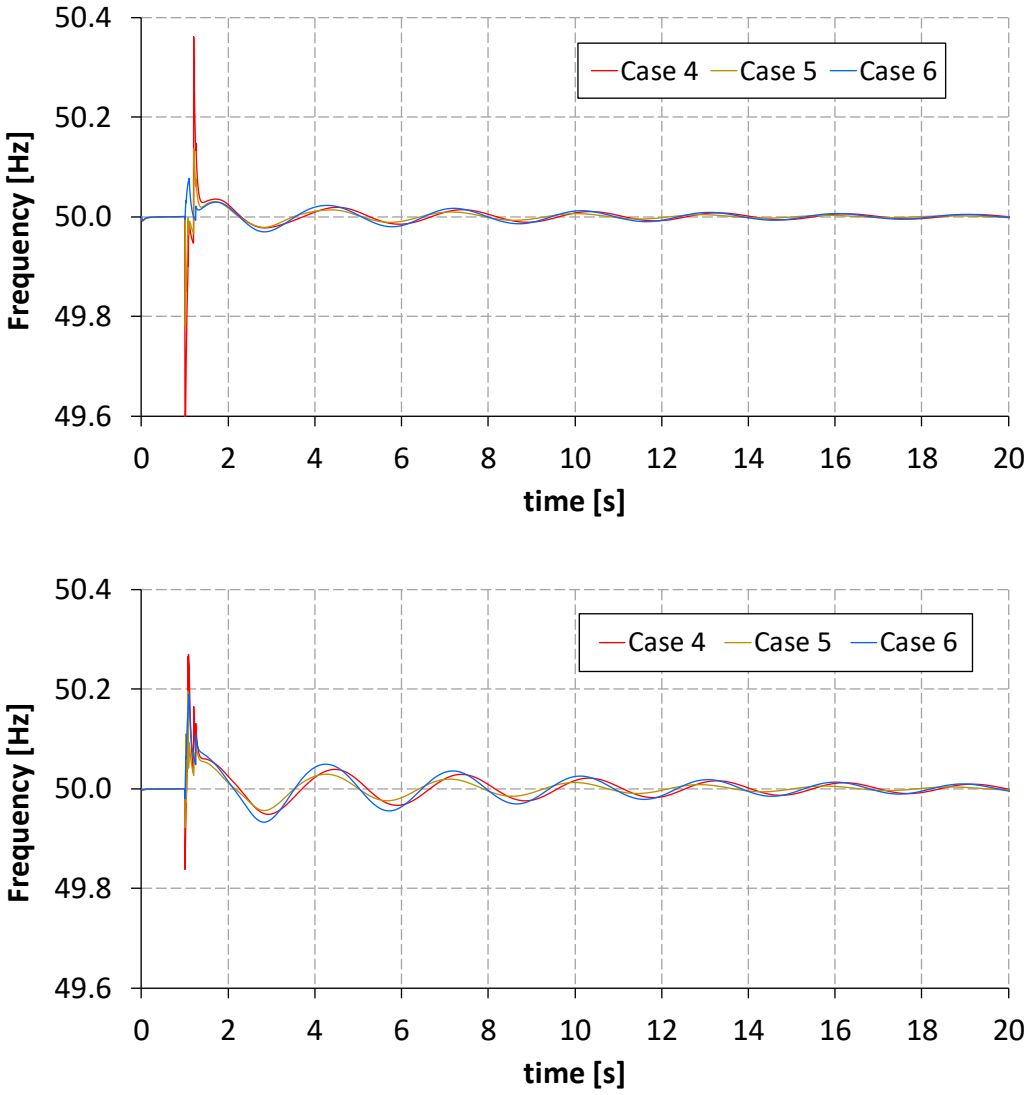

Fig. 2.19. Scenario B. Values of frequency at FNO node (top) and VLL node (bottom) in different cases.

2.2.3 Impact of the HVDC project on the power system loadability in future long-term planning scenarios

This section focuses on the transfer capacity increase across the critical section Centre South – Centre North allowed by the planned Villanova-Fano HVDC connection.

A static assessment of the maximum power transfer capacity of the 400 kV Adriatic backbone portion under study has been performed in both the current situation (named "as is" scenario) and in presence of the planned HVDC link between the Fano and Villanova nodes ("after HVDC implementation" scenario). In this last scenario, the Line Commuted Converter (LCC) technology has been considered together with the installation of synchronous compensators at the converter stations, to provide the needed reactive support. Let the bus named "S" ("Sending") be the Villanova node, and the bus "R" (Receiving") be the Fano node: the simplified single-line diagram of the new configuration is depicted in Fig. 2.20:

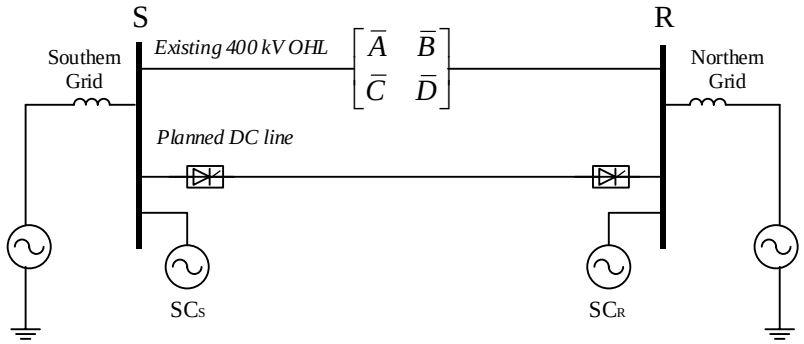

Fig.2.20. Simplified single-line diagram of the new configuration including the LCC-HVDC link and the synchronous compensators at the line terminals.

Rated power of the new HVDC link is assumed to be 1000 MW, while the overexcited output of each synchronous compensator is taken at 250 Mvar.

2.2.3.1 Forecasted scenarios

The generation mix, production forecast and demand trend, both in the European context and in the National one, are described in [119], [120].

Fig. 2.21 shows the increasing electrical demand trend in all scenarios under study: in comparison with the final value for year 2017, the DG scenario is affected by the most significant increase (+17%) because of the larger demand growth in heating and transportation sectors, while ST and the Integrated National Energy and Climate Plan (named "NECP") scenarios are characterized by smaller increases (+12% and +3%, respectively).

The installed generation capacity forecast (GW) for all scenarios considered is shown in Fig. 2.22. As a consequence of the increase in distributed generation sources and of CO_2 emissions reduction targets, the 2030 year horizon generation mix consists of a major renewable installed capacity (Fig. 2.23).

Fig. 2.24 reports the simulated number of congestion hours across the critical Centre South – Centre North section: due to the large renewable generation in Southern Italy, the power flow direction will be mainly from South to North with an increasing number of congestion hours, while the number of congestion hours in the opposite direction will decrease (down to zero hours in ST 2030 and DG 2030 scenarios). It is clear that the reinforcement of the Centre South – Centre North section on the Adriatic side is a key factor for a major renewable integration in the South of the Country.

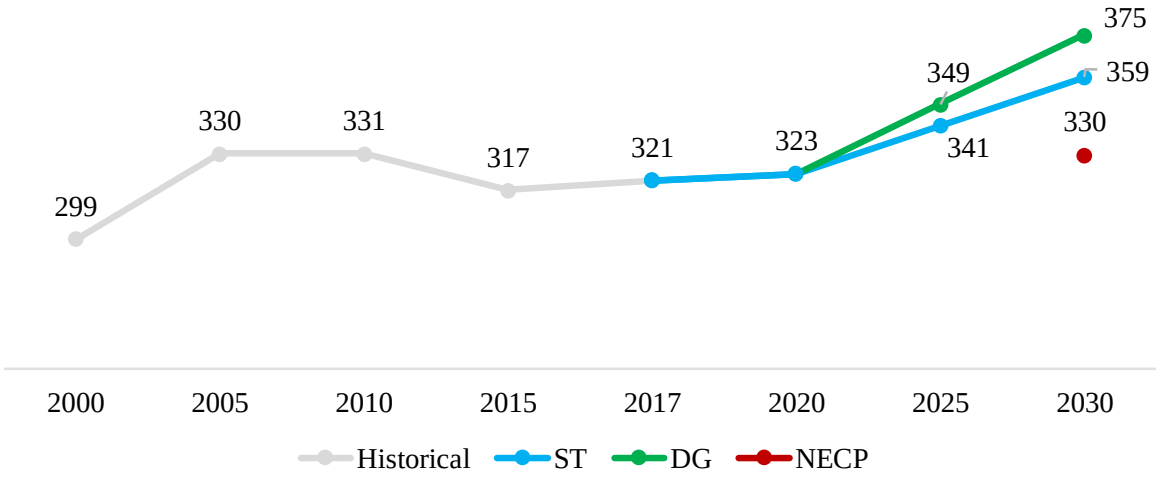

Fig. 2.21. Demand trend for Italy (TWh) in the European and National scenarios at 2030 year horizon.

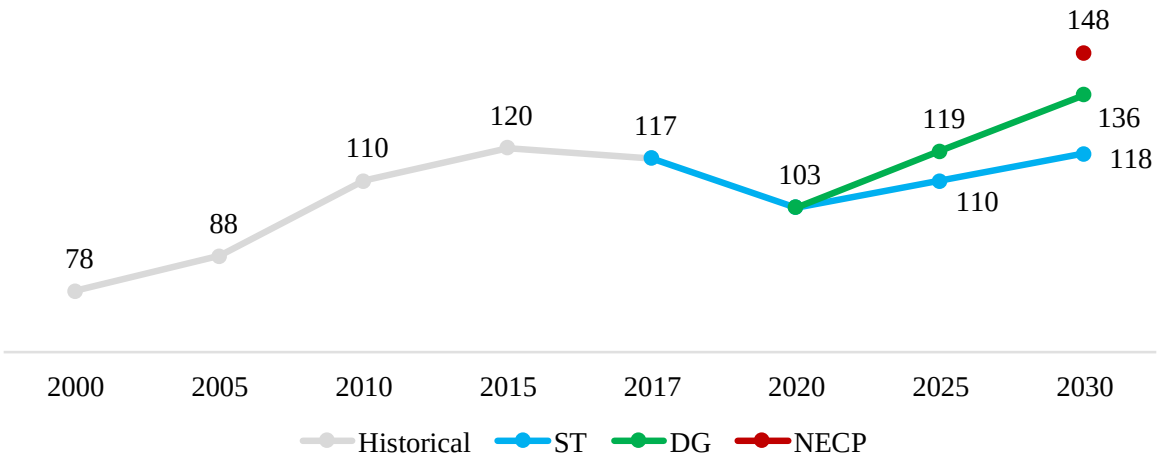

Fig. 2.22. Generation capacity forecast for Italy (GW) in the European and National scenarios at 2030 year horizon.

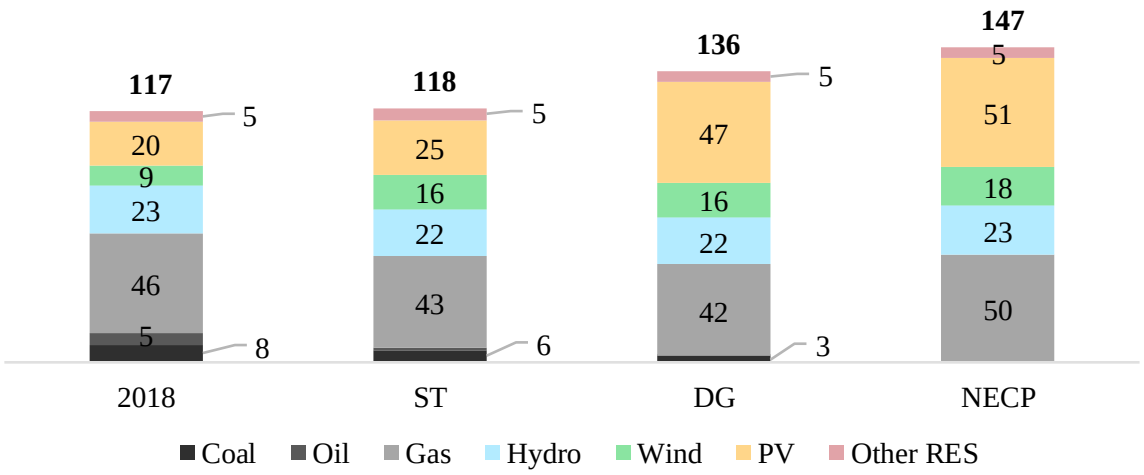

Fig. 2.23. Generation mix for Italy (GW) in the European and National scenarios at 2030 year horizon.

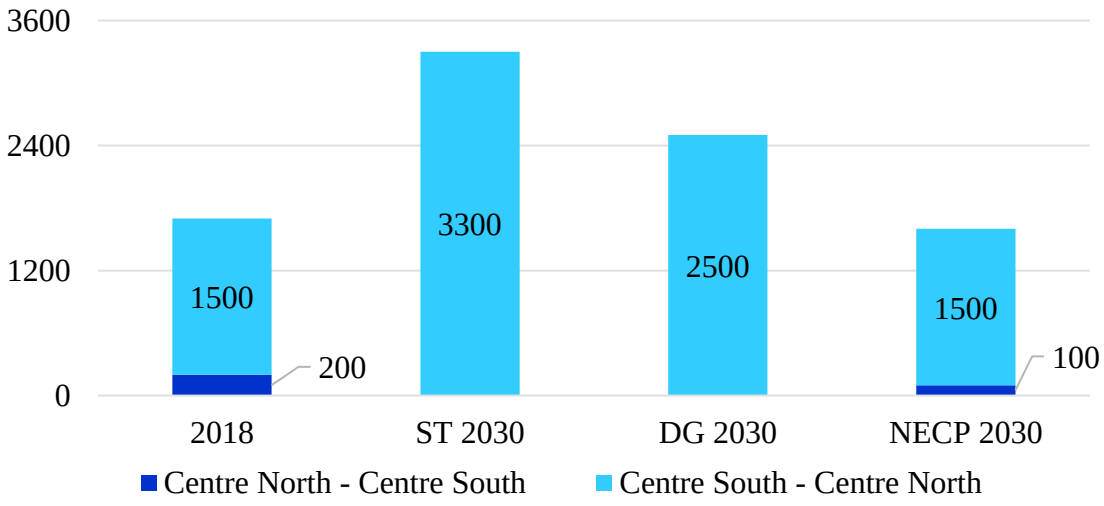

Fig. 2.24. Number of congestion hours expected in the European and National scenarios at 2030 year horizon in comparison with the present situation.

2.2.3.2 Loadability

The line loadability represents the load-carrying capacity of a transmission line operating in specific conditions. Transmission line loadability is historically represented by means of the St. Clair curves [121]. These curves represent the theoretical maximum power transmission capability of overhead lines as a function of the line length. They have been used for network planning in the power industry, being based on practical consideration and experience. In fact, in [122] the characteristics that affects the maximum transmitting current (power) on a line are presented in an analytical way. In particular, these depend on conductor thermal behavior, voltage drop across the line, power losses and steady state stability limit. In [77], the 'universal loadability curve' is reported with the same methodological approach, for uncompensated lines

and applicable to all voltage levels. Moreover, other factors that affect the loadability for long lines are highlighted in [123], [124], in terms of voltage quality and Joule losses.

Loadability curves are characterized by different regions (i.e. shorter lines), or ranges of length. Generally speaking in the first region the maximum power allowed is determined by the conductor thermal limit. In the second region, the admissible power is limited by the voltage drop limit (voltage quality constraint), ΔV_{max}. Typically, a 5% maximum voltage drop across the line is considered to adequately represent the condition of a line carrying heavy, but permissible, loads without encountering unusual operating problems.

For uncompensated lines, the first region ranges from L=0 km to roughly L=30÷100 km, depending on the conductor size, line parameters, load power factor, and voltage drop limit. The second region is wider, and can extend up to more than L=400 km. For longer lines, further regions can be determined, based on other constraints posed by line or system performance: steady-state angle stability margin, voltage stability requirements and maximum Joule losses allowed along the line.

The voltage-related capacity limits of transmission lines can be extended by means of devices for reactive power control. In particular, [125] and [126] show as synchronous condenser connected at the receiving node can increase the line loadability. Line compensation by series capacitors is a well-known, effective means to enhance transmissible power under voltage and angle constraints [1]; such an application in the Italian national transmission network, was recently proposed in [101]. It should be pointed out that the reduced line losses and improved voltage regulation and efficiency of the line also result from series compensation.

Finally, the installation of a new transmission line must be cited. This would obviously be the best long-term reinforcement option whenever a transmission line capacity limits are reached , so as to alleviate overloading by providing additional paths for power flow. It would also be beneficial by increasing the reliability of the transmission system. However, the construction of new 400 kV OHLs finds formidable obstacles in terms of authorizations and local oppositions. Local opposition to the installation of new lines could be circumvented by resorting to underground cables along part or all of the line right-of-way. However, despite the substantial increase in EHV AC cable performance [127] – [129] and an attendant decrease in unit costs, the cable line is still several times costlier than the overhead one, for a given length. These issues can be overcome through HVDC, as shown in [130]. The comparison between different HVAC and HVDC transmission options in terms of accessibility, load-carrying capability, efficiency, reliability, stability, is represented in [131].

2.2.3.3 Capability of the present 400 kV backbone – "As Is" Configuration

In order to obtain the operating envelopes in the (P,Q) plane, thermal rating and maximum/minimum voltage constraints are imposed in turn in each node of the system by using the same approach illustrated in the Chapter 1; with simple manipulations, it is possible to obtain explicit the expressions of the complex power at receiving-end as a function of voltage and current phasors as dictated by the different thermal and voltage constraints:

$$\bar{N}_{R_{i-constr}} = 3 \cdot \bar{E}_{R_{i-constr}} \cdot \bar{I}^{*}_{R_{i-constr}} \tag{2.7}$$

Where $\bar{E}_{R_{i-constr}}$ and $\bar{I}_{R_{i-constr}}$ are the receiving-end voltage and current phasors as dictated by the *i*-th constraint. Besides the terminal buses VLL and FNO, the system under study consists of three other intermediate nodes: five capability curves result by the assignation of the thermal limits and ten operating envelopes are related to maximum/minimum voltage limits in all nodes. In practice, elliptical loci in the (P_R, Q_R) complex plane are obtained by enforcing the terminal currents magnitudes equal to the thermal rating and maximum/minimum voltage magnitudes, while the phases are free to vary in the 0°÷360 ° range.

Fig. 2.25a shows the receiving-end capability curves of the "as is" configuration as dictated by the maximum current constraints: the highest point of the capability curves i.e. the maximum active power value, is associated to an exceedingly large reactive power demand at the receiving-end, and operation of the line under these conditions is not feasible due to excessive voltage drop. The operating envelopes obtained by enforcing only the maximum/minimum voltage constraints are not reported for the sake of brevity, since the highest points of the attendant capability curves are related to unfeasible operational conditions.

Only the area enclosed by both the voltage-limited and the current-limited capability curves in the (P,Q) plane, shown in Fig. 2.26b, is viable: the maximum power transfer capacity allowed in compliance with feasible operational conditions is around 1500 MW.

2.2.3.4 Capability of the HVDC system in parallel with the existing 400 kV backbone

When the proposed network reinforcements (HVDC link plus synchronous compensators) are taken into account the operating envelopes in the complex plane show a visible increase in terms of active power transfer and reactive power range enclosed (Fig. 2.25b and Fig. 2.26b). The maximum power transfer allowed by combined current and voltage limits attains more than 2400 MW.

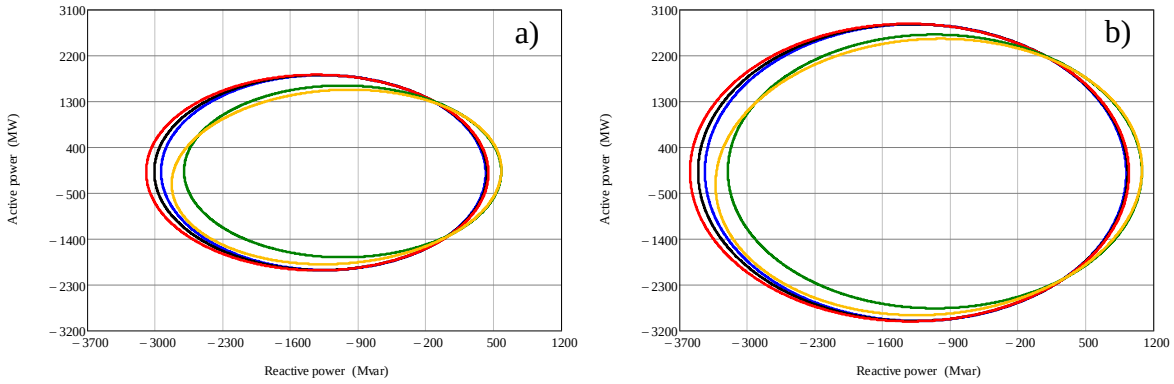

Fig. 2.25. Receiving-end (P,Q) capability curves of the “as is” (a) configuration and of the “after HVDC implementation” (b) configuration as a results of the maximum current constraints in each segment.

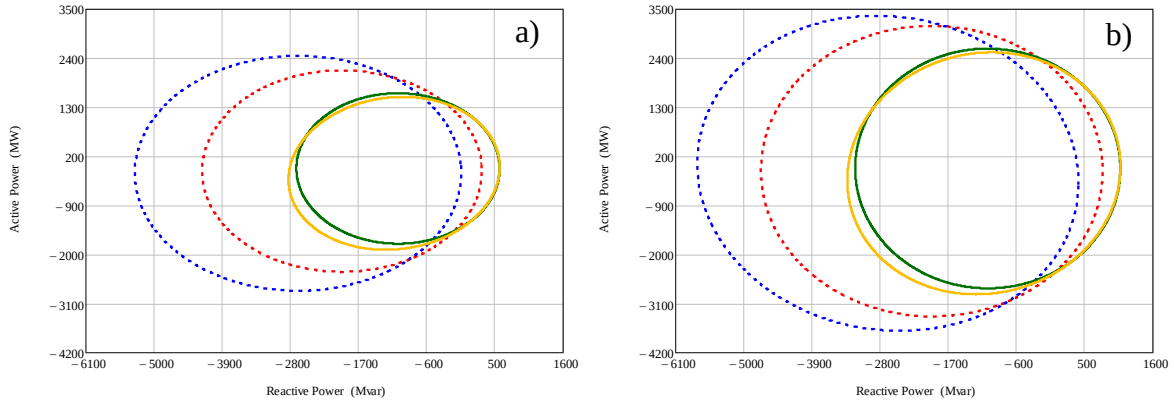

Fig. 2.26. Most voltage- and current-limited receiving-end (P,Q) capability curves of the “as is” (a) configuration and of the “after HVDC implementation” (b) configuration.

2.2.4 Conclusions

In this section, a methodology to analyse the impact of network developments on steady-state and dynamic performances in N-1 conditions has been provided, with a focus on grid security assessment and on market efficiency. The method has been applied to the assessment of different architectures for the new planned HVDC Adriatic project within the Italian transmission network, exploiting the software tools used by the Italian TSO for the secure and economic operation planning. In particular, two operating scenarios representative of critical situations with high power exchanges across the zonal structure and limited stability margins have been considered. Six cases have been analysed, accounting for different network development levels and for the further presence of the new HVDC link realized either as a LCC (with or without synchronous compensators for reactive support), or as a VSC.

Results have shown that the planned network developments reduce the risk of dynamic instability, but have a limited influence on the power transfer capacity between the two zones, and even typical LCC control allows an increase of static margins but yields limited improvement in dynamic stability. Whereas, comparable performances have been observed for the VSC technology and for the LCC integrated with synchronous compensators, although power transfer limits do not take advantage from the full capacity of the HVDC link in dynamic assessment, when dynamic stability limits are considered.

Furthermore, an assessment of the maximum power transfer capacity of the 400 kV Adriatic backbone between VLL and FNO at 2030 year horizon without and with the planned Adriatic HVDC project has been provided. The operating envelopes of both configurations were evaluated by enforcing voltage- and current-based constraints.

1. In the “as is” configuration, the considered portion of the 400 kV Adriatic backbone allows a maximum power transfer capacity of 1500 MW;
2. The implementation of the new HVDC link yields +1000 MW increase of the active power transfer along the section Centre – North / Centre – South, while the synchronous compensators at the terminal nodes provide the needed reactive support enhancing voltage profile in the vicinity of the link.

2.3 Evaluation of thermal performance for power system development

The remarkable renewable generation capacity installed in the South of Italy can determine high loading conditions of the 400 kV – 50 Hz backbones located in the area. The resultant conductors' temperature increase accelerates the deterioration of components with negative effects in terms of system reliability and economic performance. In this study, the thermal analysis of a selected set of EHV transmission lines spanning the critical section Centre South – South is carried out both in the current and in the future energy scenario at 2040 year horizon, with or without the planned developments. The conductors' temperature is calculated via the heat balance equation and corresponding resistance and losses increases are obtained. Results highlight the benefits related to the presence of the planned reinforcements.

2.3.1 Introduction

The electricity sector deregulation has emphasized, especially for the Transmission System Operator (TSO) the issue of efficient exploitation of network assets. In particular, although the evolution of electricity demand is properly forecast in short-term and in long-term windows, the presence of new and diffused power production initiatives, mostly exploiting non-programmable energy sources, can imply systematic violations of network operating constraints. In such a case, the TSO faces three possible options, i.e. reinforcing the network with new transmission lines, installing network control devices, such as FACTS and PSTs in the substations, or at least accept a more severe exploitation of the transmission assets [132]-[135].

In particular, the power flow along overhead transmission lines, usually determined by steady-state network analysis, is ultimately limited by current rating. This is determined according to the thermal performances so that, when carrying the specified current level, the conductor temperature stays below a specified threshold in standardized weather conditions, (usually depending from the installation site), and the conductor sag ensures safety distance from the ground and other conductors. However, this limit could be revised according to the actual weather conditions affecting the line operated, depending on thermal energy balance of the conductor [136]: different schemes of dynamic line rating have been realized to this purpose [137]. Dynamic thermal rating is of increasing interest in systems with high renewable penetration, especially because strong wind conditions imply higher power generation along with higher thermal rating [138]. For instance, [139] considers dynamic rating in operating condition studies for reliability analysis accounting for curtailment; whereas an overload

management strategy complying with risk levels is presented in [140]. Spatial variation of thermal rating along the line is accounted by [141] in an interpolating method.

Higher currents, and consequent higher temperature levels, can be reached in order to withstand temporary conditions, e.g. in the case of network contingencies, but they imply increased conductor temperature, involving increased power losses and higher mechanical stress of the conductor, up to the onset creep [142]. A specific attention to high temperature models is provided in [143], whereas an estimation of core temperature by means of neural networks is presented by [144]. These conditions can imply a reduction of useful lifetime of the overhead line, to be evaluated in order to plan replacement or reinforcement.

As regards system planning, [145] suggests quasi-dynamic thermal rating based on confidence levels of seasonal observations, whereas in [146] yearly operation conditions and thermal ratings are compared in terms of probability distribution functions. Moreover, [135] integrates dynamic thermal rating in stochastic transmission expansion planning, and dynamic thermal rating is involved in the framework of emission reduction in [147].

Thermal aging of overhead lines, due to overload events, is studied according to creep phenomenon in [148], and analogous estimations are embedded in network-level cascading overload estimation in [149] and in a redispatching method based on losses in [150]. Whereas, in [151] the aging failure model depending on temperature is evaluated according to Arrhenius-Weibull, and in [152] aging based on loss of tensile load is applied to spatial analysis of a line.

All evolution scenarios elaborated for the Italian power system estimate an increase of load demand and renewable generation [153]. In particular, the “Decentralized” (DEC) energy scenario at 2040 year horizon forecasts an increase of +22% in load demand and +215% in RES generation capacity installed compared with the final values for year 2018. Therefore, a method to account for aging effect of overloads in planning appears of great interest. Moreover, the reduction in average conductor aging in the presence of future network operating conditions could represent an evaluation element in cost-benefit analysis.

In this Section, a procedure to estimate the thermal performance of overhead lines is proposed and applied to the Italian power system over actual yearly operating conditions. Moreover thermally stressful conditions are evaluated in the current configuration and in an evolution scenario of network and generation/load.

2.3.2 Methodology and case study

The proposed analysis method can be divided into three parts. For the network configuration under study, according to load and generation dispatch data from economic consideration and technical forecasts, steady-state network operation is analysed by means of complete AC load flow, yielding the loading level of lines. Therefore, a proper line thermal model is subsequently implemented for each network component, in order to determine the effective conductor temperature and the consequent losses. Since these two values modify in turn the load flow solution, the two models are repeated iteratively until convergence is reached. Therefore, according to the obtained results, network-level aging indicators are determined.

In order to inspect the effect of the provisional development plan on network aging, the method is applied to different scenarios, and the difference of network aging is taken as an additional measure of planning benefit.

Since the aim is to evaluate the thermal operating conditions of overhead lines in steady-state analysis, and given that the transient behavior induced by a step variation of any input (e.g. power flowing, weather variables) is usually terminated in less than one hour [138], [143], the static thermal model provided in [136] is employed. The conductor thermal balance is given by:

$$q_c + q_r = q_s + r \cdot I^2 \tag{2.8}$$

where I is the steady state current flowing into the line, r is the conductor resistance and depending on temperature:

$$r = r_{20} \cdot k_{sk} \cdot [1 + \alpha_{20} \cdot (T_c - 20)] \tag{2.9}$$

being r_{20} the conductor resistance at 20 °C, k_{sk} is a coefficient taking into account the skin effect and α_{20} is the temperature coefficient.

The convective heat loss q_c, radiated heat loss q_r and solar heat gain q_s in (37) can be formulated as follows [154]:

$$q_c = \pi \cdot \lambda_f \cdot (T_c - T_a) \cdot N_u \tag{2.10}$$

$$q_r = E \cdot S_s \cdot \pi \cdot d \cdot (T_c^4 - T_a^4) \tag{2.11}$$

$$q_s = \beta \cdot S_i \cdot d \tag{2.12}$$

Defining:

- λ_f the air thermal conductivity;
- T_c the conductor temperature;
- T_a the ambient temperature;

- N_u the Nusselt number, which can be differently expressed depending on whether is the convective heat loss natural or forced;
- E the conductor coefficient of emissivity;
- S_s the Stefan-Boltzmann constant;
- d is the conductor diameter;
- β the conductor coefficient of absorbivity;
- S_i the solar radiated heat intensity.

Under the most unfavorable conditions, a wind speed v of 5 m/s can be assumed, and the expression (38) can be simplified as:

$$q_c = 8.55 \cdot (T_c - T_a) \cdot (v \cdot d)^{0.448} \tag{2.13}$$

Therefore, according to the electric current and the weather conditions, conductor temperature T_c is determined by solving the following fourth degree equation:

$$AT_c^4 + BT_c + C = 0 \tag{2.14}$$

Where the coefficients A, B and C are defined as:

$$A = -(E \cdot S_s \cdot \pi \cdot d) \tag{2.15}$$

$$B = [r_{20} \cdot k_{sk} \cdot \alpha \cdot I^2 - 8.55 \cdot (v \cdot d)^{0.448}] \tag{2.16}$$

$$C = [r_{20} \cdot k_{sk} \cdot I^2(1 - \alpha \cdot T_a) + \beta \cdot S_i \cdot d + 8.55 \cdot T_a \cdot (v \cdot d)^{0.448} + E \cdot S_s \cdot \pi \cdot d \cdot T_a^4] \tag{2.17}$$

Once conductor resistance $R(T_c)$ is obtained from (37), it is used in the load flow equations, expressed below the generic node i:

$$P_{g,i} - P_{d,i} = \sum_{k \in i} Y_{ik} \cdot V_i \cdot V_k \cdot cos(\vartheta_i - \vartheta_k + \varphi_{ik}) \tag{2.18}$$

$$Q_{g,i} - Q_{d,i} = \sum_{k \in i} Y_{ik} \cdot V_i \cdot V_k \cdot sin(\vartheta_i - \vartheta_k + \varphi_{ik}) \tag{2.19}$$

where the elements of nodal admittance matrix $\dot{Y}_{ik} = Y_{ik} \angle \varphi_{ik}$ are influenced by the presence of a line from node i to node k, represented with a π-circuit with temperature-dependent longitudinal resistance R

Once the load flow problem is solved, the current flowing across each line is determined and the procedure iterates determining the thermal balance. The procedure is arrested when the difference of average current loadings is less than 0.1 A and that of temperature estimates is less than 0.1 K between two consecutive iterations.

The current zonal market configuration of the Italian power system has been illustrated in previous sections (see Fig. 1.1 and Fig. 2.10). By 2021, a new zonal market configuration will involve the elimination of the Rossano virtual zone and the creation of a new Calabria market

zone [155]. However, the zonal market structure is defined on the basis of the individuation of power system sections more subject to grid congestions in some operational conditions. Once the market zones are identified, the maximum allowable power exchange between neighbouring zones is assessed [156].

This study is focused on a specific grid portion around the Centre South – South critical section of the Italian power system, depicted in Fig. 2.27. The analysis involves the 400 kV – 50 Hz overhead lines located in the area, in both the existing configuration and in the planned future one including network reinforcements.

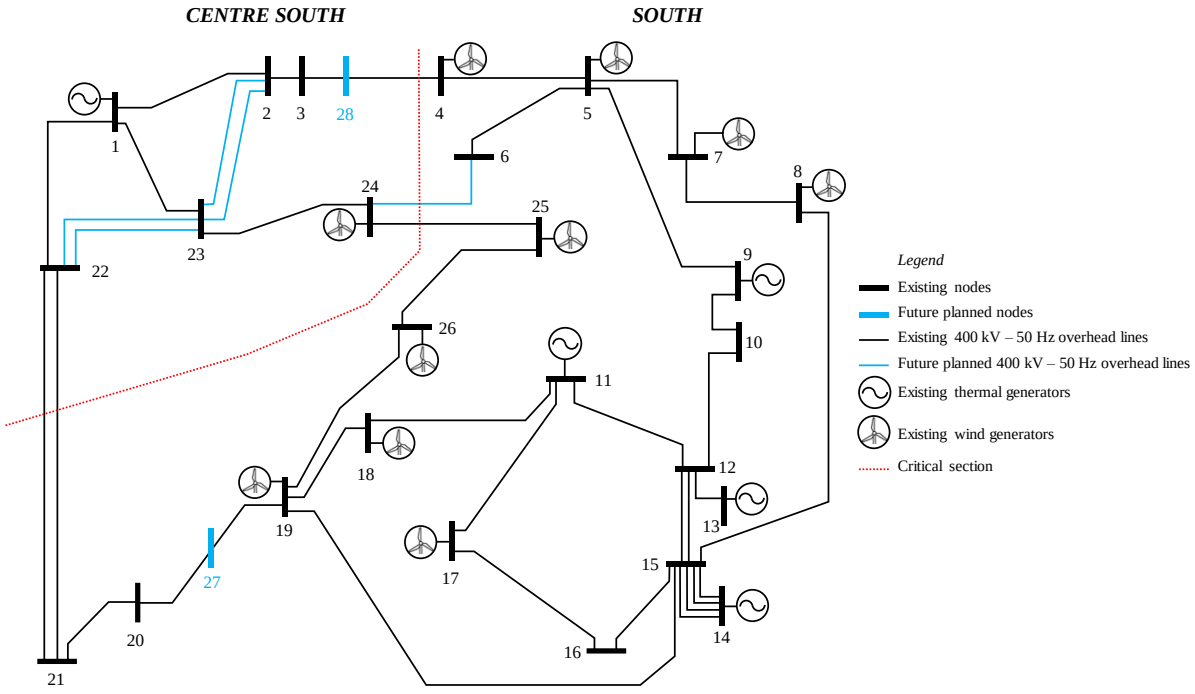

Fig. 2.27. Single line diagram of the system under study: investigated existing (in black) and future planned (in blue) transmission lines.

Nowadays, the main direction of power transfers is from the South to the North of the Country and the maximum allowable power transfer from South to Centre-South market zone is currently limited to 4600 MW, expected to be increased up to 5500 MW in the future condition including the development actions planned by the Italian TSO to avoid critical loading of the infrastructure.

The 400 kV – 50 Hz overhead transmission lines under study are equipped with Aluminium Steel-Reinforced Conductors, (ACSR),in a three conductors-bundle per phase. Conductor data are reported in Table 2.8; the cross section of the individual conductor is illustrated in Fig. 2.28.

Table 2.8. ACSR conductor technical specifications.

ACSR Conductor		
Formation	Aluminium	54 x 3.50
	Steel	19 x 2.10
Theoretical sections (mm^2)	Aluminium	519.5
	Steel	65.80
	Total	585.30
Electrical resistance at 20 °C	(Ω/km)	0.05564
Breaking load	(daN)	16852
Coeff. of thermal expansion	(K^{-1})	19.4 x 10^{-6}

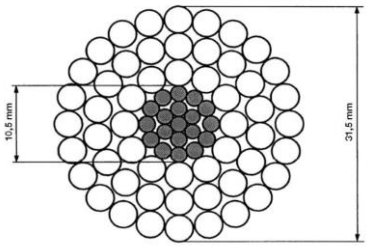

Fig. 2.28. ACSR conductor cross-section.

2.3.3 Tests results

In this sub-section the results of the study are described in the present and future planned situation. Furthermore, the analysis of loading conditions for the existing system during a year are presented.

2.3.3.1 Measured yearly loading conditions

The starting point of the analysis is represented by the yearly loading values measured for all 33 existing EHV overhead lines, referred to the system represented in Fig. 2.27. The duration curves derived from their elaboration in per unit of the thermal rating, the yearly loading (always in p.u.) and the yearly temperatures obtained by solving the heat balance equation are shown in Fig. 2.29 for the most representative transmission lines. The most relevant loading can be observed for the line L 2–3 (see Fig. 2.27) on the Tyrrhenian side, up to 120% of the thermal rating, although for a very short duration. The remaining lines under study are instead loaded well below their thermal rating. In general, higher loading conditions are observed for the transmission lines on the Tyrrhenian side, due to the presence of a more meshed 400 kV network (even besides the critical section under consideration), which collects a major amount of the power transfers from South to North of Italy.

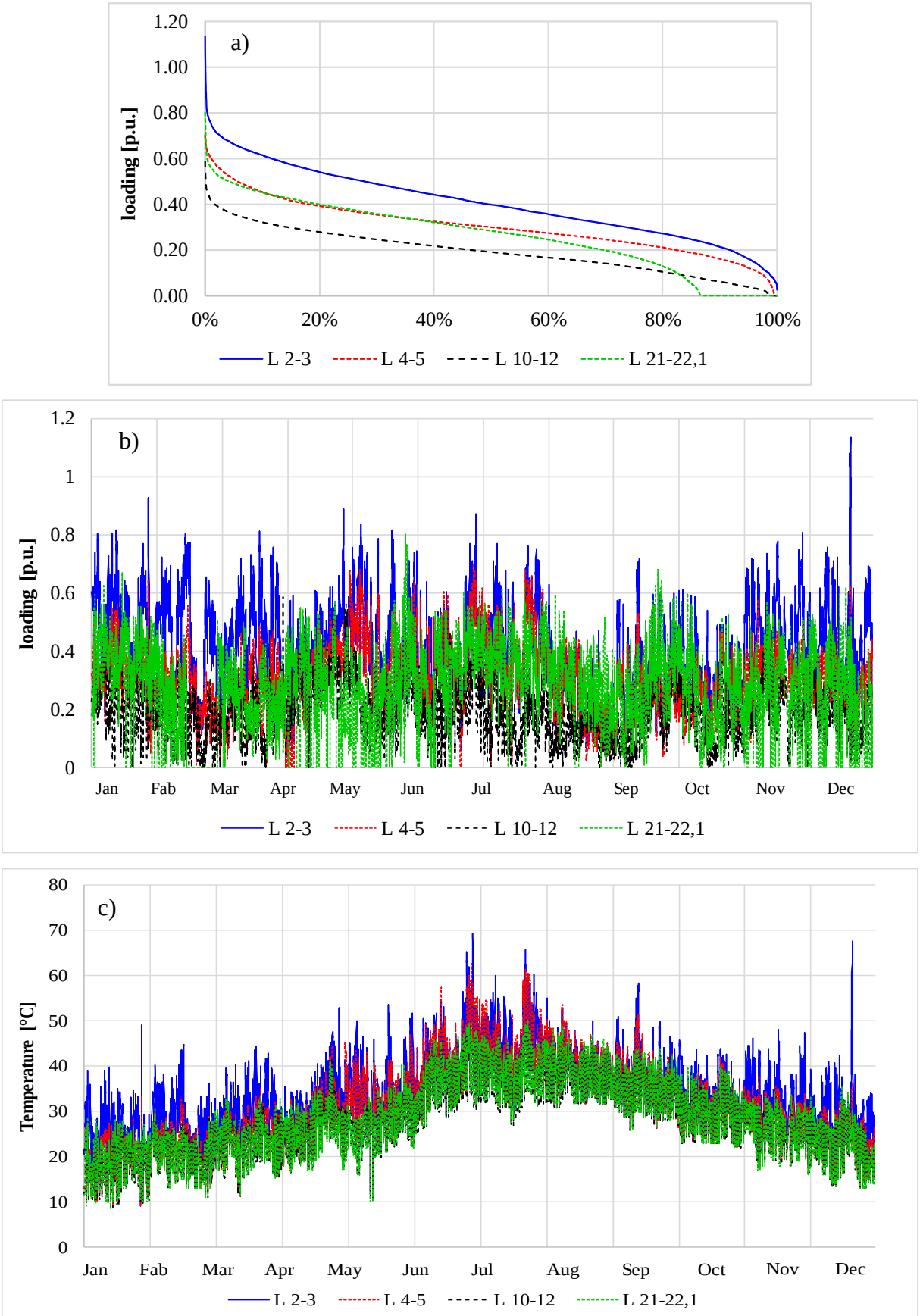

Fig. 2.29. Current loading (a), yearly loading (b) and yearly temperature (c) of the most representative EHV – OHLs under study.

2.3.3.2 Present and evolution network assessment

In order to assess the effect of network development plans on overhead line thermal performances in the network section under study, depicted in Fig. 2.27, the analysis starts from the determination of a system-level critical operating condition. This is individuated in a midday with challenging ambient conditions (air temperature 30°C, low wind and 1000 W/m² solar radiation) and remarkable renewable generation level, with an interzonal exchange at the Centre South – South border is close to the security threshold imposed at the programming stage; this is named Scenario A. It should be remarked that the analysis is run in full operating conditions (N condition) since it is not aimed at fault security assessment.

Starting from this point further scenarios are built, with main features synthesized in Table 2.9, as follows:

- Scenario B involves the same operating condition defined in Scenario A, in the presence of network development interventions included in the National Development Plan (NDP) over a ten-years horizon in the analysed section, as represented in blue in Fig. 2.27;
- Scenario C is aimed at analysing future network operating conditions, therefore it is based on the DEC future energy scenario at 2040 exploited in the NDP, characterized by a bottom-up approach with strong increases of distributed generation and of electric energy demand, pushing on end-use efficiency; moreover it considers the presence of all network development interventions planned in the NDP, involving all the national network at sub-transmission level as well, with a consequent increase of interzonal exchange limits;
- Scenario D imposes the future operating conditions in the absence of all network development interventions planned in the NDP; to this aim, the effective power exchange at zonal border is reduced by modulating zonal generation.

Load flow analysis has proved that lines are loaded at most at 60% of their rated current, showing that the network can bear stressful conditions without particular problems. The relevant distribution of line temperature levels obtained from the application of thermal model is reported in Fig. 2.30 in the boxplot form. It can be noted that ambient conditions make conductor temperature start from roughly 39 °C. In Scenario A the median value is 41.2 °C with a 48.7 °C maximum, the 25-75 percentile interval is 3.2 °C, and average value is equal to 41.8 °C. In Scenario B a moderate reduction of median, average and maximum values is observed, by 0.65, 0.20 and 0.75 °C respectively. In Scenario C, although loading is increased, the network developments imply further temperature reductions, especially for average and

maximum values (-0.8 °C and -4.1 °C with respect to Scenario A), and conductor temperature variability is smaller as well (25-75 percentile interval is 2.4 °C). Whereas, in Scenario D an increase of median and average temperatures in comparison with Scenario A is detected (by 0.6 and 0.3 °C respectively), although maximum temperature is just 47.1 °C.

Table 2.9. Present and evolution network study: features of analysed scenarios.

Features of analysed scenarios		**Scenarios**			
		A	**B**	**C**	**D**
Network elements		35	42	46	35
Centre-South	load demand [MW]	3323	3323	10684	10684
	conventional generation [MW]	1145	1145	4445	4451
	distributed generation [MW]	1332	1332	4648	4648
South	load demand [MW]	1383	1383	4647	4647
	conventional generation [MW]	2893	2893	4847	5347
	distributed generation [MW]	1828	1828	4591	4591
South-CentreSouth exchange [MW]		4600	4600	5234	4356
South-CentreSouth limit [MW]		4600	4600	5500	4600

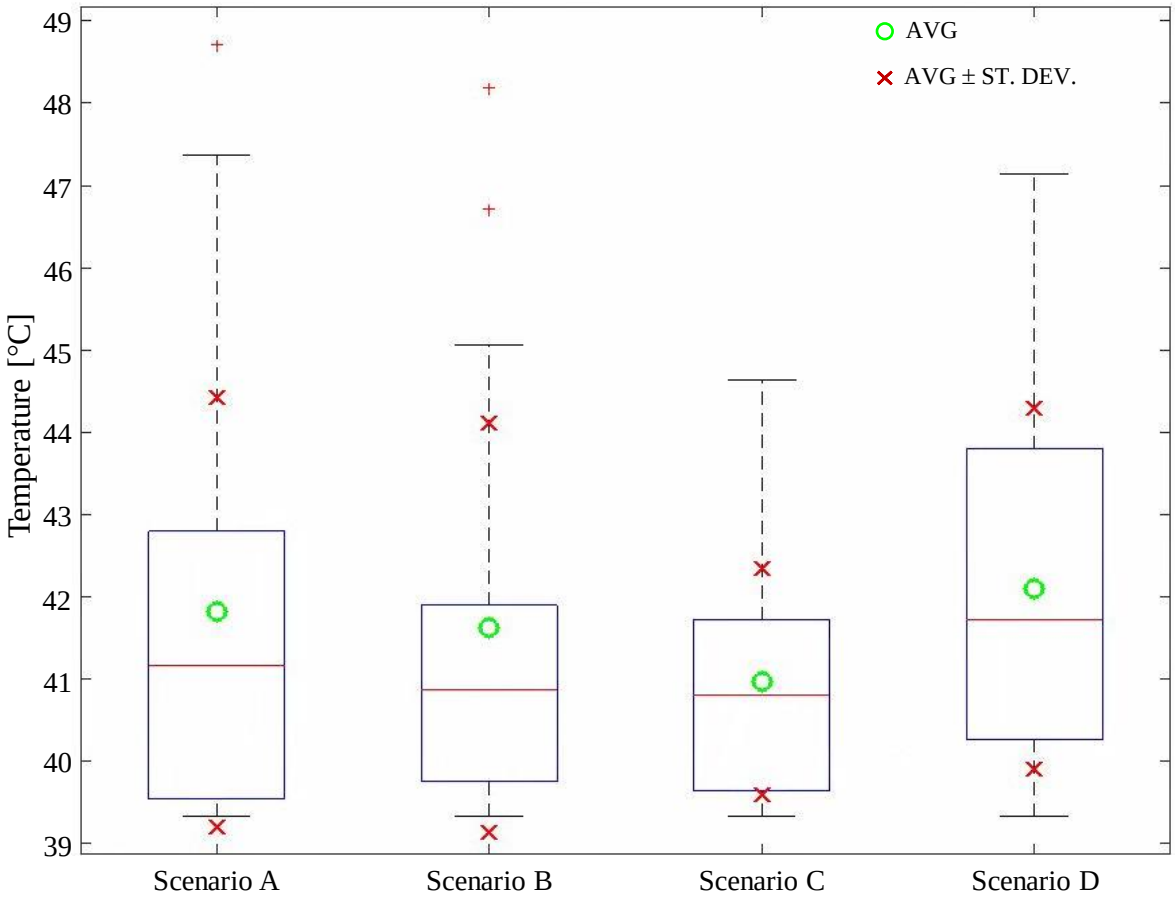

Fig. 2.30. Boxplot of conductor temperatures in the analysed scenarios.

A synthetic analysis of power losses in the four scenarios, determined at first with the standard resistance values (as reported in Table 2.8) at 30 °C temperature and subsequently with the application of the adopted thermal model, is reported in Table 2.10. It can be seen that total losses in the analysed EHV network section range from 0.2% to 0.5% of total load demand in the section, and the adoption of the thermal model allows a more precise estimation, with an increase between 9% and 35%. Losses in Scenario C are substantially lower due to increased network capacity, which reduces power flows and currents in individual lines.

Table 2.10. Active power losses estimation [MW] in analysed network section.

Active power losses estimation	**Scenarios**			
	A	**B**	**C**	**D**
Ambient temperature	24.74	21.93	11.09	24.86
Thermal model	26.98	23.85	14.98	27.00

Load-flow tests using the increased resistance values yielded by the heat balance equation are performed in scenario C and D. In the first case (scenario C), the first iteration results in an average current loading difference approximately of 0.1 A and a temperature difference less than 0.1 K: these values decrease under the selected thresholds in the second iteration. In the latter case (scenario D) an average current loading difference approximately of 5 A and a temperature difference less than 0.1 K are obtained in output from the first load-flow iteration: in the second iteration the thresholds are respected.

2.3.4 Conclusions

In this Section, a procedure to evaluate the thermal performance of overhead lines has been proposed, by means of simple polynomial equations. The model has been applied to a section of the Italian power system in order to assess of thermal stress over yearly operating conditions, highlighting lines subject to critical situations and carrying out proper correlations. Moreover, thermally stressful conditions have been evaluated in the current network configuration and in the presence of network development plans under proper future energy scenario. Simulations have proved the robustness of the EHV system and the validity of the network development project in relieving thermal performances, as well as the importance of conductor temperature update in the estimation of power flows and active power losses.

2.4 Reduced inertia power systems in high RES penetration conditions: challenges and possible solutions

In recent years, the increase of renewable generation interfaced by power electronics and the gradual shut-down of conventional power plants, are posing a serious challenge to traditional frequency control [157]. High levels of uncertainty affect the power generated by non-conventional sources, whose control and prevision are often quite difficult. Furthermore, the non-conventional generation is connected to the power system by the means of power electronic-based devices, causing a reduction of the system mechanical inertia with negative impacts on operational security. In fact, higher Rates Of Change Of Frequency (named "ROCOF") and more extreme frequency oscillations are observed in modern power systems, with reductions in the lower values (named "nadir") and increase in the higher value (named "zenith") after a system disturbance, particularly in isolated systems [158]. A major concern related to Power Electronics Interfaced Generation (PEIG) is its limited capability to support system frequency control, compared with conventional synchronous generation units [159].

In this framework, the TSOs started recognizing that with less system inertia, the power system is less capable of withstanding frequency deviations from the nominal value immediately after disturbances; the research interests have been addressed to investigating the behavior of a "weak" interconnected power system and the possible countermeasures. In literature, market designs incorporating primary frequency response in the ancillary service markets [160] have been proposed, considering the provision of inertia and the effects of uncertainties from RES [161]. Moreover, the determination of the minimum commitment cost of fast-acting storage devices for the enhancement of primary frequency responses has been provided in [162].

In the European context, the system protection and dynamics sub-group of the European Network Transmission System Operator (ENTSO-E) detected the impact of the continental Europe synchronous power systems reduced inertia when the reference incident and the system split occur. In particular, the "reference incident" is the basis for the frequency containment reserve calculations and protection scheme settings, varying with the size of the system [163].

The main objective for network planners consists in identifying a minimum level of synchronous generation penetration in the system [164], which could imply RES curtailment or additional costs for turning on/running conventional power plants. Further studies focused on the unit commitment and economic dispatch-based strategies, implementing constraints associated with the initial ROCOF following an imbalance and the level of wind curtailment [158]. Other works presented novel mixed integer linear dispatch models describing frequency

stability requirements as a function of both system inertia and maximum contingency size, with the aim of reducing operational costs and renewable curtailment [165], and optimizing the energy production and the allocation of inertial and primary frequency response. Finally, different studies proposed the implementation of the linearized inertia constraint [166] – [168] despite the strictly non-linear real behavior.

However, application of the above approaches resulted to real planning analyses met with some difficulties. Therefore, in a specific study carried out in collaboration with the Politecnico of Turin (Italy), the research activity focused on the impact of different inertia constraints implementation in the day ahead market simulator algorithm currently used for planning market study in the National context (NDP) and in the European one (European Ten Year Network Development Plan, "TYNDP") in order to obtain an economic dispatch taking into account inertia requirements in future energy scenarios.

The proposed methodology involves market analysis including significant "inertia thresholds", comparing the results in terms of overall system costs and frequency security performance, using dynamic simulations. Finally, the Technique for Order Performance by Similarity to Ideal Solution ("TOPSIS") [169], [170] is used in the multiple criteria decision analysis ("MCDA") to identify the best technical-economic compromise.

The starting point (or "base case") is represented by the market hourly results in each scenario under study. The three inertia-related constraints taken into account are:

- Minimum kinetic energy;
- Minimum available synchronous capacity;
- Maximum level of System Non-Synchronous Penetration ("SNSP", better explained in the Chapter 3 which focuses on power system flexibility).

Different values of these parameters are considered in sensitivity analyses and imposed within the market simulator algorithm to obtain the new thermal unit commitment needed to satisfy frequency security requirements.

The market simulations are then repeated in order to evaluate the performance indicators associated with following criteria:

1. Social-Economic Welfare (named "SEW");
2. CO_2 emissions;
3. Fuel consumption.

Furthermore, the hourly market results are used in input to the aggregated dynamic model [171] to evaluate the frequency performance in terms of:

4. ROCOF indicator;

5. Nadir indicator.

Finally, the different strategies (corresponding to the base case and all investigated alternatives built varying the constraints values) are compared in terms of their performance with respect to the five aforementioned criteria using the TOPSIS method, detailed in the Chapter 4 together with the Terna official market simulator algorithm.

The workflow of the entire process is depicted in Fig. 2.31.

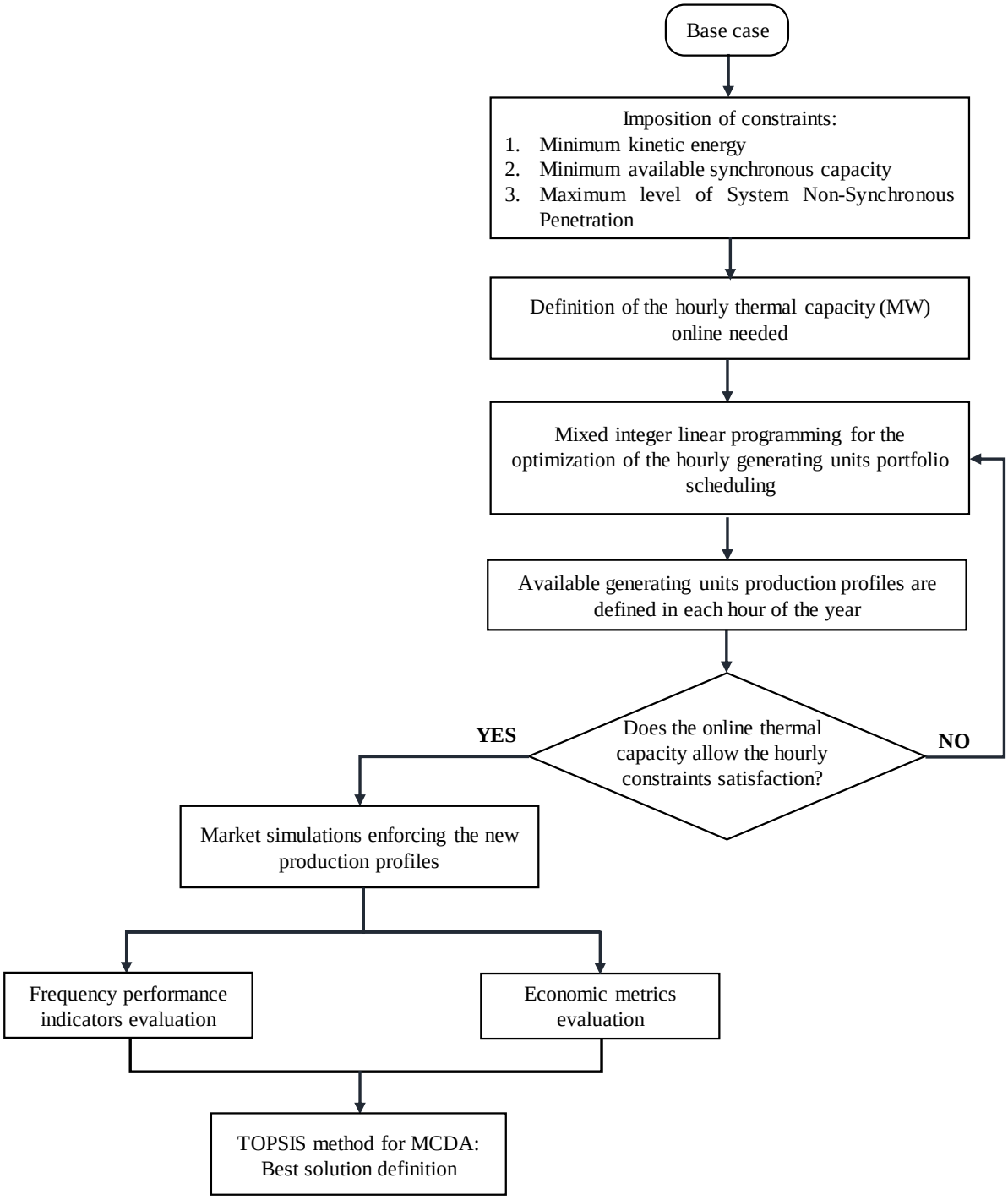

Fig. 2.31. Workflow of the proposed approach.

3. Power system flexibility assessment in transmission network expansion planning

The European electricity system is facing a deep reshaping, involving the integration of large amounts of variable decentralized generation, the digitalization process and the conventional decommissioning of power plants, whilst at the same time continuing to ensure security of supply, power system balance and competitiveness with neighboring countries [172].

As the Italian TSO, Terna is actively working to support this profound transformation of the energy landscape, performing adequacy and flexibility analysis for the Italian power system. These are two central aspects in the planning framework: system adequacy ensures that at any time the available generation capacity can meet the demand, while flexibility refers to the system ability to employ its resources to face expected and unexpected changes in generation (expecially due to the renewable sources) and load consumption while fulfilling system reliability requirements and satisfying the flexibility resources technical characteristics.

In the European framework, the Belgian TSO Elia [172] concentrated in a unique biennial report adequacy and flexibility analysis, while studies carried out by Terna are presented separately.

In particular, the "Italian Adequacy Report" [173] describes the methodology for the evaluation of conventional generating units needed to ensure the adequacy of the system in all relevant planning energy scenarios in the medium-long term horizon based on a probabilistic approach and the results obtained from its application. Moreover, the first flexibility analysis for the Italian power system based on long-term market simulations results [174] has been included in the year 2019 NDP [119]. Further studies carried out in collaboration with Politecnico of Bari University [175] focused on another important aspect of flexibility related to the exploitation level of network branches.

In the framework of the European program "Horizon 2020", Terna recently took part to the "Advanced methodology and tools taking advantage of storage and FLEXibility in transmission and distribution grid PLANning" project, named "FlexPlan". The project is funded by the European Union and coordinated by the Italian Research on the Energy System (RSE). The other partners include two European TSOs, one Distribution System Operator (DSO) and nine Universities/Research Centres, as illustrated in the Fig. 3.1.

The main objective of the FlexPlan project is the realization of a new tool for analysing transmission and distribution (T&D) grid expansion (conceived in a more and more integrated

way) options considering the deployment of new storage facilities and grid technologies (HVDC, FACTS) as well as the activation of flexibility resources located in key places.

The new tool will be developed during the next three years, and will consider all system operation costs, including those related to RES and load curtailment. Then, it will be adopted to perform integrated T&D network planning analyses in scenarios at 2030, 2040 and 2050.

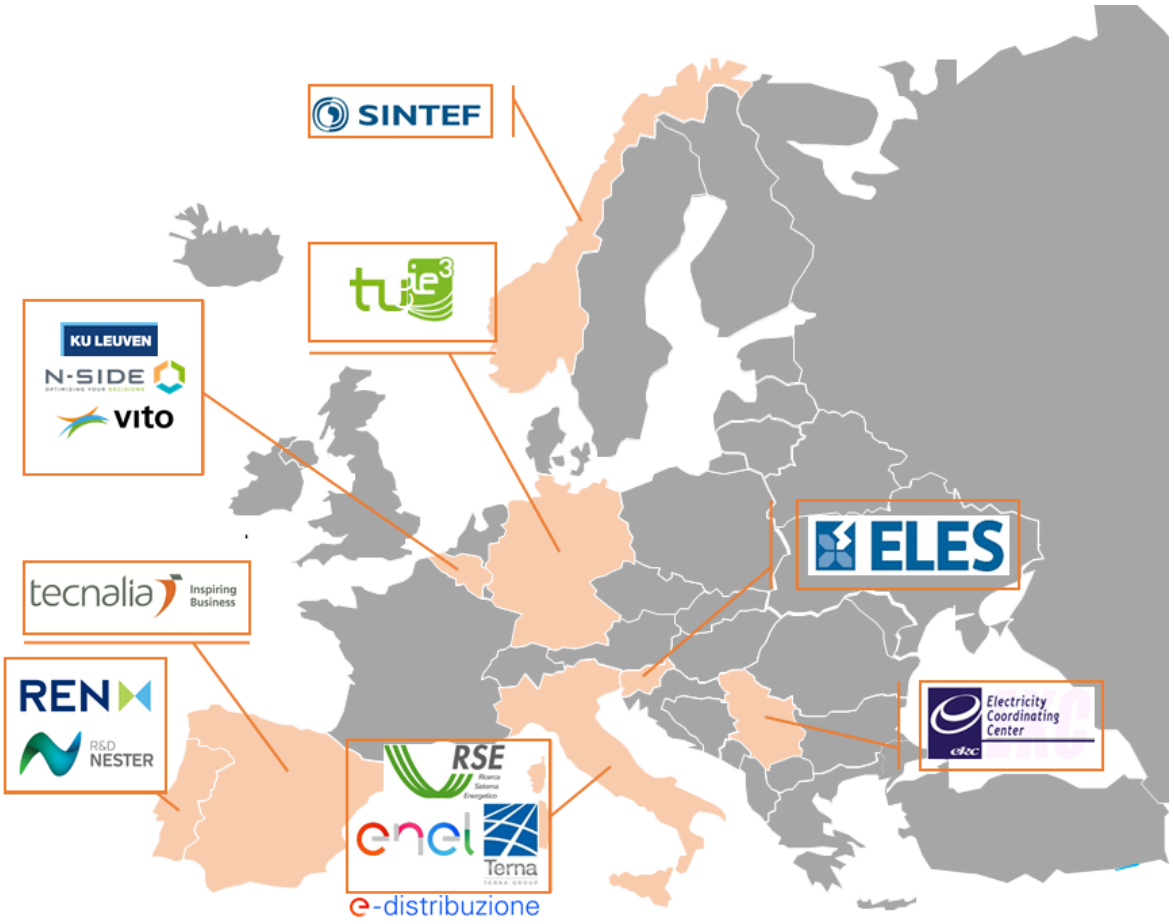

Fig. 3.1. Geographical spread of the FlexPlan Consortium.

This Section deals with the flexibility requirements assessment for the Italian power system in different planning scenarios considering both the market (in the sub-section 3.2.1) and the network (in the sub-section 3.2.2) aspects.

3.1 Introduction

The recent development of renewable distributed generation, strongly affected by the need of reaching objectives established by European Energy and Climate policies, is having an important impact on planning and operation of the power system. In this context, the TSO has to guarantee major penetration of RES generation while ensuring security of supply, efficiency and level of service.

An important barrier to the integration of RES generation is represented by the need of additional capacity for periods when renewable sources are unavailable. Besides the capacity adequacy topic [176], [177], major concerns are the magnitude and uncertainty of the ramps associated with variable generation (VG) [178] – [181]. Experiences with wind and solar generation in Electric Reliability Council of Texas (ERCOT) [182], Europe [183], and Midcontinent Independent System Operator (MISO) [184] point out to large regional VG production variations, expecially if demand changes in the opposite way. The determination of the ability of a system to integrate VG, mandatorily involves the assessment of the variability of the system's net (or "residual") load, defined as the system demand which is not met by VG production, rather than independently considering the variability of each VG technology and system demand [185]. Therefore, significant indicators of the power system flexibility are represented by the magnitude of up or down ramps in VG production, the relationship between VG production and load demand, the time occurrence of ramps and the ability of the system operator in forecasting future VG production.

In literature, the ability of the electrical system to employ its resources dealing with the changes in load demand and variable generation, is defined as the flexibility of the system [186], [187]. In [188] a power system is defined flexible if it is able to rapidly respond to large variations in demand and supply, whether scheduled or unexpected, by ramping up and down the generation output within technical and economic boundaries. The report indicates three main steps towards a flexible power system:

1. Flexibility resource identification;
2. Flexibility requirements assessment;
3. Net Flexibility Resource (NFR) evaluation, to be considered available to balance further changings related to additional VG production.

Flexibility resources (synchronous generators, demand response, interconnections [189] – [191], energy storage [192]) are required to rapidly vary their output to adequately face net load

changes. Further flexibility aspects involve the "robustness" of the transmission infrastructure [193], policy rules and market design [194], [195].

The chronological classification of the flexibility resources as provided in [196] is reported in Fig. 3.2:

Long – Term	Mid – Term	Short – Term	Super Short – Term
• A transmission system tariff to incentive wind operator; • Upgrading and expanding transmission system; • Rewiring transmission lines; • FACTS; • Super conducting fault currents limiters; • WAMS; • Line temperature monitoring; • Weather-driven tariff provisions & market rules	• Thermal units (Peak, Mid-merit, Baseload plants); • Non-thermal units (VG curtailment, Hydro power plants); • Energy Storage System (Fast response, Mid-response, Electric Vehicles); • Demand side management (Energy Efficiency Demand Response); • Developing deep, liquid day-ahead and hour ahead markets.	• Large rotating blades of variable speed wind turbine; • Geographical dispatch; • Regulation reserves; • Load following reserves; • Demand response (DR); • Consolidating balacing areas into larger entities.	• Low-voltage ride-though; • Reactive power control; • SCADA information; • Voltage control; • Output control; • Ramp rate control; • Power electronic control (governor response and initial response); • Dynamic modeling of large wind plants (prime mover dynamics)

Fig.3.2. Chronological classification of flexibility resources (from [196]).

In [197] a categorization of a power system elements as either a *flexible resources*, *flexibility sink*, or as an *intermediary* has been provided:

1. Flexibility resources:
    a. Conventional generation
    b. Dispatchable VG
    c. Interconnection
    d. Electricity Storage
    e. Demand – side measures
2. Intermediary:
    a. Transmission network
    b. Fuel storage
    c. Forecasting
    d. Market design
    e. Regulation
    f. Balancing area size
    g. Unit commitment
3. Flexibility sink:
    a. Load

b. Wind
c. Solar
d. Ocean.

The flexibility requirements are quite influenced by the system characteristics such the location of the variable sources and the load areas, the uncertainty about demand and VG profiles, the availability of flexibility resources able to cover peak load in case of necessity.

Flexibility needs to be measured: an exhaustive assessment should consider all these elements and their mutual influences.

Since in the restructured electricity business the network planners are no longer in control of the generating capacity development, it is clear that the transmission system expansion is the main driver to support the VG integration into the system. In this context, new metrics are needed in order to evaluate the impact of the growing share of RES generation on market efficiency and the ability of the transmission infrastructure to maintain the desired reliability and security standards during the current profound generation landscape transition. The transmission system flexibility is considered very important because it can reduce the overall system costs thanks to a more efficient power system operation [198].

In this Section, a methodology to assess the power system flexibility using market-based and infrastructure-based metrics is presented and the results obtained by their calculation for the real case of the Italian power system in different significant planning scenarios are illustrated.

3.2 Flexibility requirements indexes

Extensive literature reviews on power system flexibility have been recently presented in [196], [199], [200]. Some work is more focused on qualitative evaluations or theoretical developments [196]. However, the quantification of the flexibility needs and sources is an essential point for real applications together with the need of finding a compromise between computational complexity and meaningfulness of the indicators [200].

In [201] a systematic methodological approach based on a set of indicators for future power system flexibility analysis is proposed and applied to a European case study for 2020 and 2025 scenarios. Other studies referred to specific countries as Germany [202], France [203], Greece [204], the island of Ireland and the power system in Hokkaido Prefecture Japan [185] are available. Less common are the flexibility analysis on the whole European system [201], [205]. In [205] a methodology to evaluate the transmission system flexibility with respect to the generation system is proposed for highly developed power systems operating in electricity market. References [207] – [209] provided local and global indexes assessing the transmission system power margins when facing generation scenario variations. Furthermore, the proposed indexes allow the evaluation of the generation asset variation range.

In this sub-section, a set of indexes for the flexibility assessment of power systems are illustrated, and case studies involving the Italian power system are presented, evaluating its performances from the market efficiency, network security and reliability points of view. The insights gained from the application of flexibility requirements assessment methodology can be relevant in driving the new flexibility resources planning.

3.2.1 Market-based flexibility indexes

According to [201], the set of significant annual indexes measuring the RES penetration and, consequently, system flexibility requirements are provided by the reference [210]:

- RES Load penetration Index (**RLPI**), defined as the maximum hourly coverage of load by non-dispatchable renewables energy generation (wind and solar):

$$RLPI(t) = \max\left(\frac{W(t) + S(t)}{L(t)}\right) \; t = 1,2,3,\dots,8760 \tag{3.1}$$

- Renewable Energy Penetration Index (**REPI**), defined as the average value of demand covered by wind and solar generation:

$$REPI = \left(\frac{W_{annual} + S_{annual}}{E_{annual}}\right) = \frac{\sum_{t=1}^{8760} W(t) + S(t)}{\sum_{t=1}^{8760} L(t)} \tag{3.2}$$

- Renewable energy generation Curtailment Risk (**RCR**):

$$RCR = \frac{number\ of\ hours\ in\ the\ year\ with\ RL(t) < 0}{8760} \tag{3.3}$$

- Non-Synchronous Penetration ratio (**SNSP**), proposed in [205] with the aim of monitoring the system inertia and defined as:

$$SNSP(t) = \frac{W(t) + HVDC(t)_{import}}{L(t) + HVDC(t)_{export}} \tag{3.4}$$

This expression of the SNSP index derive from an original work [211] was addressed to the Irish power system, whose unique interconnector is in HVDC technology and the main renewable energy source is represented by the wind generation. The (3.4) can be easily generalized by replacing the terms $HVDC(t)_{export}$ with the general $P(t)_{export}$ and by adding the solar photovoltaic generation to the wind one. Therefore, the SNSP can be expressed as in (3.5):

$$SNSP(t) = \frac{\sum P(t)_{in_{inverter}}}{\sum P(t)_{out}} = \frac{W(t) + PV(t) + HVDC(t)_{import}}{L(t) + P(t)_{export}} \tag{3.5}$$

Where:

- $W(t)$ is the wind energy generation at time t;
- $S(t)$ is the solar energy generation (solar photovoltaic + solar thermal) at time t;
- $L(t)$ is the load at time t;
- $RL(t)$ is the residual load at time t;
- $HVDC(t)_{import}$ represents the imported power through high voltage direct current interconnections at time step t;
- $HVDC(t)_{export}$ represents the exported power through high voltage direct current interconnections at time step t.
- $P(t)_{in\_inverter}$ represents the inverter-based imported power at time t;
- $P(t)_{out}$ represents the sum of load demand and inverter-based exported power at time t;
- $PV(t)$ is the photovoltaic energy generation at time t.

The analysis performed in [201] on the European power system at 2020 and 2025 year horizon considering 25 different renewable energy generation profiles allowed the estimation of the four described indicators, as reported in the Fig. 3.3 – Fig. 3.6. In Fig. 3.3 and Fig. 3.4 the circle center represents the average value and circle size represents the standard deviation of the indexes under the examined 25 different meteorological years.

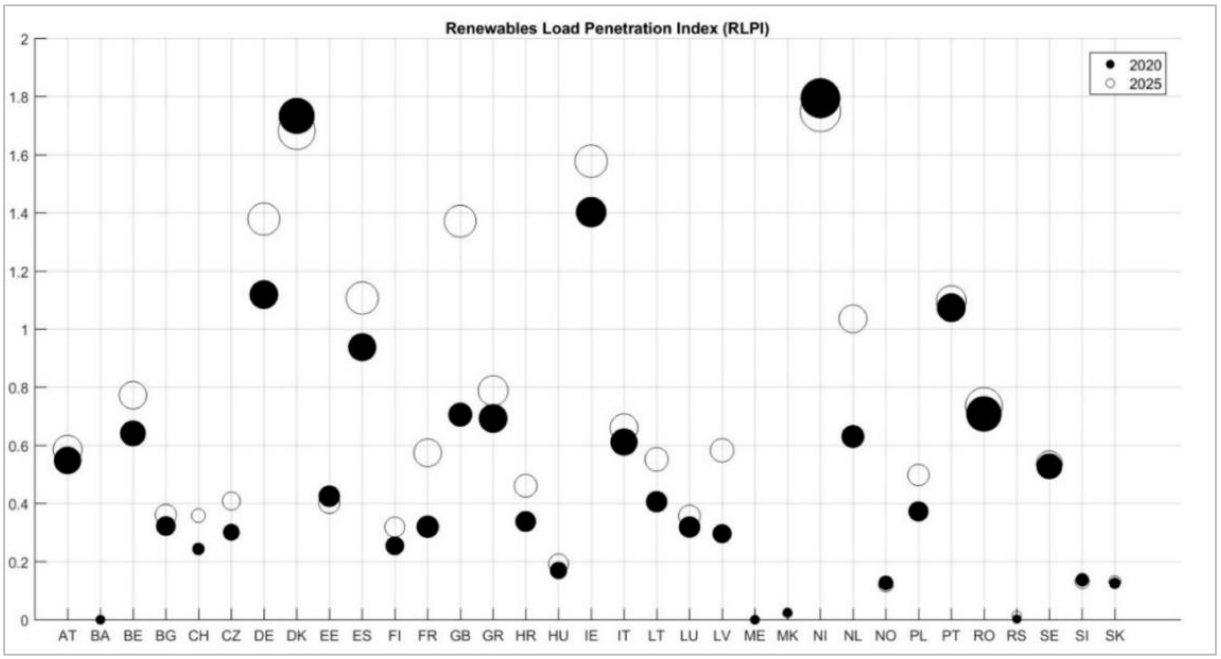

Fig. 3.3. Renewables Load Penetration Index (RLPI), (from [201]).

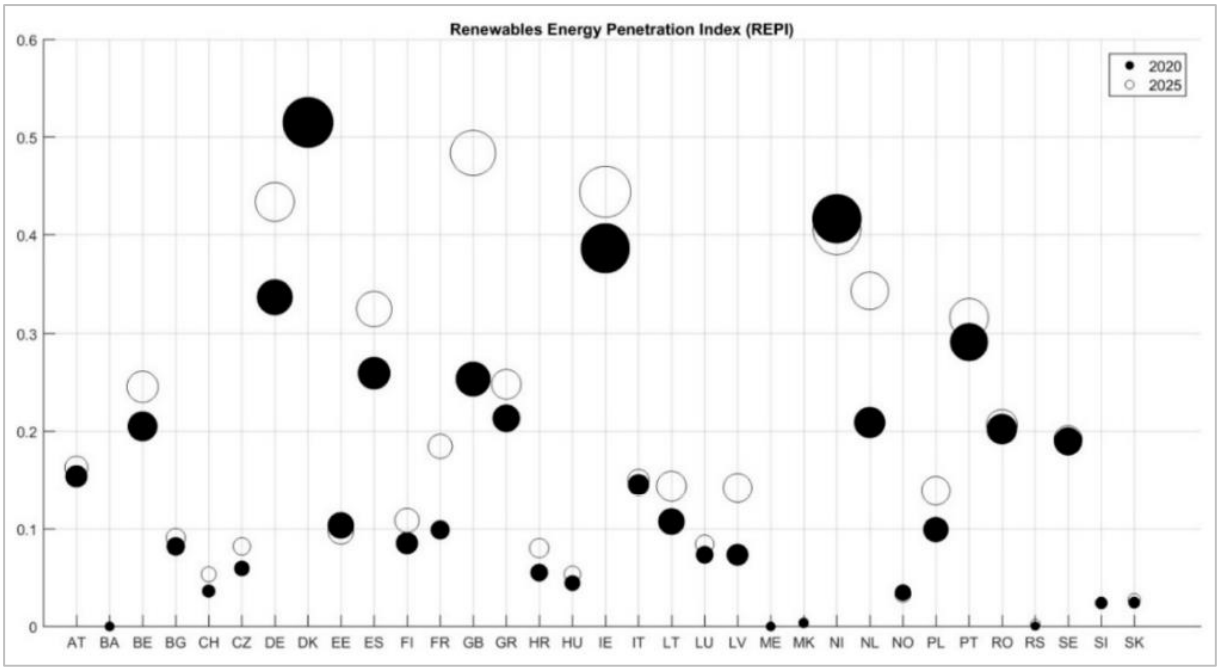

Fig. 3.4. Renewable Energy Penetration Index (REPI), (from [201]).

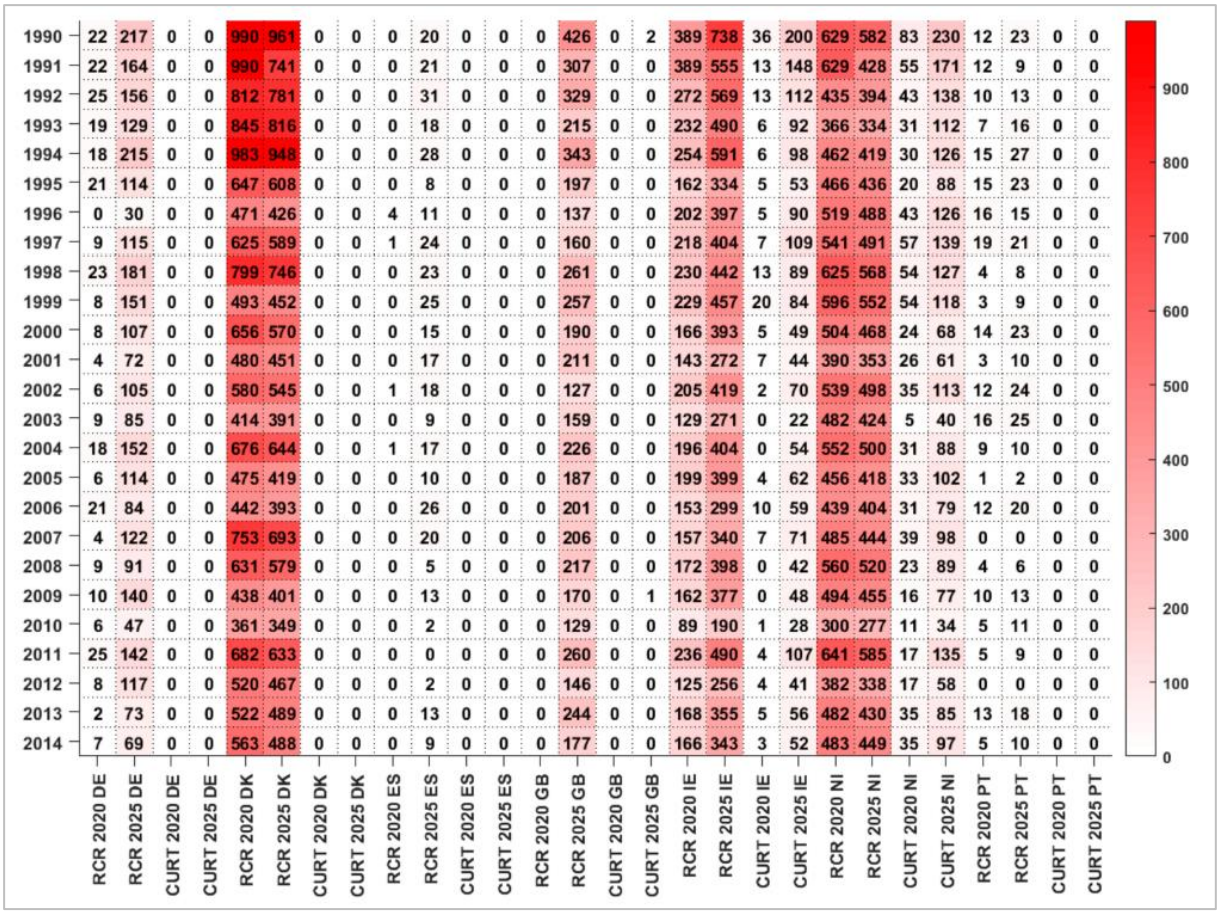

Fig. 3.5. Renewables Curtailment Risk (RCR) and actual renewable curtailment, (from [201]).

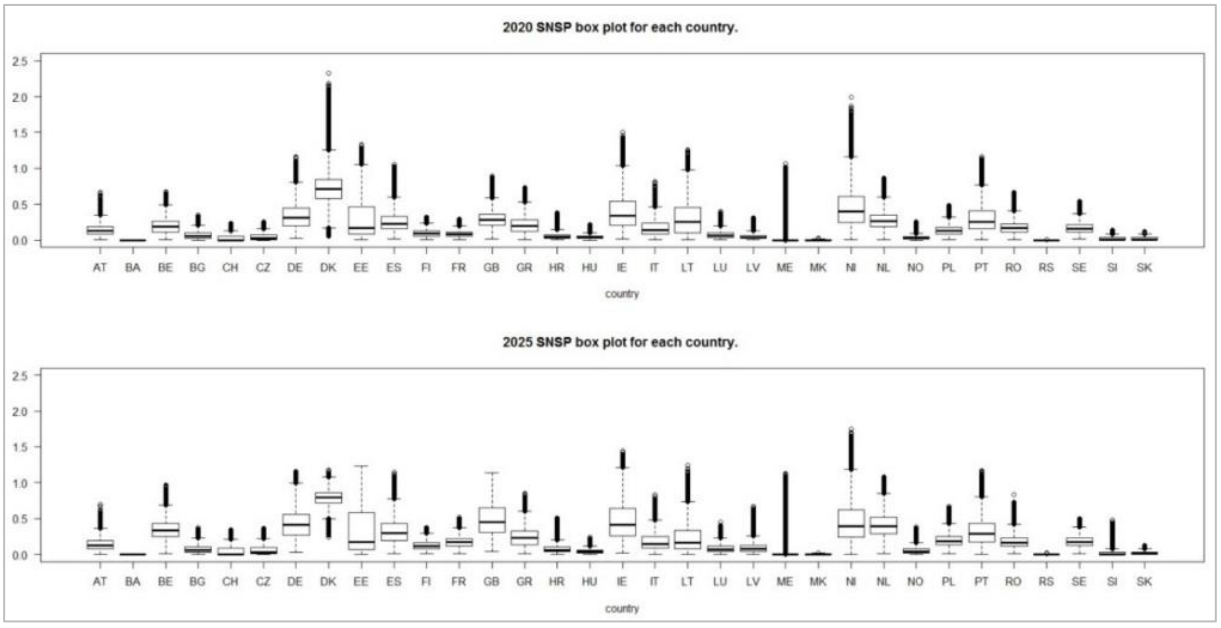

Fig. 3.6. System Non-Synchronous Penetration ratio (SNPS), (from [201]).

In the following sub-section, results obtained from the analysis for the Italian power system in most relevant planning scenarios at 2030 year horizon are reported.

3.2.1.1 Cases study and results

The analyses proposed in [174] have been performed for the Italian power system in the Sustainable Transition (ST) and Distributed Generation (DG) planning scenarios [26], [119], [212] (described in the previous Chapter 2, paragraph 2.2.3.1) and referred to 2030 year, due to ten-year horizon of the NDP.

For the sake of the clarity, a brief description of the scenarios under study is reported also in this sub-section.

- The ST scenario is defined by the means of the "bottom-up" methodology: data input on demand, technology penetration, installed capacity are collected from the TSOs and processed to build the scenario storyline. The hypothetical macro-economic trend is characterized by a moderate economic growth. Europe is in line with the achievement of 2030 targets and slightly delayed for 2040 targets and 2050 decarbonization. Electrical demand is slightly growing as well as gas demand.
- The DG scenario is defined through top-down approach: the scenario characteristics are derived from the European targets feeding market-based algorithms used to turn these targets into a generation mix for each zone. As a macro-economic trend, this scenario foresees a strong economic growth, and the replacement of coal power plants by gas power plants in electric generation. An increase in yearly electric demand is observed in the heating and transport sectors, where electric and gas vehicles achieve the emission target reduction, whereas the higher energy efficiency in buildings leads to a decreasing electric demand in domestic activities. Furthermore, the DG scenario highlights a general progress in terms of distributed generation and domestic/commercial storage thanks to a significant costs reduction of the relevant technologies.

Four different cases have been analysed: 2030 ST and 2030 DG "with" and "without" network developments, indicated by the following notation:

- A1: 2030 ST scenario **with** network developments included;
- A2: 2030 ST scenario **without** network developments included;
- B1: 2030 DG scenario **with** network developments included;
- B2: 2030 DG scenario **without** network developments included.

The Table 3.1 summarizes the results obtained from the indexes calculation for each condition in each considered scenario. Since the REPI index represents the RES penetration average value, while the RLPI index relates to the RES penetration maximum instantaneous value, this latter indicator is 3÷4 times larger than the first one. The RLPI index is greater than 1 when there is a surplus of variable RES generated energy.

Table 3.1. Results of Indexes calculation for the Italian power system in each condition in each scenario under study.

Scenarios	**Indexes**			
	Planned network development actions at 2030	***RLPI(t)***	***REPI***	***SNSP(t)***
2030 ST	Yes (A1)	0.78	0.18	0.27
	No (A2)	0.69	0.18	0.21
2030 DG	Yes (B1)	1.01	0.25	0.35
	No (B2)	0.41	0.08	0.11

It can be observed that the absence of the planned network developments leads to a reduction of indexes, particularly evident in the 2030 DG scenario due to the high RES generation capacity foreseen, while the 2030 ST scenario shows smaller reductions of indexes values in absence of development actions.

The RCR index is omitted because not relevant: only in the A1 case 3 hours of negative residual load are observed.

Solar and wind generation are undoubtedly the most developed RES. Since their production profiles are strongly affected by weather conditions, they are considered in the category of Variable Generation [186], [197], [213] and the residual load at time t is defined as:

$$RL(t) = L(t) - W(t) - S(t) \tag{3.6}$$

Starting from hourly year 2030 load values and by subtracting wind and solar energy generation at each time interval t, it is possible to evaluate the instantaneous residual load for ST and DG scenarios, both in cases with and without all planned grid developments.

Fig. 3.7 and Fig. 3.8 show the evolutions of load, residual load and RES penetration during a reference summer and winter week for the different A1, A2, B1 and B2 scenarios. Values represent the hourly expected load, wind and PV production in 2030 ST and DG and scenarios, resulting from market simulations carried out with the Terna official Day-Ahead Market Simulator (DAM) "Promed Grid" [214]. The red line is depicts the hourly residual load in a typical winter or summer week, while the yellow highlighted areas represents the wind and solar generation. A substantial difference can be observed in absence of planned network developments (A2 and B2 scenarios): the RES penetration reduction is particularly evident for the 2030 DG scenarios, as evidence of the planned grid reinforcements need in a "High RES" scenario.

The residual load evolution in a summer reference week for the year 2016 and the planning 2030 ST and DG scenarios is provided in Fig. 3.9, showing higher residual load ramps in presence of the expected high RES capacity penetration levels.

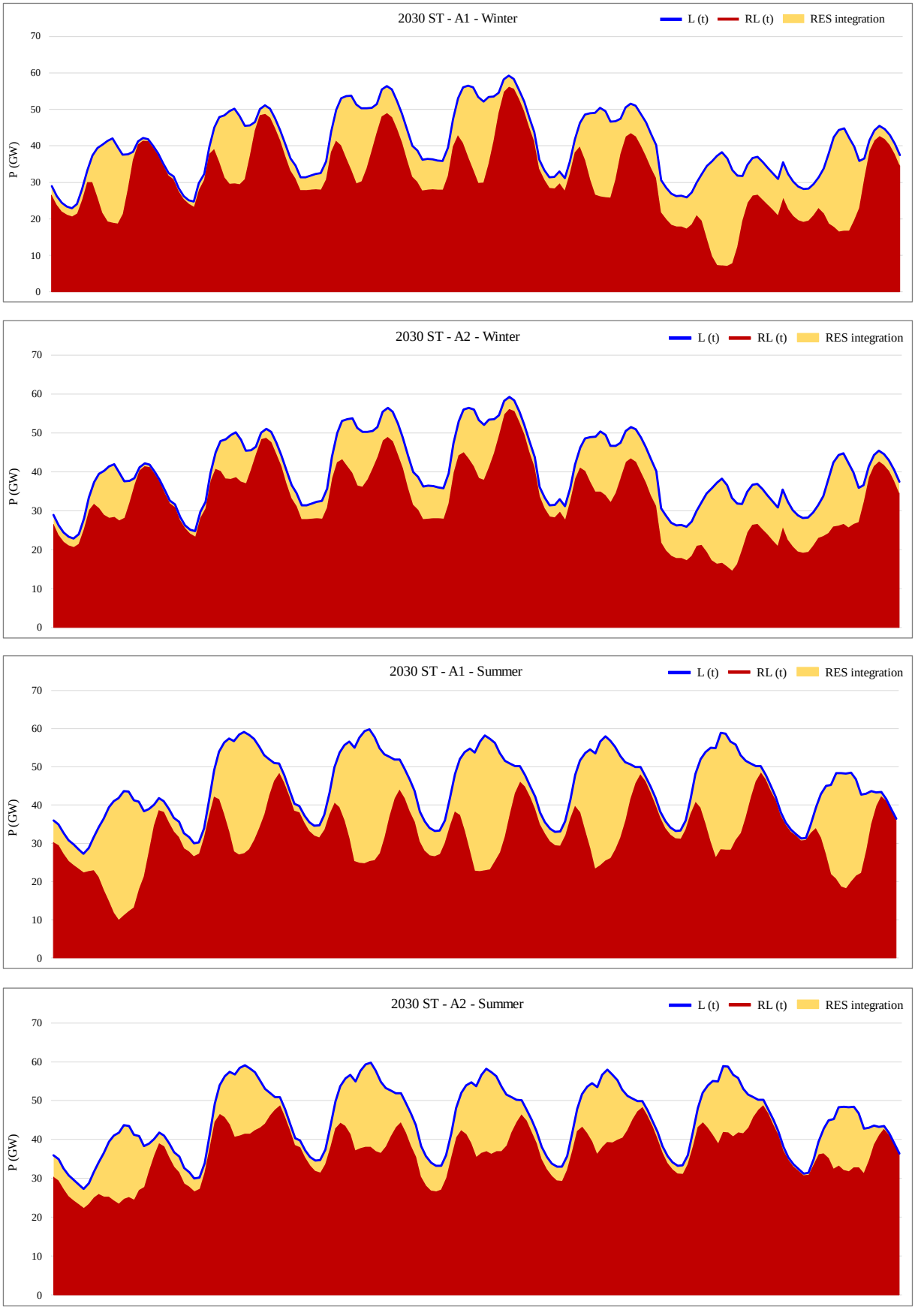

Fig. 3.7. Scenarios A1 and A2: evolutions of RL(t) and RES penetration in typical winter and summer weeks.

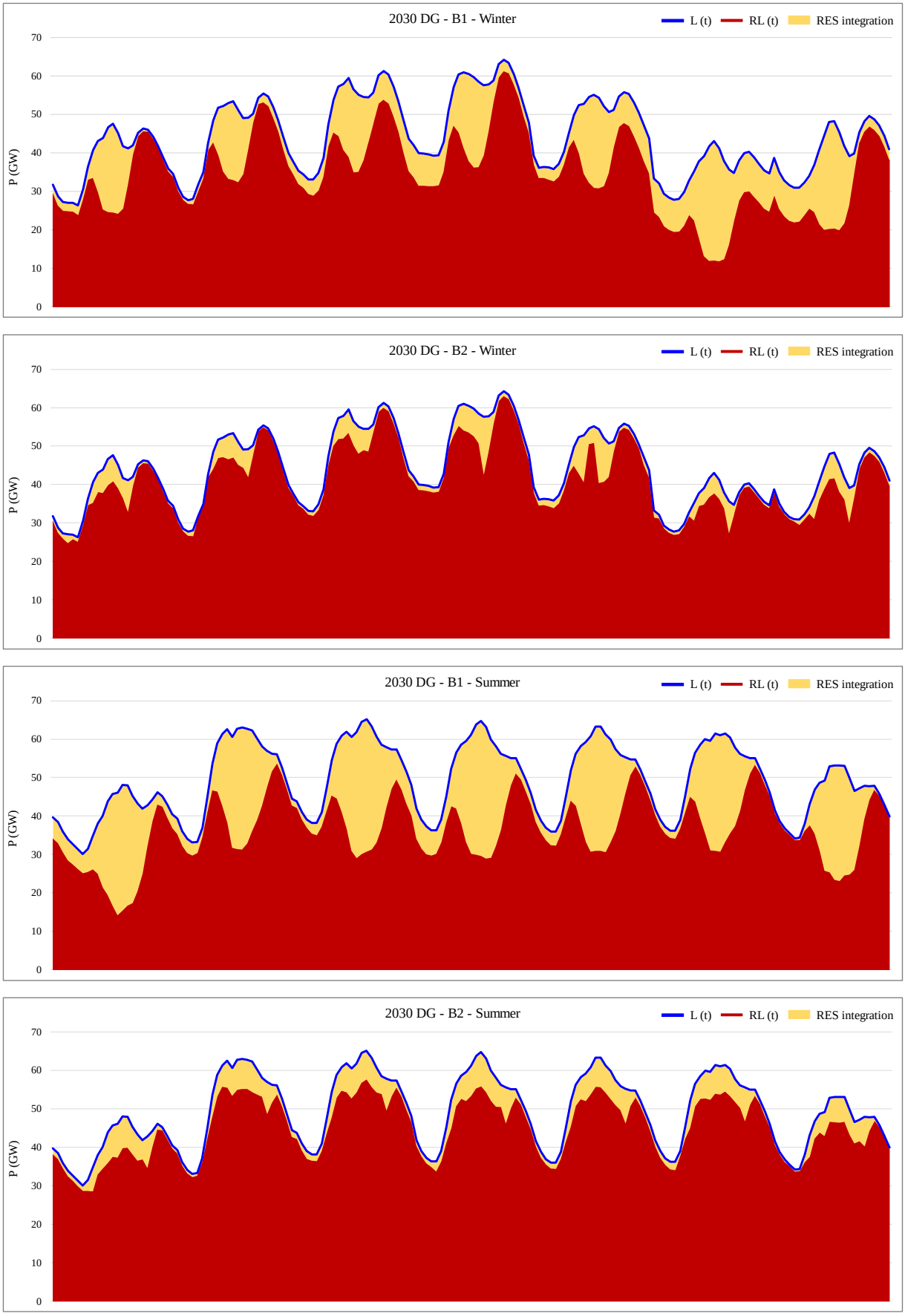

Fig. 3.8. Scenarios B1 and B2: evolutions of RL(t) and RES penetration in typical winter and summer weeks.

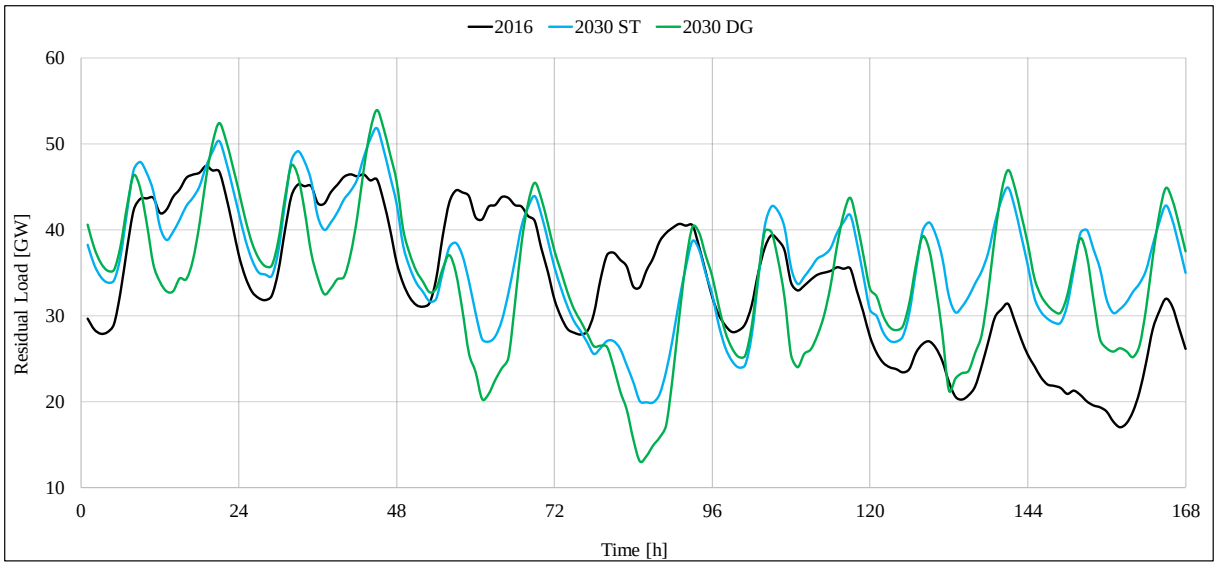

Fig. 3.9. Residual load evolution: comparison between 2030 planning scenarios (without planned network reinforcements included) and 2016 historical values.

For each new development project, the Italian NDP issued by Terna contains a detailed description of the major expected benefits [215]. Constraints to renewable energy production are locally identified (*local overgeneration*) during the hours when RES generation must be reduced in order to avoid overloads due to grid congestions. The Cost Benefit Analysis (CBA) methodology applied by Terna for all projects with associated realization costs greater than 15 M€, allows the estimate of the "B5" benefit category, corresponding to the greater increased integration of RES production thanks to a new grid development intervention.

The B5 benefit is evaluated by the means of network simulations performed using both the probabilistic and the deterministic (static load-flow) approaches [105], [216] in the presence and in absence of the new grid development intervention under study.

Table 3.2 summarizes the main projects included in 2018 NDP [217] presenting benefits in terms of RES integration and its associated B5 values, expressed in MWh.

Table 3.2. B5 benefit for some relevant planned network developments.

Development Intervention	**B5 (MWh of RES generation integrated)**		
	Area	***2030 ST***	***2030 DG***
400 kV – 50Hz overhead line "Foggia-Villanova"	Centre	206,504	2,842,008
400 kV – 50Hz overhead line "Chiaramonte Gulfi - Ciminna"	Sicily	11,940	29,130
400 kV – 50Hz overhead line "Assoro-Sorgente 2-Villafranca"	Sicily	11,940	29,130
HVDC Interconnector Italy-France	North-West	222,730	675,200

A further application of the illustrated methodology, presented in [175], has been performed for the Centre South and Centre North Italian market zones flexibility assessment, both "with" and "without" the planned Adriatic submarine HVDC link spanning the critical section.

The flexibility requirements assessment for the critical sections of the Italian power system has been carried out in the two planning scenarios representing the last years evolution of National energy policy at 2030 time horizon: the National Energy Strategy (named "NES") [109], and the Integrated National Energy and Climate Plan (named "NECP") [110]: both the generation capacity flexibility and the grid infrastructure one (reported in sub-section 3.2.3) are investigated by performing market and network simulations, drawing a set of flexibility indicators, in order to evaluate the impact of the new planned HVDC submarine link between Villanova and Fano nodes.

The two national policy scenarios under study at 2030 year horizon are substantially aligned in demand trend and generation production, (slightly higher in NECP scenario as shown in Fig. 3.10), while the import target is supposed to be the same.

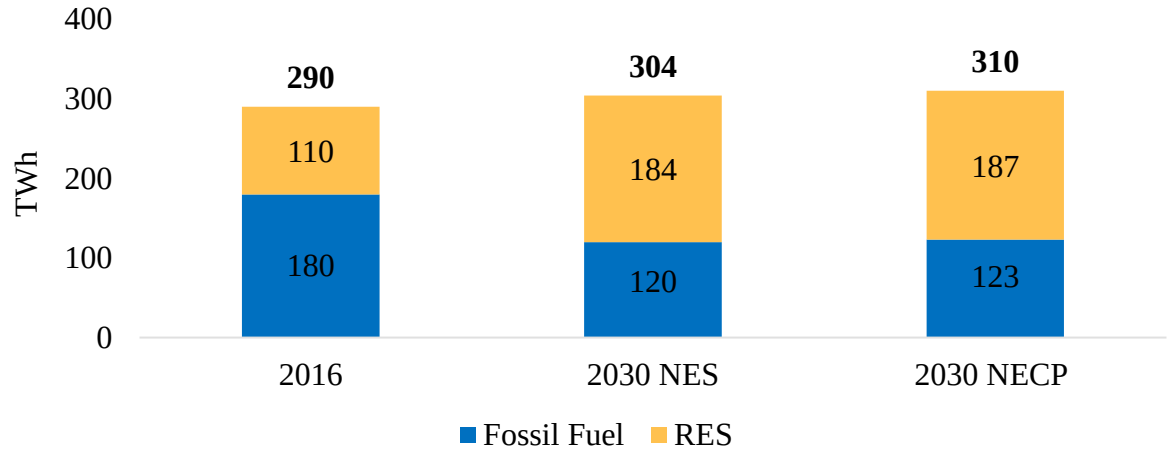

Fig. 3.10. Forecasted generation production (TWh) for national policy scenarios at 2030 year horizon.

In comparison with the NES, adopted in 2017, the new national policy NECP scenario confirms commodities values except for CO_2 prices at 2030 time horizon, which are supposed to increase [109]. Despite a minor RES installed capacity, the forecasted renewable generation is higher in the NECP scenario due to the hypothesis about the greater productivity of the variable sources. One of the main differences between the two scenarios is represented by the targets on renewable energy sources, more challenging in the NECP scenario for electricity consumption and other energy sector aspects, as illustrated in Fig. 3.11.

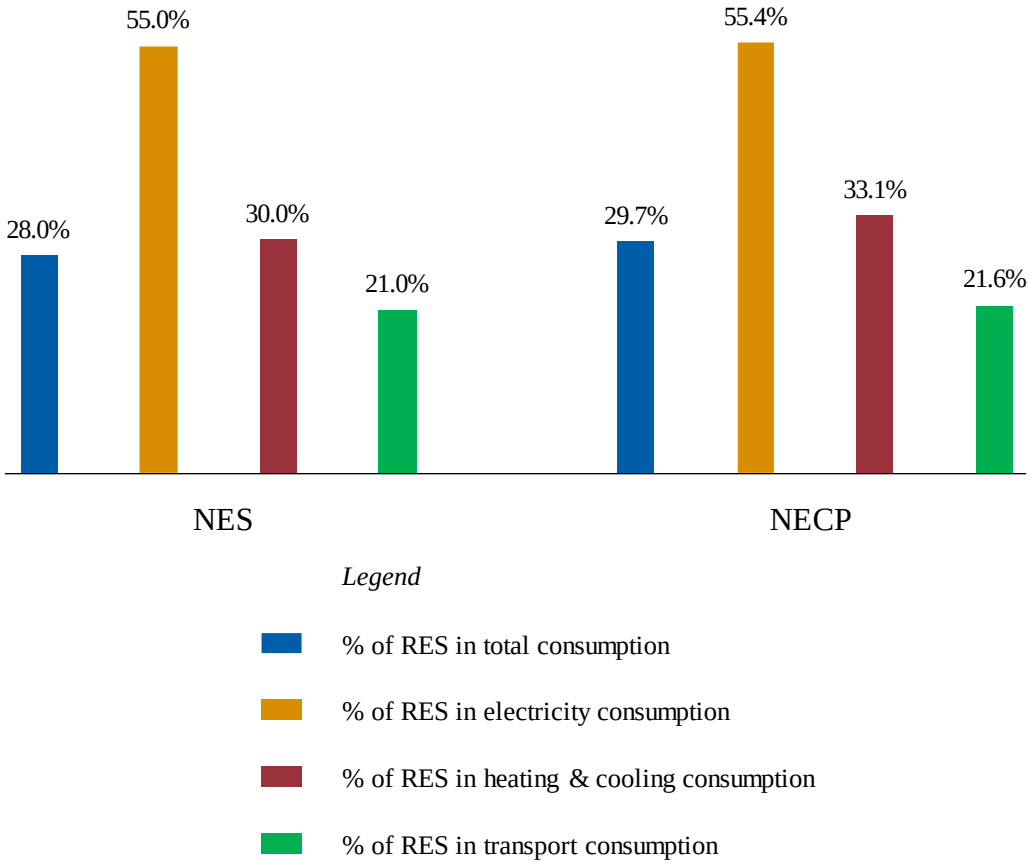

Fig. 3.11. RES targets in different consumption sectors for national policy scenarios NES and NECP at 2030 year horizon.

From the methodological point of view, the same set of flexibility indicators adopted for the flexibility requirements assessment of the whole Italian power system in the ST 2030 and DG 2030 scenarios have been evaluated, with the only difference that the analysis concerned a specific portion of the national power system in two different conditions: the Centre South and the Centre North market zones “with” and “without” the new planned submarine HVDC Adriatic link.

The inputs of NES and NECP scenarios at 2030 year horizon are used to obtain hourly consumption data and renewable generation availability. Therefore, by means of day-ahead electricity market solution with zonal structure, providing the maximization of social welfare under perfect competition assumptions, power production levels of conventional generators are determined in order to evaluate the indexes presented in section 3.2.1. for the Centre South and Centre North Italian market zones.

The results across the critical section are summarized in Table 3.3. It can be seen that the indexes increase in the presence of the planned HVDC link, pointing out to an increased ability

to integrate renewable sources. Moreover, the 2030 NES scenario is shown to be the most promising in order to improve the analysed aspects.

Table 3.3. Results of Indexes calculation for the Centre South and Centre North market zones of the Italian power system in each condition and in each scenario under study.

Scenario	**Indexes**			
	Planned HVDC	***RLPI(t)***	***REPI***	***SNSP(t)***
2030 NES	Yes	1.42	0.52	0.55
	No	1.34	0.50	0.49
2030 NECP	Yes	1.22	0.50	0.52
	No	1.14	0.49	0.47

Furthermore, the value of negative residual load $RL(t)$, representing conditions with renewables exceeding the demand, is evaluated during the 8760 hours in a year in all analysed conditions. This indicator assumes the highest value in the 2030 NES scenario in presence of the new planned HVDC Adriatic link and the lowest in the 2030 NECP scenario in absence of the same development action. In particular, the negative residual load is around of 11% in the first mentioned case and 1.8% in the latter one.

3.2.2 Grid infrastructure-based flexibility indexes

Another important aspect of flexibility is related to the exploitation level of network branches. This can be seen in a twofold manner: a moderate power flow on lines implies a safety margin to be exploited in the case of faults, moreover the flow is determined by the distribution of power injections at nodes, deriving from market equilibrium in current deregulated systems. The presence of HVDC links implies further degree of freedom, thus modifying the grid infrastructure flexibility level. It should be remarked that flow-based market solutions are gaining significant interest in literature as well as in real applications, e.g. the EUPHEMIA algorithm [218].

Taking the cue from [207] – [209], a revised version of system flexibility index is here proposed. At first, based on a complete AC power flow calculation according to market results, the active power margin of each line k at time t, $\boldsymbol{M_k(t)}$ is obtained as the difference between active power flow $\boldsymbol{F_k(t)}$ and maximum line rating $\boldsymbol{R_k}$, accounting for flow direction, i.e.:

$$M_k(t) = \begin{cases} R_k - F_k(t) & F_k(t) \geq 0 \\ R_k + F_k(t) & F_k(t) < 0 \end{cases} \tag{3.7}$$

In order to investigate the exploitability of those margins, DC power flow equations are employed. Considering a network composed of N_i nodes and N_b branches, a linear relation can

be written between the N_b–vector of active power flow on branches $\boldsymbol{F_b}$ and the (N_i – 1)-vector of net nodal power injections $\boldsymbol{P_n}$ as follows:

$$\boldsymbol{F_b} = \boldsymbol{B_b} \cdot \boldsymbol{B_{dc}^{-1}} \cdot \boldsymbol{P_n} + \boldsymbol{F_{sh}} \tag{3.8}$$

where $\boldsymbol{B_b}$ is a $N_b\ x\ (N_i - 1)$ line-node admittance matrix, $\boldsymbol{B_{dc}^{-1}}$ represents the $(N_i - 1)\ x\ (N_i - 1)$ reduced nodal admittance matrix, and the $(N_i - 1)$-vector $\boldsymbol{F_{sh}}$ accounts for the effect of phase shift transformers. By performing matrix product, the following form is derived:

$$\boldsymbol{F_b} = \boldsymbol{H} \cdot \boldsymbol{P_n} + \boldsymbol{F_{sh}} \tag{3.9}$$

where $\boldsymbol{H}$ represents the $N_b\ x\ (N_i - 1)$ line-node matrix of Power Transfer Distribution Factors (PTDFs), supposing that the injection at each node is received at slack bus [219], [220].

Usually, each PTDF $h_{k,j}$, representing the variation of flow on the line k for unit variation of power injection at bus j, ranges between -1 and 1.

The means to vary the power flow in each line within rating is given by dispatchable generation variation and non-dispatchable renewable curtailment. Let us define $\boldsymbol{\Omega_{gen}}$ as the set of nodes with dispatchable generators and $\boldsymbol{\Omega_{rnd}}$ as the set of nodes with non-dispatchable renewable generators. Therefore, in the presence of positive power flow on line k, the most bounding margin is the positive one, and dispatchable generation with positive PTDF can be limited. Redispatching Margin Index (RMI) for the line k is defined as follows, where $\boldsymbol{h_{k,j}^{+}}$ stands for positive PTDF values:

$$RMI_k(t) = \sum_{j \in \Omega_{gen}} h_{k,j}^{+} \quad if\ F_k(t) \geq 0 \tag{3.10}$$

Whereas, renewable curtailment tends to rating bound of the line in the presence of negative PTDF $\boldsymbol{h_{k,j}^{-}}$. Non-dispatchable Margin Index (NMI) for the line k is defined as follows:

$$NMI_k(t) = \sum_{j \in \Omega_{rnd}} h_{k,j}^{-} \quad if\ F_k(t) \geq 0 \tag{3.11}$$

In the case of negative power flow on line k, $\boldsymbol{h_{k,j}^{+}}$ and $\boldsymbol{h_{k,j}^{-}}$ replace each other in (3.10) and (3.11).

System level indexes at time t of redispatching margin $\boldsymbol{SRMI(t)}$ and non-dispatchable renewable margin $\boldsymbol{SNMI(t)}$ are defined as follows:

$$\boldsymbol{SRMI(t)} = \frac{\sum_{k=1}^{Nb}[|RMI_k(t)| \cdot M_k(t)]}{\sum_{\boldsymbol{k=1}}^{\boldsymbol{N_b}} M_k(t)} \tag{3.12}$$

$$\boldsymbol{SNMI(t)} = \frac{\sum_{k=1}^{Nb}[|NMI_k(t)| \cdot M_k(t)]}{\sum_{\boldsymbol{k=1}}^{\boldsymbol{N_b}} M_k(t)} \tag{3.13}$$

Flexibility is positively evaluated by comparison of different network configurations, or of different operating condition, for smaller values of indexes, since they would imply higher margins and lower PTDFs on the analysed lines.

The presence of HVDC links is modelled through coupled power injection-withdrawal at extreme nodes, as depicted in Fig. 3.12, and exchange power values from market results are determined according to their position across zones, in order not to exceed technical limits [219]. Therefore, they are directly accounted into the set of nodes with dispatchable generator $\boldsymbol{\Omega_{gen}}$ to determine (55) and (56), and their presence allows to modify margins in (52).

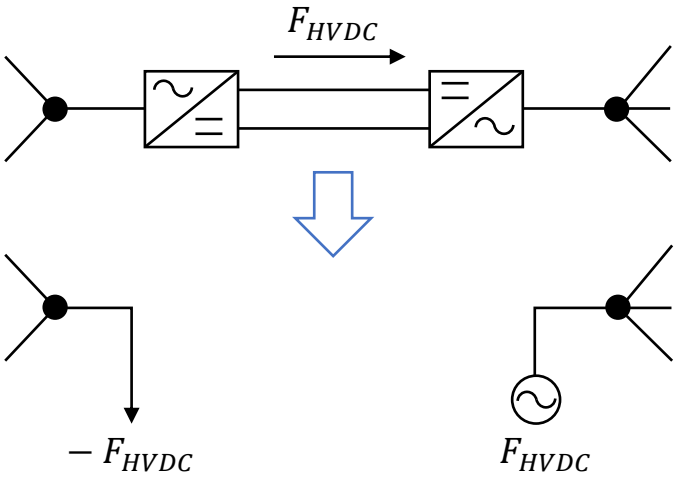

Fig. 3.12. Schematization of HVDC line model.

3.2.2.1 Case study and results

In this sub-section, the resulting values of $SRMI(t)$ and $SNMI(t)$ indexes evaluated for the real case study of the critical section Centre South – Centre North of the Italian power system in presence and in absence of the planned HVDC Adriatic link in the most recent national policy scenario NCEP at 2030 year horizon, are reported.

The generation and consumption levels associated with the scenario under study are applied to a network model including the development projects at 2030, solved by means of SPIRA, the official tool adopted by Terna for static planning studies, yielding power flows on branches and relevant margins. From the network model, the PTDF matrix is evaluated and indexes presented in sub-section 3.2.2 are eventually determined for the Centre South and Centre North Italian market zones, exploiting the MatPower environment [221]. The analysed network section involves 190 generation nodes and 170 lines.

When present, the planned HVDC Adriatic link is supposed to carry its maximum rated power (i.e. 1000 MW) from Centre South (Villanova) to Centre North (Fano) when renewable production exceeds a specified threshold, with a proportional reduction otherwise.

In Table 3.4 the flexibility indexes of the grid infrastructure calculated with respect to all EHV-HV transmission lines (nominal voltage above 100 kV) across the critical section Centre South – Centre North, for 2030 NECP scenario in both conditions "with" and "without" the planned Adriatic submarine HVDC link across the critical section are reported. The indexes are calculated in the presence of high renewable production and consequent maximum power transfer along the planned HVDC link when present. It can be observed that in the presence of the planned HVDC link both indexes reduce, pointing out higher availability of the network in the case flexible operation is required.

Table 3.4. Results of Indexes calculation for the Centre South and Centre North market zones of the Italian power system in each condition and in each scenario under study.

Scenario	**Indexes**		
	Planned HVDC	***SRMI(t)***	***SNMI(t)***
2030 NECP	Yes	6.53	10.23
	No	7.05	10.95

3.3 Conclusions

In order to assess the usefulness of the flexibility requirements assessment methodology in planning studies proposed in [201], [206], the values a set of significant indicators involving both market and network simulations have been calculated in two different real planning cases study: (1) the whole Italian power system in the European 2030 ST and DG scenarios with and without the planned network developments included and (2) the critical section Centre South – Centre North in the two national policy 2030 NES and NCEP scenarios with and without the planned HVDC Adriatic link included.

The main results can be summarized as follows:

1. The selected market-based indexes are evaluated for the Italian power system. In the 2030 ST scenario, without planned network development actions, a value of RLPI of 0.69 is obtained, while introducing development actions, the same index reaches the value of 0.78, with a percentage increasing of more 11.7%. In the 2030 DG scenario, the RLPI value grows from 0.41, without planned network development actions, to 1.01 in presence of planned network development actions, with a percentage increase close to 147.5%.

   The REPI index shows the most significant value in the 2030 DG scenario in presence of all network reinforcements, when the percentage of load covered by wind and solar energy reaches up to 25%. The same percentage drastically drops to the 8% when the development actions are not included.

   By the analysis of the SNSP index small variation is observed in the 2030 ST scenario (from 0.27 in the case "with" to 0.21 in the case "without" planned interventions), while a more significant changing is registered in the 2030 DG scenario where the index drops from 0.35 to 0.11 with and without network developments respectively;

2. The same market-based indexes are evaluated for the specific portion of the Italian power system Centre South – Centre North. The impact of the planned HVDC Adriatic link is quantified results in an increase of all indexes values in the two national policy scenarios.

   Moreover, grid infrastructure assessment based on power flow margin and flexibility analysis through DC power flow model and PTDFs have been performed in the 2030 NCEP scenario. Results have proved that the HVDC connection allows an improvement in flexibility indicators, and the validity of the method for real-sized power systems.

4. Cost-effective Target Capacity assessment in the energy transition: the Italian methodology

The transmission capacity increase within and between Member States is likely to play an essential role in maintaining the European power system operation secure and economic ensuring the growing RES generation integration.

Long-term transmission expansion planning in a restructured electricity market environment needs adequate methods able to balance different technical and economic objectives, such as: the TSOs congestion revenues, the producers bidding strategies (related to the ongoing synchronous power units phase-out), the social welfare resulting from end users electricity prices and the long-term fixed and operational costs associated with investments in transmission network expansion.

In this context, the TSOs are required, both from the Regulators and the other market participants, to address the investments in a cost-effective way, considering all mentioned different objectives, and with the aim to:

- maximize the Socio-Economic Welfare (SEW);
- minimize the investments risk;
- enhance power system security and reliability;
- reduce new transmission infrastructure environmental impact.

Furthermore, the analysis of the long-term transmission expansion planning is strongly affected by the market architecture: in the Italian context, the transmission sector is a monopoly, while power generation and distribution sectors are market competitive areas. Terna is responsible for the Italian power system planning, operation and maintenance and has to ensure a non-discriminatory access to the market.

In recent years, an output-based incentive-regulation mechanism has been set up in order to attract and prioritise the TSO investments where the benefits in terms of system efficiency are higher. In 2017 the Italian Energy Regulatory Authority (ARERA) requested Terna to assess the “Target Capacity”, defined as the efficient level of transmission capacity to be realized, for each boundary of the Italian power system in each significant planning scenario.

This Section deals with a novel methodology developed to the Italian TSO in order to assess an optimal level of transfer capacity based on the simultaneous investigation of capacity increases at all relevant market sections. The congestion hours and the average values of hourly price spreads resulting from market simulations are the indicators used to select the additional

capacities to implement in the reference grid. The new capacity is then verified by means of network and market analysis in order to confirm that related benefits outweigh the costs.

The proposed methodology has been developed during the year 2018 and launched for public consultation in order to collect all relevant stakeholders' (independent academic, experts consulting and utilities companies) feedbacks. It has been applied to the Italian case for two relevant 2030 contrasting energy scenarios: different development strategies are defined and the most cost-effective have been chosen by the means of the "least regret" criterion as the objectives for the Italian TSO.

The second edition of the target capacity report is foreseen to be issued at the end of year 2020: the updated methodology has been launched for public consultation at the end of July and the main innovations with respect to the previous version are illustrated in sub-section 4.6 of this thesis.

4.1 Introduction

In recent years, the unbundling of the electricity sector together with the profound energy landscape transformation have raised new challenges to network planners and regulators. The climate and energy objectives defined at the European level aim at deepening the integration of the European power markets [201] and the electricity sector is recognized as one of the main contributors to the energy transition. Consequently, network expansion planning became a very complex multi-objective problem [222],[223] including: the efficient location of transmission expansion developments, the mitigation of transmission congestion, the security and reliability requirements fulfilling, the nondiscriminatory access to generation resources and the market participants competition facilitation [224].

New methods are required to identify cost-effective development strategies in presence of increased uncertainties about load and generation trends, fuel availability and cost, market rules and government policies, transmission infrastructure realization costs, [225 – 228].

In the national context, in 2017 the ARERA requested the Italian TSO to define the "Target Capacity", i.e. defined as the efficient transmission capacity to be realized, for each relevant internal section and external border of the Italian power system, in each significant planning scenario.

In this Section the novel developed iterative methodology and the results obtained by its first application [229] are presented. To assess the additional transmission capacity both market simulations based on zonal models and network simulations based on detailed network topology have been performed, so as to include in the analysis economic considerations (e.g. market design, regulation schemes, generation costs and generation units bidding strategy) and technical network aspects (e.g. flow distribution on lines, losses, and operational constraints on network topology and reliability). Furthermore, the analysis has been performed in the two contrasting scenarios at the 2030 study horizon, i.e. the ST and the DG scenarios [26], [119], [212], with the aim to consider the uncertainty affecting the provisional load, generation capacity trend, commodities and resources prices in a long-term view.

In literature, several mathematical optimization, heuristic and meta-heuristic methods have been proposed to resolve the transmission expansion problem and identify robust development strategies in uncertain environment. A complete literature review on transmission expansion planning models is presented in [230].

The first category (mathematical optimization) includes all approaches expressing the transmission planning as an optimization problem: once the objective function is defined, it is

subjected to all relevant technical and economic constraints manageable by the algorithm. The solution is obtained by means of different techniques, such as linear programming [231], [232], non-linear programming, mixed integer linear programming [222], [233], and mixed integer non-linear programming [224]. The practical limitation to the use of the optimization methods is the substantial computational efforts (often non compatible with TSOs tasks timing) and the need for simplifications reducing the quantity of transmission expansion problem aspects under consideration.

In [230] the heuristic methods are defined as "*techniques that, instead of using a classical optimization approach, go step-by-step generating, evaluating, and selecting expansion options, with or without the user's help*". Some works based on the heuristic approach are [234], describing a transmission expansion tool based on "least effort" criterion, and [235] presenting a transmission expansion model based on the decomposition in different investment and operation subproblems and [236] proposing a branch and bound technique to solve the investment sub-problem.

With the aim of developing a methodology able to find feasible solutions to the target capacity assessment request, obtaining reasonable computational times while taking into account all relevant information about the main characteristics of the whole interconnected European power market and the detailed national grid topology for transmission (400 – 230 kV) and sub-transmission (150 – 132 kV) voltage levels, an heuristic approach is adopted. This kind of approach allows to fix robust sub-optimal development strategies in a multi-scenario analysis, exploring a large research solution space under the constraints deriving from empirical evidences. Three different custom-written tools enclosing the specific characteristics and inherent complexity of the Italian power system in the restructured competitive environment are adopted: demand hourly profiles, reliability and security costs, multiple contingencies, ohmic losses, hydrological scenarios and bidding strategies are all aspects considered in the Day Ahead zonal Market, Ancillary Services zonal Market and Grid Reliability and Adequacy nodal network simulators in our analyses.

The developed approach represents a relevant novelty in planning methods, overcoming the techniques adopted by the other European TSOs for similar scopes in methodological rigor and completeness, as confirmed by an independent academic reviewer in [237]. In fact, the yearly "Network Option Assessment Report" ("NOA") carried out by the Great Britain System Operator "National Grid" [238] aims at recommending in which development projects proposed by the Transmission Owners ("TOs") there should be investment during the coming year, performing a market analysis consistent with the significant energy scenarios [239] and the

system requirements identified in the “Electricity Ten Years Statement” [240] and providing a prioritization of the candidate options. The “Power System Needs 2030 and 2040 Report” [241] of ENTSO-E is a partial exercise detecting the one cross-border cost-efficient capacity specific dimension. Moreover, this latter analysis is performed in one energy scenario, and the only Socio-Economic Welfare benefit is evaluated (“SEW-based” needs). However, both mentioned practices adopted only market simulations performed through a single tool.

The iterative methodology developed detects the cost-efficient target capacity for each internal section and external border of the Italian power system in a multi-scenario analysis including network topology details, evaluating several benefits and exploring new solutions able to increase the interconnection levels also besides the transmission capacity provided by the already planned projects, avoiding the risk of profitable investments underestimation.

Custom-written software tools enclosing the specific characteristics of the Italian power system in the restructured competitive environment are adopted.

The main contributions of the proposed approach are:

1) the formulation of a new heuristic methodology for assessing the cost-effective additional transmission capacity;
2) the identification of different development strategies (one for each considered scenario) on the basis of an iterative process which determines and tests the increases of transmission capacity;
3) the construction of marginal cost and benefit curves of new transmission capacity for each section/border in each considered planning scenario.

4.2 Regulatory Framework

In the March 2002 European Council of Barcelona, an electricity interconnection target equivalent to at least 10% of the installed generation capacity for Member States by 2005 was established. In October 2014, the Council concluded that "the European Commission supported by the Member States will take urgent measures in order to ensure the achievement of a minimum target of 10% of existing electricity interconnections, as a matter of urgency, and no later than 2020". Furthermore, the European Commission proposed to extend the interconnection target to the 15% by 2030.

These one-size-fits-all interconnection targets received heavy criticisms, among others by the Agency for the Cooperation of Energy Regulators (ACER) [242], by the Council of European Energy Regulators [243] and by the Italian Energy Regulatory Authority [244], [245], concerning the risks of building inefficient transmission capacity (because benefits could be smaller than costs), to a potential risk of under-investment (when additional capacity above the interconnection target would be efficient) and to double counting effects when used in a cost-benefit analyses or in a multi-criteria analysis.

Also for this reason, after a public consultation in 2015 [246], ARERA proposed the concept of target capacity, meaning the transmission capacity which is economically efficient to build, because its benefits outweigh its costs.

The concept of target capacity was initially proposed in 2012 by ACER in its Opinion 06/2012 on the draft TYNDP 2012 [247]: "*since the main purpose of the TYNDP is to identify the investment gaps, notably with respect to cross border capacities, the Agency expects ENTSO-E to develop a specific assessment of cross-border capacities. The aim should be to identify a target value (MW) for the additional transfer capacities at cross-border boundaries*". In the same Opinion, ACER acknowledge the complexity related to the quantification of the target and the possibility to identify capacity ranges according to each scenario assumptions and each sensitivity case. We note that ACER initially proposed the concept of target capacity as the efficient additional capacity (beyond the existing capacity).

In order to help identify an optimal level of interconnection capacity between bidding zones, ENTSO-E introduced the definition and calculation of target capacities at each border in the TYNDP 2014 and refined them in the ENTSO-E Regional Investment Plans 2015 and in the TYNDP 2016. In particular, the target capacity for every boundary between bidding zones corresponds to the value above which further transmission capacity realization would not be beneficial, because the economic benefit corresponding with the additional capacity cannot

outweigh the deriving costs. We note that under such a definition (retained by ARERA), the target capacity is the total efficient capacity at a specific boundary.

However, still in the TYNDP 2018, ENTSO-E refrained to quantify the target capacity at individual boundaries and only provided some general indications referring to a few main boundaries of the European power system.

After carrying out a second consultation in 2017, ARERA adopted its Decision 884/2017 [248], which requested the Italian transmission system operator Terna to prepare during the year 2018 a report about the identification of the target capacities for the relevant network boundaries of the Italian power system.

In year 2018, as already envisaged during the public consultations, ARERA adopted an output-based regulatory scheme [249], [250], which rewards the commissioning of new transmission capacity at a number of boundaries of the Italian power system (till the target capacity level). No rewards are foreseen for capacity increases which exceed the target capacity.

For each boundary, the maximum reward (which is granted to Terna when the target capacity is reached) is defined as a combination of a percentage of congestion revenues during the years 2016 and 2017 and of a percentage of the benefit related to the increase of socio-economic welfare at that boundary. The choice of these parameters aims at providing more rewards for capacity increases at the boundaries where congestion revenues and expected benefits are higher.

If the increase of transmission capacity does not reach the target capacity, the reward is granted as a part of the maximum reward proportionally to the ratio between the capacity increase and the difference between the target capacity and the previously available capacity.

ARERA also decided to request two reviews of the target capacity report by two different academic independent experts. One of them was appointed by ARERA and the other one by Terna. The reviews were carried out in 2019-2020, and results are publicly available [237], [251].

4.3 Methodology

The purpose of the target capacities' assessment methodology is to identify the additional cost-effective transfer capacity between internal bidding zones and at external borders of the Italian power system in order to support the definition of the output-based regulatory scheme rewarding the increases of transmission capacities and facilitate the development of an efficient and economical electricity transmission system, fulfilling the system needs defined in the Ten Year National Network Development Plan ("NDP").

It is worth highlighting that the proposed methodology does not replace the cost-benefit analysis associated to planned projects included in the yearly NDP, neither it is aimed at verifying the individual planned projects usefulness. It instead provides the cost-effective level of interconnection within the national transmission system and to other external borders. It aims at addressing the complexity of multiple capacity increases at several boundaries and at exploring an optimal development of the entire transmission system under study. Such a dimension is hardly addressed by the traditional cost benefit analyses of individual projects, which cannot provide a holistic view.

As the target capacity across a market section/border is defined as the "cost-effective transfer capacity" the present methodology is based on the definition of a marginal cost curve at each boundary and on an iterative process defining the marginal benefit of the new capacity addition for each section/border in each relevant planning scenario.

The target capacity assessment method has been developed consistently with Regulator directives and the draft methodology launched for public consultation in the first half of 2018: relevant stakeholders' feedbacks supported improving the approach before its application.

The present methodology provides the efficient target capacity in 2030 year horizon for each scenario under study, with a single study year approach; the least regret analysis technique [238], [252], [253] is then applied to decide the unique recommended development strategy.

The initial network (or "base case") is made up of the existing grid plus the projects that have a strong chance of being implemented by the date of the considered scenarios.

In order to build the initial point of the interested sections/borders marginal benefit curve, the "Take Out One at the Time" (TOOT) method [254] is applied, in compliance with the cost-benefit analysis performed in the European context: as the base case reflects a future grid situation in which the aforementioned additional network developments are presumed to be realized, the projects under assessment are removed from the forecasted network structure (one at a time, hence the name of the method) to evaluate the changes to the benefit indicators.

Starting from the base case, an iterative approach is used. All sections/borders of the power system under study are simultaneously investigated in order to determine the following parameters:

- Condition A (C_{dA}), is the ratio between the *k*-th section/border average of absolute market energy hourly price spreads in the *i*-th iteration and in the *s*-th scenario, $\Delta p_{i,k}^{s}$ and the marginal investment cost of the *i*-th transmission capacity unitary increase on the *k*-th section/border, $MC_{i,k}$:

$$C_{dA} = \frac{\frac{1}{8760}\sum_{r=1}^{8760}\left|\Delta p_{i,k}^{s}\right|}{MC_{i,k}} = \frac{\left|\overline{\Delta p_{i,k}^{s}}\right|}{MC_{i,k}} \tag{4.1}$$

- Condition B (C_{dB}), is the number of congestion hours across the *k*-th section/border H_k

$$C_{dB} = H_k \tag{4.2}$$

A section/border is considered suitable for additional transfer capacity installation if any of the two parameters triggers the respective reference threshold, named L_{dA} and L_{dB}.

Once a threshold is triggered on one (or more) section/border, additional transmission capacity is implemented on it (or them) using the "Put IN one at the Time" (PINT) method [254]: the reference case reflects an initial state of the grid without the capacity increases under assessment, which are then added one at a time to this reference case in order to evaluate the variations in load flows and other indicators.

The new transfer capacity $AC_{i,k}$ is put on the *k*-th section/border of the reference grid and the associated marginal costs and benefits are evaluated. If the ratio between the marginal benefit and the marginal cost of the *i*-th transmission capacity increase on the *k*-th section/border respects the condition:

$$\frac{MB_{i,k}}{MC_{i,k}} > 1 \tag{4.3}$$

then, the additional transfer capacity usefulness is confirmed and a point on the individual section/border marginal cost-benefit curve is depicted.

The methods adopted for the marginal cost and the marginal benefit evaluation are detailed in sub-sections 4.3.1 and 4.3.2 respectively.

The iterative process stops when no section/border presents favorable conditions to new additional capacity, which means that C_{dA} and C_{dB} thresholds are not triggered or, if they are, the condition (4.3) is not satisfied.

Finally, at each section/border the marginal cost and benefit curve is enriched with values related to the last iteration. Explicative examples of the *k*-th section/border marginal cost and benefit curves resulting from the iterative process for two different scenarios are illustrated in Fig. 4.1.

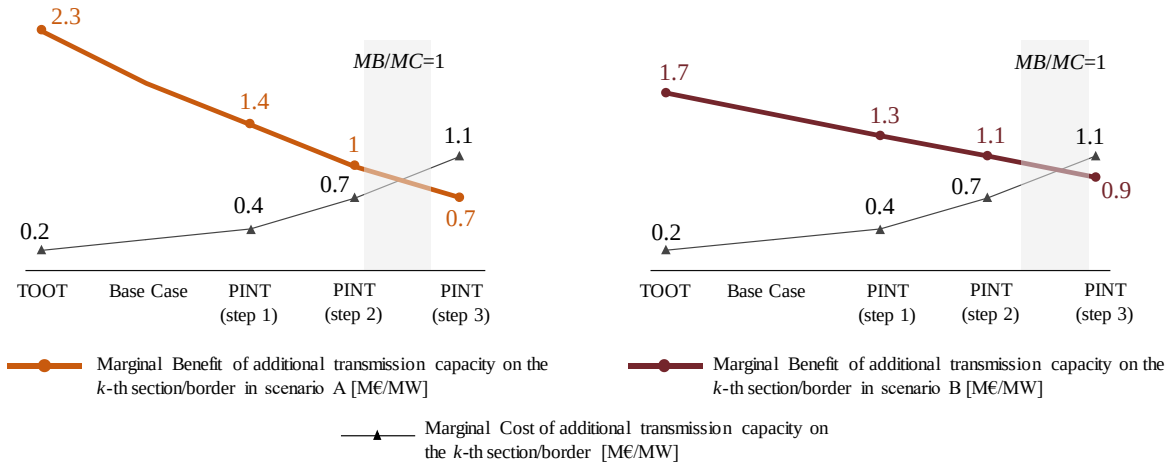

Fig. 4.1. Examples of the k-th section/border marginal cost and benefit curves resulting from the iterative process for two different scenarios.

The cost-effective transmission capacity increase for the *k*-th section/border in the *s*-th scenario, χ_k^s, is defined around the intersection of the marginal cost and benefit curves as expressed in (4.4):

$$\chi_k^s = \sum_{i=1}^{N^+} AC_{i,k}^s + AC_{l,k}^s \cdot \frac{MB_{l,k}^s}{MC_{l,k}^s} \tag{4.4}$$

Where:

- N^+ represents the number of iterations for which the condition (4.3) is satisfied for the *i*-th transmission capacity increase on the *k*-th section/border in the *s*-th scenario $AC_{i,k}^s$;
- $AC_{l,k}^s$ is the "last" transmission capacity increase on the *k*-th section/border, corresponding to the last iteration in the *s*-th scenario;
- $\frac{MB_{l,k}^s}{MC_{l,k}^s}$ represents the ratio between the marginal benefit and the marginal cost related to the last transmission capacity increase $AC_{l,k}^s$ on the *k*-th section/border in the *s*-th scenario (i.e. the capacity increase with benefits below costs).

The target capacity is then defined as:

$$TC_k^s = EC_k + \chi_k^s \tag{4.5}$$

Where EC_k is the existing transmission capacity in the *k*-th section/border.

The workflow of the entire iterative process is depicted in Fig. 4.2. The entire iterative process leads to the definition of development strategies for all power system boundaries for each scenario.

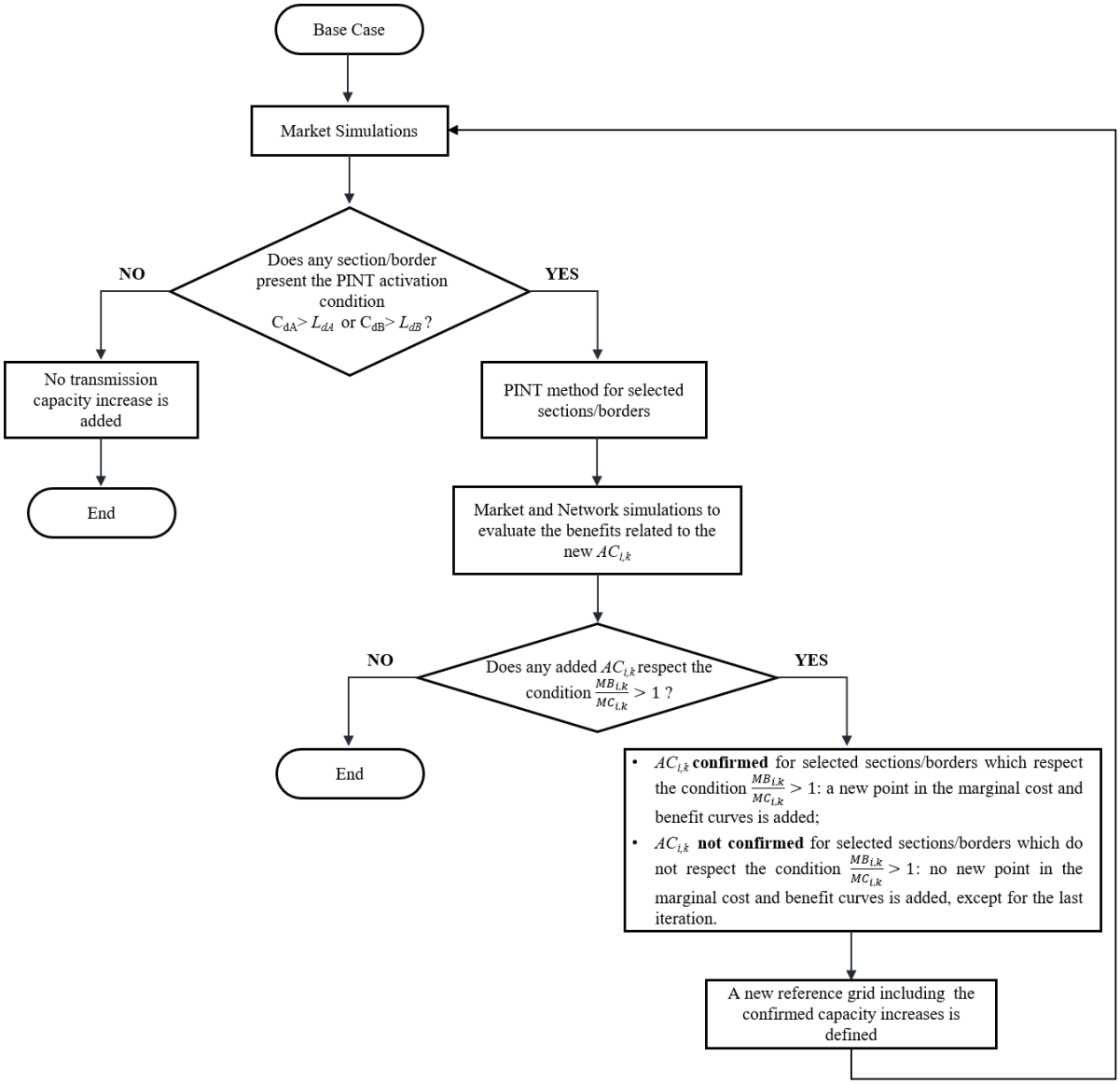

Fig. 4.2. Workflow of the iterative process.

The least regret approach applied for each border/section at contrasting scenarios allows the identification of the unique value to aim for.

4.1.1 Marginal cost evaluation

First of all, the evaluation of the marginal cost at each section/border considers the unitary investment costs of already planned projects (included in the NDP). The order in which they are considered depends on the project progress.

If the target capacity needed on the *k*-th section/border exceeds those provided by the planned projects, further reference marginal costs must be assumed. It is clear that, in this case, the cost estimation is subject to a significant uncertainty without supporting information on the details of the projects realization. The report [255] provides useful reference values for relevant electricity infrastructure (overhead transmission lines, underground and subsea cables, onshore AC substations, and HVDC converters): the information is based on historical data collected under the TSOs and other developers experiences in electricity infrastructures realizations.
In the Italian context, Terna developed a new methodology for the assessment of standard investment costs [105], approved by the Regulator in 2017.
With particular reference to the unit investment costs of development projects affecting external borders, we assumed that Italy covers half of the total cost, in the absence of other information.
Since the capacity increases are fixed while the transmission capacity increases provided by the projects are specific, they can contribute in a different manner to the final target capacity in the subsequent iterations. Given Ω_i the set of all projects (planned or not) to be considered on the *k*-th section/border in the *i*-th iteration, the following different cases could occur:

- if the Total Transfer Capacity (TTC) provided by the ω-th project is equal to the additional capacity needed, i.e. $TTC_{\omega,k} = AC_{i,k}$, its unit investment cost $C_{\omega,k}$ (M€/MW) matches the marginal cost $MC_{i,k}$ of the additional transfer capacity $AC_{i,k}$:

$$MC_{i,k} = C_{\omega,k} = \frac{C_{tot,\omega}}{TTC_{\omega,k}} \tag{4.6}$$

- if the additional capacity step is provided by two (or more) projects, the marginal investment cost of that capacity increase is the weighted average of the unit investment costs of the considered projects.

The weighting factor of the ω-th project compared to the needed *i*-th additional transmission capacity increase on the *k*-th section/border can be expressed as:

$$x_{\omega,i,k} = \frac{AC_{i,k} - \sum_{\forall y \in Y}(TTC_{y,k} - \sum_{t=1}^{i-1} TTC_{t,y,k})}{AC_{i,k}} \tag{4.7}$$

Where Y represents the subset of Ω including the projects already considered in the same iteration or in the previous ones. Once a specific project transmission capacity increase is considered in the *i*-th iteration, it can no longer be used in the following iterations.
The marginal cost expression can be generalized as follows:

$$MC_{i,k} = \sum_{\forall \omega \in \Omega_i} x_{\omega,i,k} \cdot C_{\omega,k} \tag{4.8}$$

4.1.2 Marginal benefit evaluation

The benefit categories included in target capacity assessment methodology and evaluated through market and network simulations are listed in Table 4.1.

Table 4.1. Benefit categories included in the target capacity assessment methodology.

Code[1]	Benefit categories included	
	Description	***Simulator***
B1	Social Economic Welfare (SEW)	Day Ahead zonal market
B3	Energy Not Supplied (ENS) reduction	Grid Reliability and Adequacy nodal network
B5	RES integration	Grid Reliability and Adequacy nodal network
B7z	Zonal dispatching costs variation	Ancillary service zonal market
B7n	Nodal dispatching costs variation	Grid Reliability and Adequacy nodal network
B18	CO_2 variation	Day Ahead zonal market
B19	Non–CO_2 emissions variation	Day Ahead zonal market

[1]Code used in the Cost-Benefit Analysis carried out in the NDP.

The marginal benefits values need to be discounted to the present year, in order to allow the comparison with the expected unitary investment costs.

The marginal benefit of the *i*-th transmission capacity unitary increase on the *k*-th section/border $MB_{i,k}$ is defined as:

$$MB_{i,k} = \frac{\lambda \cdot B_{tot\ i,k}}{AC_{i,k}} \tag{4.9}$$

Where:

- $B_{tot\ i,k}$ is the yearly benefit calculated at the *i*-th iteration, including all the benefit categories listed above;
- λ is the discount factor defined setting the discount rate r at 4% (real), as provided for in [215], [254], [256], and as expressed in (4.10)

$$\lambda = \sum_{\tau=1}^{25} \frac{1}{(1+r)^{\tau}} \tag{4.10}$$

4.1.3 Least regret approach

The developed iterative methodology results in the identification of *n* development strategies (or "options"), one for each scenario under study: the least regret approach is employed to define the unique set of cost-effective target capacities to aim for. In fact, it allows to determine the worst option as the one that leads to the highest regret for the decision maker.

In this context, since the main objective is maximizing the benefit to the system, the net benefit (difference between total benefit and investment costs) is considered as the most significant indicator.

The regret related to the *n*th development strategy in the *s*-th scenario, $regret_n^s$, can be expressed as:

$$regret_n^s = NB_{ref}^s - NB_n^s \tag{4.11}$$

Where:

- NB_n^s represents the net benefit of the *n*-th option in the *s*-th scenario;
- NB_{ref}^s represents the net benefit of the reference option, i.e. the development strategy that presents the highest net benefit in the *s*-th scenario.

Selecting the development strategy with the lowest maximum regret expose the entire system to the least amount of risk. Therefore, the set of final values of target capacity respects the min-max criterion:

$$\min_s \left[\max_n \left(regret_n^s \right) \right] \tag{4.12}$$

4.4 Simulation Tools

4.4.1 Day – Ahead and Ancillary Service Zonal Market Simulators

The electricity market simulations allow the assessment of a first set of benefits (B1, B18, B19, a share of B7), leaving to the network analysis the evaluation of the remaining benefits (B3, B5, a share of B7). To this aim both Day-Ahead spot Market (DAM) and Ancillary Services Market (ASM) studies were sequentially performed, consistent with the sequential order of the real Italian power market sessions.

For DAM simulation studies the full model of the European electric grid adopted by ENTSO-E for the TYNDP 2018, depicted in Fig. 4.3, was used. This model represents the European bidding zones using a single branch to characterize the equivalent transmission capacity between interconnected market zones. The model considers a single node for each country, with the exception of Denmark, France, Greece, Italy, Luxembourg, Norway, Sweden and United Kingdom.

The DAM studies have been performed through the market simulator "Promed Grid" [214]. It carries out an optimal coordinated hydro-thermal planning of the generation portfolio with an hourly time discretization over one year, implementing the day-ahead hourly energy market, characterized by a system marginal price and by a congestion management determined through a zonal market-splitting procedure.

Promed Grid is based on a deterministic model that considers both the economic and technical aspects of the power systems: the simplified market model, the hourly load, thermal generation fleet technical data, costs and constraints associated with different fuel types, thermal unit production constraints and technical data of the hydro generation set.

The simulator determines each generating unit hourly output and the flows in the equivalent links between the different bidding zones. It also calculates further indicators pertaining to the environment impact associated with each market solution, such as the corresponding emissions (CO_2, NO_x, SO_x) and dust emissions.

The DAM simulation is carried out in two different computational phases:

1. Unit Commitment: according to a merit order and considering the system constraints, the on/off state of each thermal power unit is determined;
2. Dispatching: the coordinated hydro-thermal hourly production scheduling is defined in compliance with system constraints.

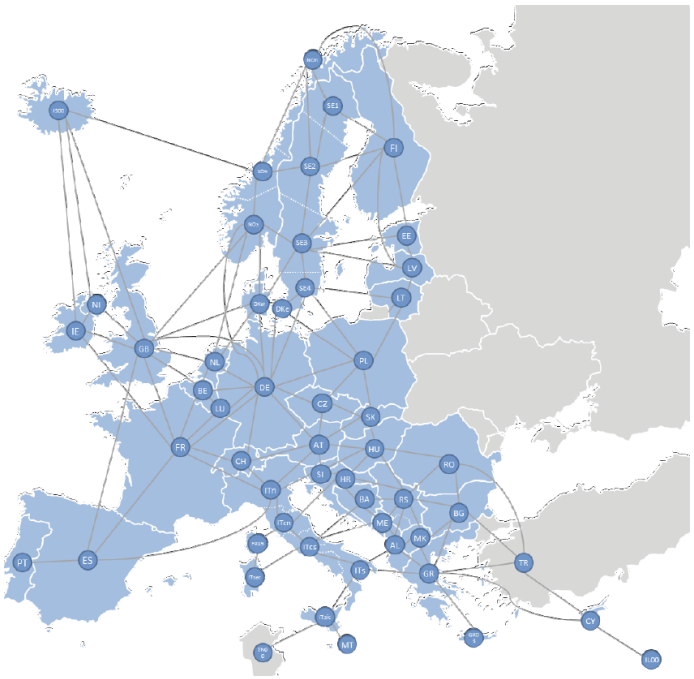

Fig. 4.3. ENTSO-E simplified market model (TYNDP 2018).

The final market solution results from an iterative converging process where a bidding strategy aimed at recovering at least each generation unit's variable costs, is revised after each iteration loop. In each loop the optimal operation generation schedule of the generating system is obtained solving a very large quadratic programming optimization problem. The objective function consists in the total variable generation costs minimization while respecting all the technical constraints.

The simulation process of the described market tool is depicted in Fig. 4.3, while some relevant applications are illustrated in [257] – [259].

The Ancillary Services Market (ASM) studies have been carried out by the means of the simulation tool "Modis" [260], [261] a multi-area market simulator specifically tailored to the Italian ASM, performing the yearly simulation of the ASM based on a pay-as-bid mechanism. It simulates ASM procurement actions for different services, such as secondary and tertiary reserve margins and real time balancing, for a whole year with hourly discretization.

Starting from the preliminary schedules of generating units resulting from the DAM simulation, Modis emulates the ASM behaviour modifying the generating schedules in order to ensure the appropriate reserve margins in each bidding zone and offsetting the gaps between demand and supply, consequent to simulated unbalances. For this reason, the deterministic model implemented in Modis belongs to the class of "security constrained differential unit commitment problems", where upward and downward regulation of the controllable variables

are made starting from an initial status inherited from the DAM solution. The objective function is the minimum rescheduling costs based on the bidding model included in the simulation tool.

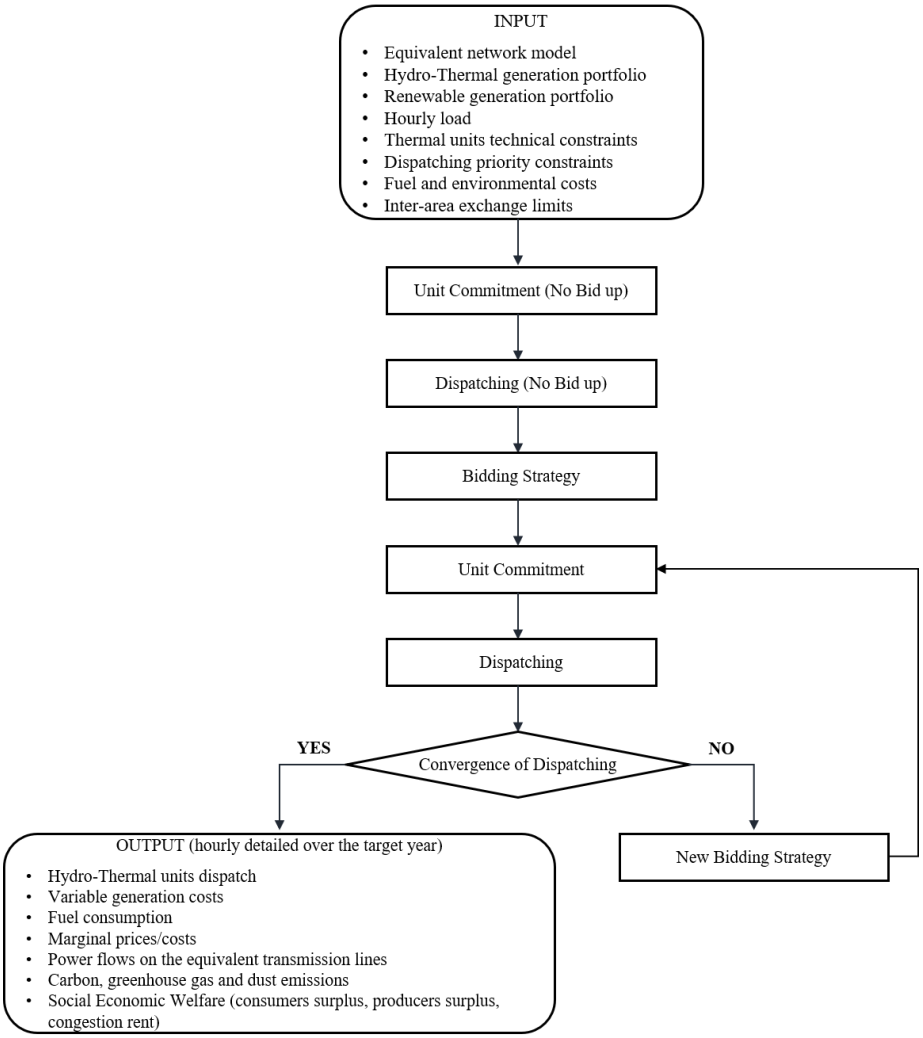

Fig. 4.3. Promed Grid simulation process.

4.4.2 Grid Reliability and Adequacy Simulator

The remaining set of benefits (B3, B5, a share of B7) are assessed through network studies based on a grid reliability and adequacy simulation model, using the Grid Reliability and Adequacy Risk Evaluator (named “GRARE”) [262].

A network model derived from the Italian transmission grid comprehensive of all the voltage levels (380, 220, 150 and 132 kV) has been used. In particular, the nodal network model consists of about 11,000 nodes, 10,000 lines and 4,000 transformers. In addition, the busbar model of the European countries has been included, considering the national loads and the generation fleet of each zone in accordance with the TYNDP 2018 scenarios, neglecting the internal transmission grid and the related network losses.

The adopted network simulator is able to evaluate large power systems reliability level through a probabilistic approach: security, operational and economic constraints are all processed in a non-sequential Monte Carlo simulation, managing multiple different stochastic variables.

At the end of each simulation, the two main power systems reliability indicators are evaluated:

- the Expected Energy Not Supplied, or "**EENS**" (in MWh) is defined as the average value of the annual not supplied demand among the several years simulated;
- the Loss of Load Expectation, or "**LOLE**" (in h/y) is defined as the expected amount of hours per time period when the available generation capacity is not sufficient to cover the demand.

In each Monte Carlo extraction, the total residual load RL is computed as follows:

$$RL = L + R - RES - IG \tag{4.13}$$

Where:

- L is the total demand of the system;
- R represents the system reserve requirements;
- RES indicates the renewable sources output (Solar, Wind and Hydro);
- IG represents the imposed production (e.g. bioenergy and geothermal).

Maintenance, faults and other power units constraints (i.e. must-run) are also considered to define the available thermal set.

The system condition is simulated by using a weekly sampling and the initial thermal Unit Commitment is obtained by the means of a mixed integer method, taking into account the requirements in terms of operational reserve to be satisfied in each bidding-zone.

The optimal power units dispatching is then evaluated by solving a linear problem according to the obtained cross-zonal exchanges and possible load-shedding events resulting from available generation and import capacity inadequate to meet the demand are identified.

In output from the simulation, power production of each power unit and energy source, EENS and LOLE indicators, and power flows are provided. This procedure is replicated and parallelized for the all weeks and the results weighted on the total tests number.

4.5 Case study and results

The proposed methodology has been built for real-world applications. The Italian power system case study is illustrated in this section.

4.5.1 Data and scenarios

Since the transmission capacity development concerns the medium-long term horizon and given the ten year view of the NDP, the target capacity assessment has been performed at 2030 year horizon in the same relevant planning scenarios adopted in the 2018 NDP cost-benefit analysis, the ST and the DG scenarios, already described in the previous Chapter 2 and Chapter 3.

The market structure adopted in the target capacity assessment is the one in force until the year 2018, depicted in Fig. 4.5. The Italian power system is divided into six different market zones (North, Centre North, Centre South, South, Sardinia and Sicily). Moreover, there are some "virtual zones" in the South and in Sicily where production is limited due to network constraints.

This structure naturally leads to the individuation of the internal sections under study:

1. IT North – IT Centre North;
2. IT Centre North – IT Centre South;
3. IT Centre South – IT South;
4. IT Sicily – IT;
5. IT Sardinia – IT.

As regards the external boundaries, although the analysis has been carried out considering the individual borders, these have been merged in assessing the global potential in terms of transmission capacity increase, according to following criteria:

- the "Northern border" comprises the borders with France, Switzerland, Austria and Slovenia. Since they are geographically and electrically connected, the transfer capacity is currently evaluated considering the mutual influence in N-1 operational conditions. Furthermore, in the first iteration, the congestion hours values and the average of absolute market energy hourly price spreads are basically aligned;
- the "Balkan border" comprises the borders with Croatia, Montenegro and Greece, for the same reasons listed above;
- the "North African border" includes the border with the Tunisia, whose detailed model is available since the interconnection project Sicily – Tunisia has been studied in the 2018 NDP [217].

Fig. 4.6 illustrates the internal sections and the merged external borders.

Fig. 4.5. Market zones of the Italian power system (year 2018).

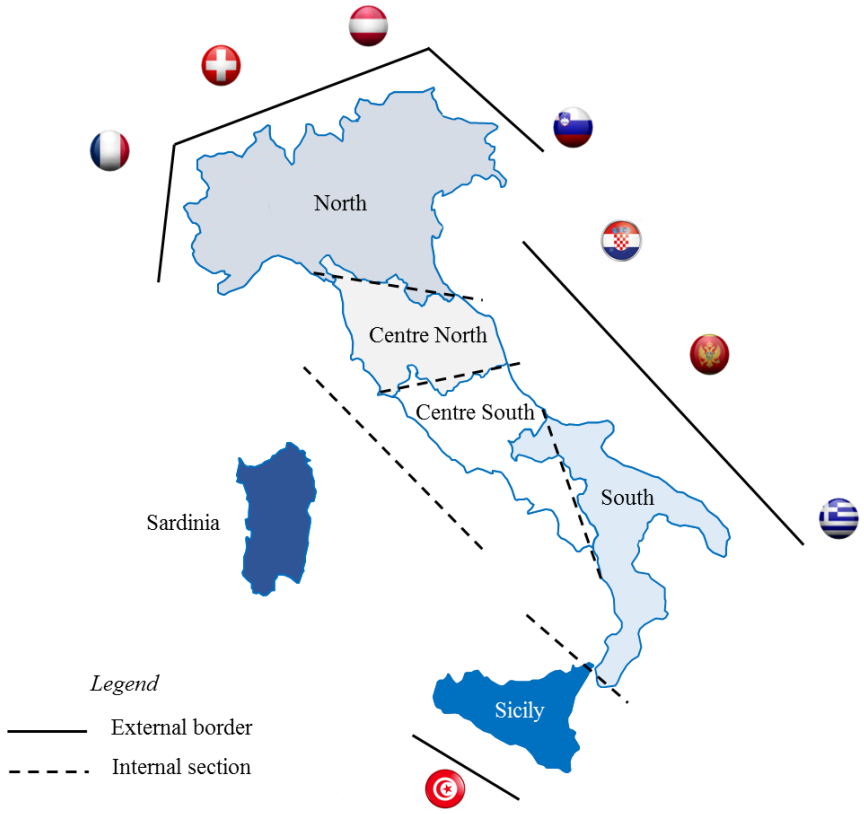

Fig. 4.6. Internal sections and external borders of Italian power system under study.

Depending on whether the transmission capacity increase involves an internal section or an external border, different sizes for the $AC_{i,k}$ are defined as follows:

$$AC_{i,k} = +400 \text{ MW if } k \text{ is an internal section}$$
$$AC_{i,k} = +500 \text{ MW if } k \text{ is an external border} \quad (4.14)$$

These values reflect the common sizes of the most of the planned or already in service projects. The threshold values L_{dA} and L_{dB} are heuristically chosen in order to have reasonable total computing time: they are differently defined for the internal market sections and for the external borders, depending on historical values of price spreads and congestions hours. Furthermore, the threshold L_{dA} is gradually decreased during the iterative process considering the progressive reduction of price spreads related to the new capacity.

Finally, the reference grid, or "base case", consists of the existing grid and of the four projects already authorized which are expected to be in service by 2025, as reported in Table 4.2 and Fig. 4.7.

Table 4.2. Planned development projects included in the base case: transmission capacity increase provided (MW) and section/border involved.

Project		TTC (MW)	Section/border involved
1	320 kV Piossasco – Grand Ile HVDC link	+1200	IT North – France
2	132 kV Brennero – Steinach link	+100	IT North – Austria
3	500 kV Villanova – Lastva HVDC link	+600	IT CSouth – Montenegro
4	380 kV Deliceto – Bisaccia link	+400	IT CSouth – IT South

Fig. 4.7. Planned projects included in the base case (listed in Table 4.2).

For the sake of the clarity, an example of marginal cost calculation for the internal section Centre South – South (named "CS – S") is illustrated in the following.

Table 4.3 summarizes the projects which contribute to build the marginal cost curve for the section Centre South – South: besides the Deliceto – Bisaccia link (useful for the description of the marginal cost curve initial point), Projects 2, 3 are already planned and included in the NDP. In the first iteration, the TTC provided by the Project 2 can saturate alone the additional capacity needed, or rather $TTC_{Pr\,2,CS-S} > AC_{1,CS-S}$. Its unit investment cost matches the marginal cost $\dot{C}_{Pr\,2} = MC_{1,CS-S}$ while the surplus ($TTC_{Pr\,2,CS-S} - AC_{1,CS-S}$) is used in the subsequent iteration, depending on its weighting factor $x_{2,Pr\,2,CS-S}$.

Table 4.3. List of ω-projects contributing to build the marginal cost curve for the section Centre South – South: transmission capacity increase provided, TTC_ω [MW], total investment cost $C_{tot,\omega}$ [M€] and marginal cost MC_ω [M€/MW].

Projects contributing to marginal cost curve building				
Project		$\boldsymbol{TTC_\omega}$	$\boldsymbol{C_{tot,\omega}}$	$\boldsymbol{MC_\omega}$
1	400 kV Deliceto – Bisaccia link	+400	86	0.22
2	400 kV Foggia – Gissi link	+500	176	0.35
3	400 kV Montecorvino – Benevento link	+200	224	1.12
4	HVDC standard project	+1000	1100	1.10

Since the transmission capacity increase required in the second iteration exceeds the TTC provided from planned Project 2 (surplus not used in the previous iteration) and Project 3, an HVDC standard project (named "Project 4") with a rated $TTC_{Project\,4,CS-S} = 1000\ MW$ and investment costs referenced to real values of similar projects is considered to saturate the residual additional capacity needed. Therefore, the projects that contribute to define the $MC_{2,CS-S}$ are Project 2, Project 3 and Project 4, considering the related weighting factors:

$$MC_{2,CS-S} = \frac{(TTC_{Pr2} - TTC_{Pr2,1})}{AC_2} \cdot \dot{C}_{Pr\,2} + \frac{TTC_{Pr3}}{AC_2} \cdot \dot{C}_{Pr\,3} + \frac{AC_2 - [(TTC_{Pr2} - TTC_{Pr2,1}) - TTC_{Pr3}]}{AC_2} \cdot \dot{C}_{Pr\,4} \quad (4.15)$$

The calculation process in subsequent iterations is illustrated in Fig. 4.8, while the marginal cost curve obtained is depicted in the Fig. 4.9.

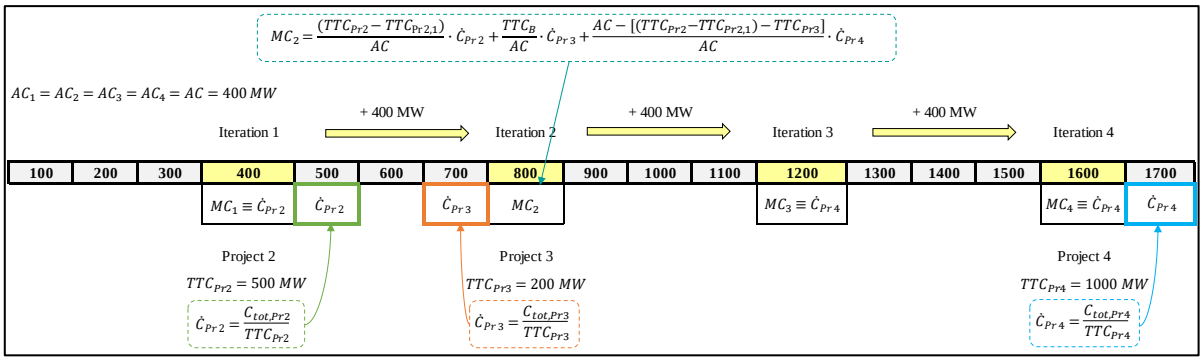

Fig. 4.8. Example of marginal cost calculation process in subsequent iterations for the internal section Centre South – South.

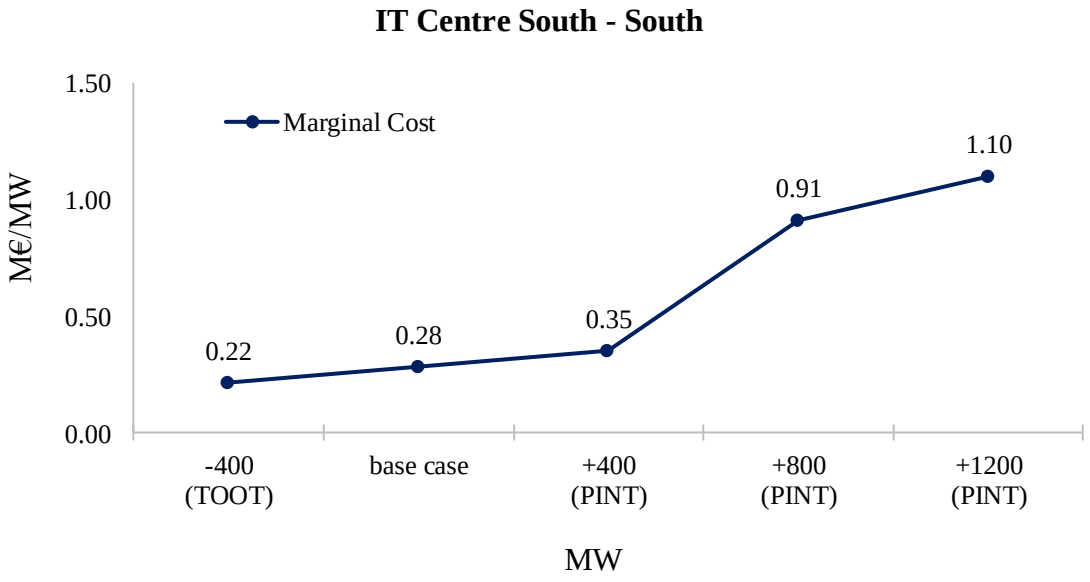

Fig. 4.9. Example of marginal cost curve description for the internal section Centre South – South.

4.5.2 Results

The cost-effective transmission capacity increases for each section/border of the Italian power system resulting from the application of the presented methodology are provided in Table 4.3 and in Fig. 4.10 for each scenario under study.

A significant variation of the transmission capacity increases assessed can be observed in the two contrasting long-term planning scenarios for the Northern border, the Balkan border and the internal IT Sicily – IT section, where the analysis in DG scenario results in transmission capacity increases of +62%, +620% and +100% respectively major than those obtained in the ST scenario, basically due to the higher distributed renewable generation to be integrated and the higher load to be supplied.

Fig. 4.11 shows the marginal cost/benefit curves for the most relevant external borders and internal sections: the dashed area highlights the intersection region between the increasing marginal cost and the decreasing marginal benefit curves. The blue and the green colors correspond to the ST scenario and to the DG scenario respectively.

Table 4.4. Cost-effective transmission capacity increases [MW] for each section/border of the Italian power system in each considered scenario.

Section/Border	χ_k^{ST}	χ_k^{DG}
Northern border – IT North	4500	7300
Balkan border – IT [1]	500	3600
North African border – IT Sicily	1200	1100
IT North – IT Centre North	500	700
IT Centre North – IT Centre South	1100	1100
IT South – IT Centre South	900	900
IT Sicily – IT [1]	900	1800
IT Sardinia – IT [1]	900	900

[1] A single boundary market zone of the Italian power system cannot be defined.

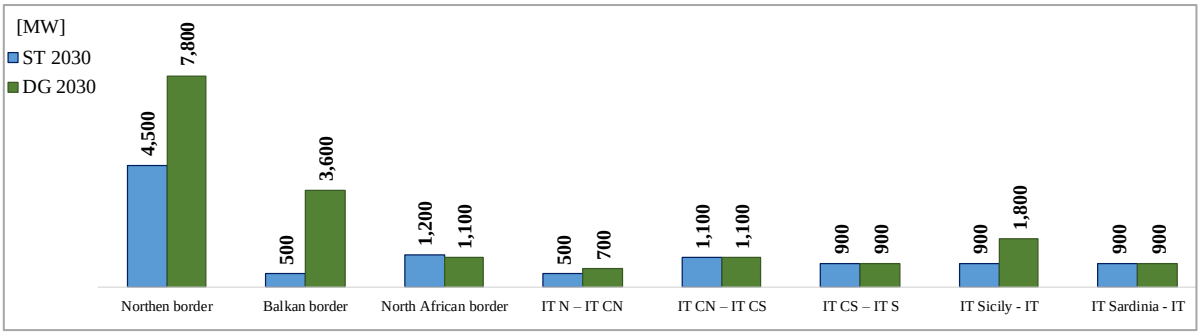

Fig. 4.10. Cost-effective transmission capacity increases [MW] for each section/border of the Italian power system in each considered scenario.

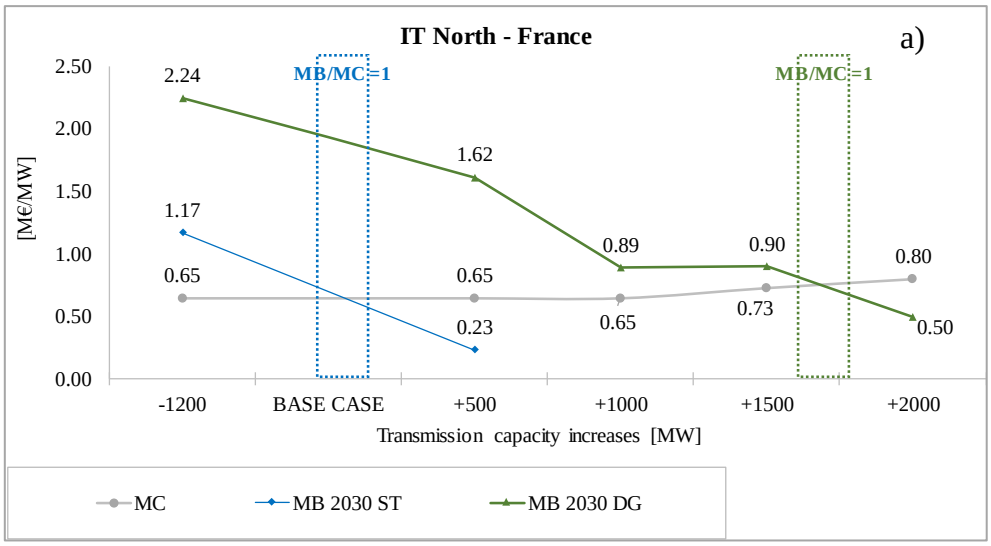
IT North - France
a)
2.50
2.00
1.50
1.00
0.50
0.00
[M€/MW]
2.24
MB/MC=1
MB/MC=1
1.62
1.17
0.89
0.90
0.80
0.65
0.65
0.73
0.23
0.65
0.50
-1200
BASE CASE
+500
+1000
+1500
+2000
Transmission capacity increases [MW]
MC
MB 2030 ST
MB 2030 DG

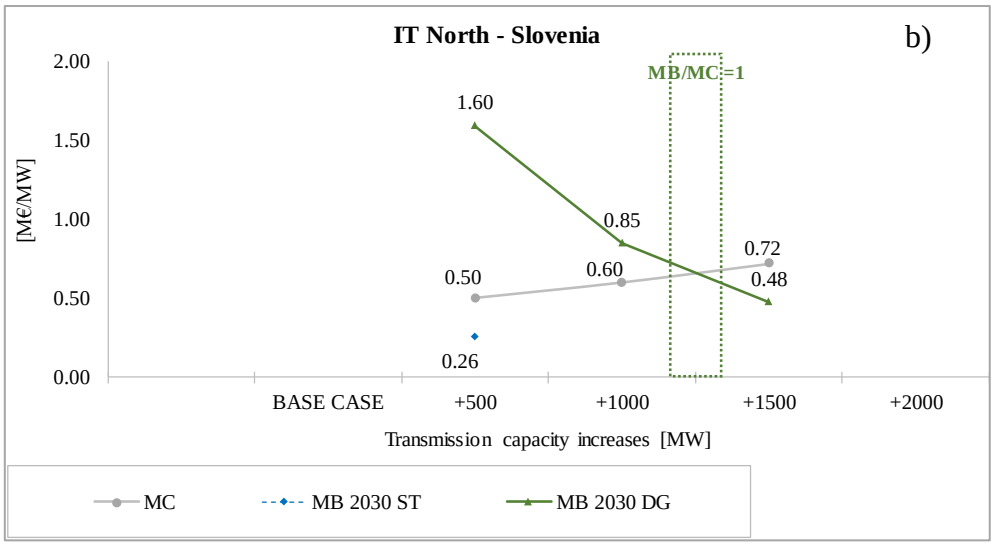
IT North - Slovenia
b)
2.00
1.50
1.00
0.50
0.00
[M€/MW]
MB/MC=1
1.60
0.85
0.72
0.50
0.60
0.48
0.26
BASE CASE
+500
+1000
+1500
+2000
Transmission capacity increases [MW]
MC
MB 2030 ST
MB 2030 DG

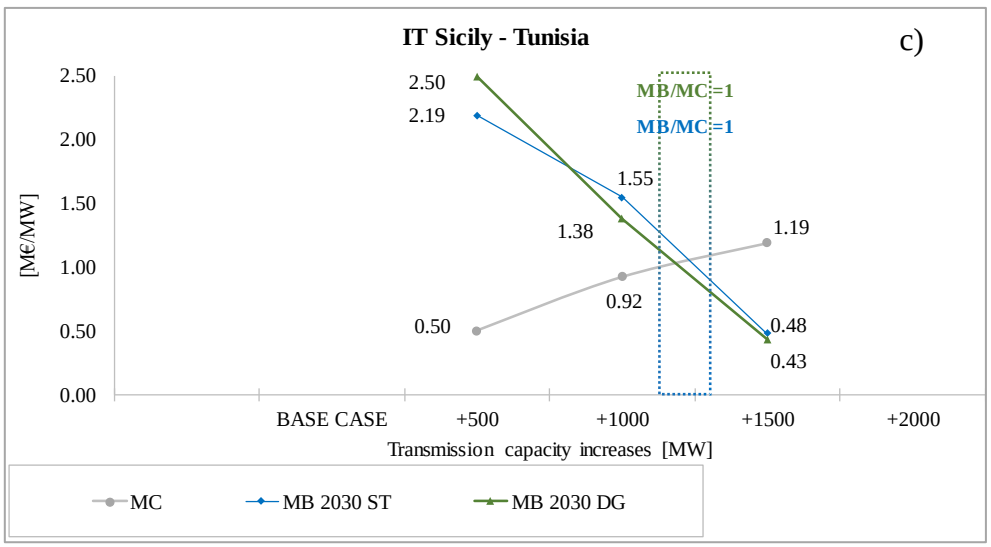
IT Sicily - Tunisia
c)
2.50
2.00
1.50
1.00
0.50
0.00
[M€/MW]
2.50
2.19
MB/MC=1
MB/MC=1
1.55
1.38
1.19
0.92
0.50
0.48
0.43
BASE CASE
+500
+1000
+1500
+2000
Transmission capacity increases [MW]
MC
MB 2030 ST
MB 2030 DG

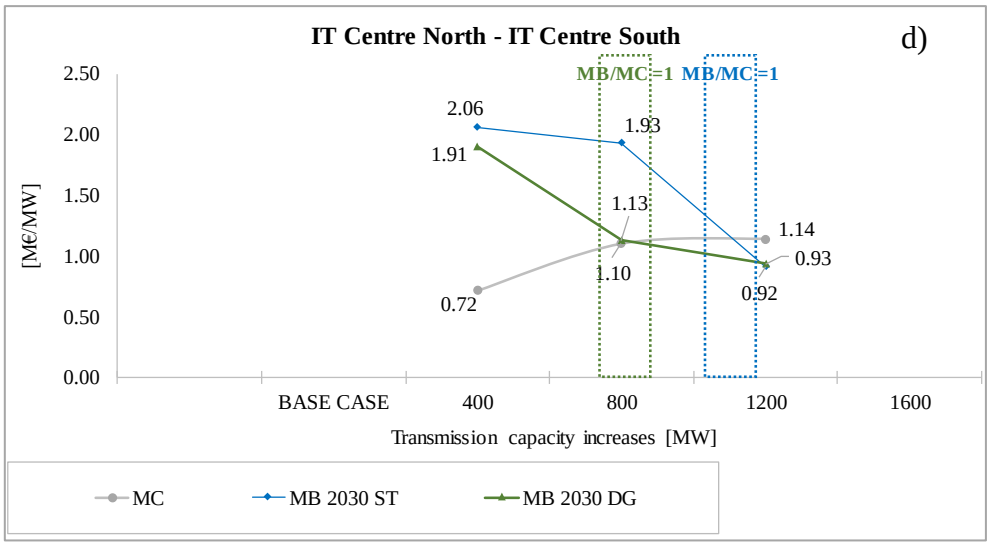
IT Centre North - IT Centre South
d)
MB/MC =1
MB/MC =1
2.06
1.93
1.91
1.13
1.14
0.93
1.10
0.72
0.92
2.50
2.00
1.50
1.00
0.50
0.00
[M€/MW]
BASE CASE
400
800
1200
1600
Transmission capacity increases [MW]
MC
MB 2030 ST
MB 2030 DG

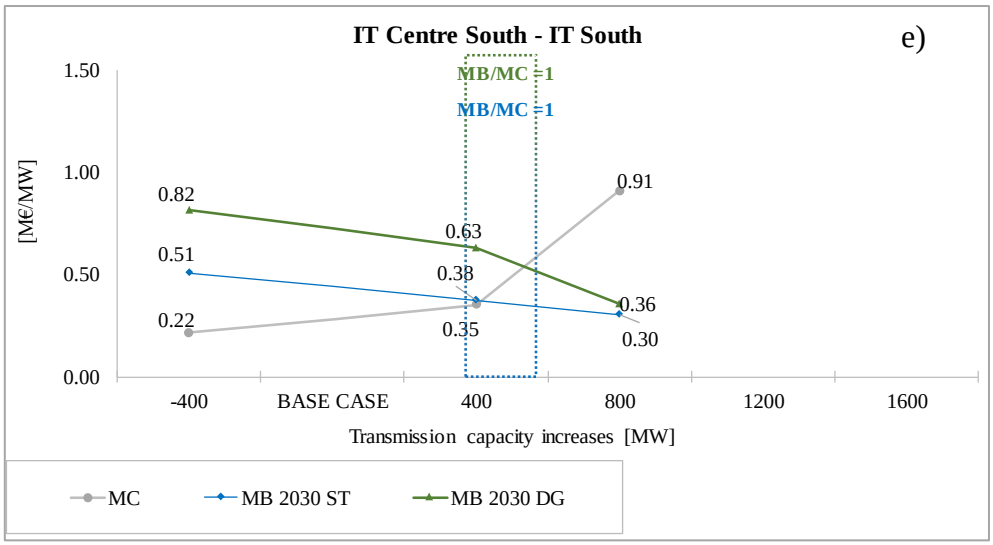
IT Centre South - IT South
e)
MB/MC =1
MB/MC =1
0.91
0.82
0.63
0.51
0.38
0.36
0.22
0.35
0.30
1.50
1.00
0.50
0.00
[M€/MW]
-400
BASE CASE
400
800
1200
1600
Transmission capacity increases [MW]
MC
MB 2030 ST
MB 2030 DG

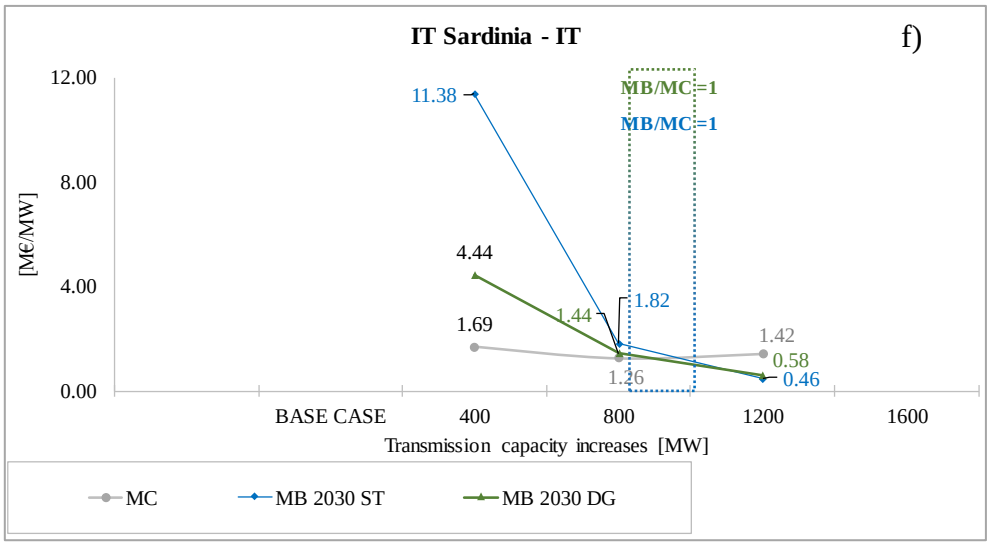
IT Sardinia - IT
f)
MB/MC =1
MB/MC =1
11.38
4.44
1.82
1.44
1.69
1.42
0.58
1.26
0.46
12.00
8.00
4.00
0.00
[M€/MW]
BASE CASE
400
800
1200
1600
Transmission capacity increases [MW]
MC
MB 2030 ST
MB 2030 DG

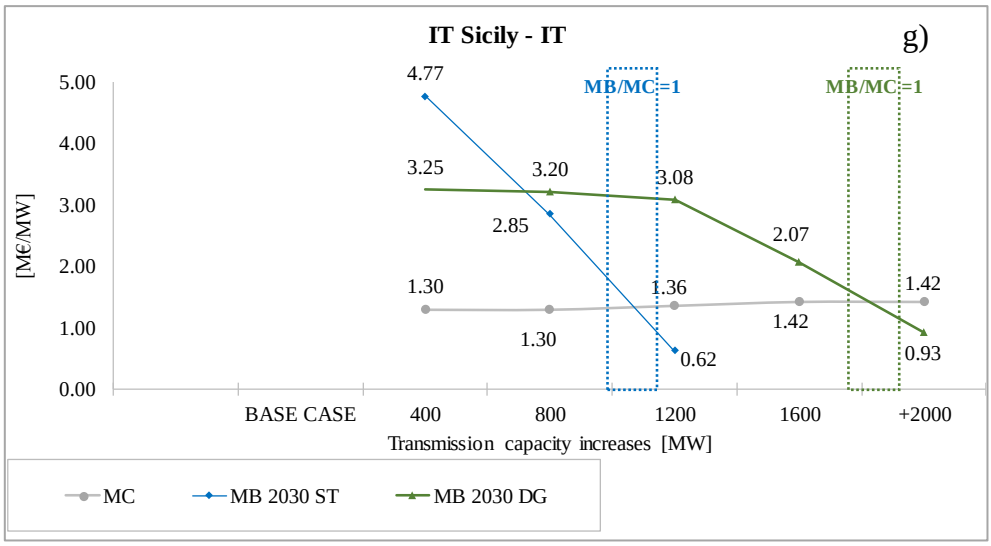

Fig. 4.11. Marginal cost/benefit curves in each considered scenario for: a) IT North – France, b) IT North – Slovenia, c) IT Sicily – Tunisia external borders; d) Centre South – Centre North, e) Centre South – South, f) Sardinia – IT; g) Sicily – IT internal sections.

Let "Option 1" and "Option 2" be the set of transmission capacity increases resulting from the application of the proposed methodology in the ST scenario and in the DG scenario respectively: the two options can be treated as different investment strategies. The only total investment cost is not exhaustive parameter for the decision maker, since the saving in network and market constraints costs associated with the new transmission capacity must be considered. The net benefit metric is then used for the economic regrets related to the different investment strategies under the two considered scenarios, allowing the decision maker (TSO) to determine the maximum risk associated with each option across different scenarios and to select the one yielding the lowest maximum regret. The net benefit related to each potential option is defined in both the two scenarios under study as reported in Table 4.5. Moreover, the worst regret is evaluated in Table 4.6.

Table 4.5. Net benefit [M€] associated to each development strategy in each scenario under study.

Scenario	$NB_{Op\,1}$	$NB_{Op\,2}$
2030 ST	449	164
2030 DG	379	319

Table 4.6. Regret [M€] associated to each development strategy in each scenario under study.

Scenario	$regret_{Op\,1}$	$regret_{Op\,2}$
2030 ST	0	285
2030 DG	0	60
Worst regret	–	**285**

The least regret criterion leads to the choice of the Option 1, since it consists in the investment strategy exposing the consumers to the minimum risk in both considered scenarios. Table 4.7 summarizes the final values of target capacity [MW] to aim for, considering the existing "winter peak" transmission capacity, $EC_{k,WP}$, in the main direction of power transfers, consistent with the TSO objective to make available the interconnection capacity in an efficient way.

Table 4.7. Results of the target capacity assessment methodology [MW].

Main direction of power flows on Section/Border	$\boldsymbol{EC_{k,WP}}$	$\boldsymbol{\chi_k^{ST}}$	$\boldsymbol{TC_k^{2030}}$
Northern border → IT North	8435	4500	12935
Balkan border → IT	500	500	1000
North African border ← IT Sicily	0	1200	1200
IT North → IT Centre North	1300	500	1800
IT Centre North → IT Centre South	2700	1100	3800
IT South → IT Centre South	4600	900	5500
IT Sicily ← IT	1100	900	2000
IT Sardinia ← IT	1028	900	1628

Let the index *I* be the "Interconnection target", defined as the ratio between the interconnection capacity with neighbouring Countries over the installed production capacity; the Table 4.8 summarizes the interconnection targets associated with the existing capacity, named "I_{EC}" and the assessed target capacity increase, named "I_{TC}" in the current (2018) and planned (ST 2030 and DG 2030) installed capacity scenarios.

Table 4.8. Interconnection targets related to the existing and assessed interconnection capacity with neighboring Countries in the current and planned scenarios under study.

Interconnection Target	**2018**	**2030 ST**	**2030 DG**
$\boldsymbol{I_{EC}}$	7.6%	7.6%	6.6%
$\boldsymbol{I_{TC}}$	13.0%	12.9%	11.2%

We can deduce that the existing interconnection level stays below the 10% target. Instead, the target capacity in output from the methodology provides index values larger than the established target in all scenarios under study.

In Fig. 4.12, the expected power flows resulting from the identified $TC_k^{ST\ 2030}$ implementation on the base case (Fig. 4.12a) are compared with the power flows resulting from scenario ST 2030 market simulations considering all the planned development actions included in the NDP 2018 (Fig. 4.12b).

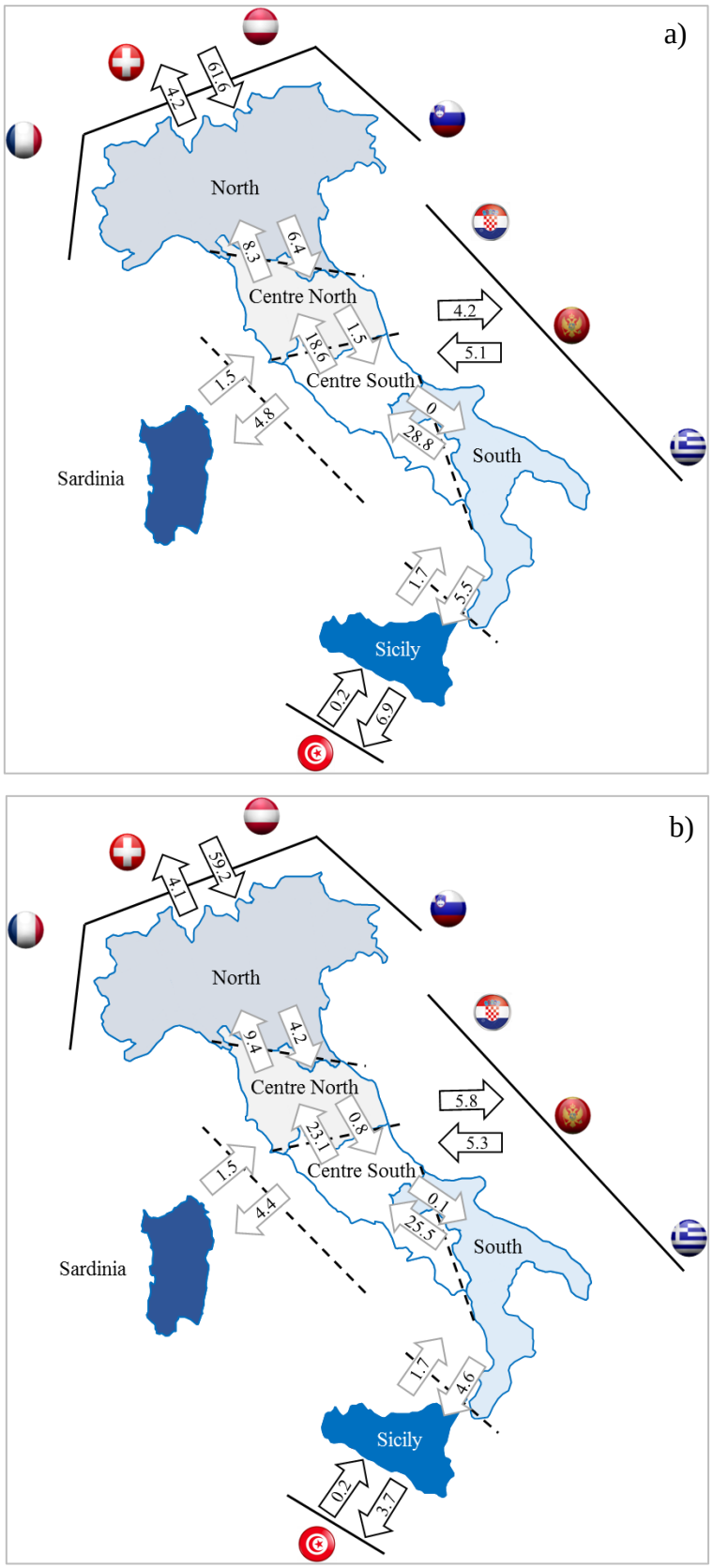

Fig. 4.12. Expected power flows (TWh) resulting from the implementation of: (a) the $TC_k^{ST\ 2030}$ on the base case; (b) all planned development projects included in the NDP 2018.

It can be observed that the power flows in the two conditions are very similar, highlighting the coherence between the target capacity assessment results and the expected power transfers considering all the already planned network reinforcements in service at 2030 aimed at increasing the power exchanges between market zones.

Finally, Fig. 4.13 and Fig. 4.14 reports the synthesis of all performed subsequent iterations in the 2030 ST and 2030 DG scenario respectively. All details concerning marginal costs and benefits in each iteration can be found in the published official report [229].

1) The section/border presents at least one of the PINT activation condition
2) The condition MB/MC > 1 is respected: the additional capacity increase is confirmed
3) A new point is added in the marginal cost and benefit curves

1) The section/border presents at least one of the PINT activation condition
2) The condition MB/MC > 1 is not respected: the additional capacity increase is not confirmed
3) No point is added in the marginal cost and benefit curves

The section/border does not present the PINT activation conditions

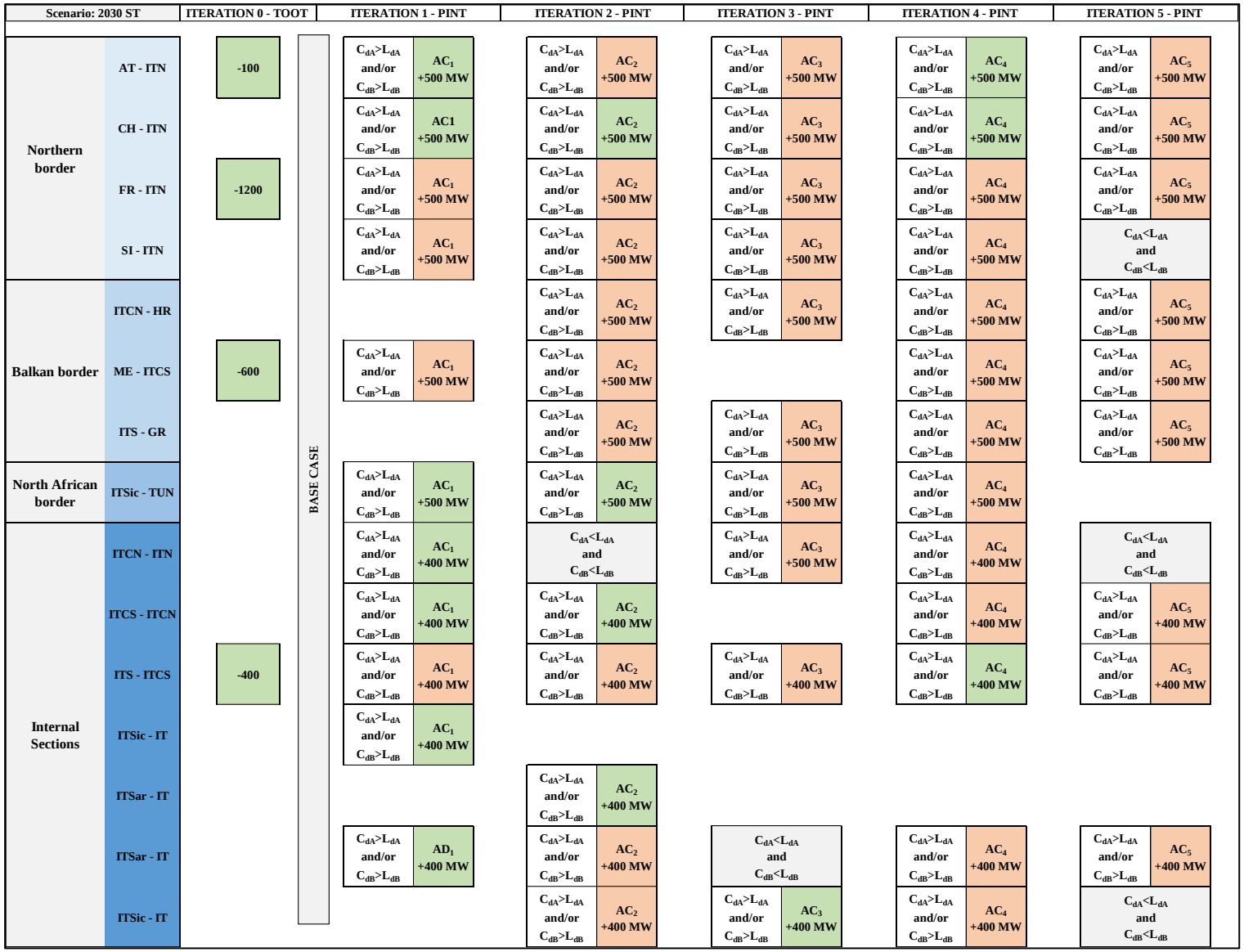

Fig. 4.13. Synthesis of all performed iterations in the scenario 2030 ST.

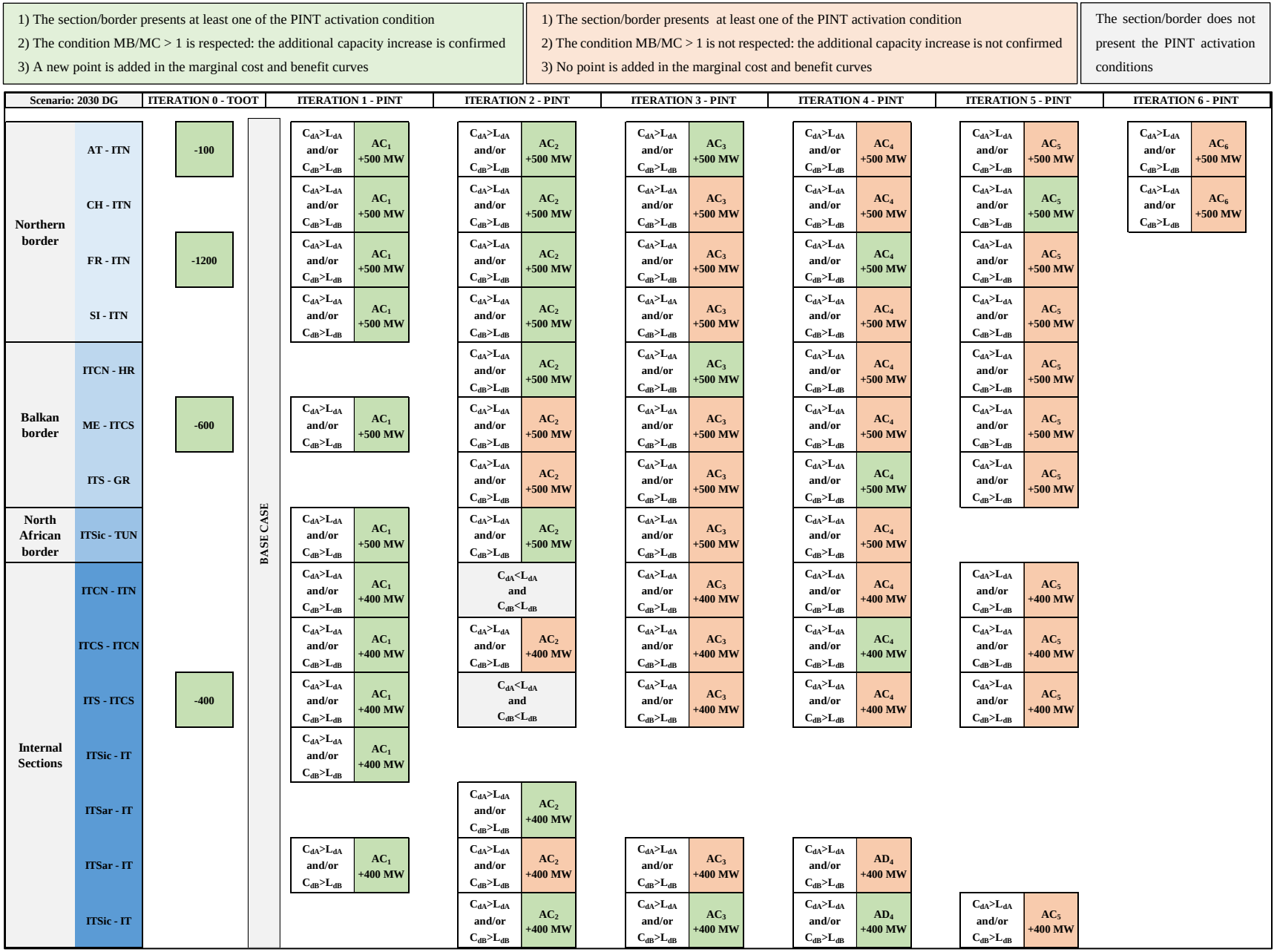

Fig. 4.14. Synthesis of all performed iterations in the scenario 2030 DG.

4.6 New developments

The first application of the proposed methodology generated great interest among academic experts, utilities and other relevant stakeholders and the Italian Regulatory Authority requested Terna to publish the second edition of the "Target Capacity" report by the end of year 2020, performing the analysis in the new significant planning scenarios adopted in the NDP 2020 [153], [263]: the "Business As Usual" (named "BAU") and the "Integrated National Energy and Climate Plan (named "NECP") scenarios.

Furthermore, some useful advices to improve the target capacity assessment methodology have been contributed by the two independent academic reviewers in their specific reports [237] and [251]. In particular, from the methodological point of view, the received suggestions cover the different aspects:

1. the use of a more rigorous approach to select the sections/borders suitable for the transmission capacity increases at the beginning of each iteration;
2. the inclusion of the operating costs, besides the already considered capital costs, in the evaluation of the reference costs for each section/border in each iteration;
3. the transmission increases $AC_{i,k}$ size reduction to the advantage of a more "granular" final solution.

With the aim of improve the developed methodology, some modifications in the methodological document have been introduced before its publication for consultation [264]. With reference to the suggestions received, the most remarkable innovations are:

1. The adoption of the "Technique for Order Preference by Similarity to an Ideal Solution" (named "TOPSIS") method to solve a Multi-Criteria Decision Making problem (MCDM) and identify the sections/borders on which the transmission capacity increases must be tested at the beginning of each iteration.

   This technique [265] finds application in a multitude of different real-world issues, and is based on the statement that the best compromise solution among several allowable options presents the shortest geometric distance from the "positive" ideal solution (A^+) and the longest geometric distance from the "negative" ideal solution (A^-).

   First of all, the decision matrix D of order $(n \times m)$ must be defined on the basis of the set of the n alternatives and the m selected criteria, as in Fig. 4.15. The generic element a_{hj} of the matrix represents the performance of the A_h $(h = 1, 2, \dots, n)$ alternative with respect to the generic C_j criterion with assigned weight w_j $(j = 1, 2, \dots, m)$.

	$C_1(w_1)$	$C_2(w_2)$	…	$C_m(w_m)$
A_1	a_{11}	a_{12}	…	a_{1m}
A_2	a_{21}	…	…	a_{2m}
.	…	…	…	…
.	…	…	…	…
A_n	a_{n1}	a_{n2}	…	a_{nm}

Fig. 4.15. Generic decision matrix.

The decision matrix D is then normalized in the X matrix (4.16), deriving each element x_{hj} as in (4.17):

$$X = \begin{bmatrix} x_{11} & \dots & x_{1m} \\ \dots & \dots & \dots \\ x_{n1} & \dots & x_{nm} \end{bmatrix} \tag{4.16}$$

$$x_{hj} = \frac{a_{hj}}{\sqrt{\sum_{p=1}^{n} a_{pj}^2}} \tag{4.17}$$

The weighted normalized decision matrix Y is obtained by multiplying each column of the X matrix for the weight associated to the correspondent criterion, as in (4.18):

$$Y = \begin{bmatrix} w_1 x_{11} & \dots & w_m x_{1m} \\ \dots & \dots & \dots \\ w_1 x_{n1} & \dots & w_m x_{nm} \end{bmatrix} = \begin{bmatrix} y_{11} & \dots & y_{1m} \\ \dots & \dots & \dots \\ y_{n1} & \dots & y_{nm} \end{bmatrix} \tag{4.18}$$

The positive ideal A^+ and negative ideal A^- solutions are determined by the means of (4.19) and (4.20) after dividing the set of criteria in two sub-set J_b (set of benefit criteria) and J_c (set of cost criteria):

$$A^+ = \left\{ \left(\max_h y_{hj} \middle| j \in J_b \right), \left(\min_h y_{hj} \middle| j \in J_c \right), h = 1, 2, \dots, n \right\} = \{ y_{1^+}, y_{2^+}, \dots, y_{n^+} \} \tag{4.19}$$

$$A^- = \left\{ \left(\min_h y_{hj} \middle| j \in J_b \right), \left(\max_h y_{hj} \middle| j \in J_c \right), h = 1, 2, \dots, n \right\} = \{ y_{1^-}, y_{2^-}, \dots, y_{n^-} \} \tag{4.20}$$

The geometric distance of each alternative from A^+ and A^- ideal solution can be calculated:

$$S_{h^+} = \sqrt{\sum_{j=1}^{m} \left(y_{hj} - y_{j^+} \right)^2} \quad for\ h = 1,2, \dots, n \tag{4.21}$$

$$S_{h^-} = \sqrt{\sum_{j=1}^{m} \left(y_{hj} - y_{j^-} \right)^2} \quad for\ h = 1,2, \dots, n \tag{4.22}$$

And the relative closeness of each alternative to the ideal solution is evaluated:

$$P_{h^+} = \frac{S_{h^-}}{S_{h^+} + S_{h^-}} \tag{4.23}$$

The P_{h^+} parameter represents the alternative performance with respect to the selected criteria and its relative importance (or weights) and lies between 0 and 1.

Finally, the ranking of alternatives based on the order of preference can be defined.

Some applications of the TOPSIS method in power systems problems are presented in [169], [266] – [268]. In the target capacity assessment context, the significant criteria selected are the four listed in Table 4.9:

Table 4.9. Selected criteria in the MCDM analysis for the PINT selection at the beginning of each iteration in the target capacity assessment methodology.

Code	Description
$\boldsymbol{C_1}$	Congestion hours [h]
$\boldsymbol{C_2}$	Price spread [€/MWh]
$\boldsymbol{C_3}$	Investment cost for transmission capacity increase [M€/MW]
$\boldsymbol{C_4}$	Project progress

In particular, the C_4 criterion is defined on a scale between 1 and 4 depending on the progress of the project considered as reference for the marginal cost on the *k*-th section/border in the *i*-th iteration:

- 1= the transmission capacity increase marginal cost refers to a standard project;
- 2= the transmission capacity increase marginal cost refers to a planned project;
- 3= the transmission capacity increase marginal cost refers to a projected scheme;
- 4= the transmission capacity increase marginal cost refers to a project in authorisation.

Table 4.10 shows the positive and the negative ideal solutions respectively to the four selected criteria:

Table 4.10. Positive and negative ideal solutions for each selected criterion.

	$C_1(w_1)$	$C_2(w_2)$	$C_3(w_3)$	$C_4(w_4)$
A^+	$\max y_{hj}$	$\max y_{hj}$	$\min y_{hj}$	$\max y_{hj}$
A^-	$\min y_{hj}$	$\min y_{hj}$	$\max y_{hj}$	$\min y_{hj}$

In line with the previous version of the methodology, the analysis will be carried out separately for the internal sections and for the external borders, in order to consider the historical differences in market signals.

The two different decision matrices are represented in Fig. 4.16 and Fig. 4.17.

		$C_1(w_1)$	$C_2(w_2)$	$C_3(w_3)$	$C_4(w_4)$
1	**AT - ITn**	$a_{EXT,11}$	$a_{EXT,12}$	$a_{EXT,13}$	$a_{EXT,14}$
2	**CH - ITn**	$a_{EXT,21}$	$a_{EXT,22}$	$a_{EXT,23}$	$a_{EXT,24}$
3	**FR - ITn**	$a_{EXT,31}$	$a_{EXT,32}$	$a_{EXT,33}$	$a_{EXT,34}$
4	**Sl – ITn**	$a_{EXT,41}$	$a_{EXT,42}$	$a_{EXT,43}$	$a_{EXT,44}$
5	**ITcn – HR**	$a_{EXT,51}$	$a_{EXT,52}$	$a_{EXT,53}$	$a_{EXT,54}$
6	**ME – ITcs**	$a_{EXT,61}$	$a_{EXT,62}$	$a_{EXT,63}$	$a_{EXT,64}$
7	**ITs – GR**	$a_{EXT,71}$	$a_{EXT,72}$	$a_{EXT,73}$	$a_{EXT,74}$
8	**ITsic – TN**	$a_{EXT,81}$	$a_{EXT,82}$	$a_{EXT,83}$	$a_{EXT,84}$

Fig. 4.16. External borders decision matrix.

		$C_1(w_1)$	$C_2(w_2)$	$C_3(w_3)$	$C_4(w_4)$
1	**ITcn - ITn**	$a_{IT,11}$	$a_{IT,12}$	$a_{IT,13}$	$a_{IT,14}$
2	**ITcs - ITcn**	$a_{IT,21}$	$a_{IT,22}$	$a_{IT,23}$	$a_{IT,24}$
3	**ITs - ITcs**	$a_{IT,31}$	$a_{IT,32}$	$a_{IT,33}$	$a_{IT,34}$
4	**ITsar - ITcn**	$a_{IT,41}$	$a_{IT,42}$	$a_{IT,43}$	$a_{IT,44}$
5	**ITsar - ITcs**	$a_{IT,51}$	$a_{IT,52}$	$a_{IT,53}$	$a_{IT,54}$
6	**ITsar - ITsic**	$a_{IT,61}$	$a_{IT,62}$	$a_{IT,63}$	$a_{IT,64}$
7	**ITsic - ITcs**	$a_{IT,71}$	$a_{IT,72}$	$a_{IT,73}$	$a_{IT,74}$
8	**ITsic - ITcal**	$a_{IT,81}$	$a_{IT,82}$	$a_{IT,83}$	$a_{IT,84}$
9	**ITcal - ITs**	$a_{IT,91}$	$a_{IT,92}$	$a_{IT,93}$	$a_{IT,94}$

Fig. 4.17. Internal sections decision matrix.

Once the "performances indexes" P_{i^+} are identified, the median values among the internal sections and the external borders are calculated and properly rounded to obtain the $AC_{i,k}$ activation reference thresholds L_{IT} and L_{EXT}. The transmission capacity increases will be tested if the condition (4.24) is verified:

$$\begin{aligned} &P_{h^+} \geq L_{IT} \text{ for internal sections} \\ &P_{h^+} \geq L_{EXT} \text{ for external borders} \end{aligned} \tag{4.24}$$

2. The inclusion of operating costs ("opex") in the marginal cost curves on the basis of (i) official data used in the cost-benefit analysis for planned projects studied in the NDP, (ii) operating costs values referred in literature for standard projects, (iii) 1.3% of capital costs in absence of specific information about the project;
3. The reduction of $AC_{i,k}$ sizes in the final steps of the iterative process to enhance the quality of the final solution. In particular, transmission capacity increases of +250 MW for external borders and +200 MW for internal sections will be tested.

Other significant changes are related to the new zonal market structure, the updated reference grid and the planning scenarios under consideration.

The target capacity assessment analysis will be performed on the new zonal market structure [155], in force by the 2021 and represented in Fig 4.18.

Fig. 4.18. New zonal market structure.

The reference grid (or "base case") will consist of the existing grid and the additional projects which have a strong possibility to be authorized during the year 2020 and completed by the year 2025, listed in Table 4.11 and illustrated in Fig. 4.19.

Table 4.11. Target capacity assessment, 2020 edition. Planned development projects included in the base case: transmission capacity increase provided (MW) and section/border involved.

	Project	**TTC (MW)**	**Section/border involved**
1	320 kV Piossasco – Grand' Ile HVDC link	+1200	IT North – France
2	220 kV Nauders – Glorenza link	+300	IT North – Austria
3	132 kV Brennero – Steinach link	+100	IT North – Austria
4	380 kV Calenzano – Colunga link	+400	IT North – IT CNorth
5	380 kV Deliceto – Bisaccia link	+400	IT CSouth – IT South

Fig. 4.19. Planned projects included in the base case (listed in Table 4.11).

The analysis will be performed at 2030 year horizon in the two energy BAU and NCEP scenarios adopted in the 2020 NDP:

- the Business-As-Usual is a technology driven scenario, projecting in future the current trends in an inertial way. Neither the 2030 energy targets established in the "Clean Energy for all Europeans Package" [269] and declined in the National context in the Italian proposal [110], nor the long-term energy targets can be reached. The demand growth is moderate and the decommissioning of coal power plants is realized only after the 2030 year horizon. Finally, the scenario forecasts minimum investments in storage systems;
- the National Climate and Energy Plan is a policy-driven scenario, designed to reflect the most recent EU requirements with regards to climate and energy targets. The electricity demand increase is mitigated by the remarkable energy efficiency measures foreseen. A total phase-out of coal power plants is achieved by 2025 and an intensive growth of renewable variable generation together with energy storage systems (both hydro pumping and electrochemical storages) can be observed.

The electrical demand trend and the generation mix forecast in both considered scenarios compared to the final values for year 2018 are illustrated in Fig. 4.20 and Fig. 4.21.

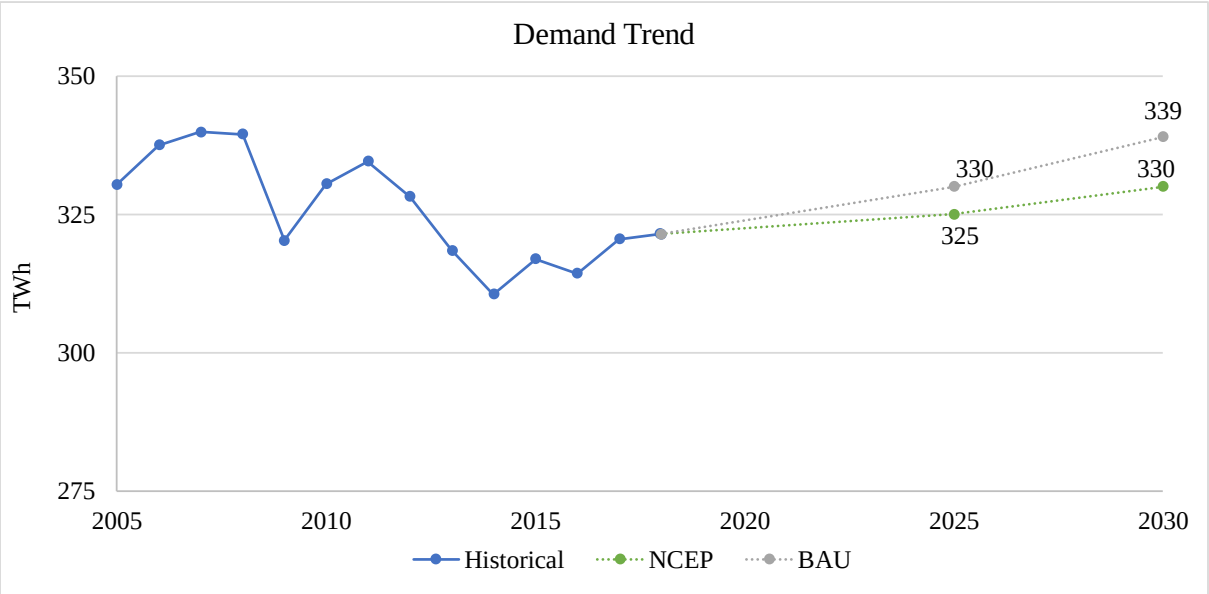

Fig. 4.20. Demand trend in planning scenarios considered for the target capacity assessment 2020.

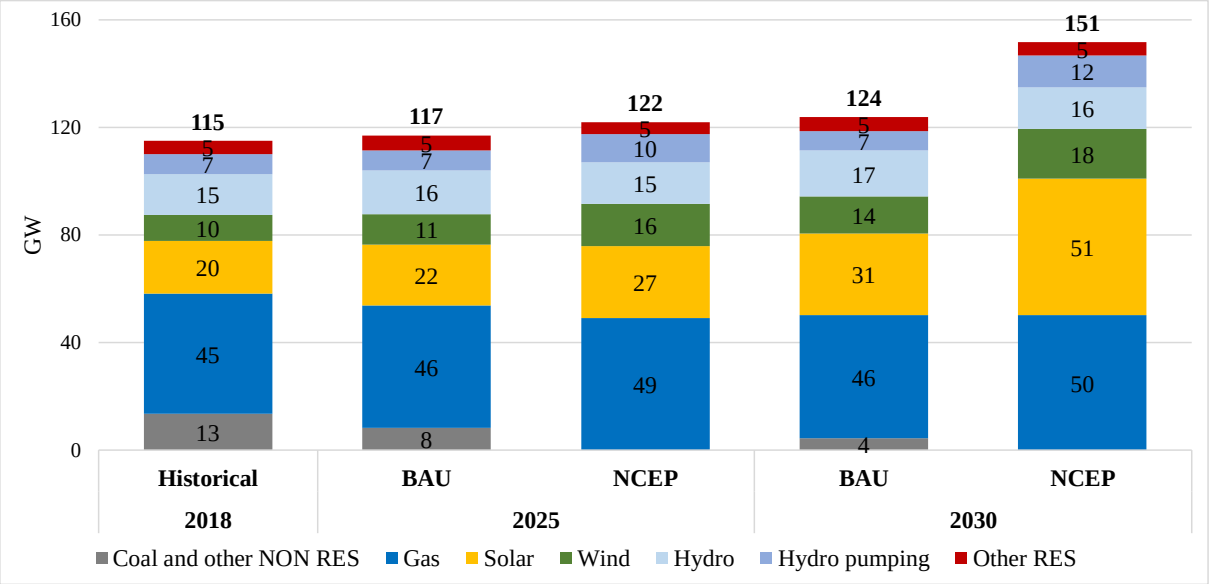

Fig. 4.21. Generation mix in planning scenarios considered for the target capacity assessment 2020.

4.7 Conclusions

New methodologies capable of designing robust development strategies in an efficient manner are needed for transmission expansion planning in the framework of competitive electricity markets.

This Section presented a novel heuristic methodology developed in the framework of the research activity in collaboration with the "Grid Planning and Interconnections Department" of Terna for the cost-effective target capacity assessment, consistently with Regulator directives and main stakeholders' feedbacks collected during its consultation. Each internal section and external boundary of the Italian power system is simultaneously studied on the basis of an iterative process in the two relevant long-term planning scenarios of year 2019 NDP, in order to obtain the possible different development strategies. In addition, the least regret approach allows the identification of the reference values for the TSO.

The outputs of this work have turned out to be relevant for policy makers, regulatory authority and market participant to assess and co-design the energy transition plan of a future European interconnected power system.

The first application of the proposed methodology dates back to year 2018: the Italian Regulator approved the identified target capacity and positive opinions have been expressed by the two academic independent reviewers of the target capacity report. The updated version of the methodology including the improvements suggested by the two academic experts and the changes in main assumptions concerning market structure, reference grid and scenarios of analysis has been recently published for consultation. The final report will be available within the end of year 2020.

Conclusions and future work

The research activity has included multiple aspects of power system planning.

Starting from the purpose of extending the capability of an underused portion of the Italian HV – EHV national transmission network, a specific application of series compensation has been assessed with the aim of exploiting the transfer capacity of a 250 km long, 230 kV – 50 Hz transmission backbone in Central Italy. The static assessment has been validated by means of extensive load-flow calculations performed both for the “isolated” backbone and considering its operation within the meshed grid.

As regards the ongoing renewable generation capacity increase, which obviously has to be integrated into the system while continuing to ensure reliability and security requirements, the offshore wind power in the Italian context have been evaluated. Furthermore, a real HVDC project increasing the transmission capacity across a critical market section of the Italian power system has been studied in static and dynamic regime, considering both LCC (plus SCs) and VSC configurations. Other aspects concerning the thermal loading performances of a specific grid portion affected by significant variable energy sources generation, and possible methods to evaluate the economic impact of the inertia reduction have also been investigated.

Methodologies for power system flexibility assessment have been proposed, based on both the market and grid-infrastructure points of view. The results obtained in relevant energy scenarios confirm the usefulness of such evaluations in planning studies.

Finally, a novel methodology developed in the framework of the research activity in collaboration with the "Grid Planning and Interconnections Department" of Terna for the target capacity assessment has been presented together with the results obtained from its first application.

Future works will deal with further applications of series compensation to active power control in comparison with some common alternative solutions (i.e. PSTs), and its impact on protective systems. Finally, in order to accomplish the goals of the FlexPlan project, the power system flexibility analysis in the new evolving scenarios will be carried out.

References

[1] P. M. Anderson and R. G. Farmer, “Series compensation of Power System”, (Book), 1996.

[2] Jancke, G., and K. F Akerstrom, "The Series Capacitor with Special Reference to its Application in the Swedish 220 kV Network," CIGRÉ paper 332, 1950.

[3] C.W. Taylor, Power System Voltage Stability, McGraw-Hill, 1994.

[4] T. J. E. Miller, Reactive Power Control in Electric Systems, New York Wiley, 1982.

[5] G. D. Breuer, H. M. Rustebakke, R. A. Gibley and H. O. Simmons, "The Use of Series Capacitors to Obtain Maximum EHV Transmission Capability". IEEE Trans. on Power Apparatus and Systems, vol. 83, no. 11, pp. 1090-1102, Nov. 1964.

[6] E. W. Kimbark, "Improvement of System Stability by Switched Series Capacitors". IEEE Trans. on Power Apparatus and Systems, vol. PAS-85, no. 2, pp. 180-188, Feb. 1966.

[7] Italian Regulatory Authority for Energy, Networks and Environment, “Disposizioni in merito alla suddivisione della rete rilevante in zone”, Deliberation 386/2018/R/EEL, July 2018, https://www.arera.it/allegati/docs/18/386-18.pdf.

[8] Terna S.p.A, “Procedura per la definizione dei limiti di transito fra le zone di mercato”, December 2016, [in Italian], online: http://download.terna.it/terna/0000/0861/14.pdf.

[9] C. F. Wagner and R.D. Evans, “Symmetrical components”, McGraw-Hill Book Co., New York, 1933.

[10] John Zaborszky and Joseph W. Rittenhouse, Electric Power Transmission, Ronald Press, New York, 1954.

[11] Turan Gönen, Electric Power Transmission System Engineering, John Wiley & Sons, Inc., New York, 1988.

[12] Edward W. Kimbark, “A new look at Shunt Compensation”, IEEE Trans., v. PAS-102, n.1, Jan 1983.

[13] Jancke, Gunnar and K. F Àkerstrom, "The Series Capacitor in Sweden," Electrical Engineering, March 1952, p. 222-227.

[14] Batho, J. L., J. E. Hardy, and N. Tolmunen, "Series Capacitor Installations in the B.e. Hydro 500 kV System," IEEE Trans., v. PAS-96, n. 6., Nov./Dec. 1977, p. 1767-1776.

[15] Maneatis, 1. A., E. J. Hubacher, W. N. Rothenbuhler, and J. Sabath, "500 kV Series Capacitor Installations in California," IEEE Trans., v. PAS-890 1970, p. 1138-1149.

[16] F. Iliceto and E. Cinieri, "Comparative Analysis of Series and Shunt Compensation Schemes for AC Transmission Systems," IEEE Trans., v. PAS-96, n. 6, Nov./Dec. 1977, p. 1819-30.

[17] P.M. Anderson, Analysis of Faulted Power Systems, IEEE Power System Engineering Series, Piscataway, NJ: IEEE Press, 1995.

[18] The Calculation of Short-Circuit Currents in Three-Phase A.C. Systems, IEC 60909.

[19] IEEE Recommended Practice for System Grounding of Industrial and Commercial Power Systems, IEEE Std. 3003.1, 2019.

[20] F. Iliceto, Impianti Elettrici, Patron Editore, 1981.

[21] S. Zalzar and E.F. Bompard, “The Impacts of an Integrated European Dayahead and Intraday Electricity Market on Market Performance: The Iberian Region Case”, Proc. 13th IEEE PowerTech, Milan, Italy, 23-27 June 2019.

[22] European Commission, “Renewable energy, Moving towards a low carbon economy”, 2018.

[23] Global Wind Energy Council, “Global Wind Statistics 2017”, 14.2.2018.

[24] O. Anaya-Lara, J. O. Tande, K. Uhlen, K. Merz, “Offshore Wind Energy Technology”, John Wiley and Sons Ltd, 2018.

[25] Wind Europe, “Offshore Wind in Europe – Key trends and statistics 2017”, February 2018.

[26] ENTSO-E, “TYNDP 2018 Scenario Report”.

[27] S. Kota, S. B. Bayne, S. Nimmagadda, “Offshore wind energy: a comparative analysis of UK, USA and India”. Renewable and Sustainable Energy Reviews vol. 41, pp. 685-694, 2015.

[28] F. Hvelplund, P. A. Østergaard, N. I. Meyer, “ Incentives and barriers for wind power expansion and system integration in Denmark”. Energy Policy, vol. 107, pp. 573-584, 2017.

[29] A. Colmenar-Santos, J. Perera-Perez, D. Borge-Diez, “Offshore wind energy: A review of the current status, challenges and future development in Spain”. Renewable and Sustainable Energy Reviews, vol. 64, pp. 1-18, 2016.

[30] X. Zhao, L. Ren, “Focus on the development of offshore wind power in China: Has the golden period come?”, Renewable Energy, vol. 81,pp. 644-657, 2015.

[31] H. P. Simao, W. B. Powell, C. L. Archer, W. Kempton, “ The challenge of integrating offshore wind power in the US electric grid. Part II: Simulation of electricity market operations”. Renewable energy, vol. 103, pp. 418-431, 2017.

[32] L. Hirth, S. Müller, “System-friendly wind power: How advanced wind turbine design can increase the economic value of electricity generated through wind power”. Energy Economics, vol. 56, pp. 51-63, 2016.

[33] B. Aluisio, M. Dicorato, G. Forte, M. Trovato, “Hybrid energy storage system optimization for improving wind power integration”, Proc. of Power Systems Computation Conference (PSCC) 2016, Genoa, Italy, 20-24 June 2016, pp. 1-6.

[34] C. Qin, G. Saunders, G., E. Loth, “Offshore wind energy storage concept for cost-of-rated-power savings”, Applied Energy, vol. 201, pp. 148-157, 2017.

[35] J. A. Voormolen, H. M. Junginger, W. G. J. H. M. Van Sark, “Unravelling historical cost developments of offshore wind energy in Europe”, Energy Policy, vol. 88, pp. 435-444, 2016.

[36] C. Draxl, A. Clifton, B. M. Hodge, J. McCaa, “The wind integration national dataset (WIND) Toolkit”, Applied Energy, vol. 151, pp. 355-366, 2015.

[37] S. Cavazzi, A. G. Dutton, “An Offshore Wind Energy Geographic Information System (OWE-GIS) for assessment of the UK’s offshore wind energy potential”, Renewable Energy, vol. 87, pp. 212-228, 2016.

[38] J. Schallenberg-Rodríguez, N. García Montesdeoca, “Spatial planning to estimate the offshore wind energy potential in coastal regions and islands. Practical case: The Canary Islands”, Energy, vol. 143, pp. 91-103, 2018.

[39] Y. K. Wu, X. C. Lee, C. Y. Hu, W. H. Yang, “Evaluation of the maximum allowed capacity of offshore wind power in Taiwan based on the existing transmission capacity limits”, Proc. of 2017 IEEE-ICASIInternational Conference, 13-17 May 2017, Sapporo, Japan, pp. 590-593.

[40] A. Chaouachi, C. F. Covrig, M. Ardelean, “Multi-criteria selection of offshore wind farms: Case study for the Baltic States”, Energy Policy, vol. 103, pp. 179-192, 2017.

[41] H. J. Bahirat, B. A. Mork, H. K. Høidalen, “Comparison of wind farm topologies for offshore applications”, Proc. of IEEE PES General Meeting, 22-26 July 2012, San Diego, U.S.A., pp. 1-8.

[42] J. S. González, M. B. Payán, J. R. Santos, “Optimum design of transmissions systems for offshore wind farms including decision making under ris”, Renewable energy, vol. 59, pp. 115-127, 2013.

[43] N. Gupta, “A review on the inclusion of wind generation in power system studies”. Renewable and Sustainable Energy Reviews, vol. 59, pp. 530-543, 2016.

[44] C. L. Archer, H. P. Simao, W. Kempton, W. B. Powell, “The challenge of integrating offshore wind power in the US electric grid. Part I: Wind forecast error”. Renewable energy, vol. 103, pp. 346-360, 2017.

[45] D. R. Drew, D. J. Cannon, D. J. Brayshaw, J. F. Barlow, P. J. Coker, “The impact of future offshore wind farms on wind power generation in Great Britain”, Resources, vol. 4(1), pp. 155-171, 2015.

[46] C. Richts, M. Jansen, M. Siefert, “Determining the economic value of offshore wind power plants in the changing energy system”. Energy Procedia - 12th Deep Sea Offshore Wind R&D Conference, EERA DeepWind’2015, vol. 80, pp. 422-432, 2015.

[47] D. Flynn et al., “Technical impacts of high penetration levels of wind power on power system stability”, Wiley Interdisciplinary Reviews: Energy and Environment, vol. 6, no.2, March/April 2017, pp. 1-19.

[48] S. M. Martínez, E. G. Lázaro, A. H. Escribano, M. C. Carretón, A. Molina-Garcia, “Wind Power Curtailment Analysis under generation flexibility requirements: The Spanish case study”, Proc. of 2015 IEEE PES General Meeting, Denver U.S.A., 26-30 July 2015, pp. 1-5.

[49] E. V. Mc Garrigle, J. P. Deane, P. G. Leahy, “How much wind energy will be curtailed on the 2020 Irish power system?”, Renewable Energy, vol. 55, pp. 544-553, 2013.

[50] L. Wang, C. T. Wu, C. H. Chang, A. V. Prokhorov, “Stability evaluation of simplified Taiwan Power System connected with a large-scale offshore wind farm”, Proc. of 2015 IEEE IFEEC Conference, In Future Energy Electronics Conference (IFEEC), Taipei, Taiwan, 1-4 Nov. 2015, pp. 1-5.

[51] N. A. Cutululis, M. Litong-Palima, P. Sørensen, “Impact of offshore wind power variability on the frequency stability of European power system”, Proc. of 2014 International Conference on Wind Energy Grid-Adaptive Technologies, 20-22 Oct. 2014, Jeju, Korea, pp. 1-8.

[52] F. Díaz-González, M. Hau, A. Sumper, O. Gomis-Bellmunt, “Participation of wind power plants in system frequency control: Review of grid code requirements and control methods”, Renewable and Sustainable Energy Reviews, vol. 34, pp. 551-564, 2014.

[53] C. Sourkounis, P. Tourou, “Grid code requirements for wind power integration in Europe”, Conference Papers in Energy, vol. 2013, Article ID 437674, pp. 1-9. Hindawi Publishing Corporation.

[54] M. A. Peñalba, O. Gomis-Bellmunt, M. Martins, “Coordinated control for an offshore wind power plant to provide fault ride through capability”, IEEE Transactions on Sustainable Energy, vol. 5, no. 4, Oct. 2014, pp. 1253-1261.

[55] A. K. Pathak, M. P. Sharma, M. Bundele, “A critical review of voltage and reactive power management of wind farms”. Renewable and Sustainable Energy Reviews, vol. 51, pp. 460-471, 2015.

[56] D. N. Truong, V. T. Ngo, M. S. N. Thi, “Voltage stability enhancement of the Bac Lieu wind power system connected to power grid using a STATCOM”, Proc. of 2017 ICSSE International Conference, Ho Chi Minh, Vietnam, 21-23 July 2017, pp. 160-164.

[57] V. T. Bui, D. N. Truong, D. L. Ho, “Improve Power Oscillation Stability in A Grid Connected Wind Power System by Using A Static Var Compensator”, Proc. of 2017 ICSSE International Conference, Ho Chi Minh, Vietnam, 21-23 July 2017, pp. 200-203.

[58] M. Dicorato, G. Forte, M. Trovato, “Voltage compensation for wind integration in power systems”, Proc. of 2012 IEEE PEDG International Symposium, Aalborg,, Denmark, 25-28 June 2012, pp. 464-469.

[59] Z. H. Rather, Z. Chen, P. Thøgersen, P. Lund, “Dynamic reactive power compensation of large-scale wind integrated power system”, IEEE Transactions on Power Systems, vol. 30, no. 5, Sept. 2015, pp. 2516-2526.

[60] S. Demirbas, R. Bayindir, A. Ova, U. Cetinkaya, M. Yesil, “Stability analysis of an offshore wind farm connected to turkish electricity transmission system”, Proc. of 2016 IEEE ICRERA International Conference, 20-23 Nov. 2016, Birmingham, U.K., pp. 314-318.

[61] A. Korompili, Q. Wu, H. Zhao, “Review of VSC HVDC connection for offshore wind power integration”, Renewable and Sustainable Energy Reviews, vol. 59, pp. 1405-1414, 2016.

[62] W. Winter, D. Chan, M. Norton, E. Haesen, Á. Székely, “ Towards a european network code for HVDC connections and offshore wind integration”, Proc. of 2015 UPEC International Conference, Stoke-on-Trent, U.K., 1-4 Sept. 2015, pp. 1-6.

[63] J. N. Sakamuri, M. Altin, A. D. Hansen, N. A. Cutululis, Z. H. Rather, “Coordinated control scheme for ancillary services from offshore wind power plants to AC and DC grids”, Proc. of 2016 IEEE PES General Meeting, Boston, U.S.A., 17-21 July 2016, pp. 1-5.

[64] A. F. Abouzeid, A. A. Daoud, S. S. Dessouky, J. M. Guerrero, “ Factors affecting offshore wind power integration to grid through VSC-HVDC”, Proc. of 2016 MEPCON Conference, Cairo, Egypt, 27-29 Dec. 2016, pp. 184-189.

[65] Y. Fu, C. Wang, W. Tian, M. Shahidehpour, “Integration of large-scale offshore wind energy via VSC-HVDC in day-ahead scheduling”. IEEE Transactions on Sustainable Energy, vol. 7, no. 2, Apr. 2016, pp. 535-545.

[66] A. A. van Der Meer, M. Ndreko, M. Gibescu, M. A. van der Meijden, “The effect of FRT behavior of VSC-HVDC-connected offshore wind power plants on AC/DC system dynamics”. IEEE Transactions on Power Delivery, vol. 31, no. 2, April 2016, pp. 878-887.

[67] M. Edrah, K. L. Lo, O. Anaya-Lara, A. Elansari, “Impact of DFIG Based Offshore Wind Farms Connected Through VSC-HVDC Link on Power System Stability”, Proc. of 11th IET International Conference on AC and DC Power Transmission, Birmingham, U.K., 10-12 Feb. 215, pp. 1-7.

[68] A. A. van Der Meer, M. Ndreko, J. A. Bos, M. Gibescu, M. A. M. M. van der Meijden, W. L. Kling, “ Stability assessment of VSC-HVDC connected large-scale offshore wind power: A North-Sea region case study”. Proc. of 2015 IEEE PowerTech, Eindhoven, The Netherlands, 29 June – 2 July 2015, pp. 1-6.

[69] Terna S.p.A.; Italian Network Code, Annex A.17, “Wind farms: General connection rules to HV networks – Protection, regulation and control system” (in Italian).

[70] K. R. Padiyar, FACTS Controllers in Power Transmission and Distribution, India, New Delhi:New Age International, 2007.

[71] T. Johnson, K. N. Shubhanga, “Loop flow performance of interconnected power systems with HVDC links”, 2016 IEEE ICPEICES International Conference, Delhi, India, 4-6 July 2016, pp. 1-6.

[72] P. Kundur, J. Paserba, V. Ajjarapu, G. Andersson, A. Bose, C. Canizares, N. Hatziargyriou, D. Hill, A. Stankovic, C. Taylor, T. Van Cutsem, V. Vittal “Definition and classification of power system stability -IEEE/CIGRE Joint Task Force on Stability Terms and Definitions”, IEEE Trans. Power Syst., vol.19, no. 3, Aug. 2004, pp. 1387-1401.

[73] K. Sharifabadi, L. Harnefors, H.-P. Nee, R. Teodorescu, S. Norrga, Design Control and Application of Modular Multilevel Converters for HVDC Transmission Systems, New York, NY, USA:Wiley, 2016.

[74] M. Crappe, Electric Power Systems: Wiley, 2008.

[75] D. L. Osborn, “Designing self-contingent HVDC systems with the AC systems”, Proc. of 2016 IEEE Power and Energy Society General Meeting (PESGM), Boston, MA, 17-21 July 2016, pp. 1-4.

[76] N. G. Hingorani, L. Gyugyi, Understanding FACTS Concepts and Technology of Flexible AC Transmission Systems, IEEE Press, 1999.

[77] P. Kundur, Power System Stability and Control. McGraw- Hill, the EPRI Power System Engineering Series, 1994.

[78] J. Beerten, O. Gomis-Bellmunt, X. Guillaud, J. Rimez, A. van der Meer, D. Van Hertem, “Modeling and control of HVDC grids: a key challenge for the future power system”, Proc. of 2014 PSCC Conf., 18-22 Aug. 2014, Wroclaw, Poland, pp. 1-21.

[79] D. Lee Hau Aik, G. Andersson, “Analysis of Voltage and Power Interactions in Multi-Infeed HVDC Systems”, IEEE Trans. Power Delivery, vol. 28, no. 2, Apr. 2013, pp. 816-824.

[80] H. Yang, Z. Cai, L. Zhu, B. Zhou, D. Zhang, “A novel assessment index of LCC-HVDC system impact on short-term voltage stability of receiving-end AC system”, Electric Power Systems Research, vol. 142, Jan. 2017, pp. 125-133.

[81] A. Bidadfar, H.-P. Nee, L. Zhang, L. Harnefors, S. Namayantavana, M. Karrari, G.B. Gharehpetian, “Power system stability analysis using feedback control system modeling including HVDC transmission links”, IEEE Trans. Power Systems, vol. 31, no. 1, Jan. 2016, pp. 116-124.

[82] X. Guo, Y. Lv, W. Li, B. Li, Q. Lv, Z. Xu, “HVDC modulation principle and supplementary controller design method of non-parallel AC/DC system”, Proc. of 12th IET ACDC 2016 Conf., Beijing, China, 28-29 May 2016, pp. 1-6.

[83] P. Thepparat, D. Retzmann, E. Ogée, M. Wiesinger, “Smart Transmission System by HVDC and FACTS”, Proc. of 2013 IEEE PowerTech Conf., Grenoble, France, 16-20 June 2013, pp. 1-6.

[84] T. Bandaru, U. Dhawa, D. Chattarjee, T. Bhattacharya, “Improving the Transient Stability by Modifying the Power Exchange by the HVDC Transmission”, Proc. of 20th NSPC Conf., Tiruchirappalli, India, 14-16 Dec. 2018, pp. 1-6.

[85] G. Macchia, M. Trovato, M. Dicorato, G. Forte, “Modelling of VSC-HVDC with power synchronization method including frequency support”, Proc. of 2019 AEIT HVDC International Conference - Florence, Italy, 9-10 May 2019, pp. 1-6.

[86] O.D. Adeuyi, M. Cheah-Mane, J. Liang, N. Jenkins, “Fast Frequency Response From Offshore Multiterminal VSC-HVDC Schemes”, IEEE Trans. Power Delivery, vol. 32, no. 6, Dec. 2017, pp. 2442-2452.

[87] A. Fuchs, M. Imhof, T. Demiray, M. Morari, “Stabilization of Large Power Systems Using VSC-HVDC and Model Predictive Control”, IEEE Trans. Power Delivery, vol. 29, no. 1, Feb. 2014, pp. 480-488.

[88] L. Sigrist, F. Echavarren, L. Rouco, P. Panciatici, “A fundamental study on the impact of HVDC lines on transient stability of power systems”, Proc. of 2015 IEEE Eindhoven PowerTech Conf., Eindhoven, The Netherlands, 29 June-2 July 2015, pp. 1-6.

[89] J. Xu, G. Karady, J. Qin “Controls of embedded HVDC system for system dynamic performance enhancement”, Proc. of 2017 IEEE PES-GM, 16-20 July 2017, Chicago, IL, U.S.A., pp. 1-5.

[90] S. Arunprasanth, U.D. Annakkage, C. Karawita, R. Kuffel, “Impact of VSC HVdc on AC System Generation”, Proc. of 13th IET ACDC 2017 Conference, Manchester, UK, 14-16 Feb. 2017, pp. 1-6.

[91] A. L’Abbate, F. Careri, R. Calisti, S. Rossi, A. Zani, “Long-term transmission expansion planning towards future European network development: analyses on HVDC corridors”, Proc. of EEM 2018 Conf., 27-29 June 2018, Lodz, Poland, pp. 1-6.

[92] A. Tosatto, T. Weckesser, S. Charzivasileiadis, “Market Integration of HVDC Lines: internalizing HVDC losses in market clearing”, IEEE Trans. Power Systems, vol. 35, no. 1, Jan. 2020, pp. 451-461.

[93] S. Delikaraoglou, P. Pinson, “Optimal allocation of HVDC interconnections for exchange of energy and reserve capacity services”, Energy Systems, vol. 10, n. 3, Aug. 2019, pp. 635-675.

[94] L. Castaing, M.-S. Debry, G. Bareux, O. Beck, “Optimal Operation of HVDC Links Embedded in an AC Network”, Proc. of 2013 IEEE PowerTech Conf., Grenoble, France, 16-20 June 2013, pp. 1-6.

[95] A.S.C. Leavy, W.A. Bukhsh, K.R.W. Bell, “Optimal Operation of the Western Link Embedded HVDC Connection”, proc. of 2018 PSCC Conf., 11-15 June 2018, Dublin, Ireland, pp. 1-6.

[96] S. Weck, S. Rüberg, J. Hansons, “Planning and Design Methodology for a European HVDC Overlay Grid”, Proc. of 13th IET ACDC 2017 Conference, Manchester, UK, 14-16 Feb. 2017, pp. 1-6.

[97] B. Aluisio, M. Dicorato, G. Forte, M. Trovato, A. Sallati, C. Gadaleta, C. Vergine, F. Ciasca, “The application of a flow-based methodology for yearly network analysis according to market data”, Proc. of 2017 EEM Conf., Dresden, Germany, 2017, pp. 1-6.

[98] B. Matthes, S. Spieker, D. Klein, C. Rehtanz, “Impact of a minimum remaining available margin adjustment in flow-based market coupling”, Proc. of 2019 IEEE Milan PowerTech Conf., Milan, Italy, 23-27 June 2019, pp. 1-6.

[99] F. Kunz, “Quo Vadis? (Un)scheduled electricity flows under market splitting and network extension in central Europe”, Energy Policy, vol. 116, May 2018, pp. 198-209.

[100] A. Kaushal, D. Van Hertem, “An Overview of Ancillary Services and HVDC Systems in European Context”, Energies, vol. 12, issue 18, Sept-2, 2019, paper n. 3481.

[101] L. Michi, E. M. Carlini, M. Migliori, F. Palone, S. Lauria, “Uprating studies for a 230 kV-50 Hz Overhead Line”, Proc. of 2019 IEEE Milan PowerTech Conf., Milan, Italy, 23-27 June 2019, pp. 1-6.

[102] Terna, Allegato A.24 al Codice di Rete: Individuazione zone della rete rilevante, rev. 04, Jan. 2019, [in Italian] online: https://download.terna.it/terna/0000/1142/92.pdf.

[103] Joint Working Group CIGRE/CIRED C1.29, “Planning criteria for future transmission networks in the presence of a greater variability of power exchange with distribution systems”, March 2017.

[104] M. Chiandone, G. Sulligoi, S. Massucco, F. Silvestro, “Hierarchical Voltage Regulation of Transmission Systems with Renewable Power Plants: an overview of the Italian case”, proc. of 3rd IET RPG 2014 conference, Naples, Italy, 24-25 Sept. 2014, pp.1-5.

[105] Terna S.p.A., Allegato A.74 al Codice di Rete: Metodologia Analisi Costi-Benefici - ACB 2.0, rev. 01, Feb. 2019, [in Italian] online: https://download.terna.it/terna/0000/1009/13.pdf.

[106] M. Migliori, S. Lauria, L. Michi, G. Donnini, B. Aluisio, C. Vergine, “Renewable sources integration using HVDC in parallel to AC traditional system: the Adriatic project”, Proc. of 2019 AEIT HVDC International Conference, Florence, Italy, 9-10 May 2019, pp. 1-6.

[107] L. Michi, G. Donnini, B. Aluisio, M. Migliori, C. Vergine, M. Dicorato, G. Forte, “The DC power planning for network flexibility in the multi-area power system”, Proc. of 2019 AEIT International Annual Conference, Florence, Italy, 18-20 Sept. 2019, pp. 1-6.

[108] D. Van Hertem, O. Gomis-Bellmunt, J. Liang, “HVDC Grids: For Offshore and Supergrid of the Future”, IEEE Press-Wiley, 2016.

[109] Italian Ministry of Infrastructures and Economic Development, “National Energy Strategy” [in Italian], online: https://www.mise.gov.it/images/ stories/documenti/BROCHURE_ENG_SEN.PDF.

[110] Italian Ministry of Infrastructures and Economic Development, “Italian National Energy and Climate Package”: https://www.mise.gov.it/images/stories/documenti/Proposta_di_Piano_Nazionale_Integrato_per_Energia_e_il_Clima_Italiano.pdf.

[111] C. Bruno, L. Campisano, M. Ciccotelli, L. Franchi, G. Giannuzzi, M. Salvetti, R. Zacheo and R. Zaottini, “CRESO and SICRE: Modern Environments for Power System Static and Dynamic Analysis”, PowerGrid Europe, May 26-28, 2009, Cologne, Germany.

[112] L. Michi, G. Donnini, P Capurso, A. Caldarulo Bugliari, F. Falorni, M. Quadrio, D.Canever, L. Giorgi, “An overview of the HVDC transmission system models in planning tools: the Italian experience”, Proc. of 2019 AEIT HVDC Int. Conf., Florence, Italy, 9-10 May 2019, pp. 1-6.

[113] L. Michi, E.M. Carlini, T. Baffa Scirocco, G. Bruno, R. Gnudi, G. Pecoraro, C. Pisani, “AC Transmission Emulation Control Strategy in VSC-HVDC systems: general criteria for optimal tuning of control system”, Proc. of 2019 AEIT HVDC Int. conf., Florence, Italy, 9-10 May 2019, pp. 1-6.

[114] Terna, Allegato A.11 Codice di Rete: “Criteri generali per la taratura delle protezioni delle reti a tensione uguale o superiore a 110 kV”, rev. 01, Jul. 2018 [in Italian] online https://download.terna.it/terna/0000/0105/28.pdf.

[115] C. Mosca, F. Arrigo, A. Mazza, E. Bompard, E. Carpaneto, G. Chicco, P. Cuccia, “Mitigation of frequency stability issues in low inertia power systems using synchronous compensators and battery energy storage systems”, IET Generation, Transmission and Distribution, vol. 13 no. 17, Sept. 2019, pp. 3951-3959.

[116] F. Palone, M. Marzinotto, M. Rebolini, S. Gentili, G. M. Giannuzzi, M. Schembari, S. Lauria, “Impact of renewable generation on commutation failures in multiinfeed HVDC systems: a real case study”, in Proc. 11th IET Int. Conf. on AC and DC Power Transmission, Birmingham, Feb. 2015.

[117] C. Guo, C. Zhao, A. Montanari, A.M. Gole, X. Xiao, “Investigation of hybrid bipolar HVDC system performances” Zhongguo Dianji Gongcheng Xuebao (Proceedings of the Chinese Society of Electrical Engineering), Vol. 32, No. 10, April 2012, pp. 98-104.

[118] Z. Li, R. Zhan, Y. Li, Y. He, J. Hou, X. Zhao, X.P. Zhang, “Recent developments in HVDC transmission systems to support renewable energy integration. Global Energy Interconnection, vol. 1, n. 5, dec. 2018, pp. 595-607.

[119] Terna S.p.A., Year 2019 Italian National Development Plan, [in Italian] online: http://download.terna.it/terna/0000/1188/36.PDF.

[120] Terna S.p.A., Statistical data, Year 2017, [in Italian], Available online: https://download.terna.it/terna/0000/0964/27.PDF.

[121] H.P. St. Clair, “Practical concepts in capability and performance of transmission line,” in proc. of the AIEE Pacific General Meeting, Vancouver, B.C., Canada, 1–4, Sept. 1953.

[122] R.D. Dunlop, R. Gutman and P.P. Marchenko, “Analytical development of loadability characteristics for EHV and UHV transmission lines,” IEEE Trans. Power Apparatus and Systems, vol. PAS-98, no. 2, pp. 606-613, March- April 1979.

[123] D. Lauria, G. Mazzanti and S. Quaia, The Loadability of Overhead Transmission Lines. Part I: Analysis of Single-Circuits, IEEE Trans. Power Delivery, February 2014, vol. 29, n. 1, 29-37.

[124] D. Lauria, G. Mazzanti and S. Quaia, “The Loadability of Overhead Transmission Lines. Part II: Analysis of Double- Circuits and Overall Comparison,” IEEE Transactions on Power Delivery, vol. 29, no. 2, April 2014, pp. 518-524.

[125] D. Lauria and S. Quaia, “Loadability Increase in Radial Transmission Lines through Reactive Power Injection”, Proc. of the 6th International Conference on Clean Electrical Power – ICCEP 2017, Santa Margherita Ligure (Italy), 27-29 June, 2017.

[126] D. Lauria and S. Quaia, "Transmission Line Loadability Increase through Series compensation," 2018 International Symposium on Power Electronics, Electrical Drives, Automation and Motion (SPEEDAM), Amalfi, 2018, pp. 1019-1024.

[127] F. M. Gatta, and S. Lauria, "Very long EHV cables and mixed overhead-cable lines. Steady-state operation," in Proc. 2005 IEEE St. Petersburg Power Tech Conf., St. Petersburg (Russia) June 2005, Paper n. 297.

[128] F. M. Gatta, A. Geri, S. Lauria, and M. Maccioni, "Steady-state operating conditions of very long EHVAC cable lines," Electric Power Systems Research, vol. 81 n. 7, pp. 1525-1533, July 2011.

[129] F. M. Gatta, A. Geri, S. Lauria, and M. Maccioni, "Steady-state operating conditions of very long EHVAC cable lines: Two case studies," Electric Power Systems Research, vol. 83 n. 1, pp. 160-169, Feb. 2012.

[130] R. Benato, A. Chiarelli, S. D. Sessa, R. D. Zan, M. Rebolini and M. Pazienza, "HVDC Cables Along with Highway Infrastructures: the “Piedmont-Savoy” Italy-France Intertie," 2018 AEIT International Annual Conference, Bari, 2018, pp. 1-6.

[131] A. Mohammed, et al. "Evaluation of EHV and AC/DC technologies for integration of large-scale renewable generation in Saudi Arabian network." IET Generation, Transmission & Distribution, 2018, vol. 13, no.4, pp. 575-581.

[132] G. Blanco, F. Olsina, F. Garces, C. Rehtanz, “Real Option Valuation of FACTS Investments Based on the Least Square Monte Carlo Method”, IEEE Trans. Power Syst., vol. 26, no. 3, Aug. 2011, pp. 1389-1398.

[133] K. Soleimani, J. Mazloum, “Considering FACTS in Optimal Transmission Expansion Planning”, Engineering, Technology & Applied Science Research, vol. 7, no. 5, Oct. 2017, pp.1987-1995.

[134] O. Ziaee, O. Alizadeh-Mousavi, F.F. Choobineh, “Co-Optimization of Transmission Expansion Planning and TCSC Placement Considering the Correlation Between Wind and Demand Scenarios”, IEEE Trans. Power Syst., vol. 33, no. 1, Jan 2018, pp. 206-215.

[135] J. Zhan. W. Liu, C.Y. Chung, “Stochastic Transmission Expansion Planning Considering Uncertain Dynamic Thermal Rating of Overhead Lines”, IEEE Trans. Power Systems, vol. 34, no. 1, Jan. 2019, pp. 432-443.

[136] IEEE Standard 738-2012, “IEEE Standard for Calcuating the Current-Temperature Relationship of Bare Overhaed Conductors”, Oct. 2012.

[137] D. A. Douglass, J. Gentle, H.M. Nguyen, W.A. Chisholm, C. Xu, T. Goodwin, H. Chen, S. Nuthlapati, I.S. Grant, J. Jardini, R. Kluge, P. Traynor, C. Davis, “A Review of Dynamic Thermal Line Rating Methods with Forecasting”, IEEE Trans. Power Delivery, vol. 34, no. 6, Dec. 2019, pp. 2100-2109.

[138] M. Rahman, F. Atchison, V. Cecchi, “Grid Integration of Renewable Energy Sources: Utilization of Line Thermal Behavior”, proc. of 2019 SoutheastCon, Huntsville, AL, USA, 11-14 Apr. 2019.

[139] H. Shaker, H. Zareipour, M. Fotuhi-Firuzabad, “Reliability Modeling of Dynamic Thermal Rating”, IEEE Trans. Power Delivery, vol. 28, no. 3, July 2013, pp. 1600-1609.

[140] Y. Huang, C. Guo, Y. Wen. Y. Wang, X. Zhang, J. Zhang, “Overload strategy of transmission and transformation equipment for safety operation”, proc. of 2014 IEEE PES General Meeting, National Harbor, MD, USA, 27-31 July 2014.

[141] D. Sidea, I. Baran, T. Leonida, “Weather-based assessment of the overhead line conductors thermal state”, proc. of 2015 IEEE Eindhoven PowerTech, Eindhoven, The Netherlands, 29 June-2 July 2015.

[142] IEEE Standard 1283-2013 “IEEE Guide for Determining the Effects of High-Temperature Operation on Conductors, Connectors, and Accessories”, August 2013.

[143] J. Rodriguez Alvarez, J. Azurza Anderson, C.M. Franck, “Validation of a thermal model for overhead transmission lines at high conductor temperature”, proc. of 2016 IEEE PES General Meeting, Boston, MA, USA, 17-21 July 2016.

[144] S. Zhai, H. Ji, Z. Ying, “A Model for Calculating Core Temperature of Bare Overhead Conductor Based on Neural Network”, proc. of 2nd International Conference on Mechatronics, Control and Automation Engineering (MCAE 2017), Shenzhen, China, 17-18 Sept. 2018.

[145] F. Song Y. Wang, H. Yan, X. Zhou, Z. Niu, “Increasing the Utilization of Transmission Lines Capacity by Quasi-Dynamic Thermal Ratings”, Energies, vol. 12, iss.5, March-1 2019, paper n. 792.

[146] D. Alali, H. Griffiths, L.M. Cipcigan, A. Haddad, “Assessment of Line Overloading Risk for Transmission Networks”, proc. of 11th IET Int. Conf. on AC and DC Power Transmission, Birmingham, UK, 10-12 Feb. 2015.

[147] P. Pytlak, P. Musilek, J. Doucet, “Using Dynamic Thermal Rating Systems to Reduce Power Generation Emissions”, proc. of 2011 IEEE PES General Meeting, Detroit, MI, USA, 24-28 July 2011.

[148] K. Kopsidas, S.M. Rowland, B. Boumecid, “A Holistic Method for Conductor Ampacity and Sag Computation on an OHL Structure”, IEEE Trans. Power Delivery, vol. 27, no. 3, July 2012, pp. 1047-1054.

[149] S. Liu, C. Cruzat, K. Kopsidas, “Impact of transmission line overloads on network reliability and conductor ageing”, proc. of 2017 IEEE Manchester PowerTech, Manchester, UK, 18-22 June 2017.

[150] K. Kopsidas, C. Tumelo-Chakonta, C. Cruzat, “Power Network Reliability Evaluation Framework Considering OHL Electro-Thermal Design”, IEEE Trans. Power Systems, vol. 31, no. 3, May 2016, pp. 2463-2471.

[151] W. A. Vasquez, D. Jayaweera, J. Jativa-Ibarra, “Advanced Aging Failure Model for Overhead Conductors”, proc. of 2017 IEEE ISGT Europe Conf., Torino, Italy, 26-29 Sept. 2017.

[152] P. Musilek, J. Heckenbergerova, M. M. I. Bhuiyan, “Spatial Analysis of Thermal Aging of Overhead Transmission Conductors”, IEEE Trans. Power Delivery, vol. 27, no. 3, July 2012, pp. 1196-1204.

[153] Terna S.p.A., National Network Development Plan, 2020. Available online: https://download.terna.it/terna/Piano%20di%20Sviluppo%202020_8d7db1ffa4ca9e7.pdf.

[154] F. M. Gatta, Impianti Elettrici, Società Editrice Esculapio, Vol.1.

[155] Italian Regulatory Authority for Energy, Networks and Environment, Deliberation 103/2019/R/EEL. Available online: https://www.arera.it/allegati/docs/19/103-19.pdf.

[156] Terna S.p.A. “Procedura per la definizione dei limiti di transito fra le zone di mercato”, online: https://download.terna.it/terna/Procedura_limiti_di_scambio_V19_2020_8d77a42edf096ee.pdf.

[157] C. Mosca, E. Bompard, B. Aluisio, M. Migliori, C. Vergine and P. Cuccia, "HVDC for frequency stability under RES penetration: the Sardinia island case," 2019 AEIT HVDC International Conference (AEIT HVDC), Florence, Italy, 2019, pp. 1-6.

[158] P. Daly, D. Flynn and N. Cunniffe, "Inertia considerations within unit commitment and economic dispatch for systems with high non-synchronous penetrations," 2015 IEEE Eindhoven PowerTech, Eindhoven, 2015, pp. 1-6.

[159] J. Zhu, J. M. Guerrero, W. Hung, C. D. Booth, nad G. P. Adam, "Generic inertia emulation controller for multi-terminal voltage-source-converter high voltage direct current systems", IET Renewable Power Generation vol. 8., issue 7, pp. 740-748, Sep. 2014.

[160] E. Ela, V. Gevorgian, A. Tuohy, B. Kirby, M. Milligan and M. O'Malley, "Market Designs for the Primary Frequency Response Ancillary Service—Part I: Motivation and Design," IEEE Trans. Power Syst., vol. 29, no. 1, pp. 421–431, 2014.

[161] W. Li, P. Du and N. Lu, "PFR ancillary service in low-inertia power system," IET Gener. Transm. Distrib., vol. 14, no. 5, pp. 920–930, 2020.

[162] T. Xu, W. Jang and T. Overbye, "Commitment of Fast-Responding Storage Devices to Mimic Inertia for the Enhancement of Primary Frequency Response," IEEE Trans. Power Syst., vol. 33, no. 2, pp. 1219–1230, 2018.

[163] ENTSO-E WG SPD, “Frequency Stability Evaluation Criteria for the Synchronous Zone of Continental Europe”, March 2016.

[164] H. Gu, R. Yan, and T.K. Saha, “Minimum synchronous inertia requirement of renewable power systems”, IEEE Trans. Power Syst., vol. 33. no. 2, pp. 1533–1543, 2018.

[165] S. Pöschel-Løvengreen and P. Mancarella, “Frequency response constrained economic dispatch with consideration of generation contingency size”, Proc. PSCC 2018, Dublin, Ireland, 11-15 June 2018.

[166] H. Ahmadi and H. Ghasemi, “Security-constrained unit commitment with linearized system frequency limit constraints”, IEEE Trans. Power Syst., vol. 29, no. 4, pp. 1536–1545, 2014.

[167] F. Teng, V. Trovato and G. Strbac, "Stochastic Scheduling With Inertia-Dependent Fast Frequency Response Requirements," IEEE Trans. Power Syst., vol. 31, no. 2, pp. 1557–1566, 2016.

[168] Y. Wen, W. Li, G. Huang and X. Liu, "Frequency Dynamics Constrained Unit Commitment With Battery Energy Storage," IEEE Trans. Power Syst., vol. 31, no. 6, pp. 5115–5125, 2016.

[169] A. Mazza and G. Chicco, “Application of TOPSIS in distribution systems multi-objective optimization,” Proc. 9th World Energy System Conference, Suceava, Romania, 28-30 June 2012, pp. 625–633.

[170] C.L. Hwang and K. Yoon, Multiple attribute decision making. Methods and applications: a state-of-the-art survey. Berlin and New York: Springer-Verlag, 1981.

[171] C. Mosca, F. Arrigo, A. Mazza, et al., “Mitigation of frequency stability issues in low inertia power systems using synchronous compensators and battery energy storage systems,” IET Gener. Transm. Distrib., vol. 13, no. 17, pp. 3951–3959, 2019.

[172] Belgian Transmission System Operator, “Adequacy and flexibility study for Belgium 2020 – 2030”, 2019, Available online: https://www.elia.be/en/electricity-market-and-system/adequacy/adequacy-studies.

[173] Terna S.p.A., “Rapporto Adeguatezza Italia 2019”, [in Italian], available online: https://download.terna.it/terna/Rapporto%20Adeguatezza%20Italia%202019_8d71cb7ff32ad37.pdf.

[174] L. Michi, M. Migliori, A. C. Bugliari, B. Aluisio, G. M. Giannuzzi and E. M. Carlini, "Transmission network expansion planning: towards enhanced renewable integration," 2018 AEIT International Annual Conference, Bari, 2018, pp. 1-5.

[175] L. Michi et al., "The DC power planning for network flexibility in the multi-area power system," 2019 AEIT International Annual Conference (AEIT), Florence, Italy, 2019, pp. 1-5.

[176] A. Keane et al., "Capacity Value of Wind Power," in IEEE Transactions on Power Systems, vol. 26, no. 2, pp. 564-572, May 2011.

[177] D. Kavanagh, A. Keane and D. Flynn, "Capacity Value of Wave Power," in IEEE Transactions on Power Systems, vol. 28, no. 1, pp. 412-420, Feb. 2013.

[178] J. Adams, M. O’Malley, K. Hanson, K. Connolly, K. Jefferies, W. Lasher, C. Loutan, B. Bagen, M. Patel, J. Nish and W. Coste, “Flexibility Requirements and Potential Metrics for Variable Generation: Implications for System Planning Studies,” Aug. 2010. [Online]. Available: http://www.nerc.com/files/IVGTF_Task_1_4_Final.pdf.

[179] EirGrid and SONI, “Ensuring a Secure, Reliable and Efficient Power System in a Changing Environment”, June 2011.

[180] CAISO, “Flexible Resource Adequacy Criteria and Must-Offer Obligation”, Feb. 2014.

[181] CAISO, “Flexible Ramping Products”, Aug. 2014.

[182] E. Ela and B. Kirby, “ERCOT Event on February 26, 2008: Lesson Learned”, July 2008.

[183] H. Holttinen et al., “Variability of load and net load in case of large scale distributed wind power,” in Proc. 10th International Workshop on large-Scale Integration of Wind Power into Power Systems as well as on Transmission Networks for Offshore Wind Power Plants, Aarhus, Denmark, Aug. 2011.

[184] N. Nivad, G. Rosenwald and D. Chatterjee, “Ramp Capability for Load Following in MISO Markets,” July 2011.

[185] E. Lannoye, M. O’Malley, A. Tuohy, D. Flynn, P. Daly, “Assessing Power System Flexibility for Variable Renewable Integration: A Flexibility Metric for Long-Term System Planning”, CIGRE Science and Engineering Journal, vol. 3., pp. 26-39, 2015.

[186] E. Lannoye, D. Flynn and M. O’Malley, “Evaluation of power system flexibility,” IEEE. Trans. Power Sys., vol. 27, no. 2, pp. 922–931, May 2012.

[187] H. Holttinen et al., “The flexibility workout: managing variable resources and assessing the need for power system modification,” IEEE Power and Energy Mag., vol. 11, no. 6, pp. 53–62, Nov. 2013.

[188] IEA, Empowering variable renewables: Options for flexible electricity systems. 2009.

[189] Navigant Research, “Demand Response Enabling Technologies,” May 2015.

[190] D.S. Kirschen, A. Rosso, J. Ma, and L.F. Ochoa, “Flexibility from the demand side,” in Proc. IEEE PES General Meeting, San Diego, CA, USA, 2012.

[191] M. Heleno, M.A. Matos and J.A. Pecas Lopes, “Availability and flexibility of loads for the provision of reserve,” IEEE. Trans. Smart Grid, vol. 6, no. 2, pp. 667-674, Mar. 2015.

[192] C. O'Dwyer and D. Flynn, "Using energy storage to manage high net load variability at subhourly time-scales," IEEE. Trans. Power Sys., vol. 30, no. 4, pp. 2139-2148, July 2015.

[193] E. Lannoye, D. Flynn and M. O’Malley, “Transmission, variable generation, and power system flexibility,” IEEE. Trans. Power Sys., vol. 30, no. 1, pp. 57–66, Jan. 2015.

[194] P. Denholm and M. Hand, “Grid flexibility and storage required to achieve very high penetration of variable renewable electricity,” Energy Policy, vol. 39, pp. 1817-1830, Mar. 2011.

[195] NREL, “Integrating Variable Renewable Energy in Electric Power Markets,” Apr. 2012.

[196] M.I. Alizadeh, M. Parsa Moghaddam, N. Amjady, P. Siano, M.K. Sheikh-El-Eslami, “Flexibility in future power systems with high renewable penetration: A review”, Renewable and Sustainable Energy Reviews, vol. 57, pp. 1186–1193, 2016.

[197] E. Lannoye, D. Flynn and M. O'Malley, "The role of power system flexibility in generation planning," 2011 IEEE Power and Energy Society General Meeting, Detroit, MI, USA, 2011, pp. 1-6.

[198] J. Cochran, M. Miller, O. Zinaman, M. Milligan, D. Arent, B. Palmintier, M. O'Malley, S. Mueller, E. Lannoye, A. Tuohy, B. Kujala, M. Sommer, H. Holttinen, J. Kiviluoma, S. Soonee, “Flexibility in 21st Century Power Systems”, 2014.

[199] G. Papaefthymiou, K. Dragoon, “Toward 100% renewable energy systems: Uncapping power system flexibility”, Energy Policy, no. 92, pp. 69-82, 2016.

[200] A. Ulbig, G. Andrersson, “Analyzing operational flexibility of electric power system”, Int. J. Electr. Power Energy Syst., no. 72, pp. 155-164, 2015.

[201] M. Poncela, A. Purvins, and S. Chondrongiannis, “Pan-European Analysis on Power System Flexibility”, Energies, July 2018.

[202] J. M. Alemany, B. Arendarski, P. Lombardi, P. Komarnicki, “Accentuating the renewable energy exploitation: Evaluation of flexibility options”, Int. J. Electr. Power Energy Syst., no. 102, pp. 131-151, 2018.

[203] I. F. Abdin, E. Zio, “An integrated framework for operational flexibility assessment in multi-period power system planning with renewable energy production”, Applied Energy, no.222, 2018.

[204] N. E. Koltsaklis, A. S. Dagoumas, I. P. Panapakidis, “Impact of the penetration of renewables on flexibility needs”, Energy Policy, no. 109, pp. 360-369, 2017.

[205] M. Huber, D. Dimkova, T. Hamacher, “Integration of wind and solar power in Europe: Assessment of flexibility requirements”, Energy, vol. 69, pp. 236-246, 2014.

[206] A. Capasso, A. Cervone, M.C. Falvo, R. Lamedica, G.M. Giannuzzi, R. Zaottini, “Bulk indices for transmission grid flexibility assessment in electricity market: A real application”, Electrical Power and Energy Systems, vol. 56, 2014, pp. 332-339.

[207] P. Bresesti, A. Capasso, M.C. Falvo, S. Lauria, “Power system planning under uncertainty conditions. Criteria for transmission network flexibility evaluation”, Proc. of 2003 IEEE PowerTech Conf., June 23th-26th, Bologna, Italy, pp.1-6.

[208] A. Capasso, M. C. Falvo, R. Lamedica, S. Lauria and S. Scalcino, "A new methodology for power systems flexibility evaluation," 2005 IEEE Russia Power Tech, St. Petersburg, 2005, pp. 1-6.

[209] MC. Falvo, “An approach for transmission system expansion planning in electricity market”. In: Proc. 2006 IEEE PES General Meeting Conf.

[210] ENTSO-E, Scenario Outlook and Adequacy Forecast 2015. Available online: https://docstore.entsoe.eu/Documents/SDC%20documents/SOAF/150630_SOAF_2015_publication_wcover.pdf.

[211] J. O'Sullivan, A. Rogers, D. Flynn, P. Smith, A. Mullane and M. O'Malley, "Studying the Maximum Instantaneous Non-Synchronous Generation in an Island System—Frequency Stability Challenges in Ireland," in IEEE Transactions on Power Systems, vol. 29, no. 6, pp. 2943-2951, Nov. 2014.

[212] Terna S.p.A., “Scenarios description document, 2018 Edition”, [in Italian], Available online: http://download.terna.it/terna/0000/1016/83.PDF.

[213] E. Lannoye, D. Flynn and M. O'Malley, "Assessment of power system flexibility: A high-level approach," 2012 IEEE Power and Energy Society General Meeting, San Diego, CA, 2012, pp. 1-8.

[214] P. Capurso, B. Cova, E. Elia, P. Portoghese, M. Stabile, F. Vedovelli, A. Venturini, “ Market integration in Europe: a market simulator taking into account different market zones and the increasing penetration of RES generation. Cigre General Session. 2012. Paris, August 2008, paper C1-104.

[215] Italian Regulatory Authority for Energy, Networks and Environment, Annex A to Order 627/2016, “Minimum requirements for the preparation of the Ten-Year development Plan of the national transmission network”.

[216] Terna S.p.A., “Documento metodologico per l’Applicazione dell’Analisi Costi Benefici Applicata al Piano di Sviluppo 2020”, [in Italian], Available online: https://download.terna.it/terna/Allegato%20Metodologico_8d7db2190bbcb8f.pdf.

[217] Terna S.p.A., Year 2018 Italian National Development Plan, [in Italian] online: https://download.terna.it/terna/0000/1039/76.PDF.

[218] EPEX Spot, APX, Belpex, Nord Pool Spot, OMIE, GME, and OTE, “EUPHEMIA public description,” Oct. 2013. [Online]. Available: http://www.apxgroup.com/wp-content/uploads/Euphemia-publicdescription-Nov-20131.pdf.

[219] B. Aluisio, G. Forte, M. Dicorato, M. Trovato, A. Sallati, C. Gadaleta, C. Vergine, F: Ciasca, “The application of a flow based methodology for yearly network analysis according to market data”, Proc. of 2017 EEM Internat. Conf., 6-9 June 2017, Dresden. Germany, pp. 1-6.

[220] A. Wood, B. Wollenberg, G. Sheblé, “Power Generation, Operation, and Control”, IEEE-Wiley, 2014.

[221] R.D. Zimmerman, C.E. Murillo-Sanchez, R.J. Thomas, “MATPOWER: Steady-State Operations, Planning, and Analysis Tools for Power Systems Research and Education”, IEEE Trans. Power Syst., vol. 26, no. 1, Feb. 2011, pp. 12-19.

[222] S. de la Torre, A. J. Conejo and J. Contreras, "Transmission Expansion Planning in Electricity Markets," in IEEE Transactions on Power Systems, vol. 23, no. 1, pp. 238-248, Feb. 2008.

[223] J. Rosellón, “Different Approaches Towards Electricity Transmission Expansion. Review of Network Economics”, 2003.

[224] J. H. Zhao, Z. Y. Dong, P. Lindsay and K. P. Wong, "Flexible Transmission Expansion Planning With Uncertainties in an Electricity Market," in IEEE Transactions on Power Systems, vol. 24, no. 1, pp. 479-488, Feb. 2009.

[225] M. O. Buygi, H. M. Shanechi, G. Balzer, M. Shahidehpour and N. Pariz, "Network planning in unbundled power systems," in IEEE Transactions on Power Systems, vol. 21, no. 3, pp. 1379-1387, Aug. 2006.

[226] M. O. Buygi, G. Balzer, H. M. Shanechi and M. Shahidehpour, "Market-based transmission expansion planning," in IEEE Transactions on Power Systems, vol. 19, no. 4, pp. 2060-2067, Nov. 2004.

[227] P. Linares, "Multiple criteria decision making and risk analysis as risk management tools for power systems planning," in IEEE Transactions on Power Systems, vol. 17, no. 3, pp. 895-900, Aug. 2002.

[228] Risheng Fang and D. J. Hill, "A new strategy for transmission expansion in competitive electricity markets," in IEEE Transactions on Power Systems, vol. 18, no. 1, pp. 374-380, Feb. 2003.

[229] Terna S.p.A., “Rapporto di identificazione delle capacità obiettivo 2018”. In Italian. Available online: https://download.terna.it/terna/0000/1149/78.PDF.

[230] G. Latorre, R. D. Cruz, J. M. Areiza and A. Villegas, "Classification of publications and models on transmission expansion planning," in IEEE Transactions on Power Systems, vol. 18, no. 2, pp. 938-946, May 2003.

[231] L. L. Garver, "Transmission Network Estimation Using Linear Programming," in IEEE Transactions on Power Apparatus and Systems, vol. PAS-89, no. 7, pp. 1688-1697, Sept. 1970.

[232] K. J. Kim, Y. M. Park and K. Y. Lee, "Optimal long term transmission expansion planning based on maximum principle," in IEEE Transactions on Power Systems, vol. 3, no. 4, pp. 1494-1501, Nov. 1988.

[233] J.A. Aguado, S. de la Torre, J. Contreras, A.J. Conejo, A. Martínez, "Market-driven dynamic transmission expansion planning", Electric Power Systems Research, Volume 82, Issue 1, 2012.

[234] A. Monticelli, A. Santos, M. V. F. Pereira, S. H. Cunha, B. J. Parker and J. C. G. Praca, "Interactive Transmission Network Planning Using a Least-Effort Criterion," in IEEE Transactions on Power Apparatus and Systems, vol. PAS-101, no. 10, pp. 3919-3925, Oct. 1982.

[235] G. Latorre-Bayona and I. J. Perez-Arriaga, "CHOPIN, a heuristic model for long term transmission expansion planning," in IEEE Transactions on Power Systems, vol. 9, no. 4, pp. 1886-1894, Nov. 1994.

[236] G. C. Oliveira, A. P. C. Costa and S. Binato, "Large scale transmission network planning using optimization and heuristic techniques," in IEEE Transactions on Power Systems, vol. 10, no. 4, pp. 1828-1834, Nov. 1995.

[237] F. G. L. Pilo, "Rapporto di verifica su: Rapporto di identificazione delle capacità obiettivo, 2019". [In Italian]. Available online: https://www.arera.it/allegati/operatori/pds/Rapporto_verifica_Pilo.pdf.

[238] National Grid. "Network Options Assessment". Online: https://www.nationalgrideso.com/research-publications/network-options-assessment-noa.

[239] National Grid. "Future Energy Scenarios". Online: https://www.nationalgrideso.com/future-energy/future-energy-scenarios.

[240] National Grid. "Electricity Ten Year Statement". Online: https://www.nationalgrideso.com/research-publications/electricity-ten-year-statement-etys.

[241] European Network of Transmission System Operators (ENTSO-E). "Power system Needs in 2030 and 2040". Online: https://eepublicdownloads.azureedge.net/tyndp-documents/IoSN2020.

[242] Agency for the Cooperation of Energy Regulators (ACER). Opinion 14/2017 on the draft regional lists of proposed electricity projects of common interest 2017, 10 October 2017. Available online: https://www.acer.europa.eu/Official_documents/Acts_of_the_Agency/Opinions/Opinions/ACER%20Opinion%2014-2017.pdf.

[243] Council of European Energy Regulators (CEER), "White Paper #VI on Infrastructures". 17 July 2017. Available online: https://www.ceer.eu/documents/104400/5937686/Infrastructure/a66d7d34-0922-bfa6-83bc-959706207c3b.

[244] Italian Regulatory Authority for Energy, Networks and Environment. Memoria 11 May 2015, 212/2015/I/COM, in Italian. Available online: https://www.arera.it/allegati/docs/15/212-15.pdf.

[245] Italian Regulatory Authority for Energy, Networks and Environment. Memoria 29 October 2015, 501/2015/I/COM, in Italian. Available online: https://www.arera.it/allegati/docs/15/501-15.pdf.

[246] Italian Regulatory Authority for Energy, Networks and Environment. Consultation document 1. October 2015. 464/2015/R/eel, in Italian. Available online: https://www.arera.it/allegati/docs/15/464-15.pdf.

[247] Agency for the Cooperation of Energy Regulators (ACER). Opinion 06/2012 on the European Ten Year Network Development Plan 2012. 5 September 2012. Available online: https://www.acer.europa.eu/Official_documents/Acts_of_the_Agency/Opinions/Opinions/ACER%20Opinion%2006-2012.pdf.

[248] Italian Regulatory Authority for Energy, Networks and Environment. Decision 21 December 2017. 884/2017/R/eel, in Italian. Available online: https://www.arera.it/allegati/docs/17/884-17.pdf.

[249] Italian Regulatory Authority for Energy, Networks and Environment. Decision 8 March 2018. 129/2018/R/eel, in Italian. Available online: https://www.arera.it/allegati/docs/18/129-18.pdf.

[250] Italian Regulatory Authority for Energy, Networks and Environment. Decision 20 December 2018. 698/2018/R/eel, in Italian. Available online: https://www.arera.it/allegati/docs/18/698-18.pdf.

[251] Michele Antonio Trovato, "Rapporto di identificazione delle capacità obiettivo 2018.". [In Italian]. Online:https://www.arera.it/allegati/operatori/pds/MA_TROVATO_Relazione_Finale_Target_Capacity_2018.pdf.

[252] B. Chen, J. Wang, L. Wang, Y. He and Z. Wang, "Robust Optimization for Transmission Expansion Planning: Minimax Cost vs. Minimax Regret," in IEEE Transactions on Power Systems, vol. 29, no. 6, pp. 3069-3077, Nov. 2014.

[253] M. Rahmani, R. A. Romero and M. J. Rider, "Risk/investment-driven transmission expansion planning with multiple scenarios," in IET Generation, Transmission & Distribution, vol. 7, no. 2, pp. 154-165, Feb. 2013.

[254] European Network of Transmission System Operators (ENTSO-E). "3rd ENTSO-E Guideline for cost benefit analysis of grid development projects". 2019. Available online: https://docstore.entsoe.eu/Documents/TYNDP%20documents/Cost%20Benefit%20Analysis/191023_CBA3_Draft%20for%20consultation.pdf.

[255] Agency for the Cooperation of Energy Regulators (ACER). Report on unit investment cost indicators and corresponding reference values for electricity and gas infrastructure. 2015. Available online: http://www.acer.europa.eu/Official_documents/Acts_of_the_Agency/Publication/UIC%20Report%20%20-%20Electricity%20infrastructure.pdf.

[256] Agency for the Cooperation of Energy Regulators (ACER). Opinion 01/2014 on the ENTSO-E Guideline for CBA of Grid Development Projects. 31 January 2014. Available online: https://www.acer.europa.eu/Official_documents/Acts_of_the_Agency/Opinions/Opinions/ACER%20Opinion%2001-2014.pdf.

[257] V. Canazza, C. Giannotti, A. Venturini, "Cross border electricity exchanges between Italy, Switzerland and Germany: scenarios of competition among the European Power Markets and signals for interconnection investmens", Cigre Session, 2014.

[258] P. P. Pericolo, V. Canazza, D. Canever, B. Cova, A. Venturini, P. Marannino, F. Zanellini, "Use of Zonal and Nodal Market Simulators in Transmission Network Planning: Application to The Italian System", Cigre Session, 2008.

[259] E. M Carlini, P. P. Pericolo, F. Vedovelli, B. Cova, A. Venturini, “Impact of CO2 Reduction Targets on Transmission Capacity Expansion dictated by the Power Market Clearing: Application to the Italian and French Systems”, Cigre Session, 2010.

[260] P. Vicini, F. H. Schulze, M. Stabile, M.; M. Cabano, A. Venturini, “A new optimization tool for security constrained unit commitment in systems with high res penetration in the GCC region”. The 14th GCC –CIGRE International Conference and 23rd Exhibition for Electrical Equipment, 2017.

[261] A. Rossi, M. Stabile, C. Puglisi, D. Falabretti and M. Merlo, "Evaluation of the energy storage systems impact on the Italian ancillary market", Sustainable Energy Grids and Networks, vol. 17, pp. 100178, 2019.

[262] O. Bertoldi, M. Innorta, G. De Martini, “New issues in bulk power system planning”. Cigre Session, Vol. 1 of 2, Report 37-106, August 1996.

[263] European Network of Transmission System Operators (ENTSO-E). “TYNDP 2020 – Scenario Report”. Online: https://www.entsos-tyndp2020-scenarios.eu/.

[264] Terna S.p.A., “Metodologia per l’identificazione delle capacità obiettivo 2020. Documento di consultazione”. [in Italian]. Available Online: https://www.terna.it/it/sistema-elettrico/rete/piano-sviluppo-rete/preparazione-pds-consultazioni.

[265] C. L. Hwang, K. Yoon. Multiple attribute decision making: methods and applications a state-of-the-art survey. Berlin: Springer. 1981.

[266] J.R.S.C. Mateo, TOPSIS, Multi Criteria Analysis in the Renewable Energy Industry, Springer, 2012, pp. 43 – 48.

[267] D. Streimikiene, T. Baleˇzentis, Multi-criteria assessment of small scale CHP technologies G.-H. Tzeng, J.-J. Huang, Multiple Attribute Decision Making: Methods and Applications, Chapman and Hall/CRC Press, 2011.

[268] M. Socorro García-Cascales, J. M. Sánchez-Lozano, “Geographical Information Systems (GIS) and Multi-Criteria Decision Making (MCDM) methods for the evaluation of solar farms locations: Case study in south-eastern Spain”, Renewable and Sustainable Energy Reviews. 24 (2013). 544 – 546.

[269] European Commission. “Clean Energy for all Europeans”, Available Online: file:///C:/Users/a393033/Downloads/MJ0319092ENN.en.pdf.